# Morphological and molecular investigations on life history of benthic diatoms

# Morphological and molecular investigations on life history of benthic diatoms

形態観察と分子生物学的解析にもとづく付着珪藻の生活史に関する研究

Shiho Kamakura
鎌倉　史帆

Graduate School of Bioscience and Biotechnology
Fukui Prefectural University

March 2023

Committee:
Shinya Sato, Supervisor
Hiroaki Suetake, Co-supervisor
David G. Mann

# CONTENTS

# GENERAL INTRODUCTION

## Diatoms and their diversity

Diatoms are microalgae distributed throughout various aquatic and subaerial environments from acidic to alkaline, tropical to arctic, and marine to brackish/fresh waters (Round et al. 1990, Mann 1999). They are an important contributor to global primary productivity, representing approximately 20% of the total, and play a key role in the biogeochemical cycling of carbon and silica (Nelson et al. 1995, Mann 1999). It is proposed that the number of diatom species is in the tens of thousands (Mann & Vanormelingen 2013). Diatom cells are enveloped by silica cell walls called the frustule, which are composed of two thecae. Each theca comprises a valve and girdle bands, which are the structures linking two thecae to one another (Fig. 1). Diatoms are classified for convenience into the 'centric' and the 'pennate' species based on the valve symmetry.

Diatoms have benthic and planktonic life forms. Planktonic diatoms have received attentions because their production of toxins or the outbreak of red tides have a negative impact on industry (Hallegraeff 1993). Benthic diatoms are ecologically less understood compared to planktonic diatoms because they are more difficult to sample and quantify than planktonic diatoms (Round et al. 1990).

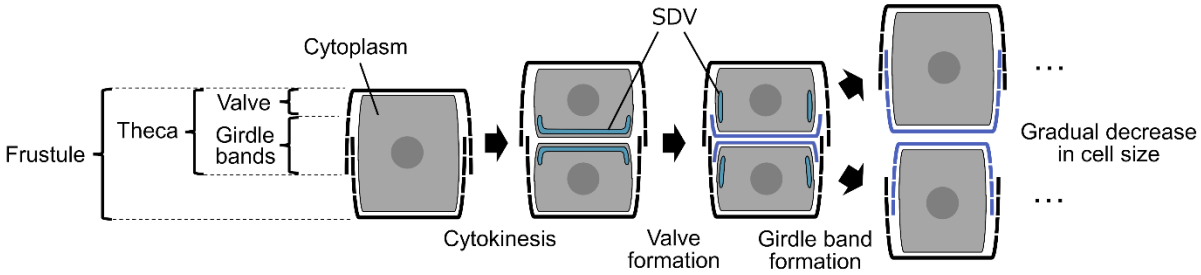


**Fig. 1.** Cell division and cell wall formation in diatoms. The diatom cell wall, called frustule, is formed within silica deposition vesicles (SDVs) through cell division. The blue lines depict newly formed frustules.

**Life cycle and sexual reproduction:** During cell division, new daughter valves are formed inside the mother cell (Fig. 1). For this structural reason in the cell wall, most species exhibit consistent reduction in cell size during the vegetative phase (Round et al. 1990). When cells become smaller than a certain size threshold, many diatoms become sexually potent, i.e. they can perform sexual reproduction when external conditions permit. The cell size thresholds and environmental cues that trigger sexual reproduction differ among species (Edlund & Stoermer 1997). Sexual reproduction ends up with the formation of an enlarged zygote, called the auxospore, in which a new vegetative cell is formed, called an initial cell, which represents the largest cell size in their life cycle. Apart from the canonical life cycle of diatoms as above, some exceptions are known, including an avoidance of size reduction (e.g.: von Stosch 1965, Round 1972, Rose & Cox 2013) or abrupt size enlargement without sexual reproduction (Gallagher 1983, Sato et al. 2008). The length of the

diatom life cycle, determined by the frequency of sexual reproduction and rate of cell size reduction, has been estimated to range from several months to several decades depending on the species (Mann 1988). Information on diatom sexual reproduction will help us to understand their population dynamics, however, only a few species have been examined for sexual reproduction relative to the total number of diatom species (Davidovich & Davidovich 2022).

**Endosymbiosis:** Eukaryotic organelles are thought to have arisen from the endosymbiotic incorporation of bacteria within archaea or ancestral eukaryotes. It is estimated that mitochondria have evolved from an ancestor related to *α*-proteobacteria, which were acquired more than 1.5 billion years ago, and that plastids have evolved from cyanobacteria that were acquired 1-1.5 billion years ago (Dyall et al. 2004). Determining the evolutionary events that led to the emergence of organelles is crucial for comprehending the evolution of eukaryotic cells and genomes. However, these organelles have diverged from their nearest bacterial relatives due to their ancient origins, thus providing limited information on the early stages of the transformation of free-living bacteria into organelles. This process involves a reduction in the genome size of the symbiont, the development of mechanisms by which the host cell controls the behavior of the symbiont (Zachar & Boza 2020) and the acquisition of the machinery to import proteins from the host to the symbiont, which is proposed to be the most decisive step in the establishment of the organelle (Theissen & Martin 2006). Furthermore, uniparental organellar inheritance, which is observed in a wide range of sexual eukaryotes, is thought to be one of the control forms of the organelle (symbiont) by the host cell (Kuroiwa 2010).

Diatoms do not have the ability to fix nitrogen, however, some genera have adapted to low nitrogen concentrations by establishing symbioses with diazotrophic bacteria (Foster & Zehr 2019). Diatom species belonging to the family Epithemiaceae have unique intracellular structures, the 'spheroid bodies' (Drum & Pankratz 1965, Geitler 1977), which are derived from nitrogen-fixing cyanobacterial symbionts (Prechtl et al. 2004, Nakayama et al. 2011). The spheroid body is much younger than mitochondria and plastid, with an estimated origin at about 12 Ma, according to the fossil record and molecular phylogenetic analysis (Nakayama et al. 2011). Therefore, the spheroid body has received an attention as a good model to provide new insights into the early stages of organelle evolution (Kneip et al. 2007, Trapp et al. 2012, Nowack & Weber 2018).

**Morphology:** Frustules have diverse and intricate hierarchical structures, including micrometer-scale exteriors and fine structures on the order of tens to hundreds of nanometers. Most diatom species are defined by their frustule morphology. The species-specific morphology and structure of diatoms has been discussed to be tied to their function and to contribute to the fitness of individuals (reviewed in Finkel & Kotrc 2010). The morphogenesis of frustules occurs in silica deposition vesicles (SDVs, Fig. 1), which are compartments separated by lipid bilayer membranes located immediately beneath the plasma membrane of dividing daughter cells (Pickett-Heaps et al. 1990, Kröger & Poulsen 2008). The morphology of the SDV and its internal forming frustule is controlled by cytoskeletons in the vicinity of the SDV (Pickett-Heaps et al. 1990, Tesson & Hildebrand 2010a). The cytoskeleton defines the position of the outer edge of the valve and

structures (Tesson & Hildebrand 2010a, b), and influences the pattern of the pores (Pickett-Heaps et al. 1990). Furthermore, some proteins involved in silica mineralization and frustule formation have been identified (reviewed in Fattorini & Maier 2021). The biosynthesis of silica frustules with varied morphologies is not only of biological significance, but are of interest in terms of their application to technologies for the massively parallel production of silica nanomaterials by self-assembly (Kröger & Poulsen 2008). To date, it is still unclear what genes and molecular mechanisms regulate the diverse morphology of frustules.

Generally, the morphology of frustules is highly stable trait within a species. However, environmental factors are known to cause plastic changes in the morphology of the valves in some diatom species. Some of the documented factors include temperature, silica concentration, pH, nutrient/heavy metals concentration, light intensity, and salinity (reviewed in Kociolek and Stoermer 2010, Su et al. 2018). If certain environmental cues are known to trigger a certain morphology within a taxon, this information can be a valid indicator of those environmental parameters (Cox 1995) in the ecological and water quality assessment of the current or past states of aquatic habitats. To date, considering the number of diatom species, there are only tiny proportion of diatoms whose morphological responses to environmental factors has been studied in culture experiments (Cox 2014).

## Culture-based experiment of diatoms

Culture experiments are effective means of studying diatom life cycles (Mann & Chepurnov 2004) as they allow the monitoring of cell division and size reduction in a population derived from a single cell. For sexually reproducing species, the experiments provide valuable insights into their life cycle, including maximum and minimum cell sizes. Observations of sexual cells in culture also provides insights into sexual differentiation (Shirokawa & Shimada 2013) and pheromone-mediated motility (Bondoc et al. 2019). In addition, culture experiment is effective in verifying morphological plasticity, particularly in instances where the morphology is affected by environmental factors and a single taxon may be mistaken for multiple taxa in field observations. Tracking of division and morphogenesis in culture has been facilitated by the use of PDMPO, which fluorescently labels newly forming frustules while keeping the diatom cells alive (Shimizu et al. 2001).

Besides the microscopic approaches, culture is useful to for transcriptomic study. The transcriptome refers to the set of all RNA molecules, both protein-coding mRNA and non-coding RNA (Thompson et al. 2016). The primary technologies for transcriptomic studies are microarrays and RNA sequencing (RNA-seq). Although microarray techniques can simultaneously detect the expression of thousands of genes, they are not ideal for detecting novel transcripts (Morozova et al. 2009). On the other hand, RNA-Seq gained popularity after 2008, with an advent of high-throughput DNA sequencing technology (Wilhelm et al. 2008), in that mRNA is fragmented and translated into cDNA, which is then sequenced using random primers. The number of reads for a given sequence is directly proportional to the expression level of genes and is an absolute indicator of their expression. In comparison to microarrays, RNA-Seq has the advantage of being able to detect novel transcripts and their high comprehensiveness, as well as reduced sequencing costs and experimental complexity (Morozova et al. 2009, Thompson et al. 2016). This sequencing

technique has made the transcriptome a practical research method not only for model species, but also for non-model species. Culture-based transcriptomics can reveal specific gene expression profiles under designed conditions. The combination of culture and RNA-seq approaches has been used to demonstrate transcriptional responses in diatoms to various environmental factors, such as nutrient limitation (Levitan et al. 2015), temperature (Ogura et al. 2018, Pargana et al. 2019), *p*CO2 (Huang et al. 2019), exposure to heavy metals (Suzuki et al. 2022), and salinity (Cheng et al. 2014, Bussard et al. 2017, Nakov et al. 2020, Pinseel et al. 2022). Furthermore, it enables us to identify expression profiles associated with various cellular events of diatoms, such as morphogenesis (Ovide et al. 2018) and sexual reproduction (Ferrante et al. 2019, Bilcke et al. 2021) to explore novel candidate genes responsible for them.

## Outline of the thesis

This dissertation focused on the biology of benthic diatoms based on culture of the pennate *Epithemia* and the centric *Pleurosira laevis* and presented new findings on diatom diversity and life history. In **Chapter 1**, the aim was to reveal the mating system of *E. gibba* var. *ventricosa* and the mode of the inheritance of its spheroid body to elucidate whether the uniparental inheritance system has evolved. This could be a criterion to assess the degree of organellogenesis in *Epithemia*. I established an experimental system consisting of induction of sexual reproduction of this diatom and genotyping to determine from which parent the spheroid body genome was transmitted to the F1 cells. In **Chapter 2**, field observation and culture experiment were combined. I measured valve lengths of two sympatric populations of congeneric diatoms *E. gibba* var. *ventricosa* and *Epithemia* sp. from a small pond in Nakaikemi Wetland, Japan, almost 3 years. I also performed growth experiments for both taxa to investigate cell-division and size-reduction rates to better interpret measurement of natural specimens. The 'cardinal points' (Kaczmarska et al. 2013) of *E. gibba* var. *ventricosa* identified in Chapter 1, i.e., size of initial cells, the upper and lower cell size threshold for sex expression, and the minimal cell size at which division is possible, were used to interpret the data. In **Chapter 3**, I documented that the plasticity of the valve morphology in *P. laevis* is determined by salinity conditions, and these responses are highly conserved among strains established from samples collected from different salinities and continents. **Chapter 4** characterized gene expression in *P. laevis* cultivated under salinity conditions that cause morphological changes as shown in the Chapter 3, and explored genes likely involved in the regulation of diatom morphology via comparative transcriptomics.

# **LIST OF PUBLICATIONS** with the statement of the candidate's contribution

## Publications included in this dissertation

Kamakura S, Mann DG, Nakamura N, Sato S. (2021) Inheritance of spheroid body and plastid in the raphid diatom *Epithemia* (Bacillariophyta) during sexual reproduction. Phycologia 60: 265–273. DOI: 10.1080/00318884.2021.1909399 (peer-reviewed)

*The candidate developed the concept and carried out the work. The manuscript was written by the candidate in discussion with the co-authors.*

Kamakura S, Ohtsuka T, Nagumo T, Sato S. Distinct life cycles of two sympatric *Epithemia* (Bacillariophyta) taxa in Nakaikemi Wetland, Japan. (in preparation)

*The candidate developed the concept and carried out the work. Ohtsuka T. provided help concerning taxonomic background and statistical analysis. Nagumo T. supported SEM observation. The manuscript was written by the candidate in discussion with the co-authors.*

Kamakura S, Ashworth MP, Yamada K, Mikami D, Kobayashi A, Idei M, Sato S. (2022) Morphological plasticity in response to salinity change in the euryhaline diatom *Pleurosira laevis* (Bacillariophyta). Journal of Phycology 58: 631–642. DOI: 10.1111/jpy.13277 (peer-reviewed)

*The candidate developed the concept and carried out the work. Ashworth M.P. provided strains from US and provided help concerning taxonomic background. The manuscript was written by the candidate in discussion with the co-authors.*

Kamakura S, Bilcke G, Sato S. Transcriptional responses to salinity in the polymorphic euryhaline diatom *Pleurosira laevis*. (in preparation)

*The candidate developed the concept and carried out the work. The manuscript was written by the candidate in discussion with the co-author.*

## Publications not included in this dissertation

Kamakura S, Sato S. (2018) Morphology and phylogeny of 2 strains of *Epithemia* collected from Nakaikemi Wetland, Fukui, Japan. Diatom 34: 68–69. DOI: 10.11464/diatom.34.68 (peer-reviewed, in Japanese)

*The candidate developed the concept and carried out the work. The manuscript was written by the candidate in discussion with the co-author.*

Mugikura, K, Arguelles, EDLR, Kamakura S, Ohtsuka T, Sato S. (2022) First record of the invasive diatom *Cymbella janischii* from Kinki Area and morphological observation of its living cell. Diatom 38: 49–53. DOI: 10.11464/diatom.38.49 (peer-reviewed, in Japanese with English abstract)

*The candidate performed molecular investigation and wrote part of the manuscript.*

Kamakura S, Sato S. (2022) Morphological plasticity of diatom silica cell walls in response to changes in salinity. Saibou 54: 314–317. (non peer-reviewed, in Japanese)

*The manuscript was written by the candidate in discussion with the co-author.*

CHAPTER 1

# Inheritance of spheroid body and plastid in the raphid diatom *Epithemia* (Bacillariophyta) during sexual reproduction

Kamakura S, Mann DG, Nakamura N, Sato S.

This is an 'Author's Accepted Manuscript' of an article published by Taylor & Francis Group in Phycologia on 21 Apr 2021, available online: https://doi.org/10.1080/00318884.2021.1909399.

## Abstract

Diatoms belonging to the family Epithemiaceae have endosymbiont 'spheroid bodies', which have received attention as a model to provide new insights into the early stages of organelle evolution. Uniparental organelle inheritance, known in a wide range of sexually reproducing eukaryotes, is considered to be one of the key characteristics acquired during the evolution of an endosymbiont into an organelle. However, there has been no information about the inheritance of spheroid bodies. The aim of the present study was, therefore, to investigate the inheritance modes of the spheroid bodies and plastids in the isogamous diatom *Epithemia gibba* var. *ventricosa*, which we established to be heterothallic. We induced sexual reproduction of *E. gibba* var. *ventricosa* in culture, using sexually compatible mating strains that differed with respect to nucleotide polymorphisms in the spheroid body and the plastid genomes. The F1 strains were genotyped to reveal the parental origin of the spheroid bodies and plastids using parent-specific polymorphisms. The results suggested that inheritance of the spheroid bodies was uniparental (i.e. progeny have the spheroid body genome from either parent but not both) and random (i.e. with an unbiased ratio of parental origins), while that of the plastids was more complex, being predominantly uniparental but with a few biparental cases. This study is the first to report the inheritance pattern of the spheroid body and will contribute to better understand the evolutionary state of this organelle.

## Introduction

Diatoms are unicellular algae distributed widely in aquatic environments, playing a predominant role in oceanic primary production and the biogeochemical cycling of carbon and silica (Nelson *et al.* 1995; Mann 1999). Their need for silicon arises because they use it to construct their cell walls, which in turn, because of the limited wall flexibility, leads in most species to an inexorable decrease in cell size during the vegetative phase (Round *et al.* 1990). When cells become smaller than a certain size threshold, many diatoms become sexually potent, i.e. they can perform sexual reproduction when external conditions permit. Sexual reproduction ends up with the formation of an enlarged zygote, called the auxospore, in which a new vegetative cell is formed, called an initial cell, which represents the largest cell size in the life cycle.

Diatom species belonging to the family Epithemiaceae have unique intracellular structures, the 'spheroid bodies' (Drum & Pankratz 1965; Geitler 1977), which are evolutionarily derived from nitrogen-fixing cyanobacterial symbionts (Prechtl *et al.* 2004; Nakayama *et al.* 2011). While mitochondria and plastids are believed to have been acquired from endosymbiotic

prokaryotes over a billion years ago (Dyall *et al.* 2004; Yoon *et al.* 2004; Gould *et al.* 2008; Archibald 2009; Parfrey *et al.* 2011), the spheroid body is much younger, with an estimated origin at about 12 Ma, according to the fossil record and molecular phylogenetic analysis (Nakayama *et al.* 2011).

Although the spheroid body has received attention as a good model to provide new insights into the early stages of organelle evolution (Kneip *et al.* 2007; Trapp *et al.* 2012; Nowack & Weber 2018), there has been no supporting information to infer what phase of organellar evolution the spheroid body represents – this could be elucidated with further information, such as the presence or absence of a targeting system for transporting and importing protein products between the symbiont and the host (Dyall *et al.* 2004; Theissen & Martin 2006; Keeling 2011), or the development of uniparental inheritance, which is commonly seen in both mitochondria and plastids (Birky 1995, 2001; Kuroiwa 2010). In this paper, we focus on the latter. Sexual reproduction in eukaryotes involves not only the fusion of gametes and cell nuclei but also the transmission of parental organelles to the next generation. The phenomenon of uniparental organellar inheritance might have already been acquired in the eukaryotic common ancestor, which showed sexual reproduction (Goodenough & Heitman 2014). The mode of inheritance of organelle DNA has been investigated in a wide range of organisms, e.g. chlorophyte and streptophyte (Miyamura 2010), brown algae (Peters *et al*. 2004; Kato *et al*. 2006), mosses (Jankowiak-Siuda *et al*. 2008), ferns (Gastony & Yatskievych 1992), fungi (Kawano *et al*. 1987; Yang & Griffiths 1993), higher plants (Mogensen 1996) and animals (Ankel-Simons & Cummins 1996; Sutovsky & Schatten 2000). Such studies have shown that non- Mendelian, uniparental inheritance of organelle DNA is the general rule, but that there are many exceptions (Xu 2005). In diatoms, the mode of inheritance has been determined in only three cases so far – two dealt with mitochondria and the other one with plastids. Gastineau *et al*. (2013) examined the mode of mitochondrial inheritance in *Haslea ostrearia* (Gaillon) Simonsen, using *cox*1 as a genetic marker, and revealed that the mitochondria are strictly transmitted uniparentally to F1 progeny. Bagmeta *et al*. (2020) also found uniparental inheritance in *Nitzschia palea* (Kützing) W. Smith, again using *cox*1. Plastid inheritance has been studied using *rbc*L as a marker. Ghiron *et al*. (2008) studied inheritance in *Pseudo-nitzschia delicatissima* (Cleve) Heiden and found that the plastids are transmitted randomly to the F1 progeny.

In this study, we aimed at revealing the mating system of *Epithemia gibba* var. *ventricosa* (Kützing) Grunow [formerly *Rhopalodia gibba* var. *ventricosa* (Kützing) H. Peragallo & Peragallo] and the mode of the inheritance of its spheroid body, to elucidate whether a selective digestion or segregation mechanism has evolved so that the body from one parent is eliminated during sexual reproduction. This could be a criterion to assess the degree of 'organellogenesis' in *Epithemia*. Using the same pair of parental strains, we also tried to reveal the inheritance of plastids and mitochondria, in order to know whether these organelles and the spheroid body from one parent are inherited or eliminated together, or whether their fates are determined independently. To do this, we successfully genotyped parental and F1 strains with respect to polymorphisms detected within the spheroid body and plastid genomes using high throughput sequencing technology. In the case of uniparental inheritance of the spheroid body, i.e. its organellogenesis is equivalent to that of established organelles, we can expect that genetic markers in the F1 generation will be derived from a single parent; in contrast, biparental inheritance will be supported if markers of both parental strains are present in the F1.

## Material and methods

### Culture

Samples were collected from Nakaikemi Wetland, Tsuruga, Fukui Prefecture, Japan (35°39.462'N, 136°05.392'E) on 12 April 2016. *Epithemia gibba* var. *ventricosa* vegetative cells were attached to bogbean *Menyanthes trifoliata* Linnaeus and isolated by capillary pipette to establish strains. All the strains were grown at 18°C under a 12:12 h (light:dark) photoperiod with cool white light *c*. 50 μmol photons $m^{-2}$ $s^{-1}$, with CSi medium (Nakayama *et al*. 2011) with extra 1.0 mM $NaNO_3$ added to the base water collected from the field (which contained 1–5 μM of nitrogen, determined with autoanalyzer TRAACS 2000, Bran & Luebbe, Norderstedt, Germany), pre-filtered and adjusted to pH 6.2 with HCl, and sterilized through a 0.2-μm pore membrane filter (Advantec Toyo, Tokyo, Japan).

### Microscopy

For light microscopy, living cells were observed with an Axio Imager A2 (Zeiss, Oberkochen, Germany) with Axiocam 506 colour digital camera (Zeiss) and differential interference contrast (DIC) optics. For confocal laser scanning microscopy, cells were placed in Lab-Tek Chambered Coverglasses (1.0 borosilicate coverglass, Thermo Fisher Scientific, Massachusetts, USA) and observed with LSM780 (Zeiss) to determine the number of plastids (due to the complex 3-dimensional shape of the plastid, it was difficult to determine the number under light microscopy or epifluorescence microscopy). SYBR Green I Nucleic Acid Gel Stain (Takara Bio, Shiga, Japan) was added to observe spheroid bodies and left 20 min at room temperature at the final concentration of 0.1 μl $l^{-1}$.

### Genome sequencing and SNP detection

Cells of the sexually compatible strains K03 and K06 were harvested from culture plates using cell scrapers (Sumitomo Bakelite, Tokyo, Japan), transferred into microtubes and centrifuged to remove supernatant. Cell pellets were homogenized using BioMasher II (Nippi, Tokyo, Japan). DNA was extracted by DNeasy Plant Mini Kit (Qiagen, Venlo, Netherlands). Each of the DNA solutions obtained was measured for concentration using Qubit 4 fluorometer and Qubit dsDNA BR Assay Kit (Thermo Fisher Scientific). Approximately 2.0 μg and 1.6 μg of DNA were obtained from K03 and K06, respectively, and used for high throughput sequencing on an Illumina HiSeq platform (paired-end, insert size 350 bp, read length 150 bp). Sequencing yielded 95.5 Gb in K03 and 45.3 Gb in K06. These read pools were preprocessed through fastp 0.14.1 (Chen *et al*. 2018) with default parameters to remove the adapters and error-prone reads. Then, we used Platanus 1.2.4 (Kajitani *et al*. 2014) with default parameters for *de novo* assembly for each strain. Similarity search was done with local blastn 2.9.0 (Zhang *et al*. 2000) to find organellar contigs, against known organellar genome sequences of *Epithemia* or those of related raphid diatoms as queries, i.e. spheroid body [AP012549, *E. turgida* (Ehrenberg) Kützing], plastid (NC_015403; *Fistulifera solaris* Mayama, M.

Matsumoto, M. Nemoto & Tsuyoshi Tanaka) and mitochondria (MF997423; *Surirella* sp.). Because contigs showing high similarities (Evalue = 0) to each reference genome were longer in the K06 assembly, we mapped the trimmed reads of both K03 and K06 strains onto the contigs using bwa 0.6.1 (Li & Durbin 2009) to visually search for a single nucleotide polymorphism (SNP) between two parental strains with Integrative Genomics Viewer 2.4.3 (Thorvaldsdóttir *et al*. 2013), and to evaluate its credibility, i.e. whether the site is covered by unambiguously mapped reads and the coverages were high. As a result, we detected SNP only for the plastid contig, and thus, we further extended the spheroid body and mitochondrial contigs with NOVOPlasty 2.2.2 (assembly type = 'mito', Dierckxsens *et al*. 2016), using the longest contig for each spheroid body and mitochondrial genome as seeds. This procedure successfully extended the contigs, from 2,995 bp to 1,073,272 bp for the spheroid body genome and from 2,364 bp to 11,080 bp for the mitochondrial genome, and SNPs were detected only from the spheroid body genome. All the SNPs were further confirmed by Sanger sequencing with the primers listed in Table S1. Three organellar contigs in fasta format are available as a Supplementary file (https://doi.org/10.1080/00318884.2021.1909399). Alignment files in BAM format, including mapped reads of both K03 and K06, are also available upon request from the corresponding author.

## Induction of sexual reproduction and establishment of F1 strains

Sexual reproduction was induced by mixing K03 and K06 in a plastic Petri dish (90-mm diameter, STAR SDish9015 ver.2, Rikaken, Nagoya, Japan). The isolation of progeny to establish the F1 strains was less straightforward, as the two initial cells were enclosed in a robust capsule of mucilage, which was visualized with Indian ink (Fig. S1A), and thus essentially inseparable by pipette. Initially, therefore, we isolated pairs of initial cells to make a number of 'progeny strains' (i.e. derived from two initial cells). These were left for about a week until two initial cells were liberated from the perizonia and divided mitotically *c*. 2 times to make the cells free from the mucilage capsule which physically hampered the isolation of a cell. Then, from the progeny strains, we further isolated a single cell to make the F1 strain, which was genuinely clonal.

## Molecular analysis for F1 strain genotyping

The F1 strains were grown in a Petri dish for about one month to form a visible pellet when cells were collected by centrifugation. The cells were homogenized with a bioMasher II and briefly spun down (*c*. 10 s with a desktop centrifuge). Supernatant was used as PCR template for amplification of genetic marker regions. Primers were designed using Primer3Plus ver. 2.4.2 (https://primer3plus.com/cgi-bin/dev/primer3plus.cgi; Untergasser *et al*. 2012) and are listed in Table S1. Each PCR was performed in a 25-µl reaction volume that contained a final concentration of 0.625 U MightyAmp DNA Polymerase, 1×MightyAmp Buffer Ver.3 ($Mg^{2+}$, dNTP plus) (Takara Bio), 0.5 µM of forward primer, 0.5 µM of reverse primer, and 2.0 µl of template. T100 Thermal Cycler (Bio Rad, California, USA) was used, with the reaction conditions as follows: an initial denaturation at 98°C for 2 min followed by 35 cycles of denaturation at 98°C for 10 s, annealing at 60°C for 15 s and extension at 68°C for 1 min. PCR products were purified using ExoSAP- IT Express (Thermo Fisher Scientific) and sequenced with the PCR primers through Eurofins Genomics

(Tokyo, Japan). Electropherograms were inspected using ATGC ver. 7 (Genetyx Corporation, Tokyo, Japan).

## Results

### Heterothallic sexual reproduction and behaviour of the spheroid body

Sexual reproduction was studied in culture using seven clones isolated from single cells. Reproduction never occurred in monoclonal cultures, only in particular mixtures of actively growing clones, and the results of preliminary mating experiments (Table S2) could be accounted for on the basis that *E. gibba* var. *ventricosa* is heterothallic, with two mating types. The longest cells capable of sexual reproduction in our experiments were 70.6 µm long, the smallest 15.7 µm. Of the seven clones, we selected two for further study and for experiments on spheroid body and plastid inheritance, based on their vigorous growth and reproduction.

Despite the differentiation into two mating types, no differences were observed between mating cells with respect to gamete morphology and behaviour: *E. gibba* var. *ventricosa* is isogamous. The vegetative cells of each strain showed motility. Details of the sexual process were examined in mating experiments using a mixture of clones K03 (valve length, average $\pm$ $s$ = 35.3 µm $\pm$ 0.3, n = 10) and K06 (45.2 µm $\pm$ 0.7, n = 10). Within a few days after making a cross, compatible cells made pairs: mating was obviously not intraclonal, judging from the size differences between paired cells (Fig. 1). Within a couple of days after pairing, two zygotes were formed by each pair of gametangia (Fig. 2). The zygotes then expanded bipolarly to form long, approximately linear auxospores orientated perpendicularly to the long axes of the parental cells (Figs 3, 4). After several days of expansion of the auxospore, an initial cell was liberated from each auxospore and returned to the vegetative phase to repeat mitotic cell divisions (Fig. 5). The valve lengths of the initial cells were 105.0–185.0 µm (n = 100). During the entire process of auxosporulation, from pairing to auxospore maturation, the cells were enclosed in a mucilage capsule (Fig. 3, arrows indicate the limit of the capsule). The presence of two spheroid bodies and one plastid per cell was confirmed in both the parental and F1 cells with light and confocal microscopy (Figs 5–7). No quantitative data were collected on spheroid body numbers but we never observed a cell with no spheroid bodies; most of them had two, and only occasionally one or more than two during the study period. We could only stain DNA in the spheroid body in dead cells in which the nucleus remained unstained or had been lost (Figs 6, S1B).

### SNP detection

Sequence comparison of organellar genomes between the parental strains K03 and K06 revealed that the genomic fragments derived from the spheroid bodies and plastids contained SNPs that could be used to determine the parental origin of each genome in the F1 strains; unfortunately, no SNP was detected in the mitochondrial genomic fragments, so that we were unable to examine its inheritance pattern. The SNPs used to discriminate the parental strains K03 and K06 were TT and AA for the spheroid bodies, and A and C for the plastids, respectively (Fig. 8).

Because our strains were not axenic, the read pools certainly contained bacterial reads. Therefore, it was possible that misassemblies took place due to high similarities between contaminating bacterial and spheroid body/plastid genomes. However, for the spheroid body marker, we found the presence of the conserved synteny at the SNPs region along with other spheroid body genomes publicly available, i.e. those of *E. turgida* (Nakayama *et al*. 2014) and *E. gibberula* (Ehrenberg) Kützing (Nakayama & Inagaki 2017), in which at least two genes were shared and arranged in the same orientations to flank both 5' and 3' directions of the SNPs site (Fig. S2). The synteny is only found in the two spheroid body genomes sequenced so far, and not in any other bacterial genomes. The blastn search of the intergenic region (between ORF2 and 3 in Fig. S2), which contained our spheroid body SNPs, resulted in no hit to any GenBank entries. For the plastid marker, NCBI nucleotide blastn search (megablast, which works best for the target percent identity of 95%, according to the instruction given under blastn suite) resulted in many hits with diatom plastid genomes. Thus, it is reasonable to assume that the target sequences were not present in other bacterial genomes, and that our genotyping was not affected by contaminant bacteria.

## Mode of inheritance of the spheroid body and plastid

Using the 39 F1 strains that were successfully established, the flanking regions of SNPs for each organelle genome were PCR amplified and Sanger sequenced to determine the strain genotype. Almost all the electropherograms exhibited single peaks at the SNP alleles, indicating that each F1 strain possessed only one genotype for each organelle (Fig. 8; the two exceptions are described below). The ratio of parental origins for the spheroid body in the F1 strains was K03:K06 = 14:15 (Table 1), and that of plastid was 12:25 (Table 1). In 10 out of 39 F1 strains, we failed to determine the genotype of the spheroid bodies because of PCR or sequencing failures.

Among the 29 F1 strains successfully genotyped for both spheroid body and plastid, joint inheritance of K03 organelles, i.e. both the spheroid bodies and the plastid derived from clone K03, was found in three F1 strains, whereas that of K06 organelles occurred in eight F1 strains. On the other hand, mixed inheritance, i.e. spheroid bodies from K03 and the plastid from K06, or vice versa, was found in 11 and 6 strains, respectively (Table 1).

A puzzling pattern was found in two F1 strains (F1#19 and #39), which showed ambiguity at the plastid SNP site with biparental signals derived from both K03 and K06 strains (i.e. the site had double peaks in the electropherogram, of both A and C) (Fig. 8), although vegetative cells only have a single plastid.

## Discussion

The discovery of heterothallism in *Epithemia gibba* var. *ventricosa* brings yet another genus in line with the view, developed during and since the seminal work of Roshchin (Roshchin 1994; Chepurnov *et al*. 2004), that pennate diatoms are fundamentally heterothallic organisms, though with many homothallic and automictic exceptions. The heterothally and isogamous sexual

reproduction of *E. gibba* var. *ventricosa*, including pairing via the ventral sides and expansion of the auxospores perpendicular to the gametangia, agree closely with *Amphora* (Mann & Poulíčková 2010), which is consistent with their phylogenetic proximity according to molecular data (Sato *et al*. 2013; Stepanek & Kociolek 2014).

The morphology and cytology of sexual reproduction in *Epithemia* (including in species formerly classified in *Rhopalodia*) were studied in some depth by Klebahn (1896) and Geitler (1932, 1977), following much earlier but very brief reports of the process by Smith (1853–1856) and others. Both Klebahn and Geitler recorded the continuity of the spheroid bodies throughout the sexual phase (though Klebahn misinterpreted them as pyrenoids) and from their observations and illustrations it would appear that none of the bodies are lost by degradation (autodigestion): the only structures they recorded (either in the text or in their illustrations) as aborting were the two superfluous nuclei from meiosis II (Klebahn 1896, figs 9, 11; Geitler 1977, fig. 1D, E) and the superfluous nucleus from each of the acytokinetic mitoses associated with the formation of the initial valves (Geitler 1977, fig. 1n). In *E. gibba*, Klebahn's observations indicate that two spheroid bodies were present in each parent cell and that these were segregated one into each gamete (see also Geitler 1977, fig. 3e). Although we did not observe the formation, rearrangement and fusion of gametes in our material *E. gibba* var. *ventricosa*, it is reasonable to reject the possibility that the two zygotes were formed via self- fertilization of each parental cell – if this had been the case, each auxospore should have been encased within an individual mucilage capsule; however, we observed two sibling auxospores in a single capsule (Fig. S1A). Each zygote consequently had two bodies, one inherited from each compatible gamete: no division nor fusion of spheroid body was mentioned throughout the entire process of sexual reproduction Klebahn observed. However, in our F1 strains of *E. gibba* var. *ventricosa*, all the electropherograms of the spheroid body marker regions showed unambiguous single peaks at the two polymorphic sites, as seen in the parental strains, and that each F1 strain had the genotype of one parental strain, either K03 or K06. This result shows that both mating types can potentially transmit the spheroid body to the F1, but that inheritance is nevertheless strictly uniparental in this taxon. How this is achieved is unclear. Given that each zygote receives at least one spheroid body from each parent, it should contain one K03 and one K06 body and it might be expected that at least some of the F1 strains would retain this heteroplasmy. Hence, the absence of any heteroplasmic strains among the 29 F1 strains we genotyped and the 1:1 ratio of K03 and K06 in the strains suggests that either (1) the two gametic bodies segregate at the first division of the initial cell, or (2) one spheroid body is digested at random in the zygote sometime during the later development of the auxospore, before the first division of the initial cell (although neither Klebahn, nor Geitler nor ourselves observed any degenerating spheroid bodies) or (3) sorting (either random or directed) occurs during the first few vegetative divisions after auxosporulation, i.e. heteroplasmy may be eliminated stochastically (as in the plastid gene inheritance model of VanWinkel-Swift 1980; also Greiner *et al*. 2014). We cannot rule out the last- mentioned hypothesis since we were unable to genotype the initial cells themselves (see Material and Methods: we explain that isolating individual initial cells was impractical because of the mechanical strength of the mucilage capsule holding the auxospores, see Fig. S1A). Whatever the means by which heteroplasmy is avoided, the inheritance of the spheroid body is clearly not from only one of the mating types of *E. gibba* var. *ventricosa*, unlike the inheritance of plastids or mitochondria in a number of other heterothallic eukaryotes (reviewed by Xu 2005), and indeed, there is no bias as to which parental spheroid body is selected.

DeYoe *et al*. (1992) reported that the number of spheroid bodies per vegetative cell varied in *Epithemia*, depending on the availability of nitrogen; however, in our parental and F1 strains, cells predominantly contained two spheroid bodies per cell in the presence of dissolved nitrogen in our modified CSi medium, indicating tight control of spheroid body division and segregation. Other *Epithemia* species have different numbers of spheroid bodies per cell and, in at least some, the number varies during the life cycle. For example, *E. porcellus* Kützing cells generally have 4–8 bodies per cell, depending on the cell size and stage in the cell cycle, but up to 16 in initial cells and as few as 2 in the smallest cells [(Geitler 1977), as *E. zebra* var. *porcellus* (Kützing) Grunow]; *E. turgida* also contains up to 16 spheroid bodies per cell. In such taxa, it could be easier than in our species to check the mechanisms by which heteroplasmy is avoided, since stochastic loss of one parental genotype would be slower with a larger number of spheroid bodies, allowing its detection if present.

In this study, as in previous studies of Epithemiaceae (e.g. Klebahn 1896; Geitler 1932, 1977), we observed only one plastid in vegetative cells of *E. gibba* var. *ventricosa*, both in the parental and F1 strains, under light and confocal microscopy. During gametogenesis, the plastids divided and segregated, so that when the cell divided at the end of meiosis I, each gamete received one plastid, as in the related genus *Amphora* (Mann 1994; Mann & Poulíčková 2010). Not surprisingly, therefore, there were two plastids in expanding auxospores and initial cells, representing the plastids inherited from the gametes. Later, as in *Amphora* and other diatoms with one plastid per cell in normal vegetative cells, the initial cell appeared to partition the two parental plastids between the daughter cells when it divided. Given all this, it was unexpected to discover two F1 strains possessing a double peak (A/C) for the plastid marker, indicating inheritance from both parental strains. We do not know how this happened. Possibly F1 strains #19 and #39 anomalously harboured an extra plastid from one parent, so that when the initial cell divided, one daughter established a lineage containing plastids from both parents. Unfortunately, we were unaware of the heteroplasmy in #19 and #39 until afterwards, when checks with confocal microscopy were no longer possible. However, close examination of the upper auxospore in Fig. 4 suggests that this may have contained three plastids, since at the left there is a plastid fragment that appears to be separate from two larger plastids to the right. Alternatively, heteroplasmy may arise by fusion of plastids to create a single organelle with genomes from both parents to create chimaeric plastids, as in *Chlamydomonas* (e.g. VanWinkel-Swift 1980). Occasional breakdown of uniparental transmission has been suggested to be advantageous for avoiding the build-up of deleterious mutations in a lineage (through Müller's ratchet: Greiner *et al*. 2014) and even in higher plants, biparental plastid inheritance has occasionally been detected in genera such as *Passiflora* (Hansen *et al*. 2007), *Zantedeschia* (Snijder *et al*. 2007) and *Medicago* (Matsushima *et al*. 2008).

Because of the relatively recent establishment of the spheroid body endosymbiosis within Epithemiaceae (Nakayama *et al*. 2011), better understanding of the nature of the spheroid body could be a key to understanding the early development of endosymbionts into organelles. Fully established organelles, such as plastids and mitochondria, divide at the same pace as the host cell and are segregated accurately into new cells, so that the organelle is a permanent resident and further acquisition of new endosymbionts is unnecessary (Rodríguez- Ezpeleta & Philippe 2006). The diatom-diazotroph associations *Hemiaulus–Richelia* and *Rhizosolenia–Richelia* are apparently functionally equivalent to the endosymbiotic relationship of the spheroid body and *Epithemia*, in

the sense that atmospheric N is fixed and supplied to the host (Foster *et al*. 2011). The existence of these associations suggests that the nitrogen-mediated interaction between bacteria and diatoms confers ecological advantages, particularly under nitrogen depleted conditions. Nevertheless, the striking difference between these endosymbionts and the spheroid body is that the diatom–diazotroph associations are facultative: the endosymbionts are transmitted to daughter cells through vegetative division but only for a few generations, and they are occasionally absent from the hosts (Rai *et al*. 2000).

Organelles typically show smaller genome sizes than free living relatives, as a result of losing genes via transfer to the host nucleus or by being lost entirely from the organism (Timmis *et al*. 2004; Rodríguez-Ezpeleta & Philippe 2006; Archibald 2009). The reduced gene complement means that the organelle has limited functionality and is dependent on the host nucleus, and thus, unable to survive outside the host cell anymore. Furthermore, what is also striking for characterizing organelles is uniparental inheritance, which is a mechanism interpreted to be a system controlled by the host nuclear genome for maintaining homoplasmy of cytoplasmic DNA and inhibiting the evolution of the organelles via recombination (e.g. Birky 2008; Kuroiwa 2010). Synchronized division and genome size reduction have already been reported in the spheroid body (Geitler 1977; Nakayama *et al*. 2014; Nakayama & Inagaki 2017), and in the 'cyanelle' of *Paulinella chromatophora* Lauterborn, which is a primary plastid analogous to the plastids of Archaeplastida (Marin *et al*. 2005; Rodríguez-Ezpeleta & Philippe 2006). Genome size reduction is also known in the *Candidatus* taxon *Atelocyanobacterium thalassa* (UCYN-A), a nitrogen-fixing cyanobacterium suggested to have established a symbiotic relationship relatively recently with haptophytes (Thompson *et al*. 2012), although no information is available on whether the mode of its division is synchronized with host cell division or not. To our knowledge, however, no attempt has been made to reveal the mode of inheritance of these 'young' organelles during the sexual phase. Our data indicate that the spheroid body in *Epithemia gibba* var. *ventricosa* is uniparentally inherited, even though there is no link with mating type. Along with the other characteristics of the spheroid body as mentioned above, we would suggest it is at a rather late stage in organellogenesis, despite its young evolutionary age compared to plastids and mitochondria.

We detected F1 strains bearing two organelles with different parental origins, that is, spheroid bodies from strain K03 and plastids from K06, or vice versa. Although this type of heterogenic origin of plastids and mitochondria has been reported from higher plants, e.g. in bananas (Fauré *et al*. 1994) and kiwi plants (Testolin & Cipriani 1997), this is the first report to show that diatoms can also show such patterns of inheritance of organelles/endosymbionts. We do not know how common these are, since there are still very few studies of organelle inheritance in diatoms, namely of mitochondria by Gastineau *et al*. (2013) and Bagmeta *et al*. (2020), and plastids by Ghiron *et al*. (2008), all of which dealt with a single organellar inheritance. Further investigation is needed with *Epithemia* to know how the mitochondria are inherited. Unfortunately, no information on the pattern of the mitochondrial inheritance was obtained in our study, due to the lack of SNPs in our genomic fragments in the parental strains.

It should be added that the results presented here were based on a single pair of the parental strains, K03 and K06, since the marker regions showed no SNPs in other parental strains. One could, of course, argue that the inheritance pattern of the organelles observed in this study is just one of several diverse modes of inheritance, as in the slime mould *Physarum polycephalum*

Schwein (Moriyama & Kawano 2003). Our current results need to be interpreted carefully because of the sample size. However, it is worth noting that no single strain exhibited biparental inheritance of the spheroid body among the F1 strains established in this study. This implies that the host diatom has already developed a system that ensures uniparental inheritance of this newly established organelle.

## Acknowledgements

The authors thank the members of NPO Nakaikemi Net for their permission and help to collect samples. We also thank Dr. Takuro Nakayama in Tohoku University, Japan, for sharing the draft genome of *Epithemia* which was used in the search for mitochondrial genomic fragments in our preliminary dataset. NGS data analysis were performed on the NIG supercomputer at ROIS National Institute of Genetics.

## References

Ankel-Simons F. & Cummins J.M. 1996. Misconceptions about mitochondria and mammalian fertilization: implications for theories on human evolution. *Proceedings of the National Academy of Sciences of USA* 93: 13859–13863. DOI: 10.1073/pnas.93.24.13859.

Archibald J.M. 2009. The puzzle of plastid evolution. *Current Biology* 19: R81–R88. DOI: 10.1016/j.cub.2008.11.067.

Bagmet V.B., Abdullin S.R., Mazina S.E., Nikulin A.Y., Nikulin V.Y. & Gontcharov A.A. 2020. Life cycle of *Nitzschia palea* (Kützing) W. Smith (Bacillariophyta). *Russian Journal of Developmental Biology* 51: 106–114. DOI: 10.1134/ S1062360420020022.

Birky C.W. Jr. 1995. Uniparental inheritance of mitochondrial and chloroplast genes: mechanisms and evolution. *Proceedings of the National Academy of Sciences of USA* 92: 11331–11338. DOI: 10.1073/pnas.92.25.11331.

Birky C.W. Jr. 2001. The inheritance of genes in mitochondria and chloroplasts: laws, mechanisms, and models. *Annual Review of Genetics* 35: 125–148. DOI: 10.1146/annurev.genet.35.102401.090231.

Birky C.W. Jr. 2008. Uniparental inheritance of organelle genes. *Current Biology* 18: R692–R695. DOI: 10.1016/j.cub.2008.06.049.

Chen S., Zhou Y., Chen Y. & Gu J. 2018. Fastp: an ultra-fast all-in-one FASTQ preprocessor. *Bioinformatics* 34: i884–i890. DOI: 10.1093/bioinformatics/ bty560.

Chepurnov V.A., Mann D.G., Sabbe K. & Vyverman W. 2004. Experimental studies on sexual reproduction in diatoms. *International Review of Cytology* 237: 91–154. DOI: 10.1016/S0074-7696(04)37003-8.

DeYoe H.R., Lowe R.L. & Marks J.C. 1992. Effects of nitrogen and phosphorus on the endosymbiont load of *Rhopalodia gibba* and *Epithemia turgida* (Bacillariophyceae). *Journal of Phycology* 28: 773–777. DOI: 10.1111/j.0022-3646.1992.00773.x.

Dierckxsens N., Mardulyn P. & Smits G. 2016. NOVOPlasty: de novo assembly of organelle genomes from whole genome data. *Nucleic Acids Research* 45: Article e18. DOI: 10.1093/nar/gkw955.

Drum R.W. & Pankratz S. 1965. Fine structure of an unusual cytoplasmic inclusion in the diatom genus, *Rhopalodia*. *Protoplasma* 60: 141–149. DOI: 10.1007/ BF01248136.

Dyall S.D., Brown M.T. & Johnson P.J. 2004. Ancient invasions: from endosymbionts to organelles. *Science* 304: 253–257. DOI: 10.1126/science. 1094884.

Fauré S., Noyer J.L., Carreel F., Horry J.P., Bakry F. & Lanaud C. 1994. Maternal inheritance of chloroplast genome and paternal inheritance of mitochondrial genome in bananas (*Musa acuminata*). *Current Genetics* 25: 265–269. DOI: 10.1007/BF00357172.

Foster R.A., Kuypers M.M., Vagner T., Paerl R.W., Musat N. & Zehr J.P. 2011. Nitrogen fixation and transfer in open ocean diatom–cyanobacterial symbioses. *ISME Journal* 5: 1484–1493. DOI: 10.1038/ismej.2011.26.

Gastineau R., Leignel V., Jacquette B., Hardivillier Y., Wulff A., Gaudin P., Bendahmane D., Davidovich N.A., Kaczmarska I. & Mouget J.L. 2013. Inheritance of mitochondrial DNA in the pennate diatom *Haslea ostrearia* (Naviculaceae) during auxosporulation suggests a uniparental transmission. *Protist* 164: 340–351. DOI: 10.1016/j. protis.2013.01.001.

Gastony G.J. & Yatskievych G. 1992. Maternal inheritance of the chloroplast and mitochondrial genomes in cheilanthoid ferns. *American Journal of Botany* 79: 716–722. DOI: 10.2307/2444887.

Geitler L. 1932. Der Formwechsel der pennaten Diatomeen. *Archiv für Protistenkunde* 78: 1–226.

Geitler L. 1977. Zur Entwicklungsgeschichte der Epithemiaceen *Epithemia, Rhopalodia* und *Denticula* (Diatomophyceae) und ihre vermutlich symbiotischen Sphäroidkörper. *Plant Systematics and Evolution* 128: 259–275. DOI: 10.1007/BF00984562.

Ghiron J.H.L., Amato A., Montresor M. & Kooistra W.H. 2008. Plastid inheritance in the planktonic raphid pennate diatom *Pseudo-nitzschia delicatissima* (Bacillariophyceae). *Protist* 159: 91–98. DOI: 10.1016/j. protis.2007.06.002.

Goodenough U. & Heitman J. 2014. Origins of eukaryotic sexual reproduction. *Cold Spring Harbor Perspectives in Biology* 6: a016154. DOI: 10.1101/cshperspect.a016154.

Gould S.B., Waller R.F. & McFadden G.I. 2008. Plastid evolution. *Annual Review of Plant Biology* 59: 491–517. DOI: 10.1146/annurev. arplant.59.032607. 092915.

Greiner S., Sobanski J. & Bock R. 2014. Why are most organelle genomes transmitted maternally? *Bioessays* 37: 80–94. DOI: 10.1002/bies.201400110.

Hansen A.K., Escobar L.K., Gilbert L.E. & Jansen R.K. 2007. Paternal, maternal, and biparental inheritance of the chloroplast genome in *Passiflora* (Passifloraceae): implications for phylogenetic studies. *American Journal of Botany* 94: 42–46. DOI: 10.3732/ajb.94.1.42.

Jankowiak-Siuda K., Pacak A., Odrzykoski I., Wyatt R. & Szweykowska- Kulińska Z. 2008. Organellar inheritance in the allopolyploid moss *Plagiomnium curvatulum*. *Taxon* 57: 145–152. DOI: 10.2307/25065956.

Kajitani R., Toshimoto K., Noguchi H., Toyoda A., Ogura Y., Okuno M., Yabana M., Harada M., Nagayasu E., Maruyama H. *et al.* 2014. Efficient de novo assembly of highly heterozygous genomes from whole-genome shotgun short reads. *Genome Research* 24: 1384–1395. DOI: 10.1101/gr.170720.113.

Kato Y., Kogame K., Nagasato C. & Motomura T. 2006. Inheritance of mitochondrial and chloroplast genomes in the isogamous brown alga *Scytosiphon lomentaria* (Phaeophyceae). *Phycological Research* 54: 65–71. DOI: 10.1111/j.1440-1835.2006.00409.x.

Kawano S., Anderson R.W., Nanba T. & Kuroiwa T. 1987. Polymorphism and uniparental inheritance of mitochondrial DNA in *Physarum polycephalum*. *Journal of General Microbiology* 133: 3175–3182. DOI: 10.1099/00221287-133-11-3175.

Keeling P.J. 2011. Endosymbiosis: bacteria sharing the load. *Current Biology* 21: R623–R624. DOI: 10.1016/j.cub.2011.06.061.

Klebahn H. 1896. Beiträge zur Kenntniss der Auxosporenbildung I. *Rhopalodia gibba* (Ehrenb.) O. Müller. *Jahrbücher für Wissenschaftliche Botanik* 29: 595–654.

Kneip C., Lockhart P., Voß C. & Maier U.G. 2007. Nitrogen fixation in eukaryotes – new models for symbiosis. *BMC Evolutionary Biology* 7: Article 55. DOI: 10.1186/1471-2148-7-55.

Kuroiwa T. 2010. Review of cytological studies on cellular and molecular mechanisms of uniparental (maternal or paternal) inheritance of plastid and mitochondrial genomes induced by active digestion of organelle nuclei (nucleoids). *Journal of Plant Research* 123: 207–230. DOI: 10.1007/s10265-009-0306-9.

Li H. & Durbin R. 2009. Fast and accurate short read alignment with burrows-wheeler transform. *Bioinformatics* 25: 1754–1760. DOI: 10.1093/bioinformatics/btp324.

Mann D.G. 1994. The systematics of amphoroid diatoms: the life history of *Amphora arcus*. *Nova Hedwigia* 58: 335–352.

Mann D.G. 1999. The species concept in diatoms. *Phycologia* 38: 437–495. DOI: 10.2216/i0031-8884-38-6-437.1.

Mann D.G. & Poulíčková A. 2010. Mating system, auxosporulation, species taxonomy and evidence for homoploid evolution in *Amphora* (Bacillariophyta). *Phycologia* 49: 183–201. DOI: 10.2216/PH09-08.1.

Marin B., Nowack E.C. & Melkonian M. 2005. A plastid in the making: evidence for a second primary endosymbiosis. *Protist* 156: 425–432. DOI: 10.1016/j.protis.2005.09.001.

Matsushima R., Hu Y., Toyoda K. & Sakamoto W. 2008. The model plant *Medicago truncatula* exhibits biparental plastid inheritance. *Plant & Cell Physiology* 49: 81–91. DOI: 10.1093/pcp/pcm170.

Miyamura S. 2010. Cytoplasmic inheritance in green algae: patterns, mechanisms and relation to sex type. *Journal of Plant Research* 123: 171–184. DOI: 10.1007/s10265-010-0309-6.

Mogensen H.L. 1996. The hows and whys of cytoplasmic inheritance in seed plants. *American Journal of Botany* 83: 383–404. DOI: 10.2307/2446172.

Moriyama Y. & Kawano S. 2003. Rapid, selective digestion of mitochondrial DNA in accordance with the matA hierarchy of multiallelic mating types in the mitochondrial inheritance of *Physarum polycephalum*. *Genetics* 164: 963–975. DOI: 10.1093/genetics/164.3.963.

Nakayama T. & Inagaki Y. 2017. Genomic divergence within non-photosynthetic cyanobacterial endosymbionts in rhopalodiacean diatoms. *Scientific Reports* 7: 1–8. DOI: 10.1038/s41598-017-13578-8.

Nakayama T., Ikegami Y., Nakayama T., Ishida K., Inagaki Y. & Inouye I. 2011. Spheroid bodies in rhopalodiacean diatoms were derived from a single endosymbiotic cyanobacterium. *Journal of Plant Research* 124: 93–97. DOI: 10.1007/s10265-010-0355-0.

Nakayama T., Kamikawa R., Tanifuji G., Kashiyama Y., Ohkouchi N., Archibald J.M. & Inagaki Y. 2014. Complete genome of a nonphotosynthetic cyanobacterium in a diatom reveals recent adaptations to an intracellular lifestyle. *Proceedings of the National Academy of Sciences of USA* 111: 11407–11412. DOI: 10.1073/pnas.1405222111.

Nelson D.M., Tréguer P., Brzezinski M.A., Leynaert A. & Quéguiner B. 1995. Production and dissolution of biogenic silica in the ocean: revised global estimates, comparison with regional data and relationship to biogenic sedimentation. *Global Biogeochemical Cycles* 9: 359–372. DOI: 10.1029/ 95GB01070.

Nowack E.C. & Weber A.P. 2018. Genomics-informed insights into endosymbiotic organelle evolution in photosynthetic eukaryotes. *Annual Review of Plant Biology* 69: 51–84. DOI: 10.1146/annurev-arplant-042817-040209.

Parfrey L.W., Lahr D.J., Knoll A.H. & Katz L.A. 2011. Estimating the timing of early eukaryotic diversification with multigene molecular clocks. *Proceedings of the National Academy of Sciences of USA* 108: 13624–13629. DOI: 10.1073/pnas.1110633108.

Peters A.F., Scornet D., Müller D.G., Kloareg B. & Cock J.M. 2004. Inheritance of organelles in artificial hybrids of the isogamous multicellular chromist alga *Ectocarpus siliculosus* (Phaeophyceae). *European Journal of Phycology* 39: 235–242. DOI: 10.1080/09670260410001683241.

Prechtl J., Kneip C., Lockhart P., Wenderoth K. & Maier U.G. 2004. Intracellular spheroid bodies of *Rhopalodia gibba* have nitrogen-fixing apparatus of cyanobacterial origin. *Molecular Biology and Evolution* 21: 1477–1481. DOI: 10.1093/molbev/msh086.

Rai A.N., Söderbäck E. & Bergman B. 2000. Cyanobacterium-plant symbioses. *New Phytologist* 147: 449–481. DOI: 10.1046/j.1469-8137.2000.00720.x.

Rodríguez-Ezpeleta N. & Philippe H. 2006. Plastid origin: replaying the tape. *Current Biology* 16: R53–R56. DOI: 10.1016/j.cub.2006.01.006.

Roshchin A.M. 1994. *Zhiznennye Tsikly Diatomovykh Vodoroslej*. Naukova Dumka, Kiev. 170 pp.

Round F.E., Crawford R.M. & Mann D.G. 1990. *The diatoms. Morphology and biology of the genera*. Cambridge University Press, Cambridge, UK. 747 pp.

Sato S., Tamotsu N. & Mann D.G. 2013. Morphology and life history of *Amphora commutata* (Bacillariophyta) I: the vegetative cell and phylogenetic position. *Phycologia* 52: 225–238. DOI: 10.2216/12-072.1.

Smith W. 1853–1856. *Synopsis of British Diatomaceae*, vol. 2. John Van Voorst, London, UK. 107 pp.

Snijder R.C., Brown F.S. & Van Tuyl J.M. 2007. The role of plastome-genome incompatibility and biparental plastid inheritance in interspecific hybridization in the genus *Zantedeschia* (Araceae). *Floriculture and Ornamental Biotechnology* 1: 150–157.

Stepanek J.G. & Kociolek J.P. 2014. Molecular phylogeny of *Amphora* sensu lato (Bacillariophyta): an investigation into the monophyly and classification of the amphoroid diatoms. *Protist* 165: 177–195. DOI: 10.1016/j.protis.2014.02. 002.

Sutovsky P. & Schatten G. 2000. Paternal contributions to the mammalian zygote: fertilization after sperm-egg fusion. *International Review of Cytology* 195: 1–65. DOI: 10.1016/S0074-7696(08)62703-5.

Testolin R. & Cipriani G. 1997. Paternal inheritance of chloroplast DNA and maternal inheritance of mitochondrial DNA in the genus *Actinidia*. *Theoretical and Applied Genetics* 94: 897–903. DOI: 10.1007/s001220050493.

Theissen U. & Martin W. 2006. The difference between organelles and endosymbionts. *Current Biology* 16: R1016–R1017. DOI: 10.1016/j. cub.2006.11. 020.

Thompson A.W., Foster R.A., Krupke A., Carter B.J., Musat N., Vaulot D., Kuypers M.M.M. & Zehr J.P. 2012. Unicellular cyanobacterium symbiotic with a single-celled eukaryotic alga. *Science* 337: 1546–1550. DOI: 10.1126/science.1222 700.

Thorvaldsdóttir H., Robinson J.T. & Mesirov J.P. 2013. Integrative Genomics Viewer (IGV): high-performance genomics data visualization and exploration. *Briefings in Bioinformatics* 14: 178–192. DOI: 10.1093/bib/bbs017.

Timmis J.N., Ayliffe M.A., Huang C.Y. & Martin W. 2004. Endosymbiotic gene transfer: organelle genomes forge eukaryotic chromosomes. *Nature Reviews Genetics* 5: 123–135. DOI: 10.1038/nrg1271.

Trapp E.M., Adler S., Zau-ner S. & Maier U.G. 2012. *Rhopalodia gibba* and its endosymbionts as a model for early steps in a cyanobacterial primary endosymbiosis. *Endocytobiosis and Cell Research* 23: 21–24.

Untergasser A., Cutcutache I., Koressaar T., Ye J., Faircloth B.C., Remm M. & Rozen S.G. 2012. Primer3 – new capabilities and interfaces. *Nucleic Acids Research* 40: Article e115. DOI: 10.1093/nar/gks596.

VanWinkel-Swift K. 1980. A model for the rapid vegetative segregation of multiple chloroplast genomes in *Chlamydomonas*: assumptions and predictions of the model. *Current Genetics* 1: 113–125. DOI: 10.1007/BF00446957.

Xu J. 2005. The inheritance of organelle genes and genomes: patterns and mechanisms. *Genome* 48: 951–958. DOI: 10.1139/g05-082.

Yang X. & Griffiths A.J.F. 1993. Male transmission of linear plasmids and mitochondrial DNA in the fungus *Neurospora*. *Genetics* 134: 1055–1062.

Yoon H.S., Hackett J.D., Ciniglia C., Pinto G. & Bhattacharya D. 2004. A molecular timeline for the origin of photosynthetic eukaryotes. *Molecular Biology and Evolution* 21: 809–818. DOI: 10.1093/molbev/msh075.

Zhang Z., Schwartz S., Wagner L. & Miller W. 2000. A greedy algorithm for aligning DNA sequences. *Journal of Computational Biology* 7: 203–214. DOI: 10.1089/ 10665270050081478.

**Table 1.** Parental origin of spheroid body and plastid in all 39 F1 strains. '–' denotes sequencing failure.

| F1 strain # | Spheroid body | Plastid |
|---|---|---|
| 1 | K06 | K06 |
| 2 | K06 | K03 |
| 3 | K06 | K06 |
| 4 | K06 | K03 |
| 5 | K03 | K06 |
| 6 | K03 | K06 |
| 7 | K03 | K06 |
| 8 | – | K03 |
| 9 | K06 | K06 |
| 10 | K03 | K06 |
| 11 | K03 | K03 |
| 12 | K03 | K06 |
| 13 | K06 | K06 |
| 14 | K03 | K03 |
| 15 | K06 | K03 |
| 16 | K03 | K06 |
| 17 | K06 | K03 |
| 18 | K03 | K06 |
| 19 | K06 | K03 and K06 |
| 20 | K06 | K06 |
| 21 | – | K06 |
| 22 | – | K03 |
| 23 | K03 | K03 |
| 24 | K03 | K06 |
| 25 | K06 | K03 |
| 26 | – | K03 |
| 27 | K03 | K06 |
| 28 | K06 | K06 |
| 29 | K06 | K03 |
| 30 | K06 | K06 |
| 31 | – | K06 |
| 32 | – | K06 |
| 33 | – | K06 |
| 34 | – | K06 |
| 35 | – | K06 |
| 36 | K06 | K06 |
| 37 | K03 | K06 |
| 38 | K03 | K06 |
| 39 | – | K03 and K06 |
| Numbers of F1 strains with spheroid bodies and plastid(s) inherited from | | |
| K03 | 14 | 12 |
| K03 and K06 | 0 | 2 |
| K06 | 15 | 25 |
| Total | 29 | 39 |


**Figs 1–5.** Sexual reproduction and auxosporulation of *Epithemia gibba* var. *ventricosa*. Scale bars=10 μm. Figs 1–4 at the same scale. **Fig. 1**. Sexually compatible cells approach by their ventral sides to form a pair. Note that cell sizes are markedly different, ruling out clonal pairing. **Fig. 2**. Rearranging zygotes after gamete fusion. Two zygotes formed per pair. **Fig. 3**. Zygotes expand perpendicularly along long axis of parental cells. Arrows indicate the limit of mucilage capsule. **Fig. 4**. Two auxospores formed per pair. Arrowheads indicate spheroid bodies (same for Fig. 5). **Fig. 5**. Cell in F1 strain.

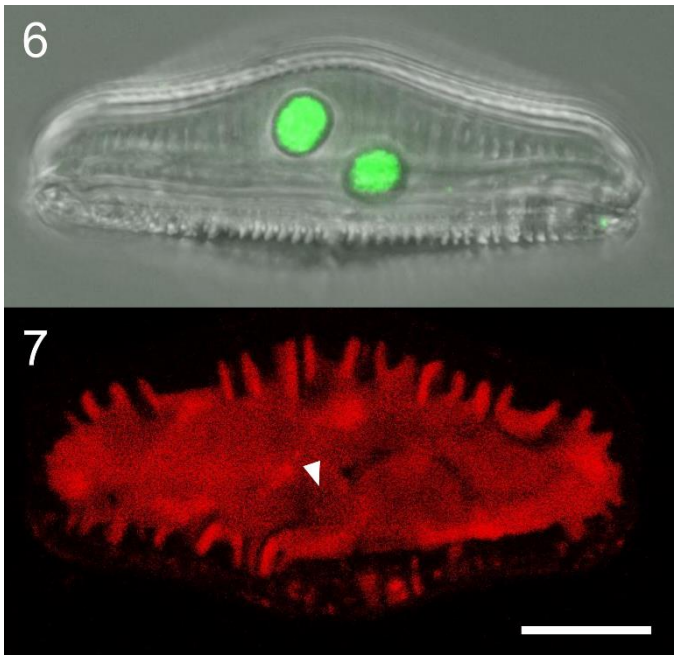


**Figs 6, 7.** Spheroid bodies and plastid, confocal laser scanning microscopy. Scale bar=10 μm. **Fig. 6**. Two spheroid bodies stained with SYBR Green. Fluorescent image merged with bright field image. **Fig. 7**. Autofluorescence of a single plastid. The plastid has two lobes, connected by a narrow bridge indicated by the arrowhead. Note that the spheroid bodies are stained in the dead cell, whereas the complex plastid shape is illustrated in the healthy cell.

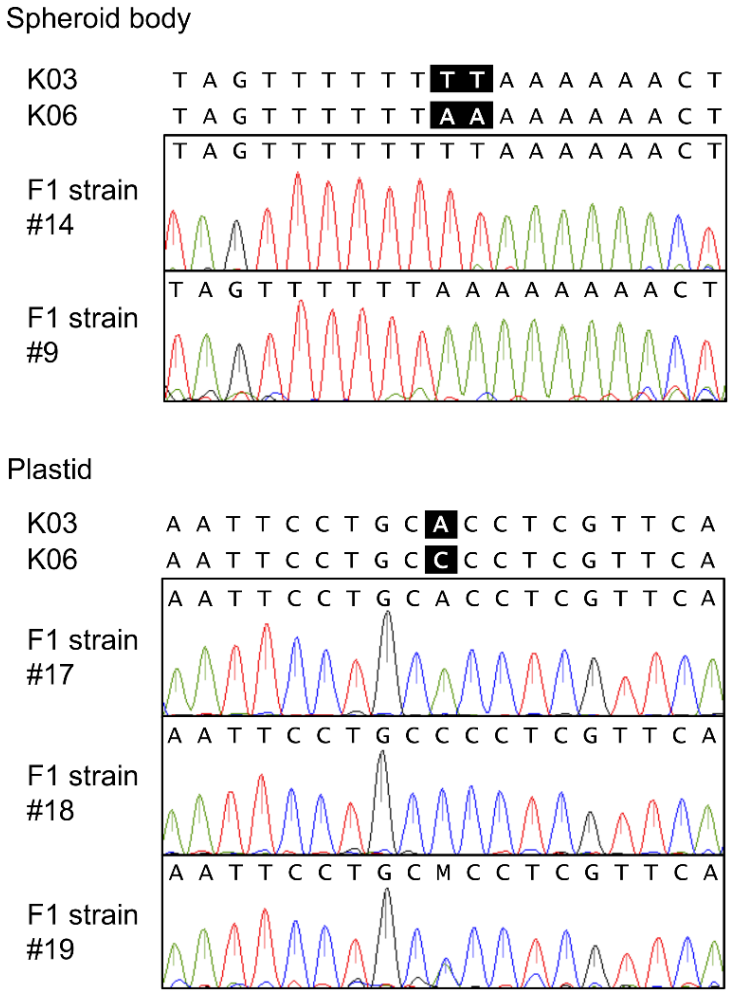


**Fig. 8.** Examples of electropherograms from amplified DNA marker regions in spheroid body and plastid of F1 strains generated by K03×K06.

**Table S1.** Primers used to amplify and sequence marker regions.

| Primer name | Sequence (5' – 3') | Target | Product length |
|---|---|---|---|
| SB_04_F | TCGTCAACAATTAGACCAGATCA | Spheroid body SNPs region | 513 bp |
| SB_04_R | CTGTGGTCAACAGGGGTAGC | | |
| CP_03_F | TTGCTAAATCAGCACCAGAGAA | Plastid SNP region | 443 bp |
| CP_03_R | GTTGCAGGTTCCGAATTTGT | | |

**Table S2.** Results of mating experiments using 7 parental strains. Plus and minus signs indicate whether sexual reproduction occurred or not, respectively.

| Parental strains | K01 | K03 | K04 | K05 | K06 | K07 | K08 |
|---|---|---|---|---|---|---|---|
| K01 | - | | | | | | |
| K03 | - | - | | | | | |
| K04 | + | + | - | | | | |
| K05 | + | + | - | - | | | |
| K06 | + | + | - | - | - | | |
| K07 | - | - | + | + | + | - | |
| K08 | - | - | + | + | + | - | - |

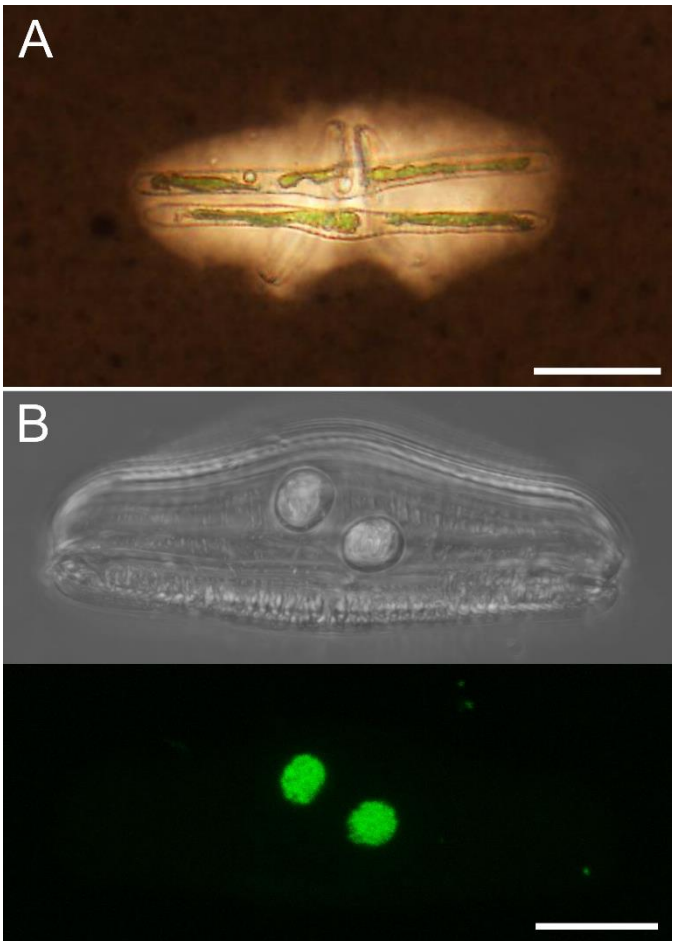


**Fig. S1**. *Epithemia gibba* var. *ventricosa*, light microscopy. **(A)** Thick mucilage capsule encasing two sibling auxospores. Mucilage is visualized by Indian ink. Scale bar=50 μm. **(B)** Confocal laser scanning microscopy; bright field (upper) and fluorescence (lower) showing spheroid bodies stained with SYBR Green. The merged image is shown in Fig. 6. Scale bar=10 μm.

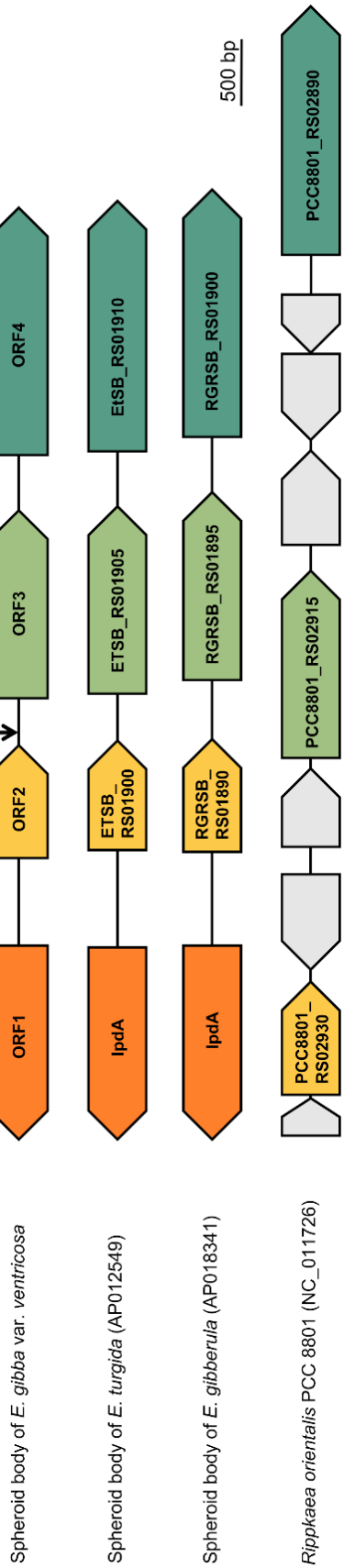


**Fig. S2.** Schematic diagram of the genome architecture around SNPs found in spheroid body genome. The SNPs found between the strains K03 and K06 in *E. gibba* var. *ventricosa* are located between the ORF2 and 3 (arrow). The gene order flanking the SNPs is same among all spheroid body genomes, whereas the order is not conserved in *Rippkaea orientalis*, a close relative of the spheroid body in free living cyanobacteria (Prechtl *et al.* 2004). ORFs with high sequence similarity (Evalue < $2E^{-170}$ with NCBI blastn search) are shown in the same colour.

CHAPTER 2

# Distinct life cycles of two sympatric *Epithemia* (Bacillariophyta) taxa in Nakaikemi Wetland, Japan

Kamakura S, Ohtsuka T, Nagumo T, Sato S.

## Abstract

The life cycle of diatoms is associated with their cell size, and characterized by a gradual decrease in size in the vegetative stage and a recovery in size through sexual reproduction. Sexual reproduction is trigged when cells become smaller than a species-specific size threshold and receive species-specific environmental cues. Few studies involving both field observation and laboratory culture have documented the life cycles and frequency of sexual reproduction in diatoms. In this study, we investigated cell size in two congeneric taxa, *Epithemia gibba* var. *ventricosa* and *Epithemia* sp. collected monthly for almost 3 years from a pond in Nakaikemi Wetland. Cultures of both taxa were established to examine rates of cell size reduction, which affects the duration of the vegetative stage. We report congeneric taxa sharing a common habitat and substratum to exhibit distinct sexual and asexual strategies.

## Introduction

Diatoms are unicellular algae with silicified cell walls. They are ubiquitous and play significant roles in the global carbon cycle as primary producers in ecosystems (Nelson et al. 1995, Mann 1999). The diatom cell wall, the frustule, resembles a pill box in that it comprises two partly overlapping halves—one being slightly smaller than the other. Bands of silica (girdle bands) enclose the cell in the mid-section of the frustule. After vegetative cell division, two daughter cells each inherit a half of the mother frustule, and a new smaller half is formed within the mother cell. Because of this, a general rule for diatoms is that repeated vegetative cell division results in a gradual decrease in the average cell size of a growing population (MacDonald–Pfitzer rule; MacDonald 1869; Pfitzer 1869, 1871). When cell size decreases to a certain size threshold, many diatoms become sexually active and reproduce sexually (Round et al. 1990). Sexual reproduction results in formation of an enlarged zygote (the auxospore), in which a new vegetative cell (an initial cell) having the largest cell size in the life cycle is formed, thereby restoring cell size (Round et al. 1990, Edlund & Stoermer 1997).

Sexual reproduction and size recovery are relatively short processes that last for a few days only (Chepurnov et al. 2004, Mann 2011) when compared to the vegetative phase which can persist for months to years. Because of the limited timeframe during which sexual events occur for diatoms, it is rare to encounter cells undergoing sexual reproduction or auxosporulation within field-collected samples. Additionally, these sexual cells (gametes, zygotes, auxospores) are fragile and disintegrate with acid cleaning, rendering their detection difficult (Edlund & Stoermer 1997). However, by monitoring vegetative cell size (valve length) within a population, the incidence of a sexual event can be identified using field-collected material. If size peaks occur (indicative of sexual

reproduction), an estimate of the timing/seasonality of sexual reproduction and degree/speed of cell size reduction can be made (e.g., Bellinger 1977, Round 1982, Mann 1988a, D'Alelio et al. 2009, Nishikawa et al. 2013, Jewson et al. 2010, Jewson & Bixby 2016).

Experimental culture is an effective way to study diatom life cycles (Mann & Chepurnov 2004) because cell division and size reduction in a population derived from a single cell can be monitored. For sexually reproducing species, these experiments also enable sexual reproduction to be induced, allowing for critical information regarding their life cycle (e.g., maximum and minimum cell sizes) to be obtained. Apart from the canonical life cycle of diatoms as above, variations include avoidance of size reduction (e.g.: von Stosch 1965, Round 1972, Rose & Cox 2013) or abrupt size enlargement without sexual reproduction (Gallagher 1983, Sato et al. 2008).

We measure valve lengths of two sympatric populations of congeneric raphid diatoms *Epithemia gibba* var. *ventricosa* (Kützing) Grunow and *Epithemia* sp. from a small pond in Nakaikemi Wetland, Japan, over almost 3 years. We also performed growth experiments for both taxa to investigate cell-division and size-reduction rates to better interpret measurement of field-collected specimens.

## Material and Methods

### Sample collection

Diatoms were collected from a pond in the Nakaikemi Wetland, Tsuruga, Fukui, Japan (35°39'27.7"N, 136°05'23.5"E). Because this pond was not fed by any river, major sources of diatom immigration (other than from spring groundwater or waterbird transport) can be eliminated. Furthermore, because this wetland is a Ramsar site and managed by the city administration, site (anthropogenic) disturbance is minimal. Because *Epithemia* cells attach to the roots of bogbean *Menyanthes trifoliata* Linnaeus, we cut c. 3 cm samples of bogbean roots and transferred to the laboratory once monthly from April 2016 to December 2018. All sampling occurred within the same c. 1 $m^2$ square plot.

### Observations

Samples were cleaned following Trobajo & Mann (2019). Organic matter was placed onto a coverslip and oxidized with nitric acid (1.42 g $mL^{-1}$, Wako, Osaka, Japan) on a hot plate (HP-3000, AS ONE Corporation, Osaka, Japan) at 100°C. The coverslip was then placed in a petri dish filled with distilled water and left for more than 15 min to remove residual salts. Washed frustules were mounted with Mounting Media (Wako). Photomicrographs of valves of *E. gibba* var. *ventricosa* and *Epithemia* sp. were taken on a BX-51 (Olympus, Tokyo, Japan) light microscope equipped with a DP-70 (Olympus) digital camera. While the taxon that we refer to *Epithemia* sp. has been sporadically reported from Japan, and historically referred to a variety of species, for reasons presented in our discussion we refrain from identifying it to species.

Cells were also cleaned using the drain-detergent method of Nagumo (1995). Cleaned diatom valves were then placed on a coverslip (3 mm diameter, Matsunami Glass Ind., Osaka, Japan) and coated with osmium oxide ($OsO_4$) using an ion sputter NEOC-AN (Meiwafosis, Tokyo, Japan) and observed on a S-5000 scanning electron microscope (Hitachi, Tokyo, Japan).

## Valve length

Valve lengths were measured using ImageJ version 1.5i (Schneider et al. 2012). Between 5 and 181 (*E. gibba* var. *ventricosa*), and 6 and 152 (*Epithemia* sp.) valves were measured in any given month. While low numbers of individuals reflect low taxon abundance in samples, because our sampling method was non quantitative this might not indicate their abundance in the field. Initial cells of *E. gibba* var. *ventricosa* formed via sexual reproduction are 105–185 µm (Kamakura et al. 2021). We regard large cells within this size range to be initial cells, and for them to provide indirect evidence of sexual reproduction at our sampling site. We estimate the number of wild population cohorts by fitting a Gaussian Mixture Model to logarithmic-transformed valve length data for each month, using the mclustICL function in *mclust* version 5.4.9 (Scrucca et al. 2016) based on Integrated Completed Likelihood (ICL) criterion in R version 4.0.3 (R Core Team 2020).

## Growth experiments

Single *E. gibba* var. *ventricosa* and *Epithemia* sp. cells were isolated from samples collected on June 20, 2018 from the field and placed into a 24-well plate (Thermo Fisher Scientific, Massachusetts, USA) using a capillary pipette. All strains were grown at 18°C under a 12:12 h (light:dark) photoperiod with cool white light c. 50 µmol photons $m^{-2}$ $s^{-1}$ in CSi medium (Nakayama et al. 2011), modified as follows: base water was collected from the field, pre-filtered and supplemented with 1.0 mM $NaNO_3$, adjusted to pH 6.2 with HCl, and sterilized through a 0.2-µm pore membrane filter (Advantec Toyo, Tokyo, Japan).

Cell counting and valve length measurements were performed every 6 or 7 days using 12 *E. gibba* var. *ventricosa* and 7 *Epithemia* sp. strains over 29 days of culture, each of which started with a single cell, with the numbers of measured cells varying over time: day 7 (3–7 cells), day 13 (9–30 cells), day 22 (25–126 cells), and day 29 (100–158 cells). The growth rate ($\mu$) = [ln ($N_2/N_1$)]/($T_2-T_1$), where $N_1$ and $N_2$ represent the number of cells at time $T_1$ and $T_2$ (day, $T_2 > T_1$), respectively. The division rate per day ($g$) = $\mu$/ln2, and the doubling time is 1 $g^{-1}$ (day), which we used to estimate the number of divisions for each period between observations. To identify the rate of reduction in valve length during cell division, the Δvalve length (µm) for each strain was calculated by $L_{29}-L_0$, where $L_0$ and $L_{29}$ refer to the average valve length on days 0 and 29, respectively. The Δvalve length per cell division was calculated by dividing Δvalve length by the number of divisions for the period between days 0 and 29.

## Results

### Morphology

#### *Epithemia gibba* var. *ventricosa* (Fig. 1A, 2A–E)

Valves lunate, with acute apices; ventral margin nearly straight; dorsal margin gently elevated centrally. Sculptured with 7 or 8 ribs per 10 μm, each separated by biseriate striae; striae arranged in a trellisoid pattern on flattened valve face (Fig. 2A), comprising a circular or C-shaped areole, and three rows near the raphe side of the valve. Raphe along valve face margin bisected by central nodule (Fig. 2C); canal raphe thick. Inner valve surface divided by thick ribs crossing in the direction of the valvar axis, each separated by 1 or 2 secondary thin ribs (Fig. 2D); two rows of areolae occur between thin ribs. Girdle bands open, with the open and closed ends interlacing one another (Fig. 2E).

#### *Epithemia* sp. (Fig. 1B, 2F–J)

Valves lunate, with capitate apices; ventral margin nearly straight; dorsal margin convex. Sculptured with 3–5 ribs per 10 μm, separated by 2–6 distinct rows of areolae, with 19 or 20 rows of areolae per 10 μm (with 6–9 areolae per 10 μm); valve face slightly undulated because of sunken areolae. Striae in single row, arranged in trellisoid pattern (Fig. 2F), comprising circular areolae. Raphe along valve face margin elevated, bisected by central nodule (Fig. 2H); canal raphe thick. Inner valve surface divided by thick ribs crossing in direction of valvar axis, with inter-rib distance decreasing toward apical edges (Fig. 2I); with 2–6 secondary thin ribs between thick ribs. Girdle bands open, with open and closed ends interlacing with one another (Fig. 2J).

### Field-based observation: seasonal succession in valve length

Both *E. gibba* var. *ventricosa* and *Epithemia* sp. occurred regularly at the site throughout the study period. For *E. gibba* var. *ventricosa*, valves ranged 18.1–168.2 μm length and 5.6–8.9 μm width; for *Epithemia* sp. valves ranged 30.6–53.2 μm length and 5.8–10.0 μm width (Fig. 3). Valves $>$ 105 μm length in *E. gibba* var. *ventricosa*, indicative of size recovery via sexual reproduction, occurred in April and June of 2016, March, April, and June of 2017, and April of 2018. No markedly larger valves indicative of auxospore formation were observed in *Epithemia* sp. By comparing models for the optimal number of components based on the ICL criterion, the size distribution for each month was separated into 1–4 cohorts for *E. gibba* var. *ventricosa* and into a single cohort only for *Epithemia* sp. (Fig. S1).

### Laboratory-based observation: growth rate and size reduction

The mean doubling times were 2.97 days (SE $\pm$ 0.31, 12 strains) for *E. gibba* var. *ventricosa,* and 3.45 days (SE=0.14, 7 strains) for *Epithemia* sp. (Fig. 4A). Cells of *E. gibba* var. *ventricosa* were motile and dispersed more-or-less evenly to cover the culture vessel bottom (Fig. 4B), whereas

those of *Epithemia* sp., based both on their patchy distribution in the culture vessel (Fig. 4C) and the fact that none was observed moving beneath a microscope, appeared to be less motile.

Valve lengths on day 0 (collection and isolation day) varied among strains (Fig. 5A). Succession in average valve length (relative to day 0) is presented in Figure 5B. The estimated decrease in average valve length for each population per cell division is 0.32 μm for *E. gibba* var. *ventricosa* strains, and 0.03 for *Epithemia* sp. strains (Fig. 5C).

## Discussion

### Life cycles of two *Epithemia* taxa

Despite the large number of known diatom species, the life cycle of very few of them has been described. We report the life cycles of two congeneric taxa that occur on the same substratum (and within a ~1 $m^2$ plot) by combination of field-based monitoring and laboratory culture. According to the MacDonald–Pfitzer rule, the average cell size of a population would gradually decrease over time, and then recover (Bellinger 1977, Round 1982, Jewson et al. 2010, Jewson & Bixby 2016), leading to shifts in size distribution over time. At our field site *E. gibba* var. *ventricosa* contained multiple size-class cohorts within the population. Kamakura et al. (2021) also used strains of *E. gibba* var. *ventricosa* established from a population from the same site as ours, and based on crossing experiments reported initial cells to range 105.0–185.0 μm in size. Accordingly, the several cells that we identified within this range are regarded to be initial cells (Fig. 3), suggesting that the population had reproduced sexually in the field (although the seasonality and/or frequency of this sexual event remain unknown). We found no cells $<$ 18 μm in field samples, but this is not surprising given that cells smaller than 15.7 μm are too small to undertake cell division in culture (Kamakura et al. 2021).

We found neither direct nor indirect evidence for sexual reproduction in *Epithemia* sp. in field-collected samples. Cell size in this species was basically stable, and did not obviously reduce over time. No record of sexual reproduction exists for this diatom 'species,' nor could we induce its sexual reproduction. Conversely, sexual reproduction in *E. gibba* var. *ventricosa* has been successfully induced under identical conditions (culture medium, temperature, photoperiod, and light intensity) (Kamakura, unpublished observations). Consistent with field observations for *Epithemia* sp., there was a slight reduction in cell size in culture.

Sex expression in diatoms is regulated by cell size, because size reduction during the vegetative phase corelates with the emergence of the sexual phase (Round et al. 1990). We report *Epithemia* 'sp.' to not obviously decrease in cell size over almost 3 years, indicating that the rate of size decrease in this species is extremely slow, resulting in a vegetative period that spans years or decades, or that the ability to reproduce sexually has been lost. A similarly narrow size range was reported by Mann (1988b) for *Navicula cuspidata* var. *ambigua* (Ehrenberg) Kirchner from Scotland.

Diatoms that do not reduce in cell size have been reported by, for example, von Stosch (1965), Round (1972), and Rose & Cox (2013). Geitler (1932) proposed that the mechanical

plasticity of girdle bands in the silica cell wall played an important role in avoidance of size reduction. When girdle bands are more elastic, the cytoplasm beneath them can expand during cell division, and the newly formed hypovalve can be comparably sized to the epivalve, or be even larger. We report no difference in the basic structure of girdle bands between the two taxa using SEM. Even within a species-complex, including multiple morphologically similar or identical cryptic species, the size of some species does not decrease while that of others does (Rose & Cox 2013). A strain of *Gomphonema parvulum* (Kützing) in the Kützing species-complex, with slight morphological differences, showed no gradual decrease in cell size over long-term cultivation. We cannot exclude the possibility that different degrees of cell size reduction in our two *Epithemia* taxa are because of undetected differences in cell wall mechanics.

Differences in the distribution of cells in culture vessels suggests that *Epithemia* sp. was less motile than *E. gibba* var. *ventricosa*. Raphid pennate diatoms are usually motile because of raphe-mediated mucilage secretion. It is important for heterothallic raphids to move actively to locate compatible cells for cell–cell pairing before gametangiogamy (Chepurnov et al. 2004).

## Taxonomic implications

Whether *E. gibba* var. *ventricosa* is or is not a variety of *E. gibba* (Ehrenberg) Kützing is debatable. Cultured *E. gibba* var. *ventricosa* valve lengths range 15.7–185.0 μm (Kamakura et al. 2021). Valve lengths of *Navicula gibba* (basionym of *E. gibba*) were originally described as 1/10 linie (a German unit of length) (Ehrenberg 1832), equivalent to about 212 μm. Kützing (1844) described *E. gibba* as being of 1/12 linie length (~176 μm). Van Heurck (1881) and Müller (1895, as *Rhopalodia gibba*) described valve length for this species to be 80–250 μm and 103–187 μm, respectively. Recently, Kociolek (2011) described North American populations to range 75–205 μm length. However, Kützing (1844) originally described valve length for *E. ventricosa* (basionym of *E. gibba* var. *ventricosa*) to be 1/40–1/38 linie (~53–56 μm), and referred to it as clearly smaller than *E. gibba*. Müller (1895) described *R. ventricosa* to be 37–73 μm in length (according to Van Heurck, 40–100 μm). Without no previous study having examined temporal differences in valve size for this species, we cannot ascertain if reported differences in size represent differences in stage after auxospore formation, or differences in size among populations. Peragallo & Peragallo (1900) maintained that *E. gibba* var. *ventricosa* hardly deserved separation from *E. gibba* var. *gibba*—a view even followed by recent authors (e.g., Krammer & Lange-Bertalot 1988, Lange-Bertalot et al. 2017). However, others have continued to separate these taxa into the varieties *E. gibba* var. *gibba* and var. *ventricosa* (e.g., Patrick & Reimer 1975, Watanabe et al. 2005). Our observations over 3 years reveal valve length for the Nakaikemi Wetland population to span reported ranges for both *E. gibba* var. *gibba* and var. *ventricosa*, but to mostly fall within the latter. We therefore adopt the view that *E. ventricosa* is a variety of *E. gibba*, and provisionally attribute our specimens to *E. gibba* var. *ventricosa*. Further investigation, preferably involving molecular analysis, is required to resolve the taxonomic status of these putative variants.

Our *Epithemia* sp. has been sporadically reported from Japan, and historically referred to *Rhopalodia acuminata* Krammer (Kihara et al. 2009, 2015), *R. michelorum* Krammer (Takano et al. 2009, Kamakura & Sato 2018, Sato et al. 2020) and *R. gibberula* var. *vanheurckii* Müller (Ohtsuka & Kitano 2020). No description of any of these species, however, precisely matches our specimens

in combinations of characters and their states. Our specimens have capitate and ventrally bent valve ends, as do *E.* (*R.*) *michelorum* and *R. gibberula* var. *vanheurckii,* but those of *E.* (*R.*) *acuminata* have cuneate or slightly rostrate, almost straight valve ends (Lange-Bertalot & Krammer 1987). *Epithemia acuminata* also differs from our specimens in having striae that become biserial near the fibulae (Lange-Bertalot & Krammer 1987). Our specimens are very similar to *E. michelorum*, but the characteristic C-shaped areolae diagnostic of the latter are not apparent under SEM (Krammer 1988). Additionally, our specimens have coarser areolae (12–18 in 10 μm) than *E. michelorum* (19–24 in 10 μm, Krammer 1988). *Rhopalodia gibberula* var. *vanheurckii* is most similar to our species, but its valves are narrower, its striae coarser (14–16 in 10 μm), and its areolae finer (Müller 1900). *Rhopalodia gibberula* var. *volkensii* O.Müller is also similar to our specimens in having larger valves, but its striae are much coarser (12–14 in 10 μm). Recently, Mimura & Ohtsuka (2021) reported this taxon from Fujiganaru Moor, and referred to it as *Epithemia* sp., as do we. We note that it is most similar to *R. gibberula* var. *vanheurckii* of Müller (1900), but differs in having much wider valves, and to *E. michelorum*, but differs in the density of striae and areolae. Our *Epithemia* sp. may represent a new species, but further morphological and molecular investigation is required to resolve its taxonomic status.

## Acknowledgements

We thank the members of NPO Nakaikemi Net for their permission and help to collect samples. The first author SK was supported by Morishita Jintan Scholarship Foundation. This work was financially supported by JSPS KAKENHI Grant Number 20K06726 and Grant-in-Aid for Scientific Research on Innovative Areas 21A402. We also thank Steve O'Shea, PhD, of Edanz for editing a draft of this manuscript.

## References

Bellinger EG (1977) Seasonal size changes in certain diatoms and their possible significance. Br Phycol J 12: 233–239.

Chepurnov VA, Mann DG, Sabbe K, Vyverman W (2004) Experimental studies on sexual reproduction in diatoms. Int Rev Cytol 237: 91–154.

D'Alelio D, d'Alcala MR, Dubroca L, Zingone A, Montresor M (2009) The time for sex: a biennial life cycle in a marine planktonic diatom. Limnol Oceanogr 55: 106–114.

Edlund MB, Stoermer EF (1997) Ecological, evolutionary and systematic significance of diatom life histories. J Phycol 33: 897–918.

Ehrenberg CG (1832) Über die Entwickelung und Lebensdauer der Infusionsthiere; nebst ferneren Beiträgen zu einer Vergleichung ihrer organischen Systeme. Abhandlungen der Königlichen Akademie Wissenschaften zu Berlin, Physikalische Klasse 1831: 1–154, pls I-IV. (in German)

Gallagher JC (1983) Cell enlargement in *Skeletonema costatum* (Bacillariophyceae). J Phycol 19: 539–542.

Geitler L (1932) Der Formwechsel der pennaten Diatomeen (Kieselalgen). Archiv üur Protistenkunde 78: 1–226. (in German)

Jewson DH, Bixby RJ (2016) Abundance and size change of *Hannaea baicalensis* in Lake Baikal. Eur J Phycol 51: 149–155.

Jewson DH, Granin NG, Zhdarnov AA, Gorbunova LA & Gnatovsky RY (2010) Vertical mixing, size change and resting stage formation of the planktonic diatom *Aulacoseira baicalensis*. Eur J Phycol 45: 354–364.

Kamakura S, Mann DG, Nakamura N, Sato S (2021) Inheritance of spheroid body and plastid in the raphid diatom *Epithemia* (Bacillariophyta) during sexual reproduction. Phycologia 60: 265–273.

Kamakura S, Sato S (2018) Morphology and phylogeny of 2 strains of *Epithemia* collected from Nakaikemi Wetland, Fukui, Japan. Diatom 34: 68–69. (in Japanese)

Kihara Y, Sahashi Y, Arita S, Ohtsuka T (2009) Diatoms of Yamakado Moor in Shiga Prefecture, Japan. Diatom 25: 91–105.

Kützing FT (1844) Die Kieselschaligen Bacillarien oder Diatomeen. Nordhausen, Zu finden bei W Köhne, 152 pp, 30 pls. (in German)

Kihara Y, Tsuda K, Ishii C, Ishizumi E, Ohtsuka T (2015) Periphytic diatoms of Nakaikemi Wetland, an ancient peaty low moor in central Japan. Diatom 31: 18–44.

Kociolek P (2011) *Epithemia gibba*. In: Diatoms of North America. Available at https://diatoms.org/species/epithemia_gibba (accessed on 16 September 16).

Krammer K (1988) The *gibberula*-group in the genus *Rhopalodia* O.Müller (Bacillariophyceae). II. Revision of the group and new taxa. Nov Hedw 47: 159–205.

Krammer K, Lange-Bertalot H (1988) Bacillariophyceae. 2. Teil: Bacillariaceae, Epithemiaceae, Surirellaceae. In: Süsswasserflora von Mitteleuropa, Vol. 2/2 (eds Ettl H, Gerloff J, Heynig H, Mollenhauer D). Gustav Fischer Verlag, Jena, 596 pp. (in German)

Lange-Bertalot H, Hofmann G, Werum M, Cantonati M (2017) Freshwater benthic diatoms of central Europe: Over 800 common species used in ecological assessment. Koeltz Botanical Books, Koenigstein. 942 pp.

Lange-Bertalot H, Krammer K (1987) Bacillariaceae Epithemiaceae Surirellaceae Ne ue und wenig bekannte Taxa, neue Kombinationen und Synonyme sowie Bemerkungen und Erganzung en zu der Naviculaceae. Bibl Diatom 15: 1–289. (in German)

Mann DG (1988a) Why didn't Lund see sex in *Asterionella*? A discussion of the diatom life cycle in nature. In: Algae and the Aquatic Environment (ed Round FE). Biopress, Bristol, pp. 383–412.

Mann DG (1988b) The nature of diatom species: analyses of sympatric populations. In: Proceedings of the 9th International Diatom Symposium (ed Round FE). Koeltz and Biopress, Königstein and Bristol, 293–304.

Mann DG (1999) The species concept in diatoms. Phycologia 38: 437–495.

Mann DG (2011) Size and sex. In: The diatom world (eds Seckbach J, Kociolek JP). Springer, Dordrecht, pp. 145–166.

Mann DG, Chepurnov VA (2004) What have the Romans ever done for us? The past and future contribution of culture studies to diatom systematics. Nov Hedw 79: 237–291.

Mimura T, Ohtsuka T (2021) Diatoms of Fujiganaru Moor, a valley moor situated in the warm-temperate zone in Western Japan. Diatom 37: 66–79.

Müller O (1895) *Rhopalodia* ein neues Genus der Bacillariaceen (Engler's) Botanische Jahrbucher fur Systematik, Pflanzengeschichte, und Pflanzengeographie, Leipzig. 22: 54–71. (in German)

Müller O (1900) Bacillariaceen aus den Natronthälern von El Kab (Ober-Aegypten). Hedwigia 38: 289–321, 3 pls. (in German)

Nagumo T (1995) Simple and safe cleaning methods for diatom samples. Diatom 10: 88. (in Japanese)

Nakayama T, Ikegami Y, Nakayama T, Ishida K, Inagaki Y, Inouye I (2011) Spheroid bodies in rhopalodiacean diatoms were derived from a single endosymbiotic cyanobacterium. J Plant Res 124: 93–97.

Nelson DM, Tréguer P, Brzezinski MA, Leynaert A, Quéguiner B (1995) Production and dissolution of biogenic silica in the ocean: revised global estimates, comparison with regional data and relationship to biogenic sedimentation. Global Biogeochem Cycles 9: 359–372.

Nishikawa T, Hori Y, Harada K, Imai I (2013) Annual regularity of reduction and restoration of cell size in the harmful diatom *Eucampia zodiacus*, and its application to the occurrence prediction of nori bleaching. Plankton Benthos Res 8: 166–170.

Ohtsuka T, Kitano D (2020) Diatom flora of a wet grassland on mineral soil conserved in the Ritsumeikan University Biwako-Kusatsu Campus in Shiga Prefecture, central Japan. Diatom 36: 1–12.

Patrick RM, Reimer CW (1975) The Diatoms of the United States, exclusive of Alaska and Hawaii. Vol. 2. Monographs of the Academy of Natural Sciences of Philadelphia 13. The Academy of Natural Sciences of Philadelphia, Philadelphia, 213 pp.

Peragallo H, Peragallo M (1900) Diatomées marines de France et des districts maritimes voisins. Atlas et Texte (ed Tempère MJ). Micrographe Editeur, Grez-sur-Loing, pp. pls 73–80. (in French)

Pfitzer E (1869) Über den Bau und die Zellteilung der Diatomeen. Bot Zeitung 27: 774–776. (in German)

Pfitzer E (1871) Untersuchungen über bau und entwicklung der Bacillariaceen (Diatomaceen). Botanische Abhandlungen aus dem Gebiet der Morphologie und Physiologie 2: 1–189. (in German)

R Core Team (2020) R: A language and environment for statistical computing. R Foundation for Statistical Computing, Austria. Vienna. https://www.R-project.org/

Rose DT, Cox EJ (2013) Some diatom species do not show a gradual decrease in cell size as they reproduce. Fundam Appl Limnol 182: 117–122.

Round FE (1972) The problem of reduction of cell size during diatom cell division. Nov Hedw 23: 291–303.

Round FE (1982) Auxospore Structure, initial valves and the development of populations of *Stephanodiscus* in Farmoor Reservoir. Ann Bot 49: 447–459.

Round FE, Crawford RM, Mann DG (1990) The Diatoms. Morphology and biology of the genera. Cambridge University Press, Cambridge, 747 pp.

Sato S, Mann DG, Nagumo T, Tanaka J, Tadano T, Medlin LK (2008) Auxospore fine structure and variation in modes of cell size changes in *Grammatophora marina* (Bacillariophyta). Phycologia 47: 12–27.

Sato Y, Takashimizu Y, Urabe A (2020) Diatom assemblages in the 2011 Tohoku-oki tsunami deposits and underlying soil in the Sendai Plain. Diatom 36: 85–91. (in Japanese with English abstract)

Schneider CA, Rasband WS, Eliceiri KW (2012) NIH Image to ImageJ: 25 years of image analysis. Nat Methods 9: 671–675.

Scrucca L, Fop M, Murphy TB, Raftery AE (2016) mclust 5: Clustering, classification and density estimation using gaussian finite mixture models. R J 8: 289–317.

Takano S, Akaneya K, Watanabe T, Katano N (2009) Diatoms from Akita Prefecture, northern part of Japan, part II－Diatoms from Toyokawa River. Diatom 25: 120–133. (in Japanese with English abstract)

Trobajo R, Mann DG (2019) A rapid cleaning method for diatoms. Diatom Res 34:115–124.

Van Heurck H (1881) Synopsis des Diatomées de Belgique. Atlas. Ducaju & Cie, Anvers. pls 31–77. (in French)

von Stosch HA (1965) Manipulierung der Zellgrösse von Diatomeen im experiment. Phycologia 5: 21–44. (in German)

Watanabe T, Asai K, Ohtsuka T, Tuji A, Houki A (2005) Picture book and ecology of the freshwater diatoms. Uchida-rokakuho, Tokyo, 666 pp. (in Japanese)

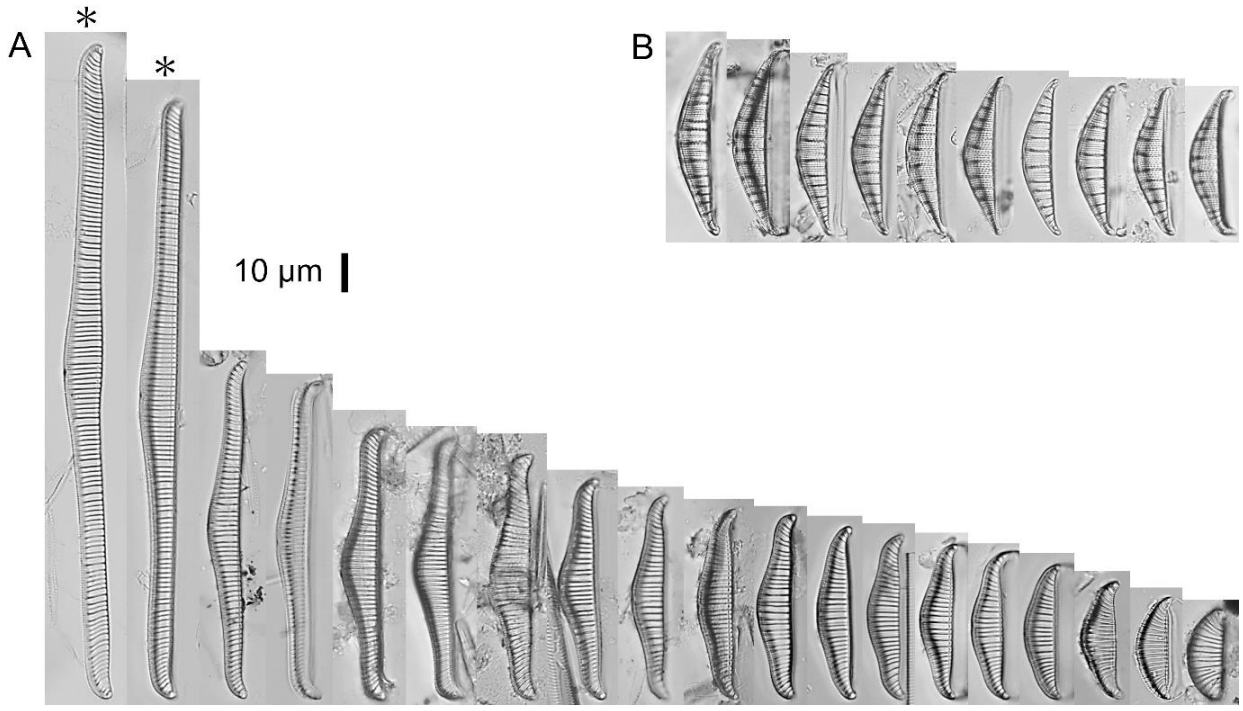


**Fig. 1.** Light-photomicrographic series depicting valve-size reduction in two *Epithemia* taxa. **(A)** *E. gibba* var. *ventricosa*. **(B)** *Epithemia* sp. Photomicrographs marked with an asterisk originate from a crossing experiment in culture (Kamakura et al. 2021); others were obtained from field-collected specimens.

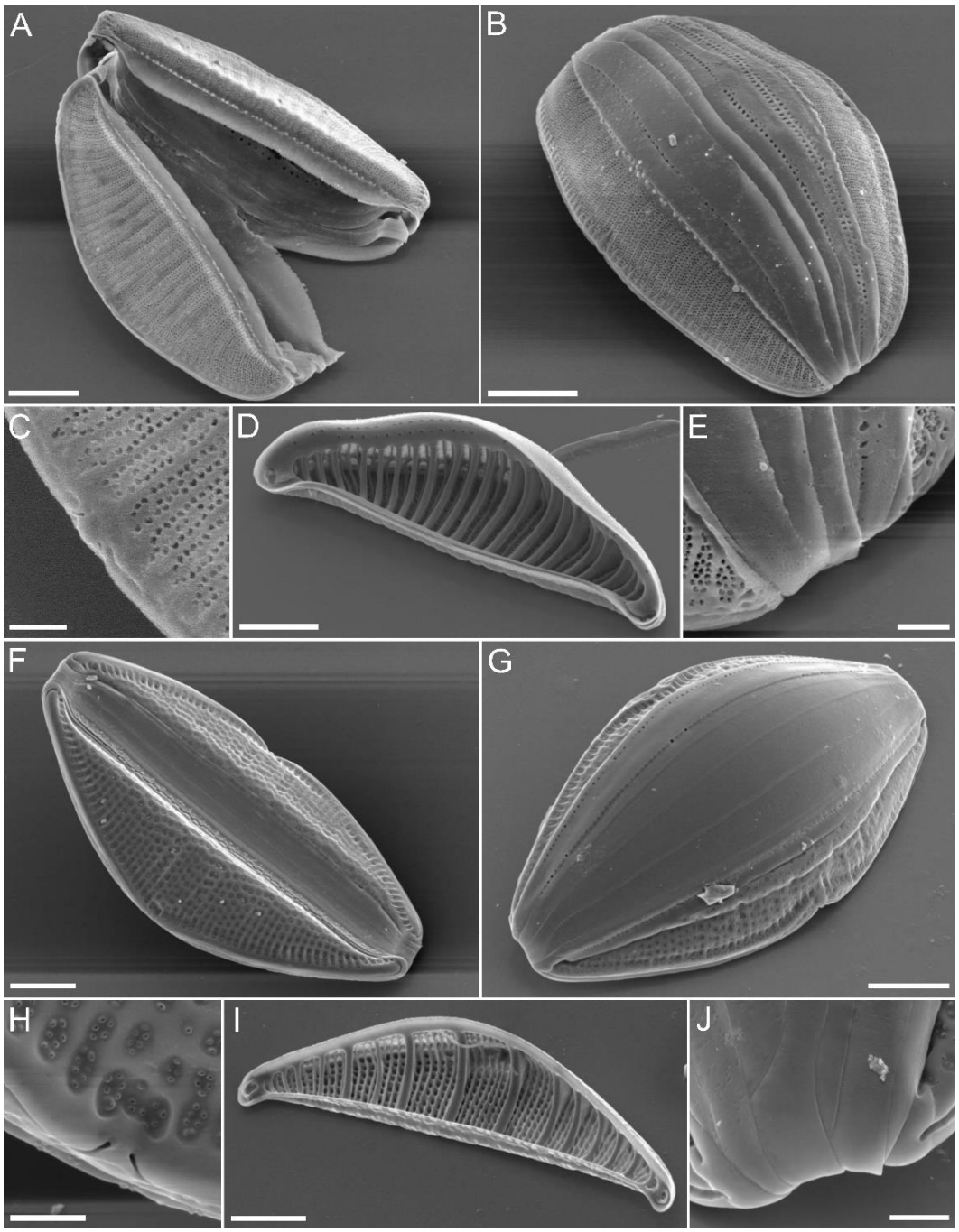


**Fig. 2.** Scanning electron microscopy images of two *Epithemia* taxa. **(A–E)** *E. gibba* var. *ventricosa*. **(A)** Disrupted frustule showing valve face. **(B)** Dorsal side of frustule. **(C)** Enlargement of valve face showing central nodule. **(D)** Internal view of valve. **(E)** Enlarged view of bottom end of frustule in **(B)**; open and closed ends of girdle bands interlace one another. **(F–J)** *Epithemia* sp. **(F)** Ventral side of frustule **(G)** Dorsal side of frustule. **(H)** Enlargement of valve face showing central nodule. **(I)** Internal view of valve. **(J)** Enlarged view of bottom end of frustule in **(G)**; open and closed ends of girdle bands interlace one another. Scale bars=5 μm **(A, B, D, F, G, I)**, and 1 μm in **(C, E, H, J)**.

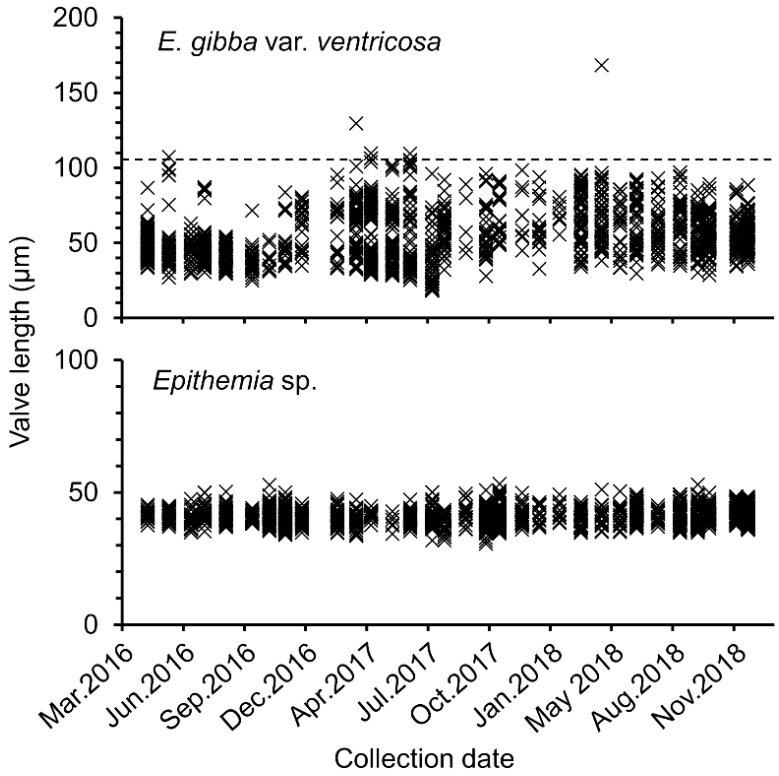


**Fig. 3.** Valve length measurements (crosses, ×) of *Epithemia gibba* var. *ventricosa* (upper) and *Epithemia* sp. (lower) in field samples collected from 2016 to 2018. The dashed line in the upper panel indicates the lower limit of initial cell *E. gibba* var. *ventricosa* valve length obtained by a crossing experiment in culture (Kamakura et al. 2021).

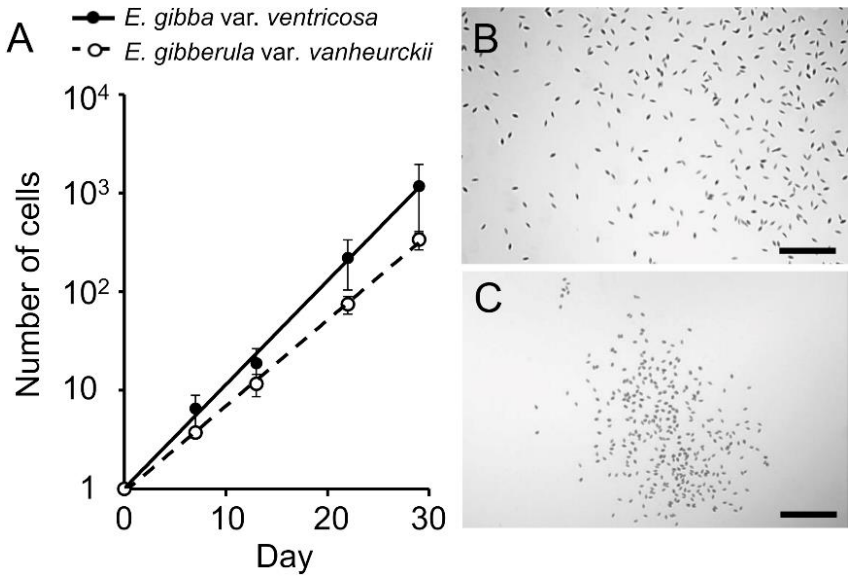


**Fig. 4.** Growth rates and patterns of two cultured *Epithemia* taxa. **(A)** Average number of cells in 12 strains of *E. gibba* var. *ventricosa* and 7 strains of *Epithemia* sp. Bars=standard error. **(B)** Cell dispersal for (motile) *E. gibba* var. *ventricosa,* and **(C)** patchy distribution for less-motile *Epithemia* sp. in culture. Scale bars=500 μm.

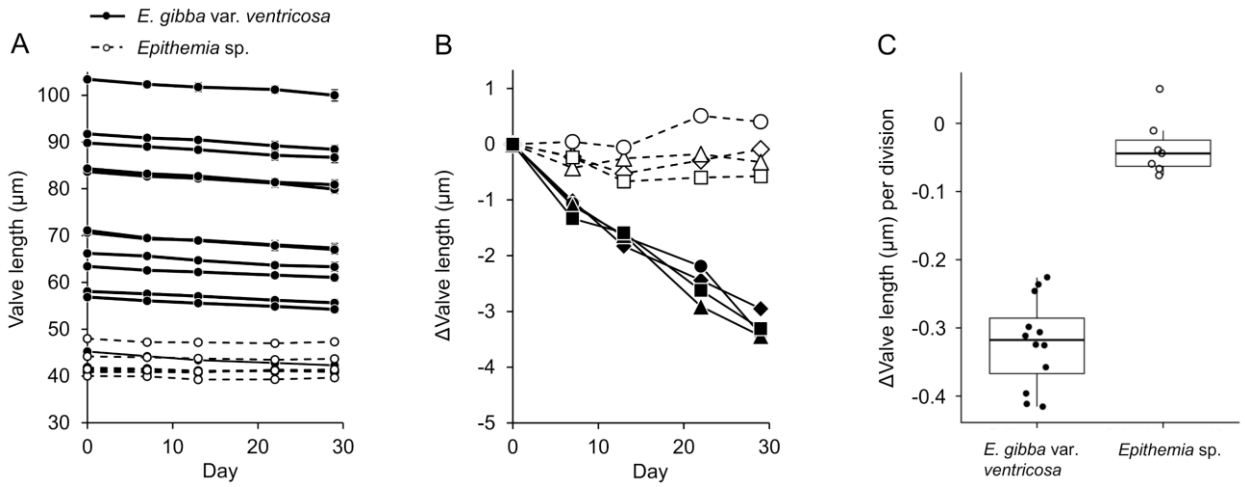


**Fig. 5.** Valve size reduction in cultured *Epithemia gibba* var. *ventricosa* (closed symbols) and *Epithemia* sp. (open symbols). **(A)** Temporal shifts in average valve length for 12 *E. gibba* var. *ventricosa* and 7 *Epithemia* sp. strains measured over a 29-d period. Bars=standard error. **(B)** Δvalve lengths of 4 representative strains from each taxon, showing average cell size change compared to valve length at day 0. Negative values indicate a decrease in size. **(C)** Δvalve lengths (µm) per division in two taxa.

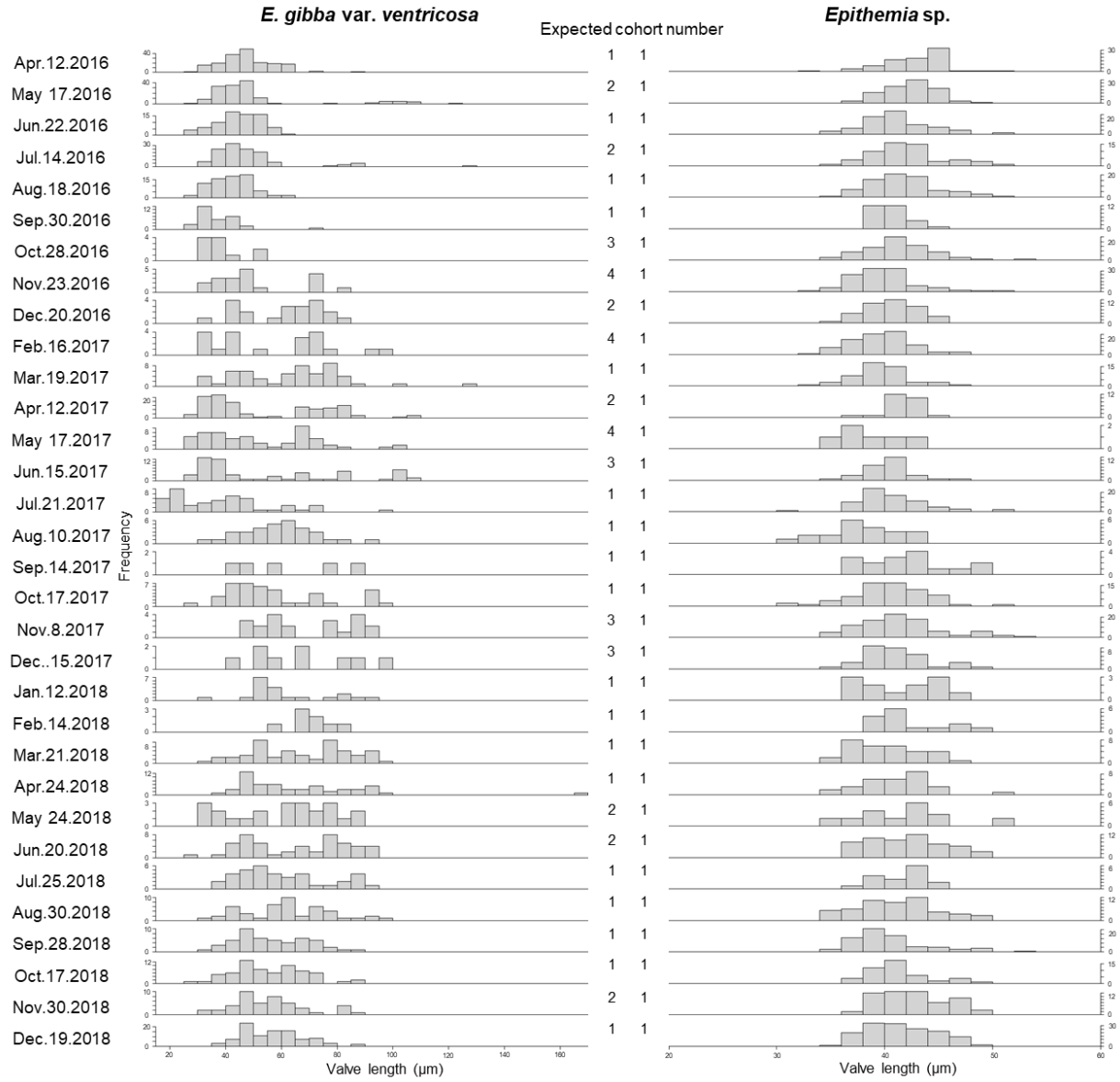


**Fig. S1.** Histograms of valve length of *E. gibba* var. *ventricosa* and *Epithemia* sp. based on field samples collected from 2016 to 2018. The number of cohorts estimated by the ICL criterion is shown for each month.

CHAPTER 3

# Morphological plasticity in response to salinity change in the euryhaline diatom *Pleurosira laevis* (Bacillariophyta)

Kamakura S, Ashworth MP, Yamada K, Mikami D, Kobayashi A, Idei M, Sato S.

This is an 'Author's Accepted Manuscript' of an article published by John Wiley & Sons, Inc. in Journal of Phycology on 7 July 2022, available online: https://doi.org/10.1111/jpy.13277.

## Abstract

*Pleurosira laevis* is a salt-tolerant diatom distributed around the world. The valve of *P. laevis* has distinct structures called ocelli, which are sharply defined areas with fine, densely packed pores. Two formae of this diatom, *P. laevis* f. *laevis* and *P. laevis* f. *polymorpha*, are distinguished from each other by their flat or dome-shaped valve faces and degree of elevation of the ocelli, respectively. In this study, we established 4 strains of *P. laevis* isolated from freshwaters or coastal areas in Japan and the United States, and tracked the formation of newly formed valves with the fluorescent SDV-specific dye PDMPO in culture under several salinity conditions. The result clearly demonstrated the morphological plasticity of the valves, controlled by environmental salinity. The *laevis* form and *polymorpha* form valves were produced at salinities of 2 and 7, respectively. The salinity thresholds dictating the morphological plasticity of the valve were consistent in all 4 strains. A similar morphology to the *polymorpha* form was reproduced in a freshwater medium with the addition of sorbitol, suggesting that osmotic pressure plays a key role in this morphological plasticity. The highly reproducible and easily manipulated change in morphology makes this diatom an ideal model for lab experiments focusing on the molecular and genetic factors involved with valve morphogenesis.

## Abbreviations

PDMPO: 2-(4-pyridyl)-5-((4-(2-dimethylaminoethylaminocarbamoyl) methoxy)phenyl)oxazole
SDV: silica deposition vesicles

## Introduction

Diatoms are microalgae distributed throughout various aquatic and subaerial environments from acidic to alkaline, tropical to polar, and marine to brackish/fresh waters (Round et al. 1990, Mann 1999a). Many diatoms grow only in the genus- or species-specific salinity conditions, and only a handful of genera and species are adapted to a wide range of salinities (Round and Sims 1981, Mann 1999b). Diatom cells are enveloped by silica cell walls called the frustule, which is composed of two thecae. Each theca comprises valve and girdle elements, band-like structures linking two thecae to one another. During cell division, new daughter cell valves are formed inside the mother cell. The morphology of a daughter valve is identical to that of a mother valve, albeit slightly smaller in length and width (Round et al. 1990). Environmental factors are known to cause plastic changes in the

morphology of the valves in some diatom species. Some of these documented factors include temperature, silica concentration, pH, nutrient/ heavy metals concentration, light intensity, and salinity (reviewed in Kociolek and Stoermer 2010, Su et al. 2018). Because diatom species are characterized and described mostly on the basis of morphology, knowledge of the breadth of morphological plasticity in a species is a taxonomic necessity. Furthermore, exposure to environmental causes (e.g., trace metals or multiple stressors, can trigger teratogenesis in the diatom frustules; reviewed in Falasco et al. 2021). If certain environmental cues are known to trigger a certain morphology within a taxon, this information can be a valid indicator of those environmental parameters (Cox 1995) in the ecological and water quality assessment of the current or past states of aquatic habitats. To date, considering the number of diatom species, there is a tiny proportion of diatoms whose morphological responses to environmental factors have been studied in culture experiments (Cox 2014).

*Pleurosira laevis* is a periphytic diatom that inhabits a wide range of salinity environments, from the river to coast. The valve of *P. laevis* has distinct structures called ocelli, which are the areas of fine, densely packed pores called porelli (Ross and Sims 1972, Round et al. 1990), surrounded by rims of silica, at both ends of the valve face. The cells form chain colonies or attach to a substratum by means of mucilaginous pads extruded from the ocelli. Taxonomically, there are two formae described for this diatom, *P. laevis* f. *laevis* and *P. laevis* f. *polymorpha*. The former *P. laevis* f. *laevis* has flat valve faces (Fig. 1), mainly observed in fresh and brackish waters (Compère 1982, Ehrlich et al. 1982, Kociolek et al. 1983, Fránková-Kozáková et al. 2007). On the other hand, *P. laevis* f. *polymorpha* has dome-shaped/ elevated valve faces with projecting ocelli (Fig. 2), found in brackish to saline waters (Hohn and Hellerman 1966, Compère 1982, Snoeijs and Weckström 2010, Bąk et al. 2020, Bilous et al. 2021). When Compère (1982) described the two formae, he also mentioned the possibility that the distinguishing characteristics of the forms (i.e., the presence or absence of the ocelli projection) could be within a range of morphological plasticity caused by a change of environmental salinity. The inference was made based on the observation of field material in which he found heterovalvar "Janus cells" (two valves in a single frustule which differ morphologically from each other, see e.g., McBride and Edgar 1998); having one valve with *laevis* form and another with *polymorpha* form (fig. 15 in Compère 1982). The presence of Janus cells is common when multiple morphological phenotypes occur within a single population or genotype (Stoermer 1967, Jordan et al. 1991, Teubner 1995, Meyer and Håkansson 1996, McBride and Edgar 1998, Andreji_c et al. 2018). Furthermore, Compère (1982) inferred that the morphological plasticity was caused by the salinity change. To support this interpretation, he referenced Li and Chiang (1979), who observed a morphological change in response to salinity in *Pleurosira socotrensis* (as *Proteucylindrus taiwanensis*) and noted that the newly formed valves in the cells they were culturing had distinctly projecting ocelli at salinities above 5. El-Awamri (2008) reported morphological variations of *P. laevis* in field material obtained from multiple localities in Egypt. El-Awamri (2008) also noted that frustules with the laevis form sometimes had newly formed daughter valves exhibiting a different morphology than the mother cell, that is, elevated ocelli and a central elevation on the valve face (ibid. fig. 3: note that he regarded these internal cells as resting spores). In this study, we report with culture experiments that the plasticity of the valve morphology in *P. laevis* is indeed determined by salinity conditions, and these responses are highly conserved among strains established from samples collected from different salinities and continents.

## Materials and methods

### Culture conditions

Three strains of *P. laevis* f. *laevis* and one strain of *P. laevis* f. *polymorpha* were established based on samples collected from different locations. They were maintained in their original salinities prior to the start of the experiments with WC medium (Guillard and Lorenzen 1972), Bolds Basal Medium (Bold and Wynne 1978), Roshchin medium (Roshchin 1994), or f/2 medium (Guillard and Ryther 1962; see Table. 1). The WC medium was prepared with distilled water for culture at salinity 0 in both the maintenance and the main experiment. Although the nutrient components can contribute to the salinity of WC medium, "effective salinity" was considered to be 0 based on a measurement by a YSI Model 63 multimeter (YSI Incorporated, Yellow Springs, OH, USA). Culture media of other salinities (i.e., 2, 3, 4, 5, 6, 7 and 30) were artificially prepared by adding "Salt stocks" described in Nakov et al. (2020), comprised of NaCl, $MgSO_4 \bullet 7H_2O$, $MgCl_2 \bullet 6H_2O$, KCl, and $CaCl_2 \bullet 2H_2O$, to WC medium. For all the media the deviation from the target salinity was 0.1, directly confirmed using the multimeter, and pH was adjusted to 8 by dropwise addition of 1 M HCl. All the media were sterilized with a membrane filter (0.2 μm pore size, Mixed Cellulose Ester, Advantec, Tokyo, Japan). The strains were grown in a flask (Nunc EasYFlask Cell Culture Flasks, Thermo Fisher Scientific, Waltham, MA, USA), kept under 18°C, 12:12 h light:dark, with cool white light, ca. 50 μmol photons $\cdot m^{-2} \cdot s^{-1}$.

### Salinity manipulation in culture

To expose strains to various salinity conditions, precultivated cells were collected and transferred to a new flask with the medium of a given salinity, by hooking a chain colony onto a glass pipette: unlike pouring inoculum into the experimental medium, the effect of the carryover of preculture medium into the experimental culture was negligible with this method.

### Growth rate measurement

All 4 strains were cultivated at salinities of 0, 2, 7, 15 and 30. Cells actively growing in culture were transferred to 12-well plates (Nunc Non-Treated Multidishes, Thermo Fisher Scientific) containing 2 mL of the same salinity medium. The number of cells grown in the culture plates was counted every 3–5 d under an inverted microscope (CKX41, Olympus, Tokyo, Japan) for 20 d. The growth rate was calculated by $\mu = [\ln (N_2/N_1)]/(T_2 - T_1)$, where $N_2$ and $N_1$ are the numbers of cells at the days $T_2$ and $T_1$, respectively, and where $T_2 > T_1$, using the two counting points ($T$) with the steepest increase in the cell numbers ($N$; Wood et al. 2005). The measurements were taken in triplicate for each strain under each salinity condition, resulting in 60 manipulations. The differences in growth rates at each salinity were statistically tested by Tukey's test at the 0.05 level of significance using R 4.0.3 (R Core Team 2020).

## Observation of morphological plasticity

The fluorescent probe PDMPO (LysoSensor Yellow/Blue DND-160, Thermo Fisher Scientific) is accumulated into the SDV and codeposited with Si so that newly forming frustules can be fluorescently labeled while keeping the diatom cells alive (Shimizu et al. 2001). We added PDMPO to the culture medium 3 days prior to observation to a final concentration of 10 nM to label newly formed valves after the change of salinity conditions, as otherwise, it is impossible to distinguish valves formed before or after the treatment. The morphology of the labeled valves was examined using a light microscope (LM; BX51, Olympus) equipped with a digital camera (DP70, Olympus). Fluorescence of PDMPO was detected using filter unit U-MWU2 (excitation wavelengths 330–385 nm, emission wavelengths >420 nm, Olympus). Individual cells were detached from chain colonies to make the observation and detection of PDMPO-labeled valves in girdle view possible. Cells were transferred into 1.5 mL microtubes with 0.3 M HCl to dissolve mucilaginous pads connecting the cells to one another, and heated at 80°C for 10 min using a dry thermo unit TAL-1G (TAITEC, Osaka, Japan), then vortexed for a few seconds. Note that the acid treatment and heating processes did not affect the subsequent observations, as there was no clear difference in the number of stained valves between treated and control (i.e., untreated) samples, and no reduction of fluorescence intensity was detected. We defined two morphological forms in the girdle view: the *polymorpha* form had valves with the ocelli projecting above the valve face, whereas the *laevis* form had non-projecting ocelli equal to (or below) the level of the valve face.

To track single cells to reveal how many divisions are required for the morphological response to salinity changes, we randomly isolated 14 individual cells in the *laevis* form from salinity 0 and transferred them to salinity 30, and 17 cells in the *polymorpha* form from salinity 30 and transferred to salinity 0. We were concerned that a small amount of the medium from the preculture would be carried over to the new salinity medium during transfer, causing a deviation from the intended salinity. Therefore, we performed this experiment at the highest salinity range set in this study (i.e., 0–30) to minimize the influence of the carry-over and ensure that the underlying contrast of "salinity at which the *laevis* form should be definitely produced" versus "salinity at which the *polymorpha* form should be definitely produced." The isolated cells were observed by LM (CKX41, Olympus) at ×200–400 magnification every day, for up to 1 week, to check the valve morphology which resulted from each division after the salinity change.

We also examined whether the morphological changes could be induced with an equivalent osmotic pressure produced with the sugar alcohol sorbitol (Wako, Osaka, Japan), using the strain HA-02. WC medium was supplemented with sorbitol in a final concentration of 0.07 and 0.23 M, which resulted in the same osmotic pressure as the media with salinities 2 and 7, respectively. After transferring the *laevis* form strains into 0.23 M sorbitol medium and *polymorpha* form strains into 0.07 M sorbitol medium, and cultivated for 3 d, PDMPO was added and the strains were kept for a further 5 d for labeling newly formed valves.

## Scanning electron microscopy (SEM)

Cells were collected into a centrifugation tube filled with distilled water, centrifuged at 800 *g* for 2 min and the supernatant discarded. This process removed the salt content from the sample. The

pellet was resuspended with a small amount of water, and a drop of the sample was placed onto a round coverslip (φ15 mm, Matsunami Glass Ind. Osaka, Japan), and cleaned as described by Trobajo and Mann (2019); briefly, the organic matter in the samples was first oxidized with nitric acid (1.42 g・mL$^{-1}$, Wako) on a hot plate (HP-3000, AS ONE Corporation, Osaka, Japan) at 100°C, and then washed with distilled water several times to dissolve the residual salts. The dried coverslip was coated with gold using an ion sputter JFC-1500 (JEOL, Tokyo, Japan) with a thickness of ca. 12 nm, and observed using an SEM SU1510 (Hitachi, Tokyo, Japan). To observe frustules with epi- and hypotheca still attached, we also washed cells in a gentler method by 5% SDS solution as described by Schmid and Schulz (1979).

## Quantifying frustule ultrastructure

To compare the finer structure of the two forms, the number of porelli per ocellus was counted using the strain HA-01 cultivated under salinities 2 and 7 for more than 1 month. All porelli in one ocellus of a valve were manually counted based on SEM images taken under a magnification ×9,500–14,000 that clearly showed an entire ocellus region with no dirt obscuring/masking porelli. The counting was repeated with 5 valves of both the *laevis* form grown under salinity 2 and the *polymorpha* form grown under salinity 7. A *t*-test at a significance level of 0.05 was conducted via Microsoft Excel to test whether there was a significant difference in the number of porelli between the two forms. Since the number could be biased by the valve length (i.e., the larger valve was expected to have more porelli), valves with somewhat equivalent lengths from the two forms were chosen for this comparison (no significant difference in the valve length was detected between them; *t*-test, $t_8 = 2.30$, $P = 0.17$). We counted the number of striae per 10 μm along a tangent of valve face under LM for the 4 strains, in both forms grown under salinities of 2 and 7, and statistically tested to check if there were any significant differences among them using R (one-way ANOVA). The stria density is one of the most widely used characters in diatom classification (Anonymous 1975). To confirm whether there is a consistent difference in valve outline between the two forms in our strains, we measured the valve length and width from 188 valves of the *laevis* form and 168 valves of the *polymorpha* form using ImageJ 1.53 k (Schneider et al. 2012), and the width/length ratio was compared. The ratio was also obtained from the literature (listed in Fig. S1 in the Supporting Information) for further comparison. To test the degree of silicification in the *laevis* and *polymorpha* forms in the strain HA-01, the amount of silicate in the frustule was measured by a silicomolybdate method (Koroleff 1983). For this measurement, the forms were grown under salinities 2 or 7 for 3 months. During this period the strain was inoculated several times, with a small amount of inoculum for each time, which ended up with almost all the cells in each form exclusively represented by the *laevis* or *polymorpha* form in salinities of 2 and 7, respectively. Cells from 15 mL of culture were then washed with 5% SDS to remove organic matter (Schmid and Schulz 1979). The chlorophyll *a* measurements (see below) were used to standardize the silicate content between the two forms. Frustules washed with SDS were collected using an 8 μm pore-sized membrane filter (Polycarbonate, Advantec), resuspended in 0.2 M NaOH solution, and dissolved by heating at 100°C for 15 min. The sample solution was neutralized with a final concentration of 0.2 M HCl and used for the estimation of silicate concentration using the molybdenum blue. A spectrophotometer UVmini 1240 (Shimadzu, Kyoto, Japan) was used to measure the absorbance values at the wavelengths of 810 nm. Based on the calibration curve

prepared using a dilutions series of Silicon Standard Solution (for atomic absorption spectrochemical analysis, Wako), the absorption values were converted to silicon content. Measurements were made in triplicate per each salinity condition.

## Measurement of chlorophyll a content

The cells of the strain HA-01 were collected through a membrane filter with a pore size of 8 μm and resuspended in 2 mL of 90% methanol. The pigment was eluted in 90% methanol for 30 min at room temperature and the absorbance values were measured at the wavelengths of 630 and 664 nm where peaks appeared (UVmini 1240, Shimadzu). The amount of eluted chlorophyll *a* was calculated by the formula Chl *a* ($\mu g \cdot mL^{-1}$) = $11.47 \times A_{664} - 0.40 \times A_{630}$ (Jeffrey and Humphrey 1975). Measurements were made in triplicate per each salinity condition.

## DNA sequencing and comparison

Cells of the 4 strains were harvested from culture flasks, transferred into microtubes and centrifuged at 800*g* for 5 min to remove supernatant. Cell pellets were homogenized using BioMasher II (Nippi, Tokyo, Japan). The DNA was extracted with a DNeasy Plant Mini Kit (Qiagen, Venlo, Netherlands). We performed PCR to amplify the small subunit 18S ribosomal DNA (SSU rDNA) gene using primers A and B developed in Medlin et al. (1988). Each reaction was carried out in a thermal cycler (LifeECO, Bioer Technology, Hangzhou, China), in a 25-μL reaction volume containing a final concentration of 1.25 U of MightyAmp DNA Polymerase, 1× MightyAmp Buffer Ver.3 ($Mg^{2+}$, dNTP plus; Takara Bio, Shiga, Japan), 0.3 μM of each primer, and 2 ng of template DNA. The amplification conditions were as follows: initial denaturation at 98°C for 2 min followed by 35 cycles of denaturation at 98°C for 10 s, annealing at 60°C for 15 s, and extension at 68°C for 1.5 min. The PCR products were purified using ExoSAP-IT Express (Thermo Fisher Scientific). Sangar sequencing was performed with the reverse and forward primers used in the PCR as well as primers SSU515+, SSU568- (Alverson et al. 2007), SSU-528F, and SSU-920R (Marin et al. 2003) using 3730xl DNA Analyzer and BigDye Terminator v3.1 Cycle Sequencing Kit (Thermo Fisher Scientific). Obtained sequences were manually aligned via BioEdit 7.2.5 (Hall 1999), along with *P. laevis* f. *laevis* (GenBank accession HQ912585), *P. laevis* f. *polymorpha* (KC309505), *P. nanjiensis* (MF578764), and *Odontella aurita* (HQ912686), which was sister to the genus *Pleurosira* in the molecular phylogeny by Li et al. (2018), and then trimmed to 1612 bp. A TCS network (Clement et al. 2000) was drawn using Popart 1.7 (Leigh and Bryant 2015) based on the nucleotide polymorphisms between the sequences.

# Results

## Growth rate

The 4 strains of *P. laevis* grew under all the conditions ranging from salinities of 0–30 (Fig. 3). Although HA-01 and 4VIII19-1 were originally collected from freshwater habitats, their growth

rates were significantly greater in saline conditions (salinities 2, 7, and 15) compared to the freshwater conditions. The growth rates of HA-02 and 25VI12-2B obtained from freshwater and marine habitats, respectively, also tended to be higher in saline conditions than in freshwater, although no significant difference was detected among them.

## Morphological plasticity

The 4 strains of *P. laevis* pre-cultivated at salinity 0 were transferred to flasks at various salinity levels (0, 2, 3, 4, 5, 6, 7 and 30), kept for 20 d, and the newly formed valves were labeled with PDMPO for 3 d. Occasionally plasmolysis took place immediately after transferring the cells into higher salinity conditions (Fig. S2 in the Supporting Information). The protoplast shrank but still attached to the valve interior at ocelli, labiate processes, and girdle element, and the cells recovered shortly (e.g., when the cells were transferred from salinity 0 to 30) they recovered from plasmolysis within approximately 2 h. Salinity change resulted in the formation of heterovalvar "Janus cells," with two opposed valves with different morphology in single cells (Fig. 4). The morphotypes of PDMPO-labeled valves (Fig. 5) were classified as either "*laevis*" form or "*polymorpha*" form, based on the projection of ocelli either level with the valve surface or above the valve surface under LM, respectively. The results showed that almost all of the valves at salinity 2 were the *laevis* form and those at 7 were *polymorpha* form, with a gradual shift in the rate of two forms under salinity conditions between 3 and 6 (Fig. 6A). We also obtained essentially the same result using a strain HA-01, with two different experimental settings: (i) cells were pre-cultured under salinity 30 to assess if the initial forms affected the outcome of the valve plasticity (Fig. 6B) and (ii) prolonged cultivation from 20 to 40 d (Fig. 6C). These results clearly showed that *P. laevis* produced both the *laevis* form and the *polymorpha* form in response to salinity. Single cells were tracked in the culture vessel to reveal that the morphological changes usually took place after the first division upon the salinity change (number of observed cells were 17 and 14, for cells transferred into salinities 0 and 30, respectively), resulting in the formation of the Janus cells. In the 0.07 M sorbitol medium (osmotic pressure was equivalent to salinity 2) the cells produced valves in *laevis* form, whereas in the 0.23 M sorbitol medium (equivalent to salinity 7) valves were in *polymorpha* type (Fig. 7). It should be mentioned, however, that in this sorbitol experiment we observed many deformed valves having rounded and an undulated valve faces in girdle view, and were unable to keep the cells alive more than a week. This difficulty could be, at least partly, caused by an overgrowth of bacteria relative to the diatom cells, most likely due to the presence of excess nutrients spurring bacterial growth.

## Quantitative and qualitative morphological analysis

The striae per 10 μm in the *laevis* form and the *polymorpha* form ranged from 13 to 19, and there was no significant difference among them (2 forms in 4 strains, Table 1). In the *laevis* form, the areolae were smaller and sporadically distributed at the central part of the valve, making the valve center somewhat hyaline (Fig. 1F). Contrarily, the areolae were larger around the center and more or less evenly distributed throughout the valve in the *polymorpha* form (Fig. 2F).

The full range of the valve length in culture was 22.0–151.4 μm. We observed occasional auxosporulation and subsequent initial cell formation within clonal strains, thus this maximum length more or less represents the maximum size in this species. There was a significant difference in the ratio of valve width/length between the two forms when valve lengths were larger than 90 μm, in that *polymorpha* form was more elliptical in valve view. On the other hand, there was no significant difference in the valve outline between the two forms when valves were smaller than 90 μm (Fig. S3 in the Supporting Information). Note that the comparison of the aspect ratio obtained from the literature did not show the same trend, as some of the valves in the *laevis* form had more elliptical valves than that of our strains (Fig. S1).

The amount of chlorophyll *a* eluted from the cells was 2.33±0.28 (average±SD, $n$=3) μg when cultivated at salinity 2, and 2.44±0.49 μg at salinity 7, with no significant difference between them. Estimated silicate content per culture standardized by chlorophyll *a* was 105.30±0.99 mmol for the culture at salinity 2, and 100.63±12.81 mmol at salinity 7, again with no significant difference between them. There was no significant difference in the number of porelli between the *laevis* form valves formed under salinity 2 and the *polymorpha* form valves formed under salinity 7 (Table S1 in the Supporting Information).

## Sequence analysis

The number of nucleotide differences in SSU rDNA gene between our four strains and publicly available sequences was calculated. There were up to 6 base differences among *Pleurosira laevis* taxa, which comprised 2 ribotypes (Fig. 8). Five of the SNPs were localized in the V4 region, and the other 1 was in a loop in their predicted secondary structure. The strains HA-01, HA- 02 (collected from freshwater locality), and 25VI12-2B (from marine) shared the same sequence with KC309505 (the sequence derived from a strain of *P. laevis* f. *polymorpha* collected in an estuarine environment on California coast). The strain 4VIII19-1 was identical to HQ912585 (*P. laevis* f. *laevis*), having 41 nucleotide differences from *P. nanjiensis*, a sister species of the *P. laevis* clade in the phylogenetic tree shown by Li et al. (2018).

## Discussion

## Growth and salinity

Our results showing a higher growth rate for *Pleurosira laevis* in saline conditions were consistent with published field observations that this species grows well in environments with a high chloride concentration (Wujek and Welling 1981, Kociolek et al. 1983, Bąk et al. 2020). In the other euryhaline diatoms, there are known cases where the optimal salinity for growth varies within a species between strains collected from different environments (Sjöqvist et al. 2015, Nakov et al. 2020). These differences might be the result of local adaptation to their respective environments. In *P. laevis,* however, even the strains originating from freshwater environments did not show optimal growth at salinity 0. In the case of *Skeletonema marinoi* documented in Pinseel et al. (2022), the optimal salinity for growth also did not necessarily correspond to the salinity conditions of the

collection localities (note that this result is different from Sjöqvist et al. 2015, which studied the *S. marinoi* population from the same locality, i.e., Baltic Sea).

## Morphological plasticity in *Pleurosira laevis*

In the present study, our *Pleurosira laevis* strains were established from samples collected from various localities in both Japan and the United States with salinities ranging from 0 to 35 (Table 1). The morphology of *P. laevis* changed between the *laevis* and *polymorpha* forms in response to salinity in all 4 strains. Therefore, this is most likely a global phenomenon for this diatom. Our results, in which nearly 100% of the valve formed above salinity 7 was *polymorpha* form, are consistent with Hohn and Hellerman (1966), in which *P. laevis* f. *polymorpha* (as *Biddulphia inusitata*) was observed in an environment with salinity 23. Judging from the fact that the *polymorpha*-like valves were also reproducible with the sorbitol medium equivalent to salinity 7, it would be reasonable to assume that the osmotic pressure plays a key role in the morphogenesis of this diatom.

Morphological responses in diatoms to salinity change have been reported in salt-tolerant species from several different families. For example, Paasche et al. (1975), Hasle and Evensen (1976) and Balzano et al. (2011) reported that silicified intercellular connecting processes became longer with increasing salinity in some *Skeletonema* species. The valve width and length vary with salinity in the raphid pennates *Gomphonema* augur (Jahn 1986) and some *Nitzschia* species (Trobajo et al. 2004, 2011). Plasticity in valve morphology is also known in finer scales; the size of areolae decreases at lower salinity in *Thalassiosira punctigera*, *T. weissflogii* (Vrieling et al. 2007), and *Cocconeis placentula* (Leterme et al. 2010). Salinity can also bring changes in the pattern, arrangement, density, or the number of striae and fultoportulae in *T. decipiens* (McMillan and Johansen 1988), *Cyclotella cryptica*, *C. meneghiniana* (Schultz 1971, Shirokawa et al. 2012), and *Stephanodiscus hantzschii* (Geissler 1986). The striking difference seen in *P. laevis* from the others is that the distinct and qualitative morphological change (i.e., the presence or absence of ocelli projection) readily recognizable under LM can be induced by only a subtle change in salinity (between 2 and 7). The distinct response to salinity in this diatom would be a potential indicator for water quality and for paleoenvironmental studies. Furthermore, the highly reproducible and easily manipulated morphological plasticity makes this diatom an ideal model for lab experiments focusing on the molecular and genetic factors involved with valve morphogenesis.

## Taxonomic implications

The striae per 10 μm of *P. laevis* reported in previous studies ranges from 12 to 18 in 10 μm (e.g., Bourrelly and Manguin 1952, Al-Saadi et al. 1979, Fránková-Kozáková et al. 2007, Cavalcante et al. 2013, Mamanazarova and Gololobova 2017, Park et al. 2017), with an exceptional case in that *P. laevis* found in Iran had 9–12/10 μm (Sharifinia et al. 2016). The striae densities in most of the valves observed in this study, from 13 to 19, fit well within this range.

Previously it has been demonstrated that the silica content of diatom cell walls can vary with salinity. Conley et al. (1989) showed that freshwater diatom frustules tended to have higher

silica content than marine diatoms. Compère (1982), on the basis of frustule observations, suggested that *Pleurosira laevis* f. *polymorpha* was more heavily silicified than f. *laevis*. In the present study, however, we found no significant difference in silica content between the frustules formed at salinities 2 and 7. As for the aspect ratio of valve view, the *polymorpha* form seems to be more elliptical than the *laevis* form, particularly in larger valves. This result would support Compère's description of *P. laevis* f. *laevis* as "broadly elliptical" and *P. laevis* f. *polymorpha* as "elliptical to subcircular."

The morphological plasticity observed in this study, the presence or absence of ocelli projection, is a dynamic response to salinity change; nevertheless, no additional physiological or morphological differences were detected between the strains grown under the salinities 2 and 7 (i.e., growth rate, degree of silicification of the frustule, nor the number of porelli per ocellus; note that there was a slight difference in the valve areolation, see Figs. 1F and 2F). Sequence analysis with SSU rDNA showed that the 4 strains and 2 GenBank entries annotated as *P. laevis* f. *laevis* and f. *polymorpha* are closely related to each other. In fact, in terms of SSU rDNA gene sequence difference, the forms and collection habitats (freshwater vs. marine/estuary) were not reciprocally monophyletic (i.e., there is not an exclusively freshwater or marine clade). The morphological difference between Compère's formae *Pleurosira laevis* f. *laevis* and *P. laevis* f. *polymorpha* are strictly environmentally derived, and there is no physiological, biogeographic, or genetic signal supporting the forma as a distinct taxon. Therefore, these 2 formae should be regarded as a synonym of *P. laevis*. Desianti et al. (2015) introduced the new combination *Pleurosira inusitata* comb. nov. as a basionym of *Biddulphia inusitata* whose description matches that of *P. laevis* f. *polymorpha*. They noted that "the new combination has priority and is available for use if the diatom known as *P. laevis* f. *polymorpha* should be considered a distinct species and not a form of *P. laevis*." Thus, given the present study, we could confidently regard this combination as superfluous.

## Plasma membranes as the molding surface for the new valves

In this study, morphological changes at the micrometer scale were detected under LM. The morphogenetic process in diatoms at this scale is believed to be driven by cytoplasmic components molding SDVs located immediately beneath the plasma membrane (Pickett-Heaps et al. 1990, Cox et al. 2012). The valve morphology and SDV molding have been explained on the basis of the pressure on the plasma membrane of the daughter cell at cleavage furrow: high tension causes a flat valve face and low tension causes undulated valve face. In the former case, the protoplasts of forming daughter cells have equally high turgor pressure and press against each other, thus the boundary between them will be usually flattened (Mann 1984, Schmid 1984, 1987, Round et al. 1990). The *laevis* form of *P. laevis* observed under lower osmotic conditions (resulting in higher membrane tension) reflects this scenario. In the marine or brackish diatoms, which have low membrane tension driven by plasmolysis, the daughter protoplasts are separated from each other, thus their plasma membranes will be rounded or grooved (Mann 1984, Schmid 1984, 1987, Round et al. 1990). The *polymorpha* form observed under higher osmotic conditions (resulting in lower membrane tension) was also consistent with this scenario. The plasticity of a domed valve face under higher osmotic conditions was also observed in *Skeletonema* species (Paasche et al. 1975,

Hasle and Evensen 1976). Fischer (1986) documented salt tolerance in some species of *Melosira*. Crawford (1978) suggested that the flat/rounded morphological plasticity of the valve in *M. lineata* may be caused by environmental factors. Given that *M. varians* in freshwater is characterized by a flat valve face, whereas brackish or marine species (e.g., *M. moniliformis* and *M. nummuloides*) have a rounded one, it is possible that these morphological differences in valve shape among the species of *Melosira* also reflect, even partly, the salinity of their habitat. The present study demonstrated that the mechanical force of osmotic pressure, which is one of the potential factors that have been estimated to provide the diatoms with morphological diversity, could drive a common morphology in at least some genera. In the fission yeast *Schizosaccharomyces pombe*, which is a rod-shaped model organism with an elastic cell wall, it was revealed that the rounded morphology of new cell ends occurring upon division is simply caused by inflation due to turgor pressure (Atilgan et al. 2015). Although diatoms possess rigid cell walls that are quite different from those of yeast, it is interesting to consider that their flexible responses in forming the rounded cell outline might be driven by the same factors. This study supports the idea that plasticity in gross morphology, such as a change of valve outline, can be induced by environmental osmotic conditions and is not solely dependent on cytoskeletal control, though various frustule morphologies in diatoms are clearly under the control of cytoskeletal elements (Tesson and Hildebrand 2010).

## Acknowledgements

The authors thank the staff of Fukui Coast Nature Center for help sampling. The authors would also like to thank Dr. Kalina Manoylov of Georgia College and State University for her advice in locating *Pleurosira* in the Savannah River. The first author SK was supported by Morishita Jintan Scholarship Foundation. This work was financially supported by JSPS KAKENHI Grant Number 20K06726 and Grant-in-Aid for Scientific Research on Innovative Areas 21A402.

## References

Al-Saadi, H. A., Pankow, H. & Huq, M. F. 1979. Algological investigations in the polluted Ashar Canal and Shatt al-Arab in Basrah (Iraq). Int. Rev. Ges. Hydrobiol. Hydrogr. 64:527–40.

Alverson, A. J., Jansen, R. K. & Theriot, E. C. 2007. Bridging the Rubicon: phylogenetic analysis reveals repeated colonizations of marine and fresh waters by thalassiosiroid diatoms. Mol. Phylogenet. Evol. 45:193–210.

Andreji_c, J. Z., Spaulding, S. A., Manoylov, K. M. & Edlund, M. B. 2018. Phenotypic plasticity in diatoms: Janus cells in four *Gomphonema* taxa. Diatom Res. 33:453–70.

Anonymous 1975. Proposals for a standardization of diatom terminology and diagnoses. Nova Hedwig. Beih. 53:323–54.

Atilgan, E., Magidson, V., Khodjakov, A. & Chang, F. 2015. Morphogenesis of the fission yeast cell through cell wall expansion. Curr. Biol. 25:2150–7.

Bąk, M., Halabowski, D., Kryk, A., Lewin, I. & Sowa, A. 2020. Mining salinisation of rivers: its impact on diatom (Bacillariophyta) assemblages. Fottea 20:1–16.

Balzano, S., Sarno, D. & Kooistra, W. H. 2011. Effects of salinity on the growth rate and morphology of ten *Skeletonema* strains. J. Plankton Res. 33:937–45.

Bilous, O. P., Genkal, S. I., Zimmermann, J., Kusber, W. H. & Jahn, R. 2021. Centric diatom diversity in the lower part of the Southern Bug River (Ukraine): the transitional zone at Mykolaiv city. PhytoKeys 178:31–69.

Bold, H. C. & Wynne, M. J. 1978. Introduction to the Algae: Structure and Reproduction. Prentice-Hall, New Jersey 516 pp.

Bourrelly, P. & Manguin, E. 1952. Algues d'eau douce de la Guadeloupe et dépendances. Recueillies par la Mission P. Allorge en 1936. Société d'Edition d'Enseignement Sup_erieur, Paris 281 pp.

Cavalcante, K. P., Tremarin, P. I. & Ludwig, T. A. V. 2013. Taxonomic studies of centric diatoms (Diatomeae): unusual nanoplanktonic forms and new records for Brazil. Acta Bot. Bras. 27:237–51.

Clement, M., Posada, D. C. K. A & Crandall, K. A. 2000. TCS: a computer program to estimate gene genealogies. Mol. Ecol. 9:1657–9.

Compère, P. 1982. Taxonomic revision of the diatom genus *Pleurosira* (Eupodiscaceae). Bacillaria 5:165–90.

Conley, D. J., Kilham, S. S. & Theriot, E. 1989. Differences in silica content between marine and freshwater diatoms. Limnol. Oceanogr. 34:205–12.

Cox, E. J. 1995. Morphological variation in widely distributed diatom taxa: taxonomic and ecological implications. In Donate, M. & Montresor, M. [Eds.] Proceedings of the 13th International Diatom Symposium, Maratea, 1994. Biopress, Bristol, pp. 335–45.

Cox, E. J. 2014. Diatom identification in the face of changing species concepts and evidence of phenotypic plasticity. J. Micropalaeontol. 33:111–20.

Cox, E. J., Willis, L. & Bentley, K. 2012. Integrated simulation with experimentation is a powerful tool for understanding diatom valve morphogenesis. Biosystems 109:450–9.

Crawford, R. M. 1978. Taxonomy and classification of diatom genus *Melosira* C.A. Agardh, III. *Melosira lineata* (Dillw.) C.A.Ag and *Melosira varians* C.A.Ag. Phycologia 17:237–50.

Desianti, N., Potapova, M. & Beals, J. 2015. Examination of the type materials of diatoms described by Hohn and Hellerman from the Atlantic Coast of the USA. Diatom Res. 30:93–116.

Ehrlich, A., Crawford, R. M. & Round, F. E. 1982. A study of the diatom *Cerataulus laevis*—The structure of the frustule. Br. J. Phycol. 17:195–214.

El-Awamri, A. F. 2008. Studies on the morphology of different valve types of the centric diatom species *Pleurosira laevis* (Ehr.) Compère. Aust. J. Basic Appl. Sci. 2:22–9.

Falasco, E., Ector, L., Wetzel, C. E., Badino, G. & Bona, F. 2021. Looking back, looking forward: a review of the new literature on diatom teratological forms (2010–2020). Hydrobiologia 848:1675–753.

Fischer, H. 1986. Osmotic behaviour of some species of *Melosira* (Bacillariophyceae) from marine and inland waters. Bot. Mar. 29:373–9.

Fránková-Kozáková, M., Marvan, P. & Geri_s, R. 2007. Halophilous diatoms in Czech running waters: *Pleurosira laevis* and *Bacillaria paxillifera*. In Kusber, W. H. & Jahn, R. [Eds.] Proceedings of the 1st Central European Diatom Meeting. Berlin, Germany, 2007. Boletim do Museu Botanico Municipal, Berlin, pp. 39–44.

Geissler, U. 1986. Experimental investigations on the variability of frustule characteristics of several freshwater diatoms. 2. The influence of different salt concentrations on some valve structures of *Stephanodiscus hantzschii* Grunow. In Ricard, M. [Ed.] Proceedings of the 8th International diatom Symposium, Paris, 1984. Koeltz, Koenigstein, pp. 59–66.

Guillard, R. R. L. & Ryther, J. H. 1962. Studies on marine planktonic diatoms. I. *Cyclotella nana* Hustedt and *Detonula confervacea* (Cleve). Gran. Can. J. Microbiol. 8:229–39.

Guillard, R. R. & Lorenzen, C. J. 1972. Yellow-green algae with chlorophyllide c. J. Phycol. 8:10–4.

Hall, T. 1999. BioEdit: a user-friendly biological sequence alignment editor and analysis program for Windows 95/98/NT. Nucleic Acids Symp. Ser. 41:95–8.

Hasle, G. R. & Evensen, D. L. 1976. Brackish water and freshwater species of the diatom genus *Skeletonema*. II. *Skeletonema potamos* comb. nov. J. Phycol. 12:73–82.

Hohn, M. H. & Hellerman, J. 1966. New diatoms from the Lewes-Rehoboth Canal, Delaware and Chesapeake Bay area of Baltimore, Maryland. Trans. Amer. Micr. Soc. 85:115–30.

Jahn, R. 1986. A study of *Gomphonema augur* Ehrenberg. The structure of the frustule and its variability in clones and populations. In Ricard, M. [Ed.] Proceedings of 8th International Diatom Symposium, Paris, 1984. Koeltz, Koenigstein, pp. 191–204.

Jeffrey, S. W. & Humphrey, G. F. 1975. New spectrophotometric equations for determining chlorophylls a, b, c1 and c2 in higher plants, algae and natural phytoplankton. Biochem. Physiol. Pflanzen. 167:191–4.

Jordan, R. W., Ligowski, L., N€othig, E. M. & Priddle, J. 1991. The diatom genus *Proboscia* in Antarctic waters. Diatom Res. 6:63–78.

Koroleff, F. 1983. Determination of silicon. In Grasshoff, K., Ehrhardt, M. & Kremling, K. [Eds.] Methods of Seawater Analysis. Verlag Chemie, Weinheim, pp. 174–83.

Kociolek, J. P., Lamb, M. A. & Lowe, R. L. 1983. Notes on the growth and ultrastructure of *Biddulphia laevis* Ehr. (Bacillariophyceae) in the Maumee River, Ohio. Ohio J. Sci. 83:125–30.

Kociolek, J. P. & Stoermer, E. F. 2010. Variation and polymorphism in diatoms: the triple helix of development, genetics and environment. A review of the literature. Vie Milieu 60:75–87.

Leigh, J. W. & Bryant, D. 2015. PopART: Full-feature software for haplotype network construction. Methods Ecol. Evol. 6:1110–6.

Leterme, S. C., Ellis, A. V., Mitchell, J. G., Buscot, M. J., Pollet, T., Schapira, M. & Seuront, L. 2010. Morphological flexibility of *Cocconeis placentula* (Bacillariophyceae) nanostructure to changing salinity levels. J. Phycol. 46:715–9.

Li, Y., Nagumo, T. & Xu, K. 2018. Morphology and molecular phylogeny of *Pleurosira nanjiensis* sp. nov., a new marine benthic diatom from the Nanji Islands, China. Acta Oceanol. Sin. 37:33–9.

Li, C. W. & Chiang, Y. 1979. A euryhaline and polymorphic new diatom, *Proteucylindrus taiwanensis* gen. et sp. nov. Br. J. Phycol. 14:377–84.

Mamanazarova, K. S. & Gololobova, M. A. 2017. First record of diatom species *Pleurosira laevis* (Ehrenberg) Compère for Uzbekistan and Central Asia. Russ. J. Biol. Invasions 8:69–74.

Mann, D. G. 1984. An ontogenetic approach to diatom systematics. In Mann, D. G. [Ed.] Proceedings of the 7th International Diatom Symposium, Philadelphia, 1982. Koeltz, Koenigstein, pp. 113–44.

Mann, D. G. 1999a. The species concept in diatoms. Phycologia 38:437–95.

Mann, D. G. 1999b. Crossing the Rubicon: the effectiveness of the marine/freshwater interface as a barrier to the migration of diatom germplasm. In Mayama, S., Idei, M. & Koizumi, I. [Eds.] Proceedings of the 14th International Diatom Symposium, Tokyo, 1996. Koeltz, Koenigstein, pp. 1–21.

Marin, B., Palm, A., Klingberg, M. A. X. & Melkonian, M. 2003. Phylogeny and taxonomic revision of plastid-containing euglenophytes based on SSU rDNA sequence comparisons and synapomorphic signatures in the SSU rRNA secondary structure. Protist 154:99–145.

McBride, S. A. & Edgar, R. K. 1998. Janus cells unveiled: frustular morphometric variability in *Gomphonema angustatum*. Diatom Res. 13:293–310.

McMillan, M. & Johansen, J. R. 1988. Changes in valve morphology of *Thalassiosira decipiens* (Bacillariophyceae) cultured in media of four different salinities. Br. J. Phycol. 23:307–16.

Medlin, L., Elwood, H. J., Stickel, S. & Sogin, M. L. 1988. The characterization of enzymatically amplified eukaryotic 16Slike rRNA-coding regions. Gene 71:491–9.

Meyer, B. & Håkansson, H. 1996. Morphological variation of *Cyclotella polymorpha* sp. nov. (Bacillariophyceae). Phycologia 35:64–9.

Nakov, T., Judy, K. J., Downey, K. M., Ruck, E. C. & Alverson, A. J. 2020. Transcriptional response of osmolyte synthetic pathways and membrane transporters in a euryhaline diatom during long-term acclimation to a salinity gradient. J. Phycol. 56:1712–28.

Paasche, E., Johansson, S. & Evensen, D. L. 1975. An effect of osmotic pressure on the valve morphology of the diatom *Skeletonema subsalsum* (A. Cleve) Bethge. Phycologia 14:205–11.

Park, S. Y., Choi, J. S., Kim, J. H. & Kim, H. S. 2017. Morphology and physico-ecology of two rare freshwater epilithic diatoms: *Hydrosera whampoensis* and *Pleurosira laevis*. Nova Hedwig. 105:151–66.

Pickett-Heaps, J., Schmid, A. M. M. & Edgar, L. A. 1990. The cell biology of diatom valve formation. In Round, F. E. & Chapman, D. J. [Eds.] Progress in Phycological Research 7. Biopress, Bristol, pp. 1–168.

Pinseel, E., Nakov, T., Van den Berge, K., Downey, K. M., Judy, K. J., Kourtchenko, O., Kremp, A. et al. 2022. Strain-specific transcriptional responses overshadow salinity effects in a marine diatom sampled along the Baltic Sea salinity cline. ISMEJ. 16:1776–87.

R Core Team 2020. R: A language and environment for statistical computing. R Foundation for Statistical Computing. R Foundation for Statistical Computing. Vienna, Austria. Availavle at: https://www.R-project.org/ last accessed 22 June 2022.

Ross, R. & Sims, P. A. 1972. The fine structure of the frustule in centric diatoms: a suggested terminology. Br. J. Phycol. 7:139–63.

Round, F. E. & Sims, P. A. 1981. The distribution of diatom genera in marine and freshwater environments and some evolutionary considerations. In Ross, R. [Ed.] Proceedings of the 6th Symposium on Recent and Fossil Diatoms, Budapest, 1980. Koeltz, Koenigstein, pp. 301–20.

Round, F. E., Crawford, R. M. & Mann, D. G. 1990. The Diatoms: Biology and Morphology of the Genera. Cambridge University Press, Cambridge 747 pp.

Roshchin, A. M. 1994. Zhiznennye tsikly diatomovykh vodoroslej. Naukova Dumka, Kiev 170 pp.

Schmid, A. M. M. 1984. Tricornate spines in *Thalassiosira eccentrica* as a result of valve modelling. In Mann, D. G. [Ed.] Proceedings of 7th International Diatom Symposium, Philadelphia, 1982. Koeltz, Koenigstein, pp. 71–95.

Schmid, A. M. M. 1987. Morphogenetic forces in diatom cell wall formation. Cytomechanics. Springer, Berlin, Heidelberg. pp. 183–99.

Schmid, A. M. M. & Schulz, D. 1979. Wall morphogenesis in diatoms: Deposition of silica by cytoplasmic vesicles. Protoplasma 100:267–88.

Schneider, C. A., Rasband, W. S. & Eliceiri, K. W. 2012. NIH Image to ImageJ: 25 years of image analysis. Nat. Methods 9:671–5.

Schultz, M. E. 1971. Salinity-related polymorphism in the brackish water diatom *Cyclotella cryptica*. Can. J. Bot. 49:1285–9.

Sharifinia, M., Ramezanpour, Z. & Namin, J. I. 2016. Distribution of benthic centric diatom *Pleurosira laevis* (Compère, 1982) in different substrate type and physical and chemical variables. Acta Limnol. Bras. 28:e18.

Shimizu, K., Del Amo, Y., Brzezinski, M. A., Stucky, G. D. & Morse, D. E. 2001. A novel fluorescent silica tracer for biological silicification studies. Chem. Biol. 8:1051–60.

Shirokawa, Y., Karino, K. & Mayama, S. 2012. Developmental plasticity and genotype–environment interactions influence valve morphology in the *Cyclotella meneghiniana* species complex (Bacillariophyceae). Eur. J. Phycol. 47:245–53.

Sjöqvist, C., Godhe, A., Jonsson, P. R., Sundqvist, L. & Kremp, A. 2015. Local adaptation and oceanographic connectivity patterns explain genetic differentiation of a marine diatom across the North Sea–Baltic Sea salinity gradient. Mol. Ecol. 24:2871–85.

Snoeijs, P. & Weckström, K. 2010. Diatoms and environmental change in large brackish-water ecosystems. In Smol, J. P. & Stoermer, E. F. [Eds.] The diatoms: applications for the environmental and Earth sciences, 2nd edition. Cambridge University Press, Cambridge, pp. 298–333.

Stoermer, E. F. 1967. Polymorphism in *Mastogloia*. J. Phycol. 3:73–7.

Su, Y., Lundholm, N. & Ellegaard, M. 2018. Effects of abiotic factors on the nanostructure of diatom frustules—ranges and variability. Appl. Microbiol. Biotechnol. 102:5889–99.

Tesson, B. & Hildebrand, M. 2010. Extensive and intimate association of the cytoskeleton with forming silica in diatoms: control over patterning on the meso-and micro-scale. PLoS ONE 5:e14300.

Teubner, K. 1995. A light microscopical investigation and multivariate statistical analyses of heterovalvar cells of *Cyclotella* species (Bacillariophyceae) from lakes of the Berlin-Brandenburg region. Diatom Res. 10:191–205.

Trobajo, R. & Mann, D. G. 2019. A rapid cleaning method for diatoms. Diatom Res. 34:115–24.

Trobajo, R., Cox, E. J. & Quintana, X. D. 2004. The effects of some environmental variables on the morphology of *Nitzschia frustulum* (Bacillariophyta), in relation its use as a bioindicator. Nova Hedwig. 79:433–45.

Trobajo, R., Rovira, L., Mann, D. G. & Cox, E. J. 2011. Effects of salinity on growth and on valve morphology of five estuarine diatoms. Phycol. Res. 59:83–90.

Vrieling, E. G., Sun, Q., Tian, M., Kooyman, P. J., Gieskes, W. W., van Santen, R. A. & Sommerdijk, N. A. 2007. Salinity dependent diatom biosilicification implies an important role of external ionic strength. Proc. Natl. Acad. Sci. USA 104:10441–6.

Wood, A. M., Everroad, R. C. & Wingard, L. M. 2005. Chapter 18. Measuring growth rates in microalgal cultures. In Andersen, R. A. [Ed.] Algal Culturing Techniques. Elsevier Academic Press, Massachusetts, pp 269–88.

Wujek, D. E. & Welling, M. L. 1981. The occurrence of 2 centric diatoms new to the Great Lakes, USA. J. Great Lakes Res. 7:55–6.

## References for Fig. S1

Gerloff, J., Natour, R. M. & Rivera, P. 1978. Diatoms from Jordan. Willdenowia 8:261–316.

Guo-Feng, P., Guo-Xiang, L., Zheng-Yu, H. & Guo-Xiang, L. 2008. *Pleurosira laevis* (Ehrenberg) Compère, a new record freshwater diatom from China. J. Wuhan Bot. Res. 26:458–60.

Kim, Y., Suk Choi, J., Sin Kim, J., Hee Kim, S., Chan Park, J. & Won Kim, H. 2008. The effects of effluent from a closed mine and treated sewage on epilithic diatom communities in a Korean stream. Nova Hedwig. 86:507–24.

Nardelli, M. S., Bueno, N. C., Ludwig, T. A. V., Tremarin, P. I. & Bartozek, E. C. R. 2014. Coscinodiscophyceae and Fragilariophyceae (Diatomeae) in the Iguaçu River, Paraná, Brazil. Acta bot. bras. 28:127–40.

T-Krasznai, E., B-Béres, V., Kókai, Z., Buczkó, K., Balogh, C. & Török, P. 2014. Contributions to knowledge on the distribution of nine adventive or invasive algae species in Hungary. Kitaibelia 19:11–21.

Tuji, A. 2013. Algae aquae dulcis Japonicae exsiccatae. Fasc. V. nos. 81–100. 21pp. National Museum of Nature and Science, Tsukuba. Available at: https://www.kahaku.go.jp/research/db/botany/exsiccatae/index.html (last accessed 22 June 2022).

Tuji, A. & Houki, A. 2001. Centric diatoms in Lake Biwa. Lake Biwa Study Monogr. 7:1–90.

**Table 1.** List of strains used in this study.

| Strain ID | Original form[a] | Collection date | Locality | Habitat salinity | Culture medium and salinity for stock culture | Valve characteristics[c] | | GenBank accession |
|---|---|---|---|---|---|---|---|---|
| | | | | | | *laevis* form | *polymorpha* form | |
| HA-01 | *P. laevis* f. *laevis* | Oct. 1, 2017 | Kasarizaki, Amami-oshima Island, Kagoshima, Japan (28°31'45.2"N 129°41'23.0"E) | Freshwater (0) | WC or BBM (0) | 22.0×21.3 - 102.7×95.3 (15.4±0.2) | 22.5×20.4 - 97.2×91.2 (16.1±0.2) | LC715259 |
| HA-02 | *P. laevis* f. *laevis* | Oct. 4, 2020 | Mikata, Fukui, Japan (35°33'54.1"N 135°50'27.0"E) | Freshwater (0)[b] | WC (0) | 34.8×34.1 - 130.5×127.0 (15.3±0.3) | 26.9×25.5 - 151.4×134.5 (15.4±0.3) | LC715260 |
| 4VIII19-1 | *P. laevis* f. *laevis* | Aug. 4, 2019 | Port Wentworth, Georgia, USA (32°01'38.9"N 80°01'34.3"W) | Freshwater (0) | WC (0) | 31.2×31.2 - 83.9×81.0 (16.1±0.2) | 23.0×21.6-106.7×100.2 (15.4±0.2) | LC715261 |
| 25VI12-2B | *P. laevis* f. *polymorpha* | Jun. 25, 2012 | Lady' s Island, South Carolina, USA (32°24'24.0"N 80°27'25.2"W) | Marine (35) | Roshchin or f/2 (35) | 31.1×30.2 - 61.1×60.1 (15.5±0.2) | 23.8×23.0 -74.5×69.8 (14.9±0.2) | LC715262 |

[a]Original form is given according to its wild form.

[b]Salinity of this locality is mostly 0, although there is the sporadic inflow of seawater drainage from a nature center situated upstream of the sampling locality, making the maximum instantaneous salinity recorded 17.9.

[c]Length×width, minimum to maximum size in μm. Striae per 10 μm in brackets, displayed as average±SD, $n$=15.

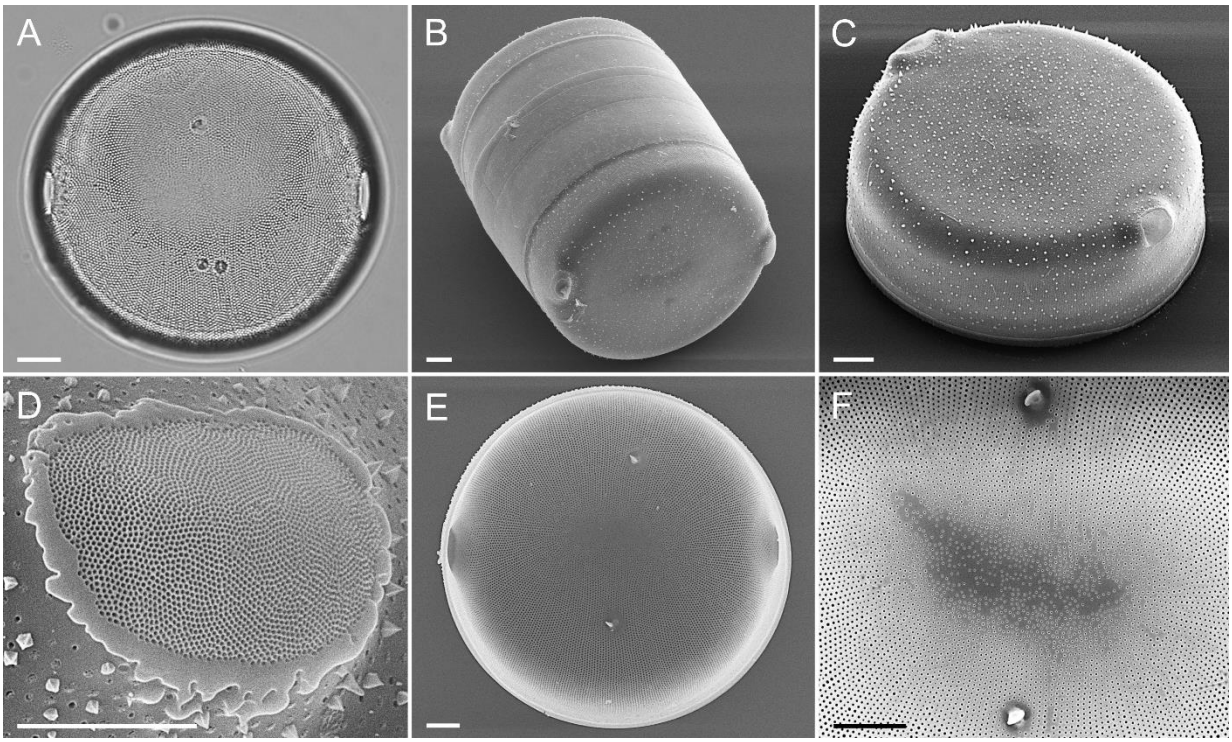


**Fig. 1.** Morphology of *laevis* form observed under LM **(A)** and SEM **(B-F)**. Strain HA-02. **(A)** Cleaned valve, with each ocellus at left and right end. Oblique view of frustule **(B)** and valve **(C)**, showing flat valve face and distinct valve mantle. **(D)** Enlarged view of ocelli, comprising fine and densely-packed pores surrounded by a heavily silicified rim. **(E)** Internal surface of the valve. **(F)** enlargement of the central area locating each labiate process at top and bottom with the somewhat hyaline central part. Note that the areolar size becomes smaller toward the hyaline part. Scale bars = 10 μm **(A-C, E, F)** and 5 μm **(D)**.

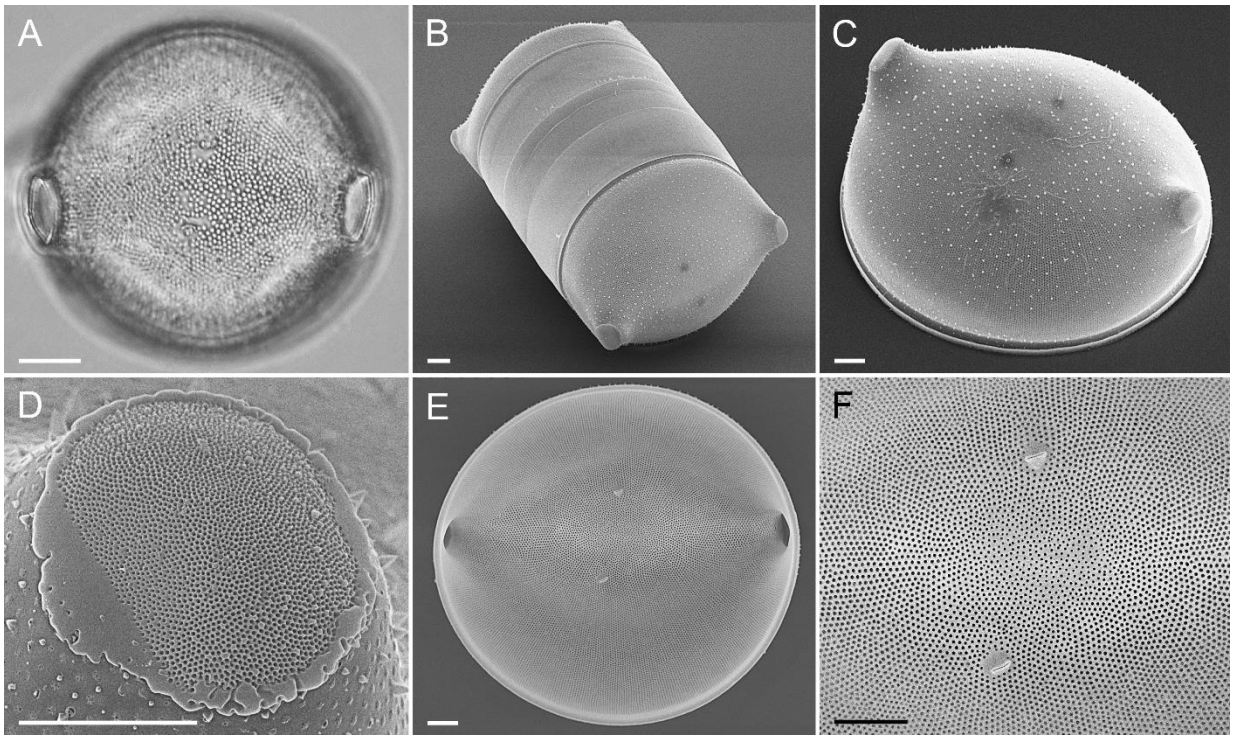


**Fig. 2.** Morphology of *polymorpha* form observed under LM **(A)** and SEM **(B-F)**. Strain HA-02. **(A)** Cleaned valve, with each ocellus at left and right end. Oblique view of frustule **(B)** and valve **(C)**, showing domed valve face and indistinct valve mantle. **(D)** Enlarged view of ocelli, comprising fine and densely-packed pores surrounded by a heavily silicified rim. **(E)** Internal surface of the valve. **(F)** enlargement of the central area with uniformly sized areolae. Scale bars = 10 μm **(A-C, E, F)** and 5 μm **(D)**.

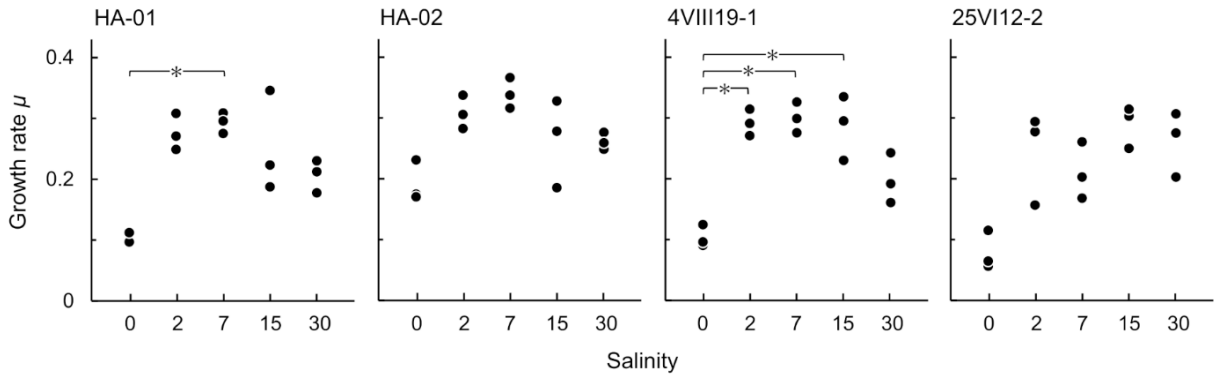


**Fig. 3.** Growth rates of strains of *Pleurosira laevis* at different salinities. Asterisks denote significant difference ($n$=3, Tukey's test, significance level <0.05). See text for growth rate calculation.

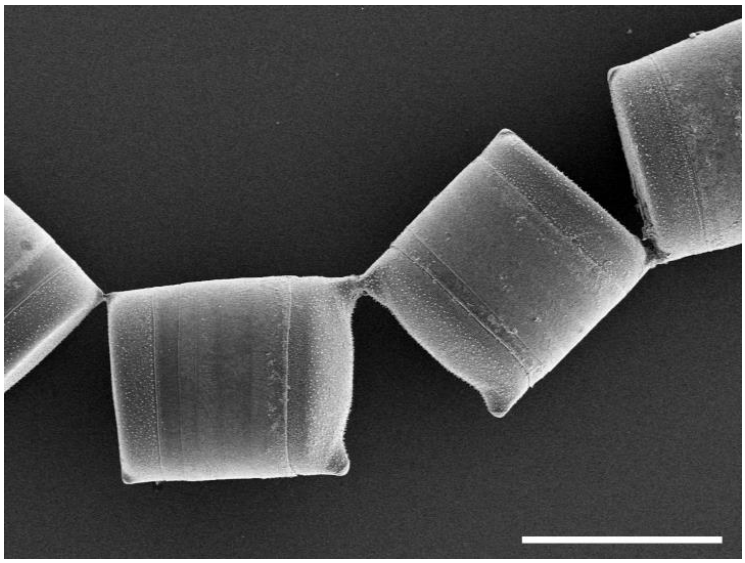

**Fig. 4.** Chain colony of *Pleurosira laevis* with two "Janus cells," which have two opposed valves in different morphology in single cells. Scale bar=100 μm.

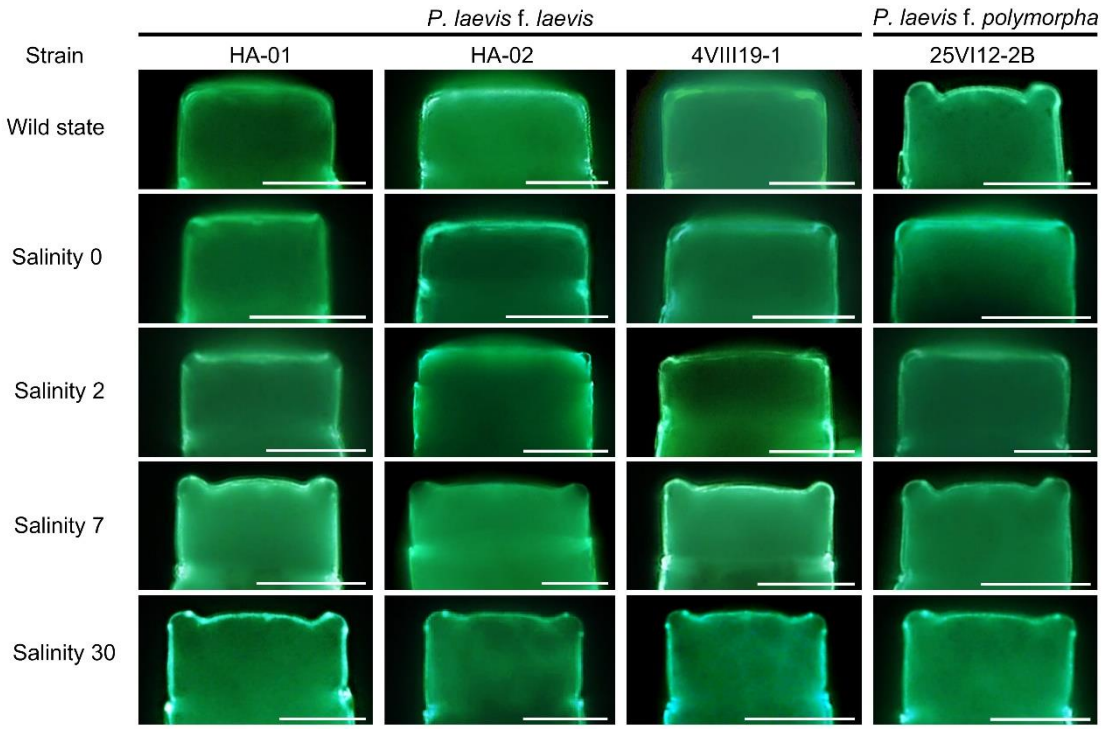


**Fig. 5.** Morphological plasticity of *Pleurosira laevis*, showing two types of valves formed depending on salinity: *polymorpha* form with the ocelli projecting above the valve face, whereas *laevis* form with non-projecting ocelli formed equal to (or below) the level of the valve face. Newly formed valves under given salinities were fluorescence-labeled with PDMPO. Scale bars=50 μm.

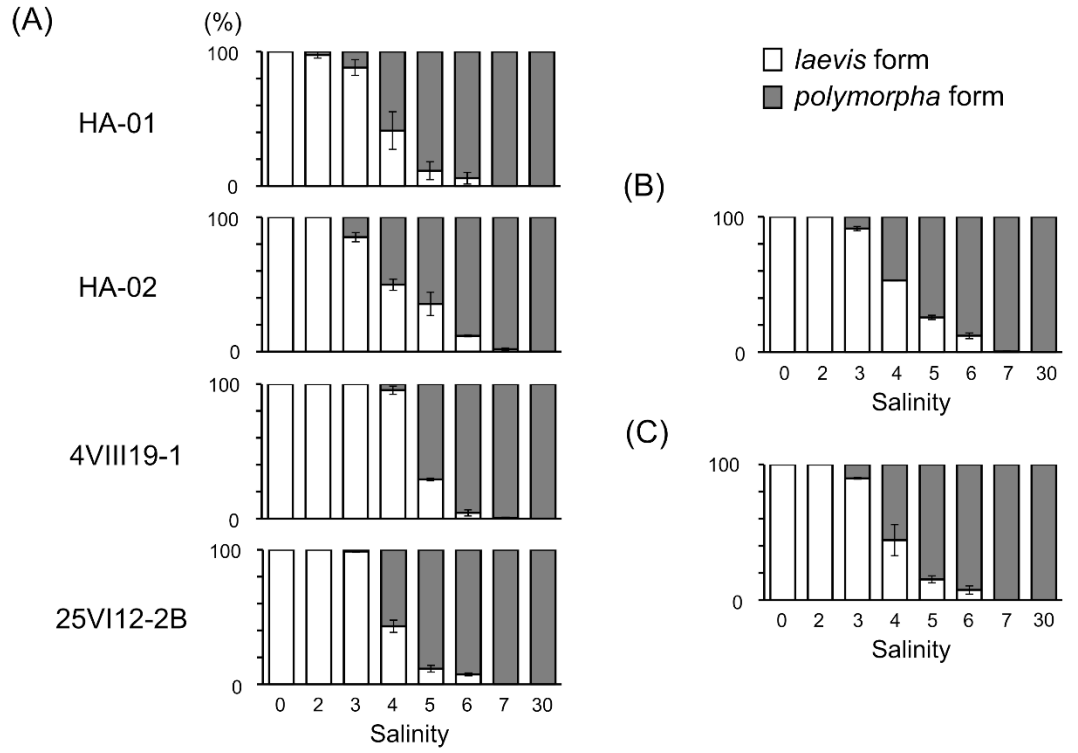


**Fig. 6.** Percentages of *laevis* vs. *polymorpha* forms produced in different salinities. **(A)** The results on day 20 after transferring strains from freshwater medium (salinity 0) to each salinity condition. Almost all valves at salinity 2 were the laevis form and those at salinity 7 were polymorpha form, with the shift in the rate of two forms between salinities 3 and 6. **(B)** The results on day 20 after transferring HA-01 from salinity 30 to each salinity condition and **(C)** prolonged cultivation with 40 days using HA-01 resulted in the same response. >50 valves were observed in each experiment. *n*=3, bars=standard error.

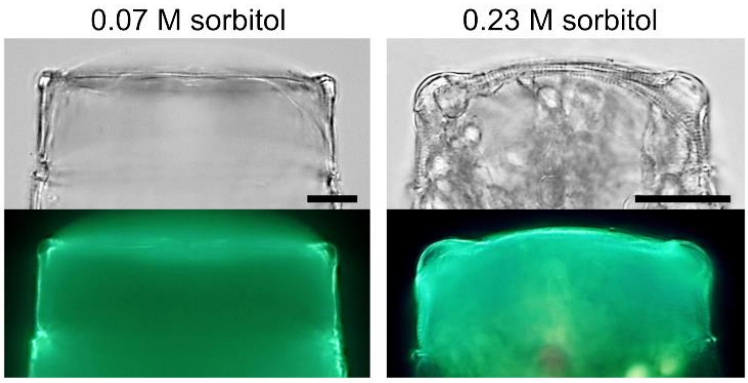


**Fig. 7.** Valves formed with growth media supplemented with 0.07 M sorbitol (equivalent osmotic pressure to the salinity of 2) and 0.23 M sorbitol (equivalent to the salinity of 7). Scale bars=20 μm.

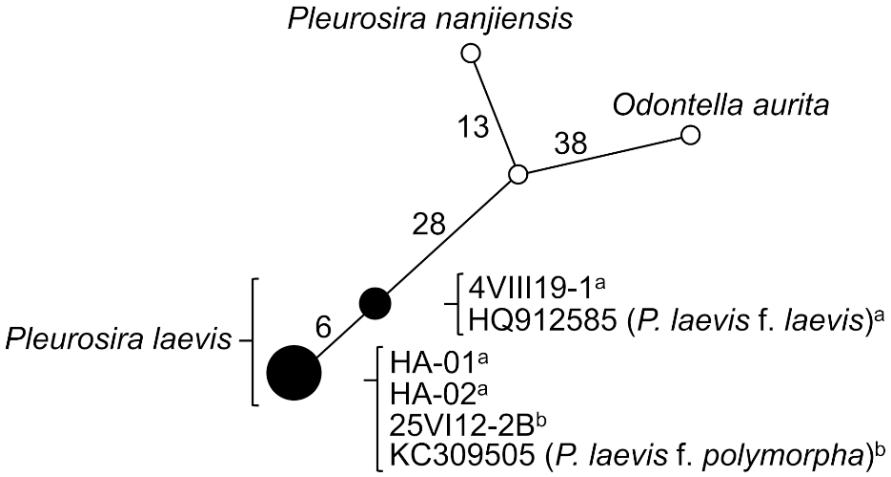


**Fig. 8.** TCS network of SSU rDNA gene ribotypes of *Pleurosira* and *Odontella aurita*. The numbers of nucleotide differences between ribotypes are shown on the branches. The circle size reflects the number of strains. An open circle is a hypothetical ribotype. Strain ID or GenBank entry is shown with different superscripts according to original habitat: a=collected from freshwater, b=collected from marine. See also Table 1 for the detailed locality.

**Table S1.** Number of porelli on the *laevis* form valves of the strain HA-01 produced under salinity 2 and *polymorpha* form valves produced under salinity 7. There was no significant difference between the conditions (*t*-test, $t_8 = 2.30$, $P = 0.12$).

| Form (salinity) | #Valve (valve length [μm]) | Number of porelli per ocellus |
|---|---|---|
| *laevis* (2) | #1 (44.9) | 2,345 |
| | #2 (40.4) | 1,380 |
| | #3 (46.9) | 2,305 |
| | #4 (47.5) | 2,396 |
| | #5 (47.1) | 2,356 |
| *polymorpha* (7) | #6 (48.7) | 1,704 |
| | #7 (46.1) | 2,470 |
| | #8 (35.5) | 1,364 |
| | #9 (34.3) | 1,205 |
| | #10 (38.4) | 1,464 |

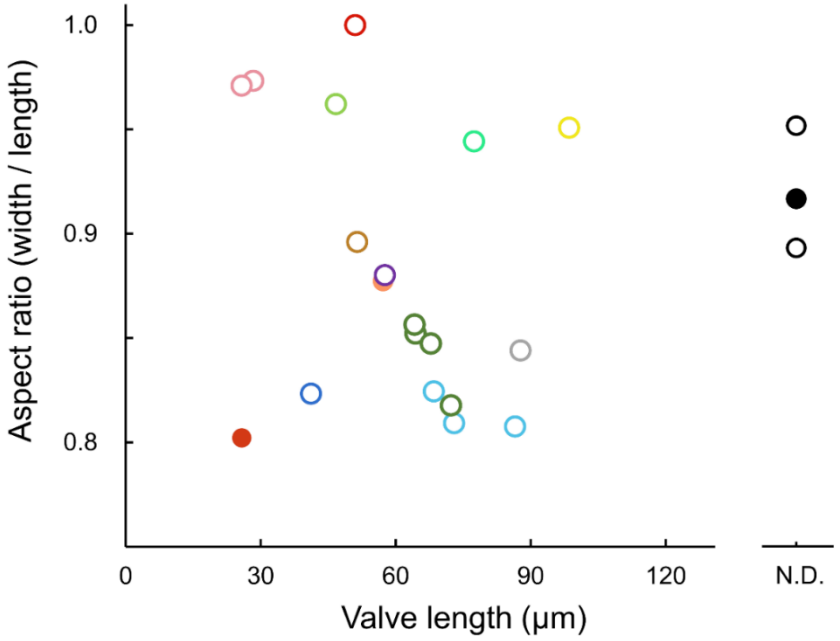


| Form | Reference | |
|---|---|---|
| *laevis* | Gerloff et al. (1978) | pl.1 - fig. 10 (illustration) |
| | Compère (1982)* | fig. 16, 17 (LM) |
| | Tuji & Houki (2001) | pl. 29 - fig. 1 (LM) |
| | Guo-Feng et al. (2008) | fig.1F (LM) |
| | Kim et al. (2008) | fig. 18 (SEM) |
| | Cavalcante et al. (2013) | fig. 12a (LM) |
| | Tuji (2013) | nos. 086 (LM, 2 figs) |
| | Nardelli et al. (2014) | fig. 35 (LM) |
| | T-Krasznai et al. (2014) | fig. 1D (LM) |
| | Sharifinia et al. (2016) | fig. 2 (LM, 4 figs) |
| | Mamanazarova & Gololobova (2017) | fig. 3 (LM), fig. 5, 6 (SEM) |
| | Park et al. (2017) | fig. 17 (SEM) |
| *polymorpha* | Hohn & Hellerman (1966) | pl. 1 - fig. 3 (illustration) |
| | Compère (1982)* | fig. 26 (LM) |
| | Bilous et al. (2021) | fig. 4D (LM) |

*Scale bars are not provided by the author.

**Fig. S1.** Valve aspect ratio based on the images from previous studies.

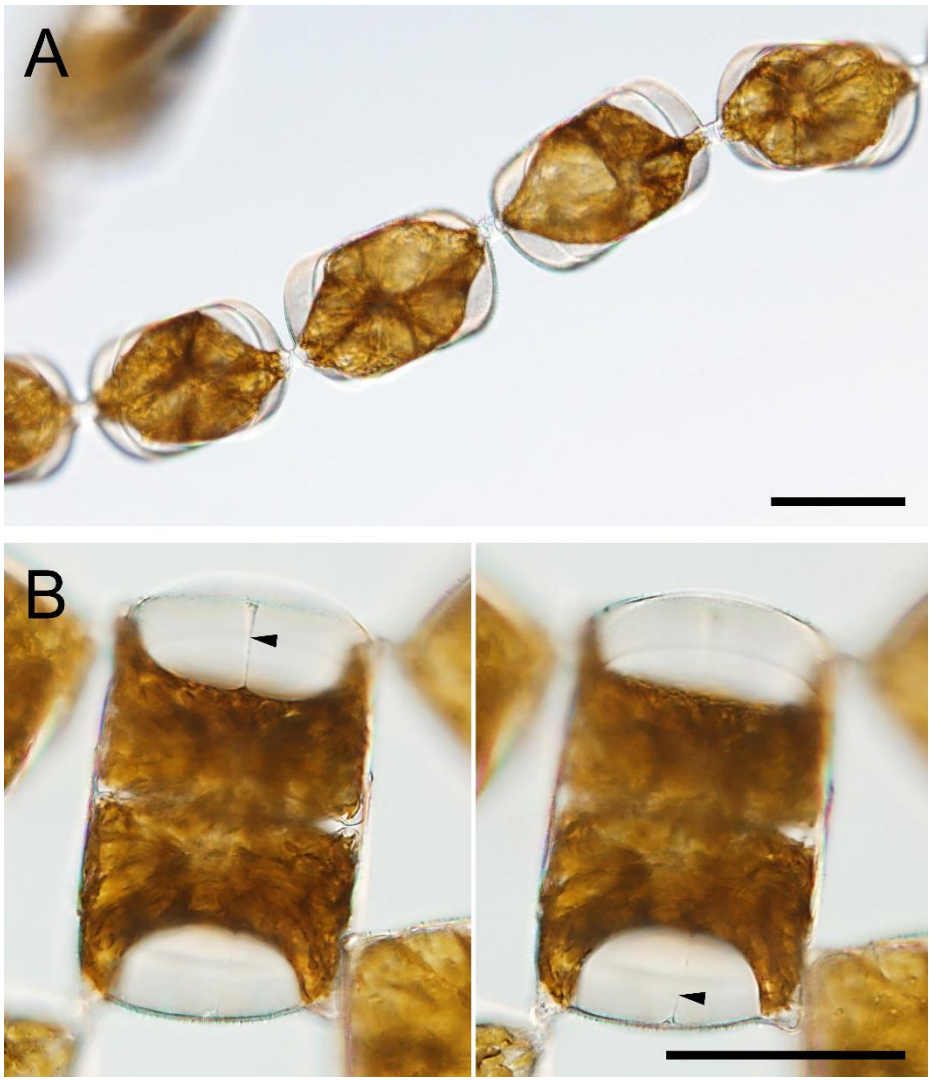


**Fig. S2.** Plasmolysed cells of *Pleurosira laevis*. **(A)** A chain colony. The protoplasts are shrunken but still attached to the valve interior at the ocelli region and girdle elements. **(B)** A cell showing cytoplasmic strands connecting (arrow heads) to the labiate processes. Same cell with different focal planes. Scale bars=100 μm.

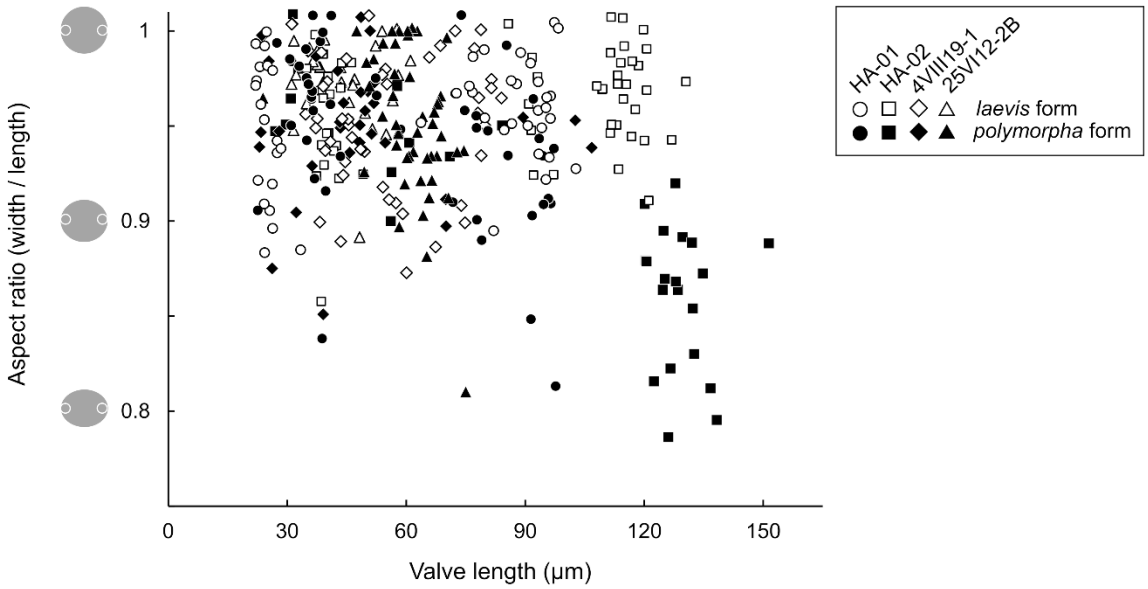


**Fig. S3.** Aspect ratio of valve view. Strains were cultivated at salinities 2 or 7 and used for measurements. The ratio of 1.0 indicates a circle. Open plot: *laevis* form, closed plot: *polymorpha* form. Plot shape represents strain.

CHAPTER 4

# Transcriptional responses to salinity in the polymorphic euryhaline diatom *Pleurosira laevis*

Kamakura S, Bilcke G, Sato S.

## Abstract

Diatoms are unicellular algae characterized by their diverse and intricate silica cell walls called frustules. The mechanism of diatom frustule morphogenesis has received attention both in the biological and nanomaterials engineering fields. However, little is known about the genetic mechanisms that regulate the morphology of frustules. We therefore aimed to search for genes that may be involved in determining the morphology in the centric diatom *Pleurosira laevis*, that can induce distinct morphological changes in its valve (flat to dome-shaped valve face) with only small differences in salinity, though comparative transcriptomes. Under the condition in which *P. laevis* produces a flat valve face, the expression of genes encoding mechanosensitive (MS) ion channels, which sense changes in membrane tension and osmotic pressure and uptake $Ca^{2+}$ into cytosol, was up-regulated. In contrast, expression of genes encoding $Ca^{2+}$ ATPases, which pump $Ca^{2+}$ out of the cell, was decreased, suggesting that intracellular $Ca^{2+}$ levels are elevated. Furthermore, genes encoding annexins, which mediate $Ca^{2+}$-dependent membrane-actin filament association, and Arp2/3, the nucleation site of new actin filaments, were up-regulated. We hypothesize that the morphogenesis related to osmotic pressure observed in some genera of diatoms may be achieved thorough an upstream response involving osmotic pressure- and membrane tension-dependent regulation of intracellular $Ca^{2+}$ levels through the gating of transporters such as mechanosensitive ion channels, and a downstream response involving $Ca^{2+}$-dependent regulation of actin dynamics at membrane contact sites.

## Introduction

Diatoms are microalgae distributed in a wide range of aquatic and terrestrial environments throughout the world. Diatoms have been proposed to number in the tens of thousands of species (Mann & Vanormelingen 2013). Their major feature is that they have cell walls called frustules composed of silica. The frustule consists of two valves and girdle elements. The morphogenesis of frustules occurs in silica deposition vesicles (SDVs), which are compartments separated by lipid bilayer membranes located immediately beneath the plasma membrane of dividing daughter cells (Pickett-Heaps et al. 1990, Kröger & Poulsen 2008). The morphology of the SDV and its internal forming frustule is controlled by cytoskeletons in the vicinity of the SDV (Pickett-Heaps et al. 1990, Tesson & Hildebrand 2010a). The cytoskeleton defines the position of the outer edge of the valve and structures (Tesson & Hildebrand 2010a, b), and influences the pattern of the pores (Pickett-Heaps et al. 1990). Furthermore, some proteins involved in silica mineralization and frustule formation have been identified (Kröger et al. 2002, Scheffel et al. 2011, De Sanctis et al. 2016, Görlich et al. 2019, Tesson et al. 2017, Trofimov et al. 2019, Nemoto et al. 2020, Heintze et al. 2022). For example, dAnk proteins were found to affect the pore pattern on the valves in the model diatom

*Thalassiosira pseudonana* (Heintze et al. 2022). Since the species-specific morphology and structure of diatoms may be tied to their function and contribute to the fitness of individuals (Finkel & Kotrc 2010). The biosynthesis of the frustules with spices specific morphologies have been a fascinating biological inquiry. In addition, morphogenesis of diatoms is of interest in terms of their application to technologies for the massively parallel production of silica nanomaterials by self-assembly (Kröger & Poulsen 2008).

Schmid (1987) proposed that the three-dimensional morphology of the valves might be controlled by the pressure on the daughter plasma membrane at cleavage furrow, exerted by turgor pressure due to extracellular osmotic pressure. The association between osmotic pressure and valve morphology is supported with morphological changes in *Skeletonema* species (Paasche et al. 1975, Balzano et al. 2011) and *Pleurosira laevis* (Kamakura et al. 2022). Kamakura et al. (2022) showed that *P. laevis* changes its valve morphology in response to the environmental osmotic pressure. *Pleurosira laevis* forms a flat valve face at salinity 2, whereas it forms a dome-shaped valve face at salinity 7. This morphological response is conserved among the strains collected from different environments. The obvious morphological plasticity seen in *P. laevis* is a rare characteristic of diatoms, and makes this species ideal for examining the underlying molecular basis of three-dimensional morphogenesis. In the present study, we aimed to characterize gene expression of *P. laevis* cultivated under the condition of salinity 2 and 7 to explore genes that are involved in the regulation of diatom morphology through comparative transcriptome analysis. Since the difference in our salinity contrast (salinity 2 *vs.* salinity 7) was not large, we expected to detect smaller number of differentially expressed genes (DEGs) involved in the osmoregulation than, for example, when comparing the response to freshwater (salinity 0) *vs.* seawater (salinity >30).

## Materials and methods

### Culture

The strains HA-01 and HA-02 of *P. laevis* obtained in Kamakura et al. (2022) were cultivated using WC medium (Guillard & Lorenzen 1972) modified to salinity 2 and 7 by adding Salt Stock described by Nakov et al. (2020). The media were adjusted to pH 8 by dropwise addition of 1M HCl, then sterilized through a membrane filter (pore size 0.2 μm, Mixed Cellulose Ester, Advantec, Tokyo, Japan). Cells were cultivated at salinity 2 or 7, 18°C, light:dark = 12:12, cold white light, *ca.* 50 μmol photons $m^{-2}・s^{-1}$, in culture flasks (Nunc EasYFlask Cell Culture Flasks, Thermo Fisher Scientific, Massachusetts, USA).

### RNA extraction and sequencing

Cells cultivated at salinity 2 or 7 for more than one month were collected on membrane filters (8 μm pore size, Polycarbonate, Advantec), and total RNA was extracted by the cetyltrimethylammonium bromide method (Imaizumi et al. 2000). The experiment was performed in triplicate for the 2 strains under the 2 salinity conditions, resulting in 12 samples. RNA

concentration was measured using a Qubit 4 Fluorometer (Thermo Fisher Scientific). cDNA libraries were prepared using TruSeq Stranded mRNA Library Prep Kit (Illumina, California, USA). Sequencing on a NovaSeq 6000 system (Illumina, paired-end, read length 100 bp) yielded 5.7-7.2 Gb of reads from each sample.

## *de novo* assembly

Pre-processing by fastp ver. 0.20.0 (Chen et al. 2018) was performed with default parameters to remove sequencing adapters and error-prone sequences from datasets. Next, *de novo* assembly was performed by Trinity ver. 2.14.0 (Grabherr et al. 2011) with default parameters combining the preprocessed data sets of total 12 paired-end reads of strains HA-01 and HA-02. Sequence redundancy was eliminated by clustering sequences with >95% homology using CD-HIT ver. 4.8.1 (Fu et al. 2012), then sequences shorter than 500 bp were removed using seqkit ver. 0.13.2 (Shen et al. 2016).

The assembled contigs were submitted to the metagenomic classifier Kaiju webserver (Menzel et al. 2016, https://kaiju.binf.ku.dk/server) against the NCBI reference protein database (nr +euk, database date 2021-02-24) with default parameters (Greedy mode, minimum match length 11, minimum match score 75, allowed mismatches 5, max E-value 0.01). Sequences classified as bacteria, archaea and opisthokonta were identified as potentially derived from contaminants in culture. The contaminant sequences were removed after DEG detection mentioned in the section below.

## Read count and differential gene expression analysis

Hereafter, the 'gene' of *P. laevis* in our analysis refers to the 'Trinity gene' in the transcriptome defined by the Trinity assembler. Note that the genes in this study contain incomplete sequences and putative transposable elements (TEs). Read counts were performed using RSEM ver. 1.3.3 (Li & Dewey 2011) with the assembled sequences as reference through the Trinity script align_and_estimate_abundance.pl, with default parameters. The counts were summed for each gene, then TMM (Trimmed mean of M value) normalized using the R package edgeR ver. 3.28.0 (Robinson & Oshlack 2010, Robinson et al. 2010). The negative binomial generalized linear model (GLM) test was performed to detect DEGs between salinity 2 and 7. Genes with FDR (False Discovery Rate) <0.05 and fold change >2 between the two salinity conditions were considered as DEGs. The analysis was performed independently for HA-01 and HA-02 by comparing expression levels at salinity 2 *vs.* 7. The number of DEGs shared between HA-01 and HA-02 was calculated by the web application 'Calculate and draw custom Venn diagrams' provided by Ghent University (https://bioinformatics.psb.ugent.be/webtools/Venn/).

To visualize the variation between samples we made a multi-dimensional scaling (MDS) plot by the 'plotMDS' function of the R package limma ver. 3.46.0 (Ritchie et al. 2015) using TMM-normalized read counts. The pairwise distances between the samples were determined based on the log2 fold changes in the 500 most variable genes (except for the contaminant sequences) between the samples. We also made a heatmap based on the Poisson distances between samples

calculated using TMM-normalized read counts by the 'PoissonDistance' function in the R package PoiClaClu ver. 1.0.2.1 (Witten 2011).

## Functional annotation

TransDecoder 5.5.0 (https://transdecoder.github.io/) was used to predict protein coding regions within transcripts and converted to amino acid sequences with '--single_best_only' option. Open reading frames were scanned against Pfam database ver. 33.1 (Mistry et al. 2021) to identify protein domains. The longest sequence for each gene was extracted via seqkit and used for functional annotation. We performed InterProScan (Jones et al. 2014) on Blast2GO ver. 6.0.3 (Conesa et al. 2005, Götz et al. 2008) against InterPro (Paysan-Lafosse et al. 2022) protein signature databases including CATH-Gene3D, SUPERFAMILY, MobiDB-lite, COILS, CDD, HAMAP, PANTHER, TIGRFAMs, PIRSF, PROSITE profiles, and SMART, using the amino acid sequences as queries. We then obtained KEGG pathway annotations via the KofamKOALA web server ver. 2022-08-01 (KEGG release 103.0, Aramaki et al. 2020, https://www.genome.jp/tools/kofamkoala/) with an E-value threshold of 0.01 (default).

We focused on the expression level of the cytoskeletons, actin and its related proteins and tubulin, which are known to be involved in the morphogenesis of the diatom frustule (Tesson & Hildebrand 2010a, b). To search for tubulins and actin-related genes in our dataset, we obtained the amino acid sequences of the model diatoms *T. pseudonana*, *Phaeodactylum tricornutum*, *Pseudo-nitzschia multiseries,* and *Fragilariopsis cylindrus* from the Joint Genome Institute (JGI) PhycoCosm (Grigoriev et al. 2021, https://phycocosm.jgi.doe.gov) and ran OrthoFinder ver. 2.5.2 (Emms & Kelly 2019) with default parameters along with our amino acid sequences of genes of *P. laevis* used for the functional annotation query. We then picked up the genes that formed orthogroups with actin-related proteins identified by Aumeier (2014) and Aumeier et al. (2015), and tubulins identified by Khabudaev et al. (2022) of the model diatoms (Table S1). Since the blastp search (Altschul et al. 1997, Schäffer et al. 2001) with an E-value=0 against our dataset did not return any hits and the hit genes (E-value>0) overlapped among queries, it was difficult to identify the genes encoding cytoskeletones and related proteins based on blastp.

The differentially expressed genes were additionally annotated with GO mapping based on blastp search against NCBI protein database (nr) on Blast2GO with an E-value threshold of 1.0E-3. Up to 10 of the hit database sequences were used for go mapping. DEGs encoding putative transporters were further subjected to the blastp search against the Transporter Classification Database (TCDB, Saier et al. 2021, https://www.tcdb.org/) and assigned TC numbers. The differentially expressed genes encoding putative TEs were additionally annotated based on the transcript nucleotide sequences by blastx ver. 2.9.0+ with E-value threshold of 0.1 against the retrotransposon protein domain database 'CORES' downloaded from the Gypsy Database (GyDB 2.0, Llorens et al. 2011, https://gydb.org/).

## Enrichment analysis

InterPro accessions significantly enriched in DEGs shared in both strains were detected via Fisher's exact test with FDR<0.05, using FatiGO (Al-Shahrour et al. 2007). The accessions assigned to all genes by InterPro Scan were used as background of the analysis. The gene ratios were calculated by dividing the count of each InterPro accession assigned to the shared up- or down-regulated genes by the total count of each accession assigned to all genes.

## Phylogenetic analysis

For phylogenetic analysis of $HCO_3^-$ transporters and TEs, multiple sequence alignments were performed using MAFFT ver. 7.480 (Katoh et al. 2002) with the '--auto' option, and sites with more than 30% gaps were removed using trimAl ver. 1.4.1 (Capella-Gutiérrez et al. 2009). Maximum likelihood trees were constructed using RAxML ver. 8.2.12 (Stamatakis et al. 2014) with the PROTGAMMAAUTO substitution model and 100 bootstrap replicates, and visualized using MEGA ver. 7.0.26 (Kumar et al., 2016). The sequence of *Odontella aurita* used in the analysis of the $HCO_3^-$ transporter was obtained through the following process: the whole transcriptome of *O. aurita* from the MMETSP database (NCBI accession SRR1294405) was pre-processed by fastp, de novo assembled by Trinity, clustered with 90% identity by CD-HIT, and then converted to amino acid sequence by TransDecoder. Orthologs from the whole transcriptome of *O. aurita* were searched for by running Orthofinder along with the amino acid sequences of $HCO_3^-$ transporters from mammals, plants, fungi, and eukaryotic algae listed in 'dataset S1' in Nakajima et al. (2013). Phylogenetic analysis of $HCO_3^-$ transporters was conducted using the amino acid sequences of $HCO_3^-$ transporters from *P. laevis*, *O. aurita*, and organisms listed in dataset S1 in Nakajima et al. (2013), as well as sequences of other diatoms that hit by blastp with the sequences of $HCO_3^-$ transporter of *P. laevis* in the annotation process. For TE analysis, we used the amino acid sequences of CoDi (Ty1/Copia-like elements from diatoms) and GyDi (Ty3/Gypsy from diatoms) provided by Maumus et al. (2009) and the sequences of selected retrotransposons from *P. laevis*, as well as retrotransposons from model organisms (Ty1 and Ty3 from *Saccharomyces cerevisiae*, Copia from *Drosophila melanogaster*, and Tnt1 from *Nicotiana tabacum*). In instances where ORFs derived from a single TE are divided into gag and pol, they were concatenated in the sequence gag-pol for further phylogenetic analysis (note that the ORFs of gag and pol of the model diatoms do not overlap.)

We performed a reconstruction of the ancestral habitat (marine or brackish) based on SSU rDNA gene phylogeny. The SSU rDNA sequences from *Pleurosira* and *Odontella*, and other species phylogenetically close to *P. laevis* (Li et al. 2018) were aligned through ClustalW (Thompson et al. 1994) and manually trimmed to 1,563 bp on BioEdit ver. 7.2.5 (Hall 1999). Maximum likelihood trees were constructed using RAxML with the GTRGAMMA substitution model and 100 bootstrap replicates. The reconstruction of the ancestral habitat were performed under the Markov k-state one-parameter model using Mesquite ver. 3.70 (Maddison & Maddison 2021). The natural growth environments of the selected diatoms were based on the collection sites provided in Roscoff Culture Collection (http://roscoff-culture-collection.org/), and of Schmidt (1875), Ashworth et al. (2013), Li et al. (2018), and Kamakura et al. (2022), as well as appendix 1 in Mann (1999).

## Results and Discussion

### Transcriptome assembly and differential gene expression analysis

The *de novo* transcriptome assembly resulted in 192,661 transcripts (117,658 genes) and the sequences was grouped into 151,568 clusters at 95% identity via CD-HIT. Then, the transcripts were reduced to 72,859 (50,070 genes) by removing sequences shorter than 500 bp. we performed a read count using this assembly as a reference and found that the number of genes detected to be expressed in HA-01 was greater than that in HA-02 by approximately 7,000 to 8,000 (Fig. S1). Protein coding regions in the transcripts were predicted by Transdecoder, yielding amino acid sequences for a total of 60,068 transcripts (33,994 partial sequences and 26,074 complete sequences). The 5,861 contaminant gene sequences identified by Kaiju were removed, resulting in a final set of 38,275 genes.

DEGs were detected with FDR<0.05 and fold change>2. The number of up-regulated genes (DEGs whose expression levels were higher in salinity 2 than salinity 7, i.e. down-regulated in salinity 7) was 2,099 in HA-01 and 2,580 in HA-02, while the number of down-regulated genes (expression levels were higher in salinity 7 than salinity 2, i.e. up-regulated in salinity 7) was 1,978 in HA-01 and 2,577 in HA-02 (Fig. 1). We focused on the functions of up- or down-regulated genes that were shared between the strains HA-01 and HA-02 to understand the core response to salinity behind the morphological plasticity in *P. laevis*.

### Intraspecific variation in responses to salinity in *P. laevis*

An MDS plot (Fig. 2A) and a Poisson-distance heatmap (Fig. 2B) showed that the samples clustered by strain rather than salinity condition. The different responses to salinity between the strains might be due to local adaptations derived from differences in natural habitats: HA-01 was collected from a purely freshwater environment, whereas HA-02 was collected from an environment with a slight salinity flux, with a sporadic inflow of seawater (Kamakura et al. 2022). Recent studies have shown that even within a single diatom species, different strains exhibit various patterns of gene expression (Pargana et al. 2019, Nakov et al. 2020, Pinseel et al. 2022).

### Overview of the functions of shared DEGs

There were more unshared DEGs than shared ones between HA-01 and HA-02 in both the up- and down-regulated gene sets (Fig. 1). InterPro scans were performed on all 38,275 genes, of which 5,280 genes were assigned one or more InterPro accessions. InterPro enrichment analysis showed NAD(P)-binding domain superfamilies (IPR017853), which are found in various enzymes, and Beta-hexosaminidase (IPR029018, IPR025705) and Glycoside hydrolase families (IPR017853, IPR015883) involved in hydrolysis of glycans were enriched in the genes up-regulated strains in salinity 2 (Fig. 1). On the other hand, in the genes down-regulated in salinity 2, the reverse transcriptase (IPR013103), ribonuclease H superfamily (IPR036397, IPR012337), zinc finger CCHC-type (IPR036875, IPR001878), and bicarbonate transporter (IPR003020, IPR011531) were

enriched. All genes assigned to zinc finger CCHC-type from the shared down-regulated genes were hit with reverse transcriptase of *Fragilaria crotonensis* by blastp search in the annotation process.

## Transmembrane transport (Fig. 3, Table S2)

The expression of a gene encoding a putative aquaporin was up-regulated in salinity 2 (TRINITY_DN11354_c0_g1, TC:1.A.8.8). Aquaporins transport water and nonpolar molecule into or out of the cell and contributes to osmoregulation (Matsui et al. 2018), and may also be involved in signal transduction by osmotic sensing (Tyerman et al. 2002, Hill et al. 2004). Consistent with our results, the up-regulation of aquaporins in *Cyclotella cryptica* and *Skeletonema marinoi* under hypoosmotic conditions has been reported (Downey et al. 2022, Pinseel et al. 2022). The betaine/carnitine/choline transporters (TC:2.A.15.1.3) and the proline/betaine transporter (EC:2.A.1.6.4), which Nakov et al. (2020) found to be differentially expressed in the long-term osmotic response of *C. cryptica*, were not found in our DEGs.

**Osmotic sensing and regulation of intracellular $Ca^{2+}$ levels:** Diatoms respond to environmental stimuli, including osmotic stress, depending on changes in calcium homeostasis (Falciatore et al. 2000). *Pleurosira laevis* is known to exhibit plastid assemblage in response to contact stimuli and light irradiation, and this response has been suggested to be essential for $Ca^{2+}$ influx into the cytosol through channels (Makita & Shihira-Ishikawa 1997, Shihira-Ishikawa et al. 2007). The genes up-regulated in salinity 2 included a putative calcium permeable stress-gated cation channel (CSC) 1-like transporter (TRINITY_DN919_c0_g2, TC:1.A.17.3). CSCs are conserved in eukaryotes and are gated by stress signals such as hyperosmotic shock, thus potentially serving as sensors that link stress stimuli to calcium-dependent downstream responses (Hou et al. 2014). Moreover, we found mechanosensitive (MS) ion channels among the shared up-regulated transporters. These channels are transmembrane proteins that directly link mechanical stimuli to ion fluxes and are responsible for sensing and responding to changes in membrane tension (Basu & Haswell 2017). The two genes (TRINITY_DN7153_c0_g1 and TRINITY_DN2800_c0_g2) were putative MscS-like (MSL) channels (TC:1.A.23.4). The MSL channels are directly gated by membrane tension and typically function to prevent cell rupture during hypoosmotic shock (Basu & Haswell 2017). The differential expression of these CSC and MS channels between the condition of salinity 2 and 7 provides the possibility that *P. laevis* is able to sense the difference in osmotic pressure and plasma membrane tension brought by such a relatively small difference in salinity. Activation of MS channels has been reported by Downey et al (2022) in *C. cryptica* in response within 3 hours after hypoosmotic exposure, but there is no report yet showing a long-term (*ca.* 1 month) upregulation as seen in *P. laevis*. In *Ph. tricornutum*, $Ca^{2+}$ signaling induced by elevated cytoplasmic $Ca^{2+}$ level upon hypoosmotic shock is important in cell volume regulation, and this elevation of cytoplasmic $Ca^{2+}$ is possibly due to $Ca^{2+}$ influxes caused by increased cell volume activating MS ion channels (Heliwell et al. 2021). We showed in Kamakura et al. (2022) that the morphological plasticity in the valve of this diatom were induced by osmotic changes brought by the addition of sorbitol to the medium, and discussed that this phenomenon could depend on the plasma membrane tension at the cleavage furrow of daughter protoplasts, which provides valve molding surfaces. Thus, it is tempting to assume that $Ca^{2+}$ signaling brought by gating of the MS channel affects the downstream expression of genes

involved in morphogenesis or cell volume regulation, eventually results in the change in valve morphology.

The three P-type ATPases, which were the most down-regulated in salinity 2, were putative $Ca^{2+}$ ATPases (TC:3.A.3.2.29) based on the TCDB annotation (TRINITY_DN4708_c0_g1, TRINITY_DN17148_c0_g1, and TRINITY_DN15658_c0_g1). $Ca^{2+}$ATPases are located in the plasma membrane or endoplasmic reticulum membrane, and pump out cytosolic $Ca^{2+}$ to the extracellular or endoplasmic reticulum, thereby decreasing intracellular $Ca^{2+}$ concentration to basal levels (Brini & Carafoli 2011). The up-regulation of influx and the down-regulation of efflux of $Ca^{2+}$ suggest that *P. laevis* directed toward maintaining intracellular $Ca^{2+}$ levels higher at salinity 2 compared to salinity 7. The regulation of cytosolic $Ca^{2+}$ levels and intracellular $Ca^{2+}$ gradient in *P. laevis* would be verified by single-cell imaging techinique, as performed in *Ph. tricornutum* (Helliwell et al. 2021).

**Sugar transport:** We found the transporters called SWEETs within the down-regulated genes (TRINITY_DN6699_c2_g2 and TRINITY_DN6073_c0_g1, TC:2.A.123.1). SWEET is a new class of sugar transporters found in 2010 (Chen et al. 2010), which are responsible for the flux of sugar molecules across the membrane and are known to be involved in various physiological processes in plants, including environmental stress responses (Breia et al. 2021, Gautam et al. 2022). Diatom genomes contain SWEET homologs (Jia et al. 2017). However, to our knowledge, there is no information on the function and the expression of this transporter in diatoms. Since sugars act as compatible solutes (Suescún-Bolívar et al. 2015), the down-regulation of SWEETs might be explained by the uptake of extracellular sugars at higher osmotic pressures, and may contribute to osmotic regulation.

**Bicarbonate transport:** Five bicarbonate transporters ($HCO_3^-$ transporters) were down-regulated in salinity 2 (TRINITY_DN24295_c0_g1, TRINITY_DN1401_c3_g2, TRINITY_DN36612_c1_g2, TRINITY_DN5264_c0_g1 and TRINITY_DN8091_c0_g1, TC:2.A.31.1 or 2). Although meanwhile one putative bicarbonate transporter (TRINITY_DN17683_c0_g1) was up-regulated in salinity 2, the enrichment analysis based on InterPro accessions showed a significant enrichment of the bicarbonate transporter in the down-regulated genes (Fig. 3). Some $HCO_3^-$ transporters have been investigated in *Ph. tricornutum.* Nakajima et al. (2013) and Nawaly et al. (2023) found that SLC4 (Solute carrier 4) -1 and 2 of *Ph. tricornutum* uptakes $HCO_3^-$ from seawater in a $Na^+$-dependent manner, and suggested that it is an effective $CO_2$ concentrating mechanism for marine diatoms to overcome $CO_2$ limitation in alkaline high-salinity water, while the SLC4-4 of *Ph. tricornutum* has a broad selectivity for cations, depending on $Na^+$, $K^+$, and $Li^+$ (Nawaly et al. 2023). The putative $HCO_3^-$ transporters of *P. laevis* may be $Na^+$ and cation dependent as seen in *Ph. tricornutum*, although they were located in different clades than these SLC4s on the phylogenetic tree (Fig. S2). The finding that *P. laevis* regulates $HCO_3^-$ transport in response to salinity may explain the culture experiment (Kamakura et al. 2022) and field observations (Wujek & Welling 1981, Kociolek et al. 1983, Bąk et al. 2020) that this diatom grows well in saline environments. All species described so far in the genus *Pleurosira* except for *P. laevis* and *P. indica* are marine (Compère 1982, Karthick & Kociolek 2011, Li et al. 2018). Moreover, it is likely that the ancestor of *P. laevis* was marine (Fig. S3), and the $HCO_3^-$ transporter is derived from the last common ancestor of *Pleurosira* clade.

## Candidate genes involved in cell wall morphogenesis

Genes encoding putative Arp2/3 and annexin were up-regulated in salinity 2 (TRINITY_DN19486_c0_g1 and TRINITY_DN914_c0_g1, Table S1). Arp2/3 serves as nucleation sites for the formation of new actin filaments. Annexins, which are known to be involved in various cellular functions, have been shown to be involved in $Ca^{2+}$ influx through the plasma membrane (Demidchik et al. 2018). Additionally, annexins link $Ca^{2+}$ signaling and actin dynamics at membrane contact sites by binding to membrane phospholipids in a $Ca^{2+}$-dependent manner, thereby organizing the relationship between the membrane and cytoskeleton (Hayes et al. 2004). Furthermore, it plays a role in plasma membrane repair through actin cytoskeleton remodeling triggered by $Ca^{2+}$ influx upon membrane injury (Koerdt et al. 2019). The activation of annexin in salinity 2 in *P. laevis* may be due to an increase in cytosolic $Ca^{2+}$ concentration as a result of channel gating by membrane tension and osmotic gradient. Although the involvement of annexin in diatom morphogenesis is not known and needs further investigation, including cellular localization analysis, it is interesting to speculate that annexin may be involved in the control of the morphology of SDV or the daughter plasma membrane to determine the resulting valve morphology on a micrometers scale.

One of the genes up-regulated in salinity 2, containing SET domain, showed a blastp hit with BacSET2 (Nemoto et al. 2020) (TRINITY_DN6649_c0_g1). The BacSET protein family is a recently identified family of methyltransferases that is up-regulated during diatom morphogenesis and potentially target long chain polyamine (LCPA) and proteins related to silica formation as substrates (Nemoto et al. 2020). The role of this protein is not clear yet, but it deserves attention as one of possible candidates for affecting valve morphology. In addition, one of the genes up-regulated in salinity 2 is a homolog of frustulin of *Fistulifera pelliculosa* (GenBank accession CAA67704) with E-value=2E-8 (TRINITY_DN3338_c0_g2). Frustulin is a family of proteins isolated from the frustules and suggested to be essential for cell wall biosynthesis of diatoms (Kröger et al. 1996), therefore its expression levels could affect the morphogenesis.

We detected differential expressions of genes of unknown function, containing ankyrin repeat (Table S4). This domain mediates protein-protein interactions and is involved in many cellular functions (Mosavi et al. 2004). It has been suggested that ankyrin repeat-bearing proteins might play a general role in silica biosynthesis in diatoms (Bilcke et al. 2021, Heintze et al. 2022). The function of the candidate genes involved in this sequence of reactions could be revealed by gene knockout or knockdown techniques as is used in studies of morphogenesis in the model diatom *T. pseudonana* (Görlich et al. 2019, Heintze et al. 2022).

## Intracellular transport

We observed several DEGs related to membrane trafficking and motor protein activity (Table S5). SDVs are believed to be generated by fusion of vesicles, possibly of Golgi origin (Schmid & Schulz 1979, Pickett-Heaps et al. 1990), thus membrane trafficking is required for frustule morphogenesis inside SDVs. Heintze et al. (2022) picked up clathrin coat proteins, Arf, Rab, and v-SNARE by proteomic analysis of SDVs as candidates for proteins involved in vesicular transport required for

SDV biogenesis in *T. pseudonana*. In addition, motor proteins such as dynein and myosin are also expected to play a potential role in diatom morphogenesis based on their ability to bind to the cytoskeleton and their involvement in vesicular transport (Shrestha et al. 2012, Tanaka et al. 2015).

## Transposable elements

Putative TEs were abundant among DEGs, particularly among those that were down-regulated in salinity 2 (Fig. 5, Table S5). This result is further supported by the enrichment of TE-related InterPro accessions among the genes down-regulated in salinity 2 (Fig. 1). TEs were also abundant in DEGs that were not shared between strains (Table S6). The TEs of *P. laevis* were found to contain both retrotransposons that move within the genome via a 'copy-and-paste' mechanism, and putative DNA transposon that move via a 'cut-and-paste' mechanism. The differentially expressed retrotransposons were distributed across the CoDi1-7 classification (Fig. S4). The putative DNA transposons were annotated as PiggyBac, Transposase IS4, and Tigger transposable element-derived protein (Table S5, S6). TEs are known to be often activated under environmental changes or stress conditions (Casacuberta & González 2013). In diatoms, up-regulation of TEs has been reported in response to thermal stress (Egue et al. 2015), high biomass density (Oliver et al. 2010), and elevated $pCO_2$ (Huang et al. 2019) in *Ph. tricornutum*, presence of grazer in *S. marinoi* (Amato et al. 2018), and cold stress in *Leptocylindrus aporus* (Pargana et al. 2019). In Pinseel et al. (2022), lower salinity condition triggered down-regulation of TEs in *S. marinoi*. TEs can induce a wide range of mutations, ranging from subtle regulatory mutations to major genomic rearrangements. Because of their ability to generate the mutations and their responsiveness and sensitivity to environmental change, they have been thought to play a relevant role in adaptation (Casacuberta & González 2013). TEs might have resulted in genetic diversity that has enabled diatoms to adapt successfully to various environments (Maumus et al. 2009) although there is no evidence for a specific role for diatoms in environmental adaptation so far.

*Pleurosira laevis* is regarded as an invasive species in Great Lakes in US and in Europe (Hulme et al. 2009, Litchman et al. 2010, Olenin et al. 2017). This diatom was first described in Hudson River, New York, US (Bailey 1842, Ehrenberg 1843), and found in Natal, Brazil (Roper 1859) and along the 'shores of North and South America' according to Pritchard (1861). However, its distribution has been expanded as documented by more recent reports of first appearances in various regions (e.g., Lake Michigan, US - Wujek & Welling 1981, Czech Republic - Fránková-Kozáková et al. 2007, China - Guo-Feng et al. 2008, Korea - Kim et al. 2008, Uzbekistan - Mamanazarova & Gololobova 2017). TEs may facilitate successful invasion of alien species by promoting rapid adaptation to the environment (Stapley et al. 2015). In some invasive plants and animals, genomic evolution resulting from TE explosions has been suggested to potentially facilitate adaptation (Liu et al. 2018, Su et al. 2021). The activation of TEs in *P. laevis* with slight salinity differences between salinity 2 and 7 might be related to the invasive aspect of this species.

## Metabolic differences of *P. laevis* between salinity 2 and 7

Mapping to metabolic pathways by KofamKoala resulted in annotations for 4,990 of the 38,275 genes. Two genes involved in Calvin cycle (EC:4.1.2.13 and EC:5.3.1.6) were down-regulated and 3

genes in TCA cycle (EC:1.3.5.1, 4.2.1.2 and EC:2.3.3.1) were up-regulated in salinity 2 (Fig. S5). Some enzymes involved in glycolysis/glycogenesis (EC:2.7.1.2, 3.1.3.11, 2.7.1.90, 4.1.2.13, 5.4.2.11 and 2.7.1.40) showed up- or down-regulation in salinity 2 (Fig. S5).

Polysaccharide chrysolaminarin (1,3-$\beta$-glucan) is a storage substance in diatoms (Kroth et al. 2008). The 1,3-beta-glucan synthase (EC:2.4.1.34), which is involved in the biosynthesis of chrysolaminarin, is down-regulated in salinity 2, while glucan 1,3-beta-glucosidase (EC:3.2.1.58), which catalyzes the reaction to produce glucose from chrysolaminarin (Table S7), was up-regulated in salinity 2. *Pleurosira laevis* likely requires less storage polysaccharide in salinity 2 than in salinity 7.

Diatoms can adjust membrane permeability by changing fatty acid and lipid composition in response to salinity (Sayanova et al. 2017). Furthermore, lipid accumulation is characteristic of the stress response in microalgae (Kumar et al. 2019). Genes encoding S-malonyltransferase (EC:2.3.1.39) involved in fatty acid biosynthesis were up-regulated in salinity 2. However, genes encoding acyl-CoA oxidase (EC:1.3.3.6), butyryl-CoA dehydrogenase (EC:1.3.8.1), acyl-CoA dehydrogenase (EC:1.3.8.7), short-chain 2-methylacyl-CoA dehydrogenase (EC:1.3.8.5) in fatty acid degradation were also up-regulated in salinity 2 (Table S7). In addition, the long-chain acyl-CoA synthetase (EC:6.2.1.3), which is involved in both biosynthesis and degradation of fatty acid, was down-regulated in salinity 2.

Genes mapped to glycerol-3-phosphate O-acyltransferase (EC:2.3.1.15) and 1-acyl-sn-glycerofl-3-phosphate acyltransferase (EC:2.3.1.51) were down-regulated in salinity 2 (Fig. S6). These enzymes catalyze the biosynthesis of phosphatidic acid (PA) from Glycero-3-phosphate. PA is a potent signaling molecule, and regulates membrane trafficking, secretion, and cytoskeletal rearrangement (Wang et al. 2006). The production of PA is trigged by both hypo- and hyper-osmotic stresses in plant (Testerink & Munnik 2005). Moreover, cytidine diphosphate-diacylglycerol synthase (CDP-DAG synthase, EC:2.7.7.41), which catalyzes the biosynthesis of cytidine diphosphate-diacylglycerol (CDP-DAG) from PA, was down-regulated in salinity 2. CDP-DAG is a key intermediate at a branching point in lipid metabolism involved in the biosynthesis of the major lipids phosphatidylinositol and phosphatidylglycerol. The CDP-DAG synthase activity modulates the signaling mediated by PA and enhance the downstream lipid production, thus regulates the levels of many intracellular lipids (Jennings & Epand 2020). The differential expression of CDP-DAG synthase suggested physiological adjustments in *P. laevis* between salinities 2 and 7.

## Stress responsive gene expression

The gene encoding Glutathione peroxidase (EC:1.11.1.9) involved in ROS degradation was down-regulated in salinity 2. Two genes encoding thioredoxin were up-regulated, and five were down-regulated in salinity 2 (Fig. 4A). Of the xanthophyll cycle, which is known to alleviate oxidative stress in addition to its function in photosynthesis (Latowski et al. 2011), violaxanthin de-epoxidase (EC:1.23.5.1) was up-regulated in salinity 2 while zeaxanthin epoxidase (EC:1.14.15.21) was down-regulated in salinity 2. Genes encoding superoxide dismutase (EC:1.15.1.1) and

peroxiredoxin (EC:1.11.1.24) involved in ROS removal were not included in the DEGs shared between the strains.

Chaperones are activated to counteract the protein aggregation and misfolding are brought by oxidative stress (Reichmann et al. 2018). In addition, heat shock proteins induced in stress conditions have chaperone functions (Hendrick & Hartl 1993). There were more shared down-regulated genes, encoding chaperones, heat shock proteins, and heat shock factors than up-regulated ones (Fig. 4B). Although we did not see significant differences in growth rates and apparent cellular stress in *P. laevis* between salinities 2 and 7 under culture experiments (Kamakura et al. 2022), the cells seem to be sensitively coping with the stress between the conditions.

## Osmolyte biosynthesis

Aquatic organisms are able to adapt to different salinities (different osmotic conditions) by maintaining osmotic balance between the external environment and their cells through transmembrane transport and the synthesis of osmolytes, also known as compatible solutes (Suescún-Bolívar et al. 2015). The organic osmolytes of diatoms are, for example, free proline and other amino acids (Liu & Hellebust 1976a, b, Dickson & Kirst 1987, Krell et al. 2007, 2008, Scholz & Liebezeit 2012), taurine (Jackson et al. 1992), dimethylsulfoniopropionate (DMSP, Lyon et al. 2011, Scholz & Liebezeit 2012, Kettles et al. 2014, Lavoie et al. 2018, Kageyama et al. 2018a) and glycine betaine (Dickson & Kirst 1987, Scholz & Liebezeit 2012, Kageyama et al. 2018b). Two genes encoding pyrroline-5-carboxylate reductase (EC:1.5.1.2, TRINITY_DN8746_c0_g1) and proline iminopeptidase (EC:3.4.11.5, TRINITY_DN71618_c0_g1), which are involved in proline biosynthesis was up-regulated in salinity 2. The former enzyme catalyzes the final step in proline synthesis, and its expression is up-regulated in *F. cylindrus* under high salinity conditions (Krell et al. 2007). Our result was the opposite of the previous study. It should be mentioned that Nakov et al. (2020) and Pinseel et al. (2022) examined transcriptional responses to different salinities after long-term acclimation (120 days and >11 days, respectively), and found that genes involved in proline biosynthesis did not show a consistent response across strains to salinity.

No DEGs were identified in the taurine biosynthesis pathway. This may be due to the low salinity and the small difference between comparisons. Nakov et al. (2020) found that the expression level of the putative gamma-glutamyltranspeptidase/glutathione hydrolase (EC:2.3.2.2 3.4.19.13) involved in taurine biosynthesis in *C. cryptica* did not significantly change at salinity 2 and 12 compared to salinity 0, but significantly decreased at salinity 24 and 36.

Ectoine is known as bacterial osmolyte (Vargas et al. 2008) and may possibly act in osmoregulation in *S. marinoi* (Pinseel et al. 2022). Genes involved in ectoine biosynthesis were not differentially expressed (aspartate kinase [EC:2.7.2.4] TRINITY_DN541_c1_g1; bifunctional aspartokinase/homoserine dehydrogenase 1 [EC:2.7.2.4 1.1.1.3] TRINITY_DN2781_c2_g1 and TRINITY_DN14712_c0_g1; aspartate-semialdehyde dehydrogenase [EC:1.2.1.11] TRINITY_DN113_c12_g1). These enzymes are the same members as those that Pinseel et al. (2022) found their expression in *S. marinoi* and are responsible for the reaction from L-aspartate through L-aspartyl-4-phosphate to L-aspartate 4-semialdehyde synthesis. Although it is insufficient for the

set of enzymes involved in the known ectoine biosynthesis pathway, Pinseel et al. (2022) presumed that either *S. marinoi* have an unknown gene for ectoine synthesis, or they can synthesize such an ectoine precursor and provide it to extracellular bacteria, which then transport the synthesized ectoine back into the diatom cell to function as osmolytes based on the fact that planktonic diatoms exchange metabolites with bacteria (Amin et al. 2015, Fenizia et al. 2020). The present results suggest that *P. laevis* is at least capable of producing precursors of ectoine although it is not known whether the expression of these genes is significantly up-regulated under even stronger osmotic conditions.

No genes involved in glycine betaine biosynthesis and DMSP biosynthesis were found. We performed a local blastp search with default parameters using the methyltransferase (included in the DMSP synthesis pathway) of *T. pseudonana* reported in Kageyama et al. (2018a) as a query against our sequences, but no homologs were found in all genes expressed in *P. laevis*. Scholz & Liebezeit (2012) exposed benthic diatoms to salinities ranging from 0.5 to 50 and examined the cellular components within 1 hour and 30 days after the salinity change by thin layer chromatography. They found that DMSP was not detected in *Achnanthes delicatula* nor *Nitzschia constricta* under both conditions. Thus, it seems that some diatom species require little or no DMSP as osmolytes in their short- and long-term salinity responses. To verify the presence or absence of genes required for DMSP biosynthesis in *P. laevis*, we need to refer to gene repertoire predicted with the whole genome sequence.

## Conclusion

Our aim was to investigate genes involved in the regulation of diatom morphology using *P. laevis*, which can induce three-dimensional morphological plasticity. Due to the osmotic pressure, the membrane tension of *P. laevis* cells will be greater in salinity 2, than in salinity 7 (Fig. 6A). The results suggested that in salinity 2, which produces a flat valve face, the intracellular $Ca^{2+}$ levels are regulated to be enhanced by the up-regulation of genes encoding mechanosensitive ion channels and down-regulation of genes encoding $Ca^{2+}$ ATPases (Fig. 6B). Furthermore, genes encoding annexin, which mediates membrane-actin filament association in a $Ca^{2+}$-dependent manner, and Arp2/3, which serves as nucleation sites for new actin filaments, were up-regulated in salinity 2. We hypothesized that the morphogenesis related to osmotic pressure may be achieved through 1) an upstream response involving osmotic pressure- and membrane tension-dependent regulation of intracellular $Ca^{2+}$ levels through the gating of transporters such as mechanosensitive ion channels, and 2) a downstream response involving $Ca^{2+}$-dependent regulation of actin dynamics at membrane contact sites. It is noteworthy that we detected the sensing of membrane tension by cells, with the change in valve morphology that has been thought to be dependent on membrane tension (Schmid 1987). In addition, the BacSET2 methyltransferase family protein and frustulin, which are suggested to be involved in furstule formation (Kröger et al. 1996, Nemoto et al. 2020), and were found as a candidate involved in the morphological plasticity. It should be noted that expression of ankyrin repeat-containing proteins of unknown function and membrane trafficking were up- or down-regulated, although their cellular localization or targets are yet unclear. In addition, we found that even small differences between salinity 2 and 7 induced regulations of

transporter activity, response to oxidative stress, physiological regulation, and TE activity in this diatom.

## Acknowledgements

The first author SK was supported by Morishita-Jintan Scholarship Foundation. This work was financially supported by JSPS KAKENHI Grant Number 20K06726 and Grant-in-Aid for Scientific Research on Innovative Areas 21A402. NGS data analysis were performed on the NIG supercomputer at ROIS National Institute of Genetics.

## References

Amin, S.A., Hmelo, L.R., van Tol, H.M., Durham, B.P., Carlson, L.T., Heal, K.R., Morales, R.L., Berthiaume, C.T., Parker, M.S., Djunaedi, B., Ingalls, A.E., Parsek, M.R., Moran, M.A. & Armbrust, E.V. (2015) Interaction and signalling between a cosmopolitan phytoplankton and associated bacteria. Nature 522: 98–101.

Al-Shahrour, F., Minguez, P., Tárraga, J., Medina, I., Alloza, E., Montaner, D. & Dopazo, J. (2007) FatiGO +: a functional profiling tool for genomic data. Integration of functional annotation, regulatory motifs and interaction data with microarray experiments. Nucleic Acids Res. 35: W91–W96.

Altschul, S.F., Madden, T.L., Schäffer, A.A., Zhang, J., Zhang, Z., Miller, W. & Lipman, D.J. (1997) Gapped BLAST and PSI-BLAST: a new generation of protein database search programs. Nucleic Acids Res. 25: 3389–3402.

Amato, A., Sabatino, V., Nylund, G.M., Bergkvist, J., Basu, S., Andersson, X.M., Sanges, R., Godhe, A., Kiørboe, T., Selander, E. & Ferrante, I.M. (2018) Grazer-induced transcriptomic and metabolomic response of the chain-forming diatom *Skeletonema marinoi*. ISME J 12: 1594–1604.

Aramaki, T., Blanc-Mathieu, R., Endo, H., Ohkubo, K., Kanehisa, M., Goto, S. & Ogata, H. (2020) KofamKOALA: KEGG Ortholog assignment based on profile HMM and adaptive score threshold. Bioinformatics 36: 2251–2252.

Ashworth, M.P., Nakov, T. & Theriot, E.C. (2013) Revisiting Ross and Sims (1971): toward a molecular phylogeny of the Biddulphiaceae and Eupodiscaceae (Bacillariophyceae). J. Phycol. 49: 1207–1222.

Aumeier, C. (2014) The cytoskeleton of diatoms: Structural and genomic analysis. PhD thesis, University of Bonn, Germany.

Aumeier, C., Polinski, E. & Menzel, D. (2015) Actin, actin-related proteins and profilin in diatoms: a comparative genomic analysis. Mar. Genomics 23: 133–142.

Balzano, S., Sarno, D. & Kooistra, W.H. (2011) Effects of salinity on the growth rate and morphology of ten *Skeletonema* strains. J. Plankton Res. 33:937–945.

Bailey, J.W. (1842) A sketch of the *Infusoria* of the family *Bacillaria*, with some account of the most interesting species which have been found in a recent or fossil state in the United States. Part II. Am. J. Sci. 42: 88–105, plate 2.

Bąk, M., Halabowski, D., Kryk, A., Lewin, I. & Sowa, A. (2020) Mining salinisation of rivers: its impact on diatom (Bacillariophyta) assemblages. Fottea 20: 1–16.

Basu, D. & Haswell, E.S. (2017) Plant mechanosensitive ion channels: an ocean of possibilities. Curr. Opin. Plant Biol. 40: 43–48.

Bilcke, G., Osuna-Cruz, C. M., Santana Silva, M., Poulsen, N., D'hondt, S., Bulankova, P., Vyverman, W., De Veylder, L. & Vandepoele, K. (2021) Diurnal transcript profiling of the diatom *Seminavis robusta* reveals adaptations to a benthic lifestyle. Plant J. 107: 315–336.

Breia, R., Conde, A., Badim, H., Fortes, A.M., Gerós, H. & Granell, A. (2021) Plant SWEETs: from sugar transport to plant-pathogen interaction and more unexpected physiological roles. Plant Physiol. 186: 836–852.

Brini, M. & Carafoli, E. (2011) The plasma membrane $Ca^{2+}$ ATPase and the plasma membrane sodium calcium exchanger cooperate in the regulation of cell calcium. Cold Spring Harb. Perspect. Biol. 3: a004168.

Capella-Gutiérrez, S., Silla-Martínez, J.M. & Gabaldón, T. (2009) trimAl: a tool for automated alignment trimming in large-scale phylogenetic analyses. Bioinformatics 25: 1972–1973.

Casacuberta, E., & González, J. (2013) The impact of transposable elements in environmental adaptation. Mol. Ecol. 22: 1503–1517.

Chen, L.Q., Hou, B.H., Lalonde, S., Takanaga H., Hartung, M.L., Qu X.Q., Guo, W.J., Kim, J.G., Underwood, W., Chaudhuri, B., Chermak, D., Antony, G., White, F.F., Shauna, S.C., Mudgett, M.B. & Frommer, W.B. (2010) Sugar transporters for intercellular exchange and nutrition of pathogens. Nature 468: 527–532.

Chen, S., Zhou, Y., Chen, Y. & Gu, J. (2018) fastp: an ultra-fast all-in-one FASTQ preprocessor. Bioinformatics 34: i884–i890.

Compère, P. 1982. Taxonomic revision of the diatom genus *Pleurosira* (Eupodiscaceae). Bacillaria 5:165–90.

Conesa, A., Götz, S., García-Gómez, J.M., Terol, J., Talón, M., Robles, M. (2005) Blast2GO: a universal tool for annotation, visualization and analysis in functional genomics research. Bioinformatics 21: 3674–3676.

Demidchik, V., Shabala, S., Isayenkov, S., Cuin, T.A. & Pottosin, I. (2018) Calcium transport across plant membranes: mechanisms and functions. New Phytol. 220: 49–69.

De Sanctis, Michael Wenzler, Nils Kröger, Wilhelm M. Malloni, Manfred Sumper, Rainer Deutzmann, Zadravec, P., Brunner, E., Kremer, W. & Kalbitzer, H.R. (2016) PSCD domains of Pleuralin-1 from the diatom *Cylindrotheca fusiformis*: NMR structures and interactions with other biosilica-associated proteins. Structure 24: 1178–1191.

Dickson, D.M.J. & Kirst, G.O. (1987) Osmotic adjustment in marine eukaryotic algae: The role of inorganic ions, quaternary ammonium, tertiary sulphonium and carbohydrate solutes. I. Diatoms and a rhodophyte. New Phytol. 106: 645–655.

Downey, K.M., Judy, K.J., Pinseel, E., Alverson, A.J. & Lewis, J.A. (2022) The dynamic response to hypo-osmotic stress reveals distinct stages of freshwater acclimation by a euryhaline diatom. Mol Ecol. DOI: 10.1111/mec.16703.

Egue, F., CHENAIS, B., Tastard, E., Marchand, J., Hiard, S., Gateau, H., Hermann, D., Morant-Manceau, A., Casse, N. & Caruso, A. (2015) Expression of the retrotransposons *Surcouf* and *Blackbeard* in the marine diatom *Phaeodactylum tricornutum* under thermal stress. Phycologia 54: 617–627.

Ehrenberg, C.G. (1843) Verbreitung und Einfluß des mikroskopischen Lebens in Süd- und Nord-Amerika. Abhandlungen der Königlichen Akademie der Wissenschaften zu Berlin, 1841: 291–445, 4 Tafel.

Emms, D.M. & Kelly, S. (2019) OrthoFinder: phylogenetic orthology inference for comparative genomics. Genome Biol. 20: 238.

Falciatore, A., d'Alcalà, M.R., Croot, P. & Bowler, C. (2000) Perception of environmental signals by a marine diatom. Science 288: 2363–2366.

Fenizia, S., Thume, K., Wirgenings, M. & Pohnert, G. (2020) Ectoine from bacterial and algal origin is a compatible solute in microalgae. Mar. Drugs 18: 42.

Finkel, Z.V. & Kotrc, B. (2010) Silica use through time: macroevolutionary change in the morphology of the diatom frustule. Geomicrobiol. J. 27: 596–608.

Fránková-Kozáková, M., Marvan, P. & Geriš, R. (2007) Halophilous diatoms in Czech running waters: *Pleurosira laevis* and *Bacillaria paxillifera*. In Proceedings of the 1st Central European Diatom Meeting. Berlin, Germany. pp. 39–44.

Fu, L., Niu, B., Zhu, Z., Wu, S. & Li, W. (2012) CD-HIT: accelerated for clustering the next-generation sequencing data. Bioinformatics 28: 3150–3152.

Gautam, T., Dutta, M, Jaiswal, V., Zinta, G., Gahlaut, V. & Kumar, S. (2022) Emerging roles of SWEET sugar transporters in plant development and abiotic stress responses. Cells 11: 1303.

Görlich, S., Pawolski, D., Zlotnikov, I. & Kröger, N. (2019) Control of biosilica morphology and mechanical performance by the conserved diatom gene Silicanin-1. Commun. Biol. 2: 1–8.

Götz, S., Garcia-Gomez, J.M., Terol, J., Williams, T.D., Nagaraj, S.H., Nueda, M.J., Robles, M., Talon, M., Dopazo, J. & Conesa, A. (2008) High-throughput functional annotation and data mining with the Blast2GO suite. Nucleic Acids Res. 36: 3420–3435.

Grabherr, M., Haas, B.J., Yassour, M., Levin, J. Z., Thompson, D.A., Amit, I., Adiconis X, Fan L., Raychowdhury R., Zeng Q., Chen, Z., Mauceli E., Hacohen, N, Gnirke, A., Rhind, N., Palma, F., Birren, B.F., Nusbaum, C., Lindblad-Toh, K., Friedman, N. & Regev, A. (2011) Full-length transcriptome assembly from RNA-Seq data without a reference genome. Nat. Biotechnol. 29: 644–652.

Grigoriev I.V., Hayes, R.D., Calhoun, S., Kamel, B., Wang, A., Ahrendt, S., Dusheyko, S., Nikitin, R., Mondo, S.J., Salamov, A., Shabalov, I. & Kuo, A. (2021) PhycoCosm, a comparative algal genomics resource. Nucleic Acids Res. 49: D1004–D1011.

Guillard, R.R. & Lorenzen, C.J. (1972) Yellow-green algae with chlorophyllide C 1, 2. J. Phycol. 8: 10–14.

Guo-Feng, P., Guo-Xiang, L., Zheng-Yu, H. & Guo-Xiang, L. (2008) *Pleurosira laevis* (Ehrenberg) Compère, a new record freshwater diatom from China. J. Wuhan Bot. Res. 26: 458–460.

Hall, T. (1999) BioEdit: a user-friendly biological sequence alignment editor and analysis program for Windows 95/98/NT. Nucleic Acids Symp. Ser. 41: 95–98.

Hayes, M.J., Rescher, U., Gerke, V. & Moss, S.E. (2004) Annexin–actin interactions. Traffic 5: 571–576.

Heintze, C., Babenko, I., Zackova Suchanova, J., Skeffington, A., Friedrich, B.M. & Kröger, N. (2022) The molecular basis for pore pattern morphogenesis in diatom silica. Proc. Natl. Acad. Sci. U.S.A 119: e2211549119.

Helliwell, K.E., Kleiner, F. H., Hardstaff, H., Chrachri, A., Gaikwad, T., Salmon, D., Smirnoff, N., Wheeler, G.L. & Brownlee, C. (2021) Spatiotemporal patterns of intracellular $Ca^{2+}$ signalling govern hypo-osmotic stress resilience in marine diatoms. New Phytol. 230: 155–170.

Hendrick, P.J. & Hartl, F.U. (1993) Molecular chaperone functions of heat-shock proteins. Annu. Rev. Biochem. 62: 349–384.

Hou, C., Tian, W., Kleist, T., He, K., Garcia, V., Bai, F., Hao, Y., Luan, S. & Li, L. (2014) DUF221 proteins are a family of osmosensitive calcium-permeable cation channels conserved across eukaryotes. Cell Res. 24: 632–635.

Hill, A., Shachar-Hill, B. & Shachar-Hill, Y. (2004) What Are Aquaporins For? J. Membrane Biol. 197: 1–32.

Huang, R., Ding, J., Gao, K., Cruz de Carvalho, M.H., Tirichine, L., Bowler, C. & Lin, X. (2019) A potential role for epigenetic processes in the acclimation response to elevated $pCO_2$ in the model diatom *Phaeodactylum tricornutum*. Front. Microbiol. 9: 3342.

Hulme, P.E. et al., eds (2009) Delivering Alien Invasive Species Inventories for Europe (DAISIE) Handbook of alien species in Europe, invading nature - springer series in invasion ecology vol. 3. Dordrecht, Netherlands, Springer, 382 pp.

Imaizumi, T., Kanegae, T. & Wada, M. (2000) Cryptochrome nucleocytoplasmic distribution and gene expression are regulated by light quality in the fern Adiantum capillus-veneris. The Plant Cell 12: 81–95.

Jackson, A.E., Ayer, S.W. & Laycock, M.V. (1992) The effect of salinity on growth and amino acid composition in the marine diatom *Nitzschia pungens*. Can. J. Bot. 70: 2198–2201.

Jennings, W. & Epand, R.M. (2020) CDP-diacylglycerol, a critical intermediate in lipid metabolism. Chem. Phys. Lipids 230: 104914.

Jia, B., Zhu, X.F., Pu, Z.J., Duan, Y.X., Hao, L.J., Zhang, J., Chen L.Q., Jeon, C.O. & Xuan, Y.H. (2017) Integrative view of the diversity and evolution of SWEET and SemiSWEET sugar transporters. Front. Plant Sci. 8: 2178.

Jones, P., Binns, D., Chang, H.Y., Fraser, M., Li, W., McAnulla, C., McWilliam, H., Maslen, J., Mitchell, A., Nuka, G., Pesseat, S., Quinn, F.A., Sangrador-Vegas, A., Scheremetjew, M., Yong, S.Y., Lopez, R. & Hunter, S. (2014) InterProScan 5: genome-scale protein function classification. Bioinformatics 30: 1236–1240.

Kageyama, H., Tanaka, Y., Shibata, A., Waditee-Sirisattha, R. & Takabe, T. (2018a) Dimethylsulfoniopropionate biosynthesis in a diatom *Thalassiosira pseudonana*: Identification of a gene encoding MTHB-methyltransferase. Arch. Biochem. Biophys. 645: 100–106.

Kageyama, H., Tanaka, Y. & Takabe, T. (2018b) Biosynthetic pathways of glycinebetaine in *Thalassiosira pseudonana*; functional characterization of enzyme catalyzing three-step methylation of glycine. Plant Physiol. Biochem. 127: 248–255.

Kamakura, S., Ashworth, M.P., Yamada, K., Mikami, D., Kobayashi, A., Idei, M. & Sato, S. (2022) Morphological plasticity in response to salinity change in the euryhaline diatom *Pleurosira laevis* (Bacillariophyta). J. Phycol. 58: 631–642.

Katoh, K., Misawa, K., Kuma, K. & Miyata, T. (2002) MAFFT: a novel method for rapid multiple sequence alignment based on fast Fourier transform. Nucleic Acids Res. 30: 3059–3066.

Karthick, B. & Kociolek, J.P. (2011) Four new centric diatoms (Bacillariophyceae) from the Western Ghats, South India. Phytotaxa 22: 25–40.

Kettles, N. L., Kopriva, S. & Malin, G. (2014) Insights into the regulation of DMSP synthesis in the diatom *Thalassiosira pseudonana* through APR activity, proteomics and gene expression analyses on cells acclimating to changes in salinity, light and nitrogen. PLoS ONE 9: e94795.

Kociolek, J.P., Lamb, M.A. & Lowe, R.L. (1983) Notes on the growth and ultrastructure of *Biddulphia laevis* Ehr. (Bacillariophyceae) in the Maumee River, Ohio. Ohio J. Sci. 83: 125–130.

Koerdt, S.N., Ashraf, A.P.K. & Gerke, V. (2019) Annexins and plasma membrane repair. Curr. Top. Membr. 84: 43–65.

Khabudaev, K.V., Petrova, D.P., Bedoshvili, Y.D., Likhoshway, Y.V. & Grachev, M.A. (2022) Molecular evolution of tubulins in diatoms. Int. J. Mol. Sci. 23: 618.

Kim, Y., Suk Choi, J., Sin Kim, J., Hee Kim, S., Chan Park, J. & Won Kim, H. (2008) The effects of effluent from a closed mine and treated sewage on epilithic diatom communities in a Korean stream. Nova Hedwig. 86: 507–524.

Krell, A., Funck, D., Plettner, I., John, U. & Dieckmann, G. (2007) Regulation of proline metabolism under salt stress in the psychrophilic diatom *Fragilariopsis cylindrus* (Bacillariophyceae). J. Phycol. 43:753–762.

Krell, A., Beszteri, B., Dieckmann, G., Glöckner, G., Valentin, K. & Mock, T. (2008) A new class of ice-binding proteins discovered in a salt-stress-induced cDNA library of the psychrophilic diatom *Fragilariopsis cylindrus* (Bacillariophyceae). Eur. J. Phycol. 43: 423–433.

Kröger, N., Bergsdorf, C. & Sumper, M. (1996) Frustulins: domain conservation in a protein family associated with diatom cell walls. Eur. J. Biochem. 239: 259–264.

Kröger, N., Lorenz, S. & Brunner, E. (2002) Self-assembly of highly phosphorylated silaffins and their function in biosilica morphogenesis. Science 298: 584–586.

Kröger, N. & Poulsen, N. (2008) Diatoms—from cell wall biogenesis to nanotechnology. Annu. Rev. Genet. 42: 83–107.

Kroth, P.G., Chiovitti, A., Gruber, A., Martin-Jezequel, V., Mock, T., Parker, M.S., Stanley, S.M., Kaplan, A., Caron, L., Weber, T., Maheswari, U., Armbrust, E.V. & Bowler, C. (2008) A model for carbohydrate metabolism in the diatom *Phaeodactylum tricornutum* deduced from comparative whole genome analysis. PLoS ONE 3: e1426.

Kumar, B. R., Deviram, G., Mathimani, T., Duc, P. A. & Pugazhendhi, A. (2019) Microalgae as rich source of polyunsaturated fatty acids. Biocatal. Agric. Biotechnol. 17: 583–588.

Kumar, S., Stecher, G. & Tamura, K. (2016) MEGA7: Molecular Evolutionary Genetics Analysis version 7.0 for bigger datasets. Mol. Biol. Evol. 33: 1870–1874.

Latowski, D., Kuczyńska, P. & Strzałka, K. (2011) Xanthophyll cycle –A mechanism protecting plants against oxidative stress. Redox Rep. 16: 78–90.

Lavoie, M., Waller, J.C., Kiene, R.P. & Levasseur, M. (2018) Polar marine diatoms likely take up a small fraction of dissolved dimethylsulfoniopropionate relative to bacteria in oligotrophic environments. Aquat. Microb. Ecol. 81: 213–218.

Li, B. & Dewey, C.N. (2011) RSEM: accurate transcript quantification from RNA-Seq data with or without a reference genome. BMC bioinformatics 12: 1–16.

Li, Y., Nagumo, T. & Xu, K. (2018) Morphology and molecular phylogeny of *Pleurosira nanjiensis* sp. nov., a new marine benthic diatom from the Nanji Islands, China. Acta Oceanol. Sin. 37: 33–39.

Litchman, E. (2010) Invisible invaders: non-pathogenic invasive microbes in aquatic and terrestrial ecosystems. Ecol. Lett. 13: 1560–1572.

Liu, M.S. Hellebust, J.A. (1976a) Effects of salinity and osmolarity of the medium on amino acid metabolism in *Cyclotella cryptica*. Can. J. Bot. 54: 938–948.

Liu, M.S. & Hellebust, J.A. (1976b) Regulation of proline metabolism in the marine centric diatom *Cyclotella cryptica*. Can. J. Bot. 54: 949–959.

Liu, C., Zhang, Y., Ren, Y., Wang, H., Li, S., Jiang, F., Yin, L., Qiao, X., Zhang, G., Qian, W., Liu, B. & Fan, W. (2018) The genome of the golden apple snail *Pomacea canaliculata* provides insight into stress tolerance and invasive adaptation. Gigascience 7: giy101.

Llorens, C., Futami, R., Covelli, L., Dominguez-Escriba, L., Viu, J.M., Tamarit, D., Aguilar-Rodriguez, J. Vicente-Ripolles, M., Fuster, G., Bernet, G.P., Maumus, F., Munoz-Pomer, A., Sempere, J.M., LaTorre, A. & Moya, A. (2011) The Gypsy Database (GyDB) of mobile genetic elements: release 2.0. Nucleic Acids Res. 39, Issue suppl_1: D70–D74.

Lyon, B.R., Lee, P.A., Bennett, J.M., DiTullio, G.R. & Janech, M.G. (2011) Proteomic analysis of a sea-ice diatom: salinity acclimation provides new insight into the dimethylsulfoniopropionate production pathway. Plant Physiol. 157: 1926–1941.

Maddison, W. P. & Maddison, D.R. (2021) Mesquite: a modular system for evolutionary analysis. Version 3.70. http://www.mesquiteproject.org

Makita, N. & Shihira-Ishikawa, I. (1997) Chloroplast assemblage by mechanical stimulation and its intercellular transmission in diatom cells. Protoplasma 197: 86–95.

Mamanazarova, K.S. & Gololobova, M.A. (2017) First record of diatom species *Pleurosira laevis* (Ehrenberg) Compère for Uzbekistan and Central Asia. Russ. J. Biol. Invasions 8: 69–74.

Mann, D.G. (1999) Crossing the Rubicon: the effectiveness of the marine/freshwater interface as a barrier to the migration of diatom germplasm. In Mayama, S., Idei, M. & Koizumi, I. [Eds.] Proceedings of the 14th International Diatom Symposium, Tokyo, 1996. Koeltz, Koenigstein, pp. 1–21.

Mann, D.G. & Vanormelingen, P. (2013) An inordinate fondness? The number, distributions, and origins of diatom species. J. Eukaryot. Microbiol. 60: 414–420.

Matsui, H., Hopkinson, B. M., Nakajima, K. & Matsuda, Y. (2018) Plasma membrane-type aquaporins from marine diatoms function as $CO_2$/$NH_3$ channels and provide photoprotection. Plant Physiol. 178: 345–357.

Maumus, F., Allen, A.E., Mhiri, C., Hu, H., Jabbari, K., Vardi, A., Grandbastien, M.A. & Bowler C. (2009) Potential impact of stress activated retrotransposons on genome evolution in a marine diatom. BMC Genomics 10: 624.

Menzel, P., Ng, K.L. & Krogh, A. (2016) Fast and sensitive taxonomic classification for metagenomics with Kaiju. Nat. Commun. 7: 1–9.

Mistry, J., Chuguransky, S., Williams, L., Qureshi, M., Salazar, G.A., Sonnhammer, E.L.L, Tosatto, S.C.E., Paladin, L., Raj, S., Richardson, L.J., Finn, R.D. & Bateman, A (2021) Pfam: The protein families database in 2021. Nucleic Acids Res. 49: D412–D419.

Mosavi, L.K., Cammett, T.J., Desrosiers, D.C. & Peng, Z. Y. (2004) The ankyrin repeat as molecular architecture for protein recognition. Protein Sci. 13: 1435–1448.

Nakajima, K., Tanaka, A. & Matsuda, Y. (2013) SLC4 family transporters in a marine diatom directly pump bicarbonate from seawater. Proc. Natl. Acad. Sci. U.S.A. 110: 1767–1772.

Nakov, T., Judy, K.J., Downey, K.M., Ruck, E.C. & Alverson, A.J. (2020) Transcriptional response of osmolyte synthetic pathways and membrane transporters in a euryhaline diatom during long-term acclimation to a salinity gradient. J. Phycol. 56: 1712–1728.

Nawaly, H., Matsui, H., Tsuji, Y., Iwayama, K., Ohashi, H., Nakajima, K. & Matsuda, Y. (2023) Multiple plasma membrane SLC4s contribute to external $HCO_3^-$ acquisition during $CO_2$ starvation in the marine diatom *Phaeodactylum tricornutum*. J. Exp. Bot. 74: 296–307.

Nemoto, M., Iwaki, S., Moriya, H., Monden, Y., Tamura, T., Inagaki, K., Mayama, S. & Obuse, K. (2020) Comparative gene analysis focused on silica cell wall formation: identification of diatom-specific SET domain protein methyltransferases. Mar. Biotechnol. 22: 551–563.

Olenin, S., Gollasch, S., Lehtiniemi, M., Sapota, M. & Zaiko, A. (2017) Biological invasions. In Biological Oceanography of the Baltic Sea (pp. 193–232). Springer, Dordrecht.

Oliver, M.J., Schofield, O. & Bidle, K. (2010) Density dependent expression of a diatom retrotransposon. Mar. Genomics 3: 145–150.

Paasche, E., Johansson, S. & Evensen, D.L. (1975) An effect of osmotic pressure on the valve morphology of the diatom *Skeletonema subsalsum* (A. Cleve) Bethge. Phycologia 14: 205–211.

Pargana, A., Musacchia, F., Sanges, R., Russo, M.T., Ferrante, M.I., Bowler, C. & Zingone, A. (2019) Intraspecific diversity in the cold stress response of transposable elements in the diatom *Leptocylindrus aporus*. Genes 11: 9.

Paysan-Lafosse, T., Blum, M., Chuguransky, S., Grego, T., Pinto, B.L., Salazar, A.G., Bileschi, L.M., Bork, P., Bridge, A., Colwell, L., Gough, J., Haft, H.D., Letunić, I., Marchler-Bauer, A., Mi, H., Natale, A.D., Orengo, A.C., Pandurangan, P.A., Rivoire, C., Sigrist, J.A.C., Sillitoe, I., Thanki, N., Thomas, D.P., Tosatto, C.E.S., Wu, H.C. & Bateman, A. (2022) InterPro in 2022. Nucleic Acids Res. gkac993.

Pickett-Heaps, J., Schmid, A.M.M. & Edgar, L.A. (1990) The cell biology of diatom valve formation. Prog. Phycol. Res. 7: 1–168.

Pinseel, E., Nakov, T., Van den Berge, K., Downey, K.M., Judy, K.J., Kourtchenko, O., Kremp, A., Ruck, E.C., Sjöqvist, C., Töpel, M., Godhe, A. & Alverson, A.J. (2022) Strain-specific transcriptional responses overshadow salinity effects in a marine diatom sampled along the Baltic Sea salinity cline. ISME J. 16: 1776–1787.

Pritchard, A. (1861) A history of infusoria, including the Desmidiaceae and Diatomaceae, British and foreign. Fourth edition enlarged and revised by J.T. Arlidge, M.B., B.A. Lond.; W. Archer, Esq.; J. Ralfs, M.R.C.S.L.; W.C. Williamson, Esq., F.R.S., and the author. pp. i-xii, 1–968, 40 pls. London: Whittaker and Co., Ave Maria Lane.

Reichmann, D., Voth, W. & Jakob, U. (2018) Maintaining a healthy proteome during oxidative stress. Mol Cell. 69: 203–213.

Ritchie, M.E., Phipson, B., Wu, D., Hu, Y., Law, C.W., Shi, W. & Smyth, G.K. (2015) limma powers differential expression analyses for RNA-sequencing and microarray studies. Nucleic Acids Res. 43: e47.

Robinson, M.D. & Oshlack, A. (2010) A scaling normalization method for differential expression analysis of RNA-seq data. Genome Biol. 11: R25.

Robinson, M.D., McCarthy, D.J. & Smyth, G.K. (2010) edgeR: a Bioconductor package for differential expression analysis of digital gene expression data. Bioinformatics 26: 139–140.

Roper, F.C.S. (1859) On the genus *Biddulphia* and its affinities. Transactions of the Microscopical Society of London 7: 1–24, pl. 1 & 2.

Saier, M.H., Reddy, V.S., Moreno-Hagelsieb, G., Hendargo, K.J., Zhang, Y., Iddamsetty, V., Lam, K.J.K, Tian, N., Russum, S., Wang, J. & Medrano-Soto, A. (2021) The Transporter Classification Database (TCDB): 2021 update. Nucleic Acids Res. 49: D461–D467.

Sayanova, O., Mimouni, V., Ulmann, L., Morant-Manceau, A., Pasquet, V., Schoefs, B. & Napier, J. A. (2017) Modulation of lipid biosynthesis by stress in diatoms. Philos. Trans. R. Soc. B 372: 20160407.

Scheffel, A., Poulsen, N., Shian, S., & Kröger, N. (2011) Nanopatterned protein microrings from a diatom that direct silica morphogenesis. Proc. Natl. Acad. Sci. U.S.A.108: 3175–3180.

Schäffer, A.A, Aravind, L., Madden, T.L., Shavirin, S., Spouge, J.L., Wolf, Y.I., Koonin, E.V. & Altschul, S.F. (2001) Improving the accuracy of PSI-BLAST protein database searches with composition-based statistics and other refinements. Nucleic Acids Res. 29: 2994–3005.

Schmid, A.M.M. (1987) Morphogenetic forces in diatom cell wall formation. Cytomechanics. Springer, Berlin, Heidelberg. pp. 183–199.

Schmid, A.M.M. & Schulz, D. (1979) Wall morphogenesis in diatoms: deposition of silica by cytoplasmic vesicles. Protoplasma. 100: 267–288.

Schmidt, A.W.F. (1875) Atlas der Diatomaceen-kunde. Series I: Heft 8. pp. pls 29–32. Aschersleben: Verlag von Ernst Schlegel.

Scholz, B. & Liebezeit, G. (2012) Compatible solutes in three marine intertidal microphytobenthic Wadden Sea diatoms exposed to different salinities. Eur. J. Phycol. 47: 393–407.

Shen, W., Le, S., Li, Y., & Hu, F. (2016). SeqKit: a cross-platform and ultrafast toolkit for FASTA/Q file manipulation. PloS one 11: e0163962.

Shihira-Ishikawa, I., Nakamura, T., Higashi, S.I. & Watanabe, M. (2007) Distinct responses of chloroplasts to blue and green laser microbeam irradiations in the centric diatom *Pleurosira laevis*. Photochem. Photobiol. 83: 1101–1109.

Shrestha, R.P., Tesson, B., Norden-Krichmar, T., Federowicz, S., Hildebrand, M. & Allen, A.E. (2012) Whole transcriptome analysis of the silicon response of the diatom *Thalassiosira pseudonana*. BMC Genomics 13: 499.

Stamatakis, A. (2014) RAxML version 8: a tool for phylogenetic analysis and post-analysis of large phylogenies. Bioinformatics 30: 1312–1313.

Stapley, J., Santure, A.W. & Dennis, S.R. (2015) Transposable elements as agents of rapid adaptation may explain the genetic paradox of invasive species. Mol. Ecol. 24: 2241–2252.

Su, Y., Huang, Q., Wang, Z. & Wang, T. (2021) High genetic and epigenetic variation of transposable elements: Potential drivers to rapid adaptive evolution for the noxious invasive weed Mikania micrantha. Ecol. Evol. 11: 13501–13517.

Suescún-Bolívar, L.P. & Thomé, P.E. (2015) Osmosensing and osmoregulation in unicellular eukaryotes. World J. Microbiol. Biotechnol. 31: 435–443.

Tanaka, A., De Martino, A., Amato, A., Montsant, A., Mathieu, B., Rostaing, P., Tirichine, L. & Bowler, C. (2015) Ultrastructure and membrane traffic during cell division in the marine pennate diatom *Phaeodactylum tricornutum*. Protist 166: 506–521.

Tesson, B. & Hildebrand, M. (2010a) Extensive and intimate association of the cytoskeleton with forming silica in diatoms: control over patterning on the meso- and micro-scale. PloS one 5: e14300.

Tesson, B. & Hildebrand, M. (2010b) Dynamics of silica cell wall morphogenesis in the diatom *Cyclotella cryptica*: substructure formation and the role of microfilaments. J. Struct. Biol. 169: 62–74.

Tesson, B., Lerch, S.J.L. & Hildebrand, M. (2017) Characterization of a new protein family associated with the silica deposition vesicle membrane enables genetic manipulation of diatom silica. Sci. Rep. 7: 1–13.

Testerink, C. & Munnik, T. (2005) Phosphatidic acid: a multifunctional stress signaling lipid in plants. Trends Plant Sci. 10: 368–375.

Thompson, J.D., Higgins, D.G. & Gibson, T.J. (1994) CLUSTAL W: improving the sensitivity of progressive multiple sequence alignment through sequence weighting, position-specific gap penalties and weight matrix choice. Nucleic Acids Res. 22: 4673–4680.

Trofimov, A.A., Pawlicki, A.A., Borodinov, N., Mandal, S., Mathews, T.J., Hildebrand, M., Ziatdinov, M.A., Hausladen, K.A., Urbanowicz, P.K., Steed, C.A., Ievlev, A.V., Belianinov, A., Michener, J.K., Vasudevan, R. & Ovchinnikova, O.S. (2019) Deep data analytics for genetic engineering of diatoms linking genotype to phenotype via machine learning. npj Comput. Mater. 5: 1–8.

Tyerman, S.D., Niemietz, C.M. & Bramley, H. (2002) Plant aquaporins: Multifunctional water and solute channels with expanding roles. Plant Cell Environ. 25: 173–194.

Wang, X., Devaiah, S.P., Zhang, W. & Welti, R. (2006) Signaling functions of phosphatidic acid. Prog. Lipid Res. 45: 250–278.

Witten, D.M. (2011) Classification and clustering of sequencing data using a Poisson model. Ann. Appl. Stat. 5: 2493–2518.

Wujek, D.E. & Welling, M.L. (1981) The occurrence of 2 centric diatoms new to the Great Lakes, USA. J. Great Lakes Res. 7: 55–56.

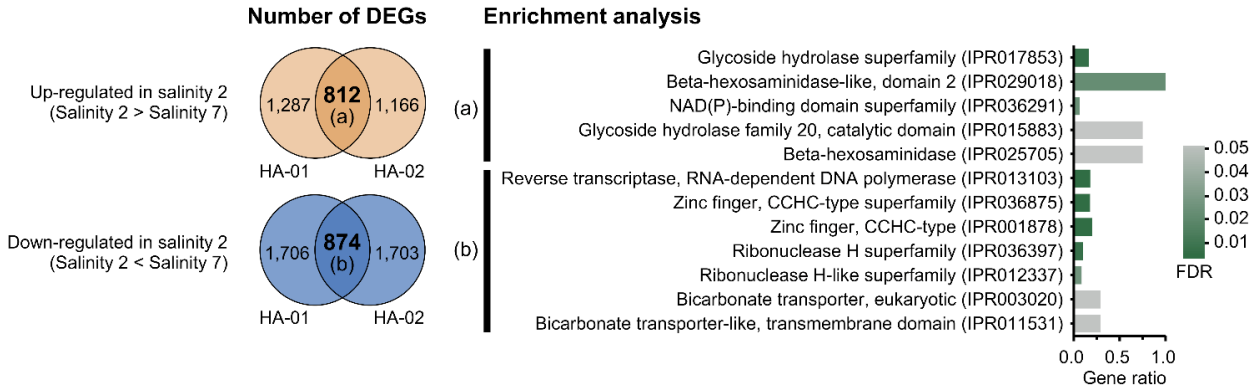


**Fig. 1.** Venn diagrams showing the intersection between differentially expressed genes (DEGs) of the 2 strains and InterPro enrichment on the shared **(a)** up and **(b)** downregulated genes.

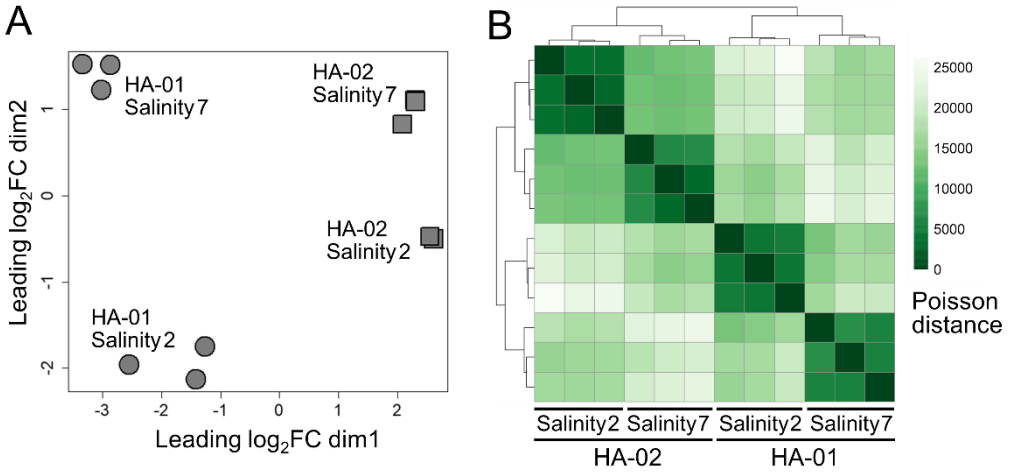


**Fig. 2.** Variation among strains in the transcriptional response of *P. laevis* to salinity 2 and 7. **(A)** Multi-dimensional scaling (MDS) plot of RNA-sequencing samples in this study. The distances between the samples were based on the $Log_2$ fold changes in the 500 most variable genes between the samples. **(B)** Poisson-distance heatmap of the full dataset. Samples were clustered firstly by strain and secondly by salinity.

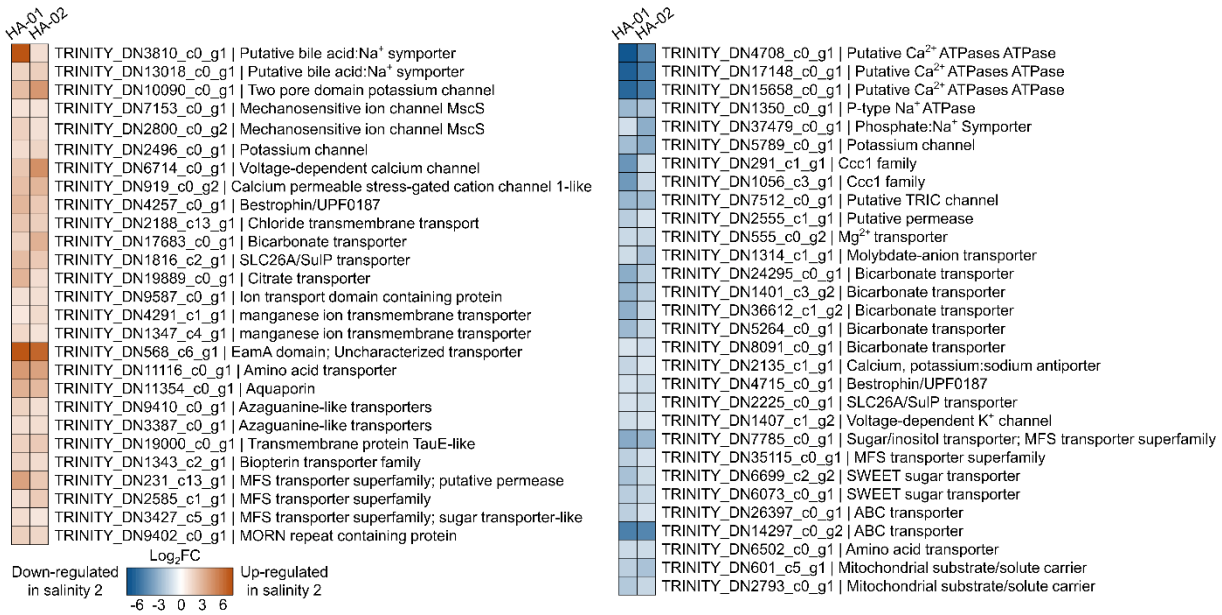


**Fig. 3.** Log2 fold changes of shared DEGs encoding transporters.

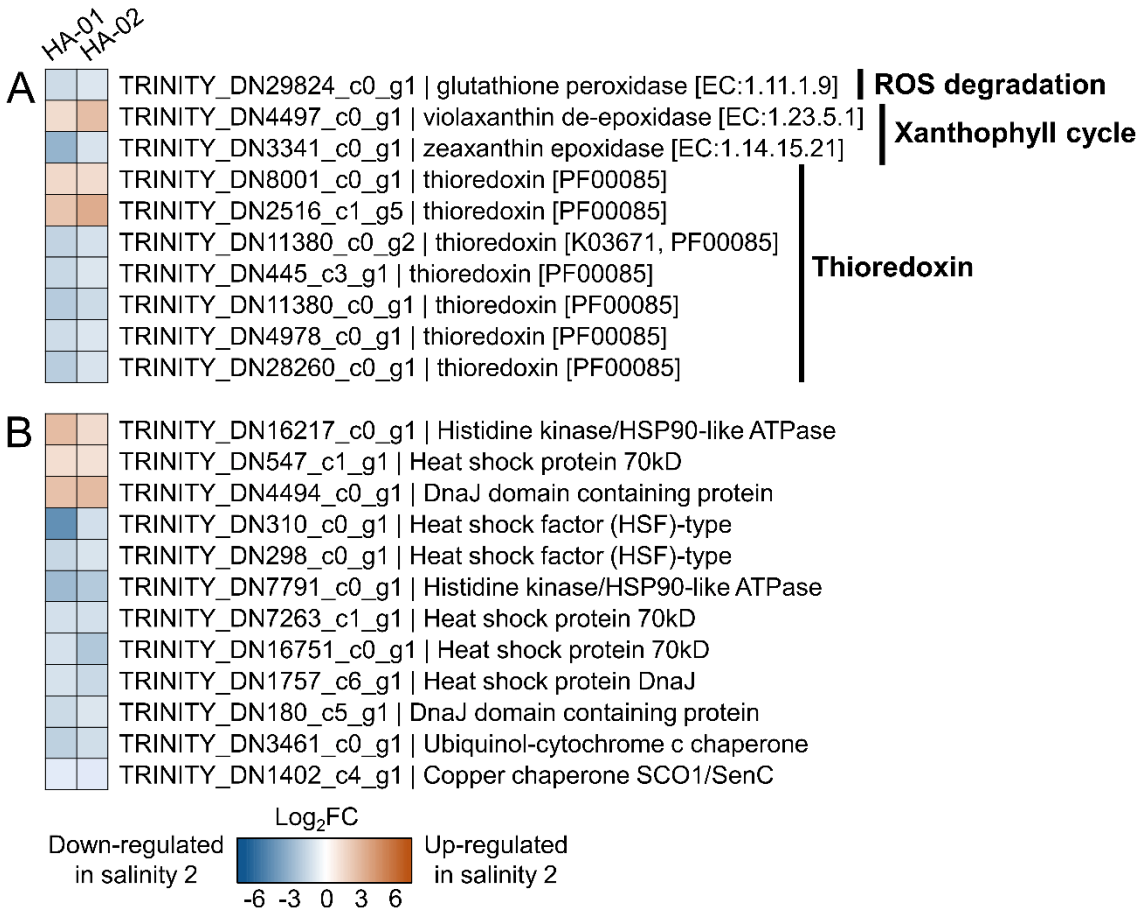


**Fig. 4.** Log2 fold changes of shared DEGs associated with stress responses. **(A)** Genes encoding proteins involved in ROS elimination processes. The PF00085 is a Pfam accession and K03671 is a K number for the KEGG database. **(B)** Genes encoding putative chaperones, heat shock proteins, and heat shock factors.

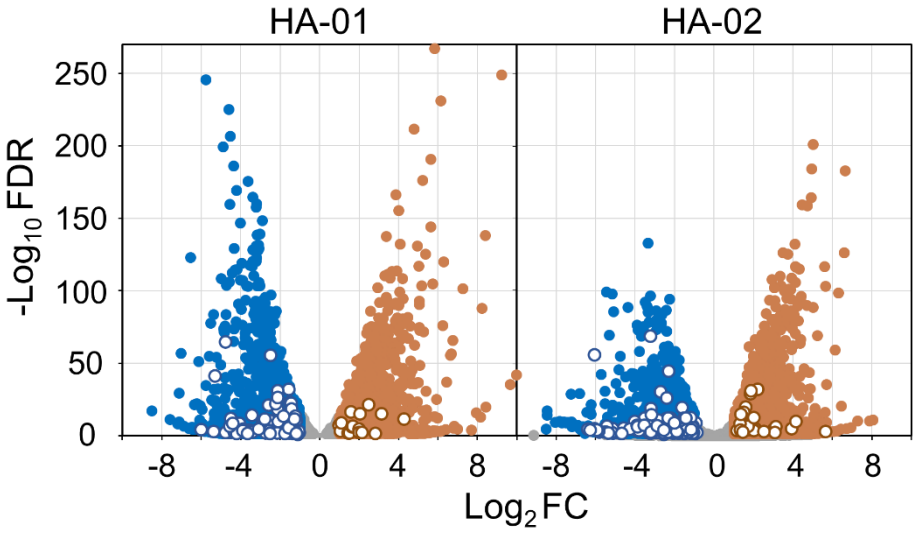


**Fig. 5.** Volcano plots for gene expression of HA-01 and HA-02 (salinity 2 *vs.* salinity 7). Brown plots indicate genes up-regulated in salinity 2, and blue plots indicate genes down-regulated in salinity 2. Open circle plots are the genes predicted to be transposable elements (TEs). Gray plots indicate genes that were not differentially expressed.

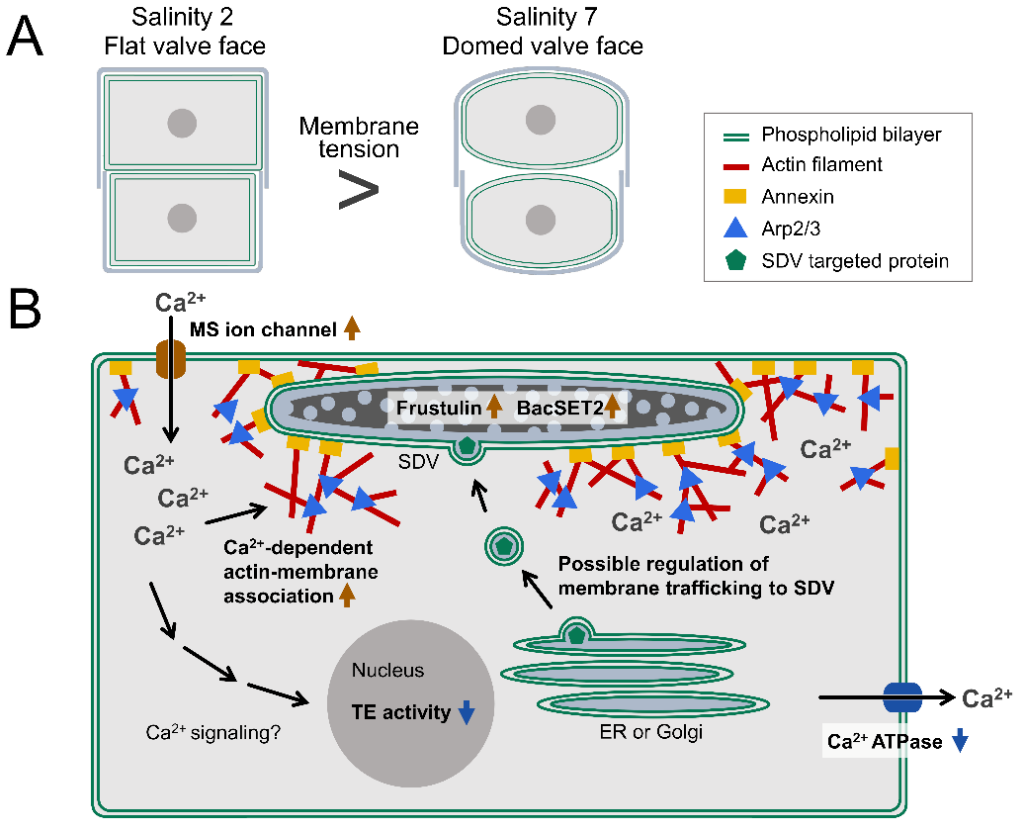


**Fig. 6.** Valve morphogenesis of *P. laevis* in response to osmotic pressure and membrane tension **(A)** Differences in membrane tension that the cells experience in forming flat or domed valves. **(B)** Schematic diagram of the regulation of cellular functions that can be involved in the formation of a flat valve. Brown and blue arrows indicate up- and down-regulation respectively, in comparison with cells with domed valves.

**Table S1.** Sequences used to search for cytoskeletons and related proteins (identified by Aumeier 2014 and Aumeier et al. 2015) and expression levels of the gene that formed an Orthogroup with them. $Log_2FC$ values are shown for DEGs only. Not DE=not differentially expressed.

| Protein | Protein sequences used for Orthofinder (JGI PhycoCosm protein ID) | Genes assigned to Orthogroup | $log_2FC$ | |
|---|---|---|---|---|
| | | | HA-01 | HA-02 |
| Actin | Thaps3\|25772; Phatr2\|51157; Psemu1\|22272; Fracy1\|171145 | TRINITY_DN71589_c0_g1 | Not DE | Not DE |
| | | TRINITY_DN9459_c0_g1 | Not DE | 1.64 |
| ADF/ cofilin | Thaps3\|4830; Phatr2\|15613; Fracy1\|206967; Psemu1\|248251 | - | - | - |
| Aip1 | Thaps3\|23728; Phatr2\|48381; Fracy1\|185021; Psemu1\|260507 | TRINITY_DN4982_c0_g2 | Not DE | Not DE |
| Annexin | Thaps3\|259626; Thaps3\|268316; Phatr2\|54190 | TRINITY_DN347_c5_g1 | Not DE | Not DE |
| | | TRINITY_DN29611_c0_g1 | Not DE | Not DE |
| | | TRINITY_DN4483_c0_g1 | Not DE | Not DE |
| | | TRINITY_DN1756_c3_g1 | 1.03 | Not DE |
| | | **TRINITY_DN914_c0_g1** | **2.44** | **2.15** |
| Annexin | Phatr2\|44109 | - | - | - |
| Arp1 | Thaps3\|269504; Phatr2\|44089; Psemu1\|239296; Fracy1\|228346 | TRINITY_DN2809_c0_g1 | Not DE | Not DE |
| | | TRINITY_DN27645_c0_g1 | Not DE | Not DE |
| | | TRINITY_DN80958_c0_g1 | Not DE | Not DE |
| Arp2/3 | Fracy1\|269231; Psemu1\|288992 | **(TRINITY_DN19486_c0_g1)*** | **(2.07)** | **(1.99)** |
| Arp4 | Thaps3\|269619; Psemu1\|324603; Fracy1\|178989 | TRINITY_DN2830_c0_g1 | Not DE | Not DE |
| Arp4 | Thaps3\|41068 | TRINITY_DN4672_c3_g1 | Not DE | Not DE |
| Arp4 | Phatr2\|20837; Psemu1\|188258 | - | - | - |
| Arp4 | Phatr2\|4515 | TRINITY_DN579_c13_g1 | Not DE | Not DE |
| Arp6 | Thaps3\|260856; Phatr2\|3281; Psemu1\|62991; Fracy1\|139659 | TRINITY_DN123_c0_g4 | Not DE | Not DE |
| | | TRINITY_DN2112_c20_g1 | Not DE | Not DE |
| Arp11 | Thaps3\|1132 | TRINITY_DN4450_c0_g1 | Not DE | Not DE |
| CAP | Thaps3\|23046; Phatr2\|20921; Fracy1\|262057; Psemu1\|249042 | TRINITY_DN8958_c0_g1 | Not DE | Not DE |
| CAPZ | Fracy1\|246923; Psemu1\|36278 | - | - | - |
| CAPZ | Phatr2\|9601 | TRINITY_DN15120_c0_g1 | Not DE | Not DE |
| | | TRINITY_DN9960_c0_g1 | Not DE | Not DE |
| CAPZ | Phatr2\|35252; Fracy1\|234298; Psemu1\|304923 | TRINITY_DN107_c10_g1 | Not DE | Not DE |
| | | TRINITY_DN8936_c3_g1 | Not DE | Not DE |
| Coronin | Thaps3\|8387; Phatr2\|45580; Psemu1\|70315 | TRINITY_DN62257_c0_g1 | Not DE | Not DE |
| | | TRINITY_DN68372_c0_g1 | Not DE | Not DE |
| | | TRINITY_DN71884_c0_g1 | Not DE | Not DE |
| | | TRINITY_DN5478_c0_g1 | Not DE | Not DE |
| Dematin | Psemu1\|324055 | - | - | - |
| Dematin | Phatr2\|45476 | TRINITY_DN21133_c0_g1 | Not DE | Not DE |
| | | TRINITY_DN74078_c0_g1 | Not DE | Not DE |
| | | TRINITY_DN27905_c0_g1 | Not DE | Not DE |
| Fascin | Thaps3\|7140; Fracy1\|235712; Fracy1\|254447 | TRINITY_DN1502_c3_g1 | Not DE | Not DE |
| | | TRINITY_DN8955_c0_g1 | Not DE | Not DE |
| | | TRINITY_DN9768_c0_g1 | Not DE | Not DE |
| Formin | Thaps3\|24787 | - | - | - |
| Formin | Phatr2\|46058; Psemu1\|212264 | - | - | - |
| Formin | Phatr2\|54229; Fracy1\|163042 | TRINITY_DN916_c0_g1 | Not DE | Not DE |
| Formin | Thaps3\|11711; Thaps3\|8340; Thaps3\|9248 | TRINITY_DN24782_c0_g1 | Not DE | Not DE |
| | | TRINITY_DN28989_c0_g1 | Not DE | -1.65 |
| Formin | Thaps3\|24070 | - | - | - |
| Formin | Thaps3\|4119; Phatr2\|46029; Phatr2\|54510 | TRINITY_DN11361_c0_g1 | Not DE | Not DE |
| | | TRINITY_DN4370_c0_g1 | Not DE | Not DE |
| Severin | Thaps3\|22984; Phatr2\|53980; Phatr2\|19089; Fracy1\|271285; Psemu1\|209419\| | TRINITY_DN1889_c0_g1 | Not DE | Not DE |
| | | TRINITY_DN3142_c0_g1 | Not DE | Not DE |
| | | TRINITY_DN3936_c0_g2 | Not DE | Not DE |
| | | TRINITY_DN61730_c0_g1 | Not DE | Not DE |

| | | | | |
|---|---|---|---|---|
| $\alpha$-tublin | Fracy1\|169390; Psemu1\|235379; Phatr2\|54534 | TRINITY_DN44742_c0_g1 | Not DE | Not DE |
| $\beta$-tubulin | Thaps3\|8069; Psemu1\|198602; | TRINITY_DN1001_c0_g1 | Not DE | Not DE |
| | Fracy1\|274017; Fracy1\|275160 | TRINITY_DN9493_c0_g1 | Not DE | Not DE |
| $\gamma$-tubulin | Thaps3\|29237; Psemu1\|296046; Fracy1\|193621 | TRINITY_DN89_c2_g1 | Not DE | Not DE |

*TRINITY_DN19486_c0_g1 was annotated as Arp2/3 but not assigned to orthogroup.

**Table S3**. Annotations and expression levels of transporters in the DEGs shared between the strains. The first column indicates the area on the Venn diagrams in Fig. 1.

| Venn diagram | Gene | InterPro accession | NCBI Blastp | | Mapping GO Term by NCBI Blastp | TCDB Blast | | | $Log_2FC$ | |
|---|---|---|---|---|---|---|---|---|---|---|
| | | | Top hit | E-value | | Family | Top hit | E-value | HA-01 | HA-02 |
| (a) | TRINITY_DN3810_c0_g1 | Putative sodium bile acid cotransporter (IPR016833, IPR038770) | GFH48748.1 \| solute carrier family 10 (sodium/bile acid cotransporter), member 7 [Chaetoceros tenuissimus] | 2.30E-102 | membrane | The Bile Acid:Na+ Symporter (BASS) Family | TC:2.A.28.3.1 | E-36 | 7.22 | 1.37 |
| (a) | TRINITY_DN10090_c0_g1 | Two pore domain potassium channel; EF-Hand 1, calcium-binding site (IPR003280, IPR013099, IPR018247) | GFH47503.1 \| hypothetical protein CTEN210_03978 [Chaetoceros tenuissimus] | 1.80E-60 | potassium ion transmembrane transport; calcium ion binding | The Voltage-gated Ion Channel (VIC) Superfamily | TC:1.A.1.7.5 | E-25 | 2.74 | 4.27 |
| (a) | TRINITY_DN2496_c0_g1 | Potassium channel domain (IPR013099, IPR003280) | EJK48158.1 \| hypothetical protein THAOC_33073 [Thalassiosira oceanica] | 4.00E-52 | potassium ion transmembrane transport | The Voltage-gated Ion Channel (VIC) Superfamily | TC:1.A.1.21.3 | E-12 | 1.46 | 1.76 |
| (a) | TRINITY_DN6714_c0_g1 | Voltage-dependent calcium channel, alpha-1 subunit (IPR002077, IPR031649, IPR027359, IPR005821, IPR043203) | GFH52780.1 \| hypothetical protein CTEN210_09256 [Chaetoceros tenuissimus] | 0 | calcium ion transport | The Voltage-gated Ion Channel (VIC) Superfamily | TC:1.A.1.11.20 | E-162 | 2.33 | 4.58 |
| (a) | TRINITY_DN919_c0_g2 | Calcium permeable stress-gated cation channel 1-like (IPR045122) | EJK45541.1 \| hypothetical protein THAOC_35845 [Thalassiosira oceanica] | 2.4E-155 | cation transmembrane transport | The Calcium-dependent Chloride Channel (Ca-ClC) Family | TC:1.A.17.3.1 | E-139 | 2.67 | 3.03 |
| (a) | TRINITY_DN4257_c0_g1 | Bestrophin/UPF0187 (IPR021134, IPR044669) | VEU38973.1 \| unnamed protein product [Pseudo-nitzschia multistriata] | 2.70E-122 | chloride transmembrane transport | The Anion Channel-forming Bestrophin (Bestrophin) Family | TC:1.A.46.2.11 | E-53 | 3.01 | 2.23 |
| (a) | TRINITY_DN2188_c13_g1 | - | GFH46765.1 \| hypothetical protein CTEN210_03239 [Chaetoceros tenuissimus] | 3.50E-06 | chloride transmembrane transport | The Autotransporter-2 (AT-2) Family | TC:1.B.40.1.5 | 0.0245 | 2.38 | 1.98 |
| (a) | TRINITY_DN17683_c0_g1 | Bicarbonate transporter, eukaryotic (IPR003020) | EJK48087.1 \| hypothetical protein THAOC_33148 [Thalassiosira oceanica] | 5.90E-26 | inorganic anion transport | The Anion Exchanger (AE) Family | TC:2.A.31.1.3 | E-10 | 1.84 | 3.23 |
| (a) | TRINITY_DN1816_c2_g1 | SLC26A/SulP transporter; STAS domain (IPR011547, IPR002645, IPR001902, IPR036513) | EEC42812.1 \| predicted protein, partial [Phaeodactylum tricornutum CCAP 1055/1] | 0 | secondary active sulfate transmembrane transporter activity | The Sulfate Permease (SulP) Family | TC:2.A.53.1.8 | E-174 | 2.78 | 2.23 |
| (a) | TRINITY_DN19889_c0_g1 | Citrate transporter-like domain; CBS domain superfamily (IPR004680, IPR046342, IPR045016) | KAG7356795.1 \| citrate transporter [Nitzschia inconspicua] | 0 | sodium ion transport | The NhaD Na+:H+ Antiporter (NhaD) Family | TC:2.A.62.1.3 | E-157 | 3.12 | 1.39 |
| (a) | TRINITY_DN13018_c0_g1 | Sodium/solute symporter superfamily; Bile acid:sodium symporter/arsenical resistance protein Acr3 | OEU08424.1 \| SBF-domain-containing protein [Fragilariopsis cylindrus CCMP1102] | 2.20E-105 | membrane (GO:0016020, GO:0016021) | The Bile Acid:Na+ Symporter (BASS) Family | TC:2.A.28.2.2 | E-52 | 1.80 | 1.98 |

| | | | | | | | | | |
|---|---|---|---|---|---|---|---|---|---|
| | | (IPR038770, IPR002657, IPR004710) | | | | | | | |
| (a) | TRINITY_DN7153_c0_g1 | Mechanosensitive ion channel MscS (IPR023408, IPR006685, IPR016688) | EEC44757.1 \| predicted protein [Phaeodactylum tricornutum CCAP 1055/1] | 4.30E-150 | transmembrane transport (GO:0055085, GO:0016020, GO:0016021) | The Small Conductance Mechanosensitive Ion Channel (MscS) Family | TC:1.A.23.4.14 | E-15 | 1.23 | 1.15 |
| (a) | TRINITY_DN2800_c0_g2 | Mechanosensitive ion channel MscS (IPR006685, IPR023408, IPR010920) | KAI2498881.1 \| mechanosensitive ion channel [Fragilaria crotonensis] | 1.50E-79 | transmembrane transport GO:0055085, GO:0016020, GO:0016021) | The Small Conductance Mechanosensitive Ion Channel (MscS) Family | TC:1.A.23.4.2 | E-13 | 1.90 | 1.28 |
| (a) | TRINITY_DN9587_c0_g1 | Ankyrin repeat; Ion transport domain (IPR002110, IPR036770, IPR005821) | GAX19398.1 \| hypothetical protein FisN_4Lh378 [Fistulifera solaris] | 1E-60 | transmembrane transport (GO:0055085, GO:0016020, GO:0034220, GO:0016021, GO:0006811, GO:0005216) | The Transient Receptor Potential Ca2+ Channel (TRP-CC) Family | TC:1.A.4.5.9 | E-06 | 1.28 | 1.32 |
| (a) | TRINITY_DN4291_c1_g1 | - | GAX22879.1 \| hypothetical protein FisN_24Lh166 [Fistulifera solaris] | 5.2E-15 | manganese ion transmembrane transport (GO:0071421, GO:0016020, GO:0005384, GO:0016021, GO:0030026) | The Gordonia Outer Membrane Porin (GjpA) Family | TC:1.B.89.1.13 | E-07 | 1.00 | 1.51 |
| (a) | TRINITY_DN1347_c4_g1 | - | VEU33986.1 \| unnamed protein product [Pseudo-nitzschia multistriata] | 3.7E-49 | manganese ion transmembrane transport (GO:0009987, GO:0016020) | The Gordonia Outer Membrane Porin (GjpA) Family | TC:1.B.89.1.13 | 0.0003 | 1.64 | 1.17 |
| (a) | TRINITY_DN568_c6_g1 | EamA domain (IPR000620) | KAG7347462.1 \| EamA-like transporter family protein [Nitzschia inconspicua] | 3.1E-50 | membrane (GO:0016020, GO:0016021) | The Drug/Metabolite Transporter (DMT) Superfamily | TC:2.A.7.3.36 | 0.0002 | 6.95 | 6.30 |
| (a) | TRINITY_DN11116_c0_g1 | Amino acid transporter, transmembrane domain (IPR01305) | EED95929.1 \| hypothetical protein THAPSDRAFT_20889 [Thalassiosira pseudonana CCMP1335] | 7.6E-118 | membrane (GO:0016020, GO:0016021) | The Amino Acid/Auxin Permease (AAAP) Family | TC:2.A.18.6.1 | E-27 | 4.17 | 3.84 |
| (a) | TRINITY_DN11354_c0_g1 | Major intrinsic protein; Aquaporin-like (IPR000425, IPR023271, IPR034294, IPR022357) | VEU35719.1 \| unnamed protein product [Pseudo-nitzschia multistriata] | 2.2E-102 | membrane (GO:0016020) | The Major Intrinsic Protein (MIP) Family | TC:1.A.8.8.1 | E-41 | 3.24 | 2.88 |
| (a) | TRINITY_DN9410_c0_g1 | Nucleobase cation symporter 2 family; Azaguanine-like transporters (IPR006043, IPR045018) | GAX20102.1 \| putative MFS transporter, AGZA family, xanthine/uracil permease [Fistulifera solaris] | 0 | transmembrane transport (GO:0015205, GO:0016021, GO:1904823) | The Nucleobase/ Ascorbate Transporter (NAT) or Nucleobase:Cation Symporter-2 (NCS2) Family | TC:2.A.40.7.3 | E-142 | 1.83 | 1.33 |
| (a) | TRINITY_DN3387_c0_g1 | Nucleobase cation symporter 2 family; Azaguanine-like | KAG7362392.1 \| xanthine/uracil/vitamin C permease [Nitzschia | 1.8E-103 | transmembrane transport | The Nucleobase/Ascorbate Transporter (NAT) or | TC:2.A.40.7.8 | E-58 | 1.37 | 1.38 |

| | | | | | | | | | | |
|---|---|---|---|---|---|---|---|---|---|---|
| | | transporters (IPR006043, IPR045018) | inconspicua]/KAG7339680.1 \| xanthine/uracil/vitamin C permease [Nitzschia inconspicua] | | | Nucleobase:Cation Symporter-2 (NCS2) Family | | | | |
| (a) | TRINITY_DN19000_c0_g1 | Transmembrane protein TauE-like (IPR002781) | NQY67781.1 \| sulfite exporter TauE/SafE family protein [Flavobacteriales bacterium] | 6.8E-22 | membrane | The 4-Toluene Sulfonate Uptake Permease (TSUP) Family | TC:2.A.102.6.3 | E-24 | 1.91 | 2.18 |
| (a) | TRINITY_DN1343_c2_g1 | Biopterin transporter family; MFS transporter superfamily (IPR039309, IPR036259) | KAI2494246.1 \| BT1-like protein [Fragilaria crotonensis] | 0 | membrane | The Folate-Biopterin Transporter (FBT) Family | TC:2.A.71.2.2 | E-39 | 1.76 | 1.46 |
| (a) | TRINITY_DN231_c13_g1 | MFS transporter superfamily (IPR011701, IPR036259) | OEU07328.1 \| MFS general substrate transporter [Fragilariopsis cylindrus CCMP1102] | 2.2E-136 | transmembrane transport | The Major Facilitator Superfamily (MFS) | TC:2.A.1.2.80 | E-43 | 3.83 | 2.25 |
| (a) | TRINITY_DN2585_c1_g1 | MFS transporter superfamily (IPR036259, IPR011701, IPR044770, IPR020846) | EED94687.1 \| hypothetical protein THAPSDRAFT_261312, partial [Thalassiosira pseudonana CCMP1335] | 1.6E-81 | transmembrane transport | The Major Facilitator Superfamily (MFS) | TC:2.A.1.66.3 | E-87 | 1.35 | 2.14 |
| (a) | TRINITY_DN3427_c5_g1 | MFS transporter superfamily; Major facilitator, sugar transporter-like (IPR036259, IPR005828, IPR005829, IPR020846) | KAG7359281.1 \| major facilitator superfamily transporter [Nitzschia inconspicua] | 2.5E-68 | transmembrane transport | The Major Facilitator Superfamily (MFS) | TC:2.A.1.82.5 | E-37 | 1.42 | 1.04 |
| (a) | TRINITY_DN9402_c0_g1 | MORN motif (IPR003409) | KOO53739.1 \| morn repeat protein [Chrysochromulina tobinii] | 4.4E-27 | transmembrane transport; calcium ion binding | The Junctophilin (JP) Family | TC:8.A.110.1.3 | E-20 | 1.96 | 1.65 |
| (a) | TRINITY_DN1645_c0_g1 | - | EEC51806.1 \| predicted protein [Phaeodactylum tricornutum CCAP 1055/1] | 1.3E-20 | transmembrane transport | The Voltage-gated Ion Channel (VIC) Superfamily | TC:1.A.1.2.8 | 0.0118 | 1.52 | 1.65 |
| (b) | TRINITY_DN4708_c0_g1 | Cation-transporting P-type ATPase, C-terminal (IPR006068, IPR023298) | KAG7371055.1 \| cation-transporting P-type ATPase [Nitzschia inconspicua] | 5.9E-42 | nucleotide binding; membrane | The P-type ATPase (P-ATPase) Superfamily | TC:3.A.3.2.29 | E-06 | -7.07 | -4.95 |
| (b) | TRINITY_DN17148_c0_g1 | P-type ATPase, cytoplasmic domain N (IPR023299) | KAI2508547.1 \| Cation transport ATPase [Fragilaria crotonensis] | 1.6E-77 | nucleotide binding; membrane | The P-type ATPase (P-ATPase) Superfamily | TC:3.A.3.2.29 | E-20 | -6.58 | -5.29 |
| (b) | TRINITY_DN15658_c0_g1 | Cation-transporting P-type ATPase (IPR001757, IPR006068, IPR023214, IPR023298, IPR036412) | KAG7359721.1 \| HAD superfamily P-type ATPase [Nitzschia inconspicua] | 0 | nucleotide binding; membrane | The P-type ATPase (P-ATPase) Superfamily | TC:3.A.3.2.29 | E-84 | -6.31 | -5.28 |
| (b) | TRINITY_DN1350_c0_g1 | Cation-transporting P-type ATPase, N-terminal (IPR004014, IPR023214;IPR006068, | KAG7371055.1 \| cation-transporting P-type ATPase [Nitzschia inconspicua] | 0 | nucleotide binding; membrane | The P-type ATPase (P-ATPase) Superfamily | TC:3.A.3.2.41 | E-163 | -2.93 | -2.38 |

| | | | | | | | | | |
|---|---|---|---|---|---|---|---|---|---|
| | | IPR023299, IPR001757, IPR044492) | | | | | | | |
| (b) | TRINITY_DN37479_c0_g1 | Sodium-dependent phosphate transport protein (IPR003841, IPR030147) | GFH53715.1 \| hypothetical protein CTEN210_10191 [Chaetoceros tenuissimus] | 0 | inorganic anion transport | The Phosphate:Na+ Symporter (PNaS) Family | TC:2.A.58.1.7 | E-95 | -1.32 | -3.36 |
| (b) | TRINITY_DN5789_c0_g1 | Potassium channel domain (IPR013099, IPR003280) | KAG7349485.1 \| Kef-type K+ transporter [Nitzschia inconspicua] | 3.2E-103 | potassium ion transmembrane transport | The Voltage-gated Ion Channel (VIC) Superfamily | TC:1.A.1.21.3 | E-09 | -2.71 | -3.43 |
| (b) | TRINITY_DN291_c1_g1 | Ccc1 family (IPR008217) | NNC39198.1 \| hypothetical protein [Acidimicrobiia bacterium] | 1.3E-38 | manganese ion transmembrane transport | The Vacuolar Iron Transporter (VIT) Family | TC:2.A.89.1.2 | E-13 | -4.38 | -1.49 |
| (b) | TRINITY_DN1056_c3_g1 | Ccc1 family (IPR008217) | EEC50371.1 \| predicted protein [Phaeodactylum tricornutum CCAP 1055/1] | 9.1E-21 | manganese ion transmembrane transport | The Vacuolar Iron Transporter (VIT) Family | TC:2.A.89.1.2 | E-07 | -4.24 | -1.59 |
| (b) | TRINITY_DN7512_c0_g1 | TRIC channel (IPR007866) | EEC49465.1 \| predicted protein [Phaeodactylum tricornutum CCAP 1055/1] | 5.5E-94 | identical protein binding; potassium ion transmembrane transport | The Homotrimeric Cation Channel (TRIC) Family | TC:1.A.62.4.2 | 0.0034 | -2.98 | -2.66 |
| (b) | TRINITY_DN2555_c1_g1 | EamA domain (IPR000620) | KAG7354052.1 \| EamA-like transporter family protein [Nitzschia inconspicua] | 5.4E-76 | membrane | The Drug/Metabolite Transporter (DMT) Superfamily | TC:2.A.7.3.53 | E-26 | -2.05 | -1.19 |
| (b) | TRINITY_DN555_c0_g2 | EamA domain; Magnesium transporter NIPA (IPR000620, IPR008521) | GFH60843.1 \| hypothetical protein CTEN210_17319 [Chaetoceros tenuissimus] | 6.4E-85 | magnesium ion transmembrane transport | The Drug/Metabolite Transporter (DMT) Superfamily | TC:2.A.7.29.4 | E-05 | -1.57 | -1.64 |
| (b) | TRINITY_DN1314_c1_g1 | Molybdate-anion transporter; MFS transporter superfamily (IPR008509, IPR036259) | KAG7365329.1 \| sugar transporter [Nitzschia inconspicua] | 0 | molybdate ion transmembrane transporter activity | The Major Facilitator Superfamily (MFS) | TC:2.A.1.40.3 | E-59 | -1.46 | -2.39 |
| (b) | TRINITY_DN24295_c0_g1 | Bicarbonate transporter-like, transmembrane domain (IPR011531, IPR003020) | EEC48580.1 \| predicted protein [Phaeodactylum tricornutum CCAP 1055/1] | 6E-38 | inorganic anion transport | The Anion Exchanger (AE) Family | TC:2.A.31.2.15 | E-18 | -3.41 | -2.02 |
| (b) | TRINITY_DN1401_c3_g2 | Bicarbonate transporter, eukaryotic (IPR011531, IPR003020) | EEC48580.1 \| predicted protein [Phaeodactylum tricornutum CCAP 1055/1 | 1.1E-39 | inorganic anion transport | The Anion Exchanger (AE) Family | TC:2.A.31.1.1 | E-08 | -3.08 | -1.94 |
| (b) | TRINITY_DN36612_c1_g2 | Bicarbonate transporter, eukaryotic (IPR011531, IPR003020) | EEC42613.1 \| predicted protein [Phaeodactylum tricornutum CCAP 1055/1] | 1.7E-61 | inorganic anion transport | The Anion Exchanger (AE) Family | TC:2.A.31.2.4 | E-29 | -3.30 | -1.57 |
| (b) | TRINITY_DN5264_c0_g1 | Bicarbonate transporter, eukaryotic (IPR011531, IPR003020) | EEC48580.1 \| predicted protein [Phaeodactylum tricornutum CCAP 1055/1] | 2.7E-124 | inorganic anion transport | The Anion Exchanger (AE) Family | TC:2.A.31.2.16 | E-46 | -2.88 | -1.61 |
| (b) | TRINITY_DN8091_c0_g1 | Bicarbonate transporter, eukaryotic (;IPR003020, IPR011531) | KAI2504608.1 \| HCO3-transporter family [Fragilaria crotonensis] | 0 | inorganic anion transport | The Anion Exchanger (AE) Family | TC:2.A.31.2.16 | E-70 | -1.12 | -1.31 |
| (b) | TRINITY_DN2135_c1_g1 | EF-hand domain; NCX, central ion-binding domain superfamily (IPR002048, IPR044880, IPR004481, IPR004837, IPR018247, IPR011992) | KAG7357370.1 \| CaCA family Na+/Ca+ antiporter [Nitzschia inconspicua] | 0 | calcium, potassium:sodium antiporter activity | The Ca2+:Cation Antiporter (CaCA) Family | TC:2.A.19.4.2 | E-99 | -1.71 | -1.07 |

| | | | | | | | | | |
|---|---|---|---|---|---|---|---|---|---|
| (b) | TRINITY_DN4715_c0_g1 | Bestrophin/UPF0187 (IPR021134) | EEC44724.1 \| predicted protein [Phaeodactylum tricornutum CCAP 1055/1] | 1.5E-25 | chloride transmembrane transport | The Anion Channel-forming Bestrophin (Bestrophin) Family | TC:1.A.46.2.5 | 0.0005 | -1.25 | -1.50 |
| (b) | TRINITY_DN2225_c0_g1 | SLC26A/SulP transporter domain (IPR011547, IPR001902) | PSC69898.1 \| sulfate transporter [Micractinium conductrix] | 2.9E-60 | sulfate transport | The Sulfate Permease (SulP) Family | TC:2.A.53.1.14 | E-66 | -1.22 | -1.40 |
| (b) | TRINITY_DN1407_c1_g2 | Voltage-dependent channel domain superfamily; Adenylyl cyclase class-3/4/guanylyl cyclase (IPR027359, IPR001054, IPR029787) | GFH57281.1 \| hypothetical protein CTEN210_13757 [Chaetoceros tenuissimus] | 0 | ion channel activity; cyclic nucleotide biosynthetic process | The Guanylate Cyclase (GC) Family | TC:8.A.85.1.8 | E-45 | -1.41 | -1.12 |
| (b) | TRINITY_DN7785_c0_g1 | Sugar/inositol transporter; MFS transporter superfamily (IPR003663, IPR005828, IPR036259, IPR020846) | KAI2500116.1 \| major facilitator superfamily-like protein [Fragilaria crotonensis] | 0 | carbohydrate transmembrane transporter activity | The Major Facilitator Superfamily (MFS) | TC:2.A.1.1.132 | E-105 | -3.51 | -2.98 |
| (b) | TRINITY_DN35115_c0_g1 | MFS transporter superfamily (IPR011701, IPR036259, IPR020846) | GFH51031.1 \| hypothetical protein CTEN210_07507 [Chaetoceros tenuissimus] | 1.2E-151 | transmembrane transport | The Major Facilitator Superfamily (MFS) | TC:2.A.1.2.104 | E-30 | -1.94 | -1.23 |
| (b) | TRINITY_DN6699_c2_g2 | SWEET sugar transporter (IPR004316) | GFH53799.1 \| hypothetical protein CTEN210_10275 [Chaetoceros tenuissimus] | 4E-28 | carbohydrate transport | The Sweet; PQ-loop; Saliva; MtN3 (Sweet) Family | TC:2.A.123.1.17 | E-16 | -2.55 | -1.46 |
| (b) | TRINITY_DN6073_c0_g1 | SWEET sugar transporter (IPR004316) | EEC51987.1 \| predicted protein [Phaeodactylum tricornutum CCAP 1055/1] | 3.3E-57 | membrane | The Sweet; PQ-loop; Saliva; MtN3 (Sweet) Family | TC:2.A.123.1.13 | E-24 | -2.06 | -1.61 |
| (b) | TRINITY_DN26397_c0_g1 | ABC transporter type 1, transmembrane domain (IPR011527, IPR036640, IPR039421) | EJK46387.1 \| hypothetical protein THAOC_34944, partial [Thalassiosira oceanica] | 3.5E-85 | nucleotide binding; transmembrane transport | The ATP-binding Cassette (ABC) Superfamily | TC:3.A.1.201.1 | E-24 | -1.97 | -1.24 |
| (b) | TRINITY_DN6502_c0_g1 | Amino acid transporter, transmembrane domain (IPR013057) | EJK67700.1 \| hypothetical protein THAOC_11234 [Thalassiosira oceanica] | 1.7E-111 | membrane | The Amino Acid/Auxin Permease (AAAP) Family | TC:2.A.18.6.8 | E-28 | -1.51 | -1.49 |
| (b) | TRINITY_DN601_c5_g1 | Mitochondrial substrate/solute carrier (IPR023395, IPR018108) | KAG7366653.1 \| mitochondrial carrier protein [Nitzschia inconspicua] | 2.3E-10 | mitochondrial transmembrane transport | The Mitochondrial Carrier (MC) Family | TC:2.A.29.14.8 | 0.0001 | -1.97 | -2.50 |
| (b) | TRINITY_DN2793_c0_g1 | Mitochondrial substrate/solute carrier (IPR002067, IPR023395, IPR018108) | GFH52009.1 \| hypothetical protein CTEN210_08485 [Chaetoceros tenuissimus] | 2.8E-172 | transmembrane transport; membrane; integral component of membrane | The Mitochondrial Carrier (MC) Family | TC:2.A.29.2.9 | E-42 | -2.24 | -1.64 |

**Table S4.** Annotations and expression levels of the shared DEGs containing ankyrin repeat. The first column indicates the area on the Venn diagrams in Fig. 1. Note that the two genes containing ankyrin repeat (TRINITY_DN3240_c5_g1 and TRINITY_DN9587_c0_g1) were listed in table S4 and S1, respectively, and are not in this table.

| Venn diagram | Gene | InterPro accession | NCBI Blastp | | Mapping GO term by NCBI Blastp | $Log_2FC$ | |
|---|---|---|---|---|---|---|---|
| | | | Top hit | E-value | | HA-01 | HA-02 |
| (a) | TRINITY_DN21_c0_g2 | Ankyrin repeat (IPR002110, IPR036770) | KAG7361234.1\|2-oxyglutarate/Fe(II) oxygenase [Nitzschia inconspicua] | 4E-108 | - | 3.79 | 3.77 |
| (a) | TRINITY_DN22764_c0_g1 | Ankyrin repeat (IPR002110, IPR036770) | KAI2501697.1\|hypothetical protein MHU86_12765 [Fragilaria crotonensis] | 8E-169 | - | 1.48 | 2.40 |
| (a) | TRINITY_DN13496_c0_g1 | Ankyrin repeat (IPR002110, IPR036770) | GFH58047.1\|hypothetical protein CTEN210_14523 [Chaetoceros tenuissimus] | 1.8E-45 | - | 6.72 | 2.12 |
| (a) | TRINITY_DN5738_c0_g1 | WGR domain; Ankyrin repeat; Poly(ADP-ribose) polymerase, catalytic domain (IPR008893, IPR002110, IPR012317, IPR036770, IPR004102, IPR036616) | KNC87483.1\|hypothetical protein SARC_00417 [Sphaeroforma arctica JP610] | 0 | glycosyltransferase activity; protein ADP-ribosylation; phosphorylation (GO:0016757, GO:0006471, GO:0016310, GO:0016740, GO:0016301, GO:0003950, GO:0005634) | 1.97 | 1.57 |
| (a) | TRINITY_DN1775_c0_g1 | Ankyrin repeat (IPR002110, IPR036770) | EJK76137.1\|hypothetical protein THAOC_02119 [Thalassiosira oceanica] | 7.9E-88 | - | 2.12 | 1.50 |
| (b) | TRINITY_DN1425_c2_g1 | Ankyrin repeat (IPR002110, IPR036770) | GFH55523.1\|hypothetical protein CTEN210_11999 [Chaetoceros tenuissimus] | 3E-175 | - | -2.42 | -1.56 |
| (b) | TRINITY_DN347_c5_g2 | Ankyrin repeat (IPR002110, IPR036770) | - | - | - | -1.52 | -1.71 |
| (b) | TRINITY_DN13936_c0_g1 | Ankyrin repeat (IPR002110, IPR036770) | GAX12363.1\|hypothetical protein FisN_1Hh296 [Fistulifera solaris] | 0.00039 | - | -1.48 | -1.43 |

**Table S5.** Annotations and expression levels of the DEGs shared between the strains, encoding proteins involved in motor protein activity and membrane trafficking. The first column indicates the area on the Venn diagrams in Fig. 1.

| Venn diagram | Gene | InterPro Accession | NCBI Blastp | | Mapping GO term by NCBI Blastp | $Log_2FC$ | |
|---|---|---|---|---|---|---|---|
| | | | Top hit | E-value | | HA-01 | HA-02 |
| **Motor protein activity** | | | | | | | |
| (a) | TRINITY_DN429_c4_g1 | Growth arrest-specific protein 8 domain (IPR025593, IPR039308) | KAG8459196.1\|hypothetical protein KFE25_005707 [Diacronema lutheri] | 2.40E-25 | axonemal dynein complex assembly; small GTPase binding; cilium; microtubule binding; protein localization; Golgi apparatus; axoneme (GO:0005856, GO:0005515, GO:0048870, GO:0005737, GO:0070286, GO:0031267, GO:0005929, GO:0097729, GO:0031514, GO:0060294, GO:0008017, GO:0008104, GO:0005794, GO:0005874, GO:0042995, GO:0005930) | 1.27 | 1.26 |
| (a) | TRINITY_DN356_c1_g3 | Metallo-beta-lactamase; Ribonuclease Z/Hydroxyacylglutathione hydrolase-like (IPR001279, IPR036866) | EEC42667.1\|predicted protein, partial [Phaeodactylum tricornutum CCAP 1055/1] | 1.40E-25 | nucleotide binding; microtubule motor activity; zinc ion binding; microtubule binding; ATP binding; N-acylphosphatidylethanolamine-specific phospholipase D activity (GO:0000166, GO:0003777, GO:0008270, GO:0008017, GO:0005874, GO:0005524, GO:0016787, GO:0007018, GO:0070290) | 1.25 | 1.52 |
| (a) | TRINITY_DN7895_c0_g1 | - | GAX18345.1\|hypothetical protein FisN_23Hh239 [Fistulifera solaris] | 9.70E-16 | cortical microtubule organization (GO:0043622) | 1.16 | 1.38 |
| (a) | TRINITY_DN21164_c0_g1 | Tetratricopeptide repeat (IPR019734, IPR011990) | EDV19007.1\|hypothetical protein TRIADDRAFT_62542, partial [Trichoplax adhaerens] | 1.90E-10 | glycosyltransferase activity; NAD+-protein-arginine ADP-ribosyltransferase activity; signal transduction; protein ADP-ribosylation; kinesin complex; microtubule (GO:0005856, GO:0016757, GO:0005737, GO:0106274, GO:0007165, GO:0006471, GO:0005871, GO:0016740, GO:0005874) | 1.12 | 1.77 |
| (b) | TRINITY_DN8102_c0_g1 | WD40 repeat; WD40/YVTN repeat-like-containing domain superfamily (IPR001680, IPR015943, IPR015943, IPR036322) | EGB09149.1\|hypothetical protein AURANDRAFT_25101 [Aureococcus anophagefferens] | 1.30E-78 | - | -3.75 | -2.41 |
| (b) | TRINITY_DN10480_c0_g2 | PIH1D1/2/3, CS-like domain; Dynein axonemal assembly factor 6 (IPR041442, IPR026697) | RYH29894.1\|hypothetical protein EON65_06950 [archaeon] | 1.10E-33 | axonemal dynein complex assembly; chaperone binding (GO:0070286, GO:0051087) | -2.52 | -1.03 |
| (b) | TRINITY_DN1470_c2_g2 | Myosin head, motor domain; IQ motif, EF-hand binding site; P-loop containing nucleoside triphosphate hydrolase (IPR001609, IPR000048, IPR036961, IPR027417) | GFH52842.1\|myosin G [Chaetoceros tenuissimus] | 0 | myosin complex; nucleotide binding; actin binding; ATP binding; cytoskeletal motor activity; hydrolase activity (GO:0016459, GO:0000166, GO:0003779, GO:0005524, GO:0003774, GO:0016787) | -1.03 | -1.41 |
| **Membrane trafficking** | | | | | | | |
| (a) | TRINITY_DN2300_c0_g1 | C2 domain; Copine, C2B domain (IPR000008, IPR035892, IPR045052, IPR037768) | EEC47209.1\|predicted protein, partial [Phaeodactylum tricornutum CCAP 1055/1] | 5.00E-21 | calcium-dependent phospholipid binding (GO:0005544) | 4.17 | 4.01 |
| (a) | TRINITY_DN3240_c5_g1 | Ankyrin repeat; v-SNARE, coiled-coil homology domain (IPR002110, IPR036770, IPR042855) | EJK65911.1\|hypothetical protein THAOC_13192 [Thalassiosira oceanica] | 8.20E-24 | calcium ion binding (GO:0005509) | 1.28 | 1.05 |

| | | | | | | | |
|---|---|---|---|---|---|---|---|
| (a) | TRINITY_DN4933_c5_g1 | Nucleotide-sugar transporter (IPR007271) | EJK69357.1\|hypothetical protein THAOC_09395 [Thalassiosira oceanica] | 4.70E-75 | pyrimidine nucleotide-sugar transmembrane transport; Golgi membrane (GO:0016020, GO:0015165, GO:0016021, GO:0008643, GO:0000139, GO:0090481) | 2.04 | 1.75 |
| (a) | TRINITY_DN171_c28_g1 | Conserved oligomeric Golgi complex subunit 8 (IPR007255) | EJK54047.1\|hypothetical protein THAOC_26404 [Thalassiosira oceanica] | 1.40E-78 | Golgi transport complex; protein transport; Golgi apparatus (GO:0017119, GO:0016020, GO:0015031, GO:0005794) | 1.45 | 1.61 |
| (a) | TRINITY_DN5526_c0_g1 | AP complex, mu/sigma subunit; Coatomer subunit zeta; Longin-like domain superfamily (IPR022775, IPR039652, IPR011012) | GFH48759.1\|hypothetical protein CTEN210_05235 [Chaetoceros tenuissimus] | 8.50E-92 | retrograde vesicle-mediated transport, Golgi to endoplasmic reticulum; protein transport; COPI-coated vesicle membrane (GO:0016192, GO:0005737, GO:0006890, GO:0016020, GO:0015031, GO:0031410, GO:0030663, GO:0005794, GO:0000139, GO:0030126) | 1.20 | 1.05 |
| (a) | TRINITY_DN3268_c1_g1 | Vacuolar protein sorting-associated protein IST1-like (IPR042277, IPR005061)f | GFH43834.1\|hypothetical protein CTEN210_00307 [Chaetoceros tenuissimus] | 6.90E-88 | protein transport (GO:0015031) | 1.76 | 1.00 |
| (a) | TRINITY_DN1771_c0_g2 | P-loop containing nucleoside triphosphate hydrolase; Dynamin; Dynamin-type guanine nucleotide-binding (G) domain (IPR027417, IPR022812, IPR030381) | NYZ17637.1\|calcium-binding protein [Azospirillum oleiclasticum] | 8.90E-06 | - | 1.66 | 1.16 |
| (a) | TRINITY_DN9209_c0_g1 | Rab GDI protein; GDP dissociation inhibitor; GDP dissociation inhibitor; FAD/NAD(P)-binding domain superfamily (IPR000806, IPR018203, IPR018203, IPR036188) | EJK68651.1\|hypothetical protein THAOC_10150, partial [Thalassiosira oceanica] | 0 | Rab GDP-dissociation inhibitor activity; small GTPase mediated signal transduction; protein transport (GO:0005092, GO:0005093, GO:0007264, GO:0050790, GO:0015031) | 2.02 | 1.78 |
| (b) | TRINITY_DN2279_c2_g1 | Vacuolar protein sorting-associated protein 13 (IPR009543, IPR026847) | KAI2491565.1\|vacuolar sorting-associated protein 13 [Fragilaria crotonensis] | 0 | lipid transport (GO:0006869) | -1.91 | -1.32 |
| (b) | TRINITY_DN768_c0_g1 | Small GTPase; P-loop containing nucleoside triphosphate hydrolase (IPR001806, IPR027417, IPR005225) | GFH45444.1\|small GTP binding protein Rab1A [Chaetoceros tenuissimus] | 5.90E-102 | GTP binding; GTPase activity (GO:0005525, GO:0003924) | -1.77 | -1.26 |
| (b) | TRINITY_DN20938_c0_g1 | P-loop containing nucleoside triphosphate hydrolase; EH domain-containing protein, N-terminal; Domain of unknown function DUF5600; Dynamin, N-terminal (IPR027417, IPR031692, IPR040990, IPR045063, IPR029945, IPR030381) | EGB05878.1\|hypothetical protein AURANDRAFT_30262 [Aureococcus anophagefferens] | 2.10E-148 | endosome; GTP binding; nucleotide binding; calcium ion binding; actin cytoskeleton organization; ATP binding (GO:0005768, GO:0005525, GO:0000166, GO:0046872, GO:0016020, GO:0005509, GO:0032456, GO:0030036, GO:0010008, GO:0005524, GO:0005886) | -1.24 | -1.05 |

**Table S5.** Putative TEs up- or down- regulated in salinity 2 in the both strains. The first column indicates the area on the Venn diagrams in Fig. 1.

| Gene | InterPro accession | NCBI Blastp | | GyDB Blastx | | $Log_2FC$ | |
|---|---|---|---|---|---|---|---|
| | | Top hit | E-value | Top hit | E-value | HA-01 | HA-02 |
| TRINITY_DN11053_c0_g1 | - | KAI2493199.1\|hypothetical protein MHU86_21348 [Fragilaria crotonensis] | 1.70E-22 | - | - | -5.09 | -3.11 |
| TRINITY_DN11950_c2_g1 | Zinc finger, CCHC-type (IPR001878, IPR036875) | KAI2490608.1\|Reverse transcriptase (RNA-dependent DNA polymerase) [Fragilaria crotonensis] | 5.60E-27 | GAG_Tnt-1 | 0.0004 | -3.58 | -6.42 |
| TRINITY_DN12997_c2_g1 | Reverse transcriptase/retrotransposon-derived protein (IPR041577, IPR043502) | NBR26683.1\|hypothetical protein [Micrococcales bacterium] | 1.20E-46 | RNaseH_HMS-Beagle | 1.00E-23 | -1.84 | -1.38 |
| TRINITY_DN14959_c0_g2 | Reverse transcriptase, RNA-dependent DNA polymerase (IPR013103, IPR036397, IPR012337) | ABY63657.1\|gag-pol/CAP62384.1\|Blackbeard [Phaeodactylum tricornutum] | 0 | RT_CoDi4.3 | 4.00E-78 | -1.85 | -1.9 |
| TRINITY_DN14959_c0_g3 | - | ACA60884.1\|gag protein [Phaeodactylum tricornutum] | 8.40E-31 | GAG_CoDi4.3 | 3.00E-35 | -3.09 | -5.96 |
| TRINITY_DN15363_c0_g1 | Reverse transcriptase, RNA-dependent DNA polymerase (IPR036397, IPR013103, IPR012337) | ACA60889.1\|pol protein [Thalassiosira pseudonana] | 0 | RT_CoDi4.5 | 9.00E-97 | -1.22 | -2.41 |
| TRINITY_DN176_c1_g1 | Reverse transcriptase, RNA-dependent DNA polymerase (IPR013103, IPR043502) | GFH45823.1\|hypothetical protein CTEN210_02297 [Chaetoceros tenuissimus] | 0 | RT_CoDi6.3 | 4.00E-45 | -1.46 | -1.01 |
| TRINITY_DN18312_c0_g3 | Reverse transcriptase, RNA-dependent DNA polymerase (IPR013103, IPR043502) | KAG7341273.1\|reverse transcriptase RNA-dependent DNA polymerase [Nitzschia inconspicua] | 0 | RT_CoDi4.5 | 3.00E-95 | -1.36 | -1.62 |
| TRINITY_DN1938_c0_g1 | Integrase zinc-binding domain (IPR041588) | MCK7501271.1\|reverse transcriptase domain-containing protein [Comamonadaceae bacterium] | 5.00E-22 | RNaseH_Diaspora | 3E-16 | -1.59 | -1.18 |
| TRINITY_DN21298_c1_g2 | - | KAI2506113.1\|Reverse transcriptase (RNA-dependent DNA polymerase) [Fragilaria crotonensis] | 1.90E-73 | - | - | -2.7 | -2.65 |
| TRINITY_DN21827_c0_g1 | - | KAI2500803.1\|Reverse transcriptase (RNA-dependent DNA polymerase) [Fragilaria crotonensis] | 5.10E-172 | RNaseH_Mtanga | 1.00E-15 | -1.63 | -2.7 |
| TRINITY_DN21991_c0_g1 | Reverse transcriptase, RNA-dependent DNA polymerase (IPR013103) | KAG7341273.1\|reverse transcriptase RNA-dependent DNA polymerase [Nitzschia inconspicua] | 0 | RT_CoDi4.5 | 1.00E-91 | -2.6 | -2.51 |
| TRINITY_DN22405_c0_g1 | Reverse transcriptase, RNA-dependent DNA polymerase (IPR013103, IPR043502) | EJK63769.1\|hypothetical protein THAOC_15555 [Thalassiosira oceanica] | 0 | INT_CoDi6.6 | 5.00E-59 | -2.55 | -2.43 |
| TRINITY_DN22792_c0_g1 | Reverse transcriptase/ retrotransposon-derived protein (IPR041577, IPR041588, IPR043502) | KAI2490057.1\|transposition [Fragilaria crotonensis] | 1.20E-56 | RNaseH_Yoyo | 1.00E-21 | -4.06 | -3.99 |

| | | | | | | | |
|---|---|---|---|---|---|---|---|
| TRINITY_DN22892_c1_g2 | - | MCK7499178.1\|hypothetical protein [Comamonadaceae bacterium] | 1.80E-140 | RNaseH_CopiaSL_23 | 1.00E-11 | -4.58 | -5.51 |
| TRINITY_DN24020_c1_g1 | - | KAI2512927.1\|Reverse transcriptase (RNA-dependent DNA polymerase) [Fragilaria crotonensis] | 7.90E-50 | RNaseH_CopiaSL_23 | 0.0007 | -2.78 | -2.25 |
| TRINITY_DN24263_c0_g1 | Reverse transcriptase/Diguanylate cyclase domain (IPR000477, IPR043128, IPR043502) | GAX23113.1\|hypothetical protein FisN_UnNu094 [Fistulifera solaris] | 1.30E-30 | RT_Cer1 | 2.00E-27 | -1.29 | -1.87 |
| TRINITY_DN24727_c0_g1 | PiggyBac transposable element-derived protein (IPR029526) | AYV87236.1\|MAG: hypothetical protein Sylvanvirus41_1, partial [Sylvanvirus sp.] | 2.20E-14 | - | | -4.45 | -4.23 |
| TRINITY_DN25351_c0_g2 | Zinc finger, CCHC-type (IPR001878, IPR036875) | KAI2490608.1\|Reverse transcriptase (RNA-dependent DNA polymerase) [Fragilaria crotonensis] | 3.20E-46 | GAG_Retrosat-2 | 0.00002 | -3.87 | -3.84 |
| TRINITY_DN28282_c0_g1 | - | KAH9089508.1\|hypothetical protein Ae201684P_007677 [Aphanomyces euteiches] | 6.50E-05 | RNaseH_GypsySL_11 | 4E-12 | 1.02 | 1.46 |
| TRINITY_DN28388_c0_g1 | - | MCP4746268.1\|reverse transcriptase family protein [Desulfobacteraceae bacterium] | 6.00E-12 | - | | -1.03 | -1.18 |
| TRINITY_DN29047_c0_g1 | Zinc finger, CCHC-type (IPR001878, IPR036875) | KAG7364547.1\|hypothetical protein IV203_037749 [Nitzschia inconspicua] | 6.20E-06 | GAG_Tma | 0.003 | -1.29 | -1.19 |
| TRINITY_DN29819_c0_g1 | - | KAI2493200.1\|Reverse transcriptase (RNA-dependent DNA polymerase) [Fragilaria crotonensis] | 4.20E-73 | RT_CopiaSL_05 | 3.00E-06 | -3.54 | -4.35 |
| TRINITY_DN29898_c0_g1 | Reverse transcriptase, RNA-dependent DNA polymerase (IPR036397, IPR013103, IPR001584, IPR012337) | ACA60878.1\|gag-pol polyprotein [Phaeodactylum tricornutum] | 0 | RT_CoDi2.4 | 3.00E-93 | -1.97 | -2.05 |
| TRINITY_DN32369_c0_g1 | Reverse transcriptase, RNA-dependent DNA polymerase (IPR013103) | KAI2490200.1\|Reverse transcriptase (RNA-dependent DNA polymerase) [Fragilaria crotonensis] | 7.00E-118 | RT_CoDi4.5 | 2.00E-50 | -1.82 | -2.16 |
| TRINITY_DN3255_c0_g3 | PiggyBac transposable element-derived protein (IPR029526) | XP_034824097.1\|piggyBac transposable element-derived protein 3-like [Maniola hyperantus] | 1.20E-13 | RNaseH_Real | 0.83 | 2.98 | 3.77 |
| TRINITY_DN35736_c0_g1 | - | KAG7342125.1\|reverse transcriptase RNA-dependent DNA polymerase [Nitzschia inconspicua] | 2.00E-53 | RT_1731 | 1.00E-05 | -4.22 | -3.37 |
| TRINITY_DN36035_c0_g1 | - | KAI2493200.1\|Reverse transcriptase (RNA-dependent DNA polymerase) [Fragilaria crotonensis] | 7.30E-38 | RT_Retrofit | 3.00E-10 | -4.55 | -5.2 |
| TRINITY_DN36380_c0_g1 | - | MCH94884.1\|retrovirus-related Pol polyprotein from transposon TNT 1-94 [Trifolium medium] | 8.90E-04 | GAG_CoDi7.1 | 6.00E-06 | -1.37 | -1.97 |
| TRINITY_DN440_c0_g2 | Reverse transcriptase, RNA-dependent DNA polymerase (IPR013103) | KAI2503956.1\|Reverse transcriptase (RNA-dependent DNA polymerase) [Fragilaria crotonensis] | 6.50E-45 | RT_CoDi3.1 | 1.00E-60 | -1.73 | -1.26 |

| | | | | | | | |
|---|---|---|---|---|---|---|---|
| TRINITY_DN4426_c4_g1 | - | KAI2490608.1\|Reverse transcriptase (RNA-dependent DNA polymerase) [Fragilaria crotonensis] | 6.30E-09 | - | | -6.02 | -5.09 |
| TRINITY_DN46482_c0_g2 | - | KAG7344469.1\|reverse transcriptase RNA-dependent DNA polymerase [Nitzschia inconspicua] | 3.60E-04 | RT_Osvaldo | 9E-24 | -1.54 | -1.98 |
| TRINITY_DN51460_c0_g1 | Reverse transcriptase, RNA-dependent DNA polymerase (IPR013103, IPR043502) | KAI2494468.1\|Reverse transcriptase (RNA-dependent DNA polymerase) [Fragilaria crotonensis] | 2.10E-83 | RT_CoDi4.5 | 9.00E-91 | -2.52 | -4.71 |
| TRINITY_DN540_c3_g2 | Reverse transcriptase, RNA-dependent DNA polymerase (IPR013103, IPR036397, IPR001584, IPR012337) | ACA60912.1\|gag-pol polyprotein [Phaeodactylum tricornutum] | 0 | INT_CoDi7.1 | 9.00E-143 | -1.17 | -1.3 |
| TRINITY_DN5578_c0_g1 | Reverse transcriptase, RNA-dependent DNA polymerase (IPR013103) | KAG7341273.1\|reverse transcriptase RNA-dependent DNA polymerase [Nitzschia inconspicua] | 0 | RT_CoDi4.5 | 2.00E-108 | -1.77 | -3.43 |
| TRINITY_DN62452_c0_g1 | Reverse transcriptase/Diguanylate cyclase domain (IPR043128, IPR043502) | MCK7501271.1\|reverse transcriptase domain-containing protein [Comamonadaceae bacterium] | 1.60E-22 | INT_marY1 | 0.00001 | -3.11 | -3.28 |
| TRINITY_DN6416_c0_g1 | Reverse transcriptase, RNA-dependent DNA polymerase (IPR013103) | KAI2491145.1\|Reverse transcriptase (RNA-dependent DNA polymerase) [Fragilaria crotonensis] | 2.00E-64 | RNaseH_CoDi2.4 | 3.00E-48 | -1.23 | -1.42 |
| TRINITY_DN666_c8_g1 | PiggyBac transposable element-derived protein (IPR029526) | XP_034824097.1\|piggyBac transposable element-derived protein 3-like [Maniola hyperantus] | 1.20E-75 | TR_LsGINGER2-1_Repbaseaccession_Ginger2-1_LS | 0.4 | -2.18 | -1.62 |
| TRINITY_DN7129_c0_g1 | - | KMZ58833.1\|hypothetical protein ZOSMA_7339G00010, partial [Zostera marina] | 3.40E-122 | RNaseH_CopiaSL_23 | 4E-17 | -1.57 | -4.11 |
| TRINITY_DN7894_c1_g1 | - | KAI2512927.1\|Reverse transcriptase (RNA-dependent DNA polymerase) [Fragilaria crotonensis] | 1.50E-88 | RNaseH_Mtanga | 2.00E-23 | -4.36 | -2.69 |

**Table S6.** Putative TEs up- or down- regulated in salinity but not shared among the strains (TEs contained in parcels other than (a) and (b) in the Venn diagram in Fig. 1). $Log_2FC$ values are shown for DEGs only. Not DE=not differentially expressed.

| Gene | Sequence description | GyDB Blastp | | $Log_2FC$ | |
|---|---|---|---|---|---|
| | | Top hit | E-value | HA-01 | HA-02 |
| TRINITY_DN11030_c0_g1 | Reverse transcriptase (RNA-dependent DNA polymerase) | RT_Sto-4 | 0.0000003 | not DE | -1.89 |
| TRINITY_DN11278_c0_g1 | Reverse transcriptase (RNA-dependent DNA polymerase) | RT_CoDi4.4 | 7E-37 | not DE | 1.21 |
| TRINITY_DN1147_c9_g1 | Reverse transcriptase (RNA-dependent DNA polymerase) | RT_CoDi4.3 | 1E-58 | not DE | 1.77 |
| TRINITY_DN11667_c0_g1 | gag protein | AP_CoDi4.3 | 5E-14 | not DE | -1.98 |
| TRINITY_DN11892_c0_g2 | Reverse transcriptase (RNA-dependent DNA polymerase) | RNaseH_CopiaSL_09 | 2E-09 | not DE | 1.93 |
| TRINITY_DN11970_c0_g1 | pol protein | INT_412 | 0.00000001 | not DE | -3.60 |
| TRINITY_DN120_c8_g1 | Reverse transcriptase (RNA-dependent DNA polymerase) | RNaseH_pCretro6 | 2E-21 | not DE | -1.16 |
| TRINITY_DN12194_c0_g1 | transposase IS4 | - | - | not DE | -5.36 |
| TRINITY_DN12594_c0_g2 | gag-polypeptide of LTR copia-type | GAG_CoDi6.3 | 2E-66 | not DE | -3.88 |
| TRINITY_DN1293_c25_g1 | gag protein | GAG_CoDi4.3 | 1E-14 | not DE | 2.93 |
| TRINITY_DN13080_c0_g1 | Reverse transcriptase (RNA-dependent DNA polymerase) | RT_CoDi2.4 | 5E-80 | not DE | -2.30 |
| TRINITY_DN13173_c0_g1 | pol protein | RNaseH_CoDi4.3 | 7E-30 | not DE | -3.96 |
| TRINITY_DN13257_c1_g1 | Reverse transcriptase (RNA-dependent DNA polymerase) | RT_CoDi2.4 | 1E-77 | not DE | -1.87 |
| TRINITY_DN13333_c0_g1 | transposase IS4 | - | - | not DE | -2.29 |
| TRINITY_DN13609_c1_g1 | Reverse transcriptase (RNA-dependent DNA polymerase) | RT_CoDi4.5 | 3E-75 | not DE | -2.44 |
| TRINITY_DN13780_c0_g1 | Reverse transcriptase (RNA-dependent DNA polymerase) | RT_DRM | 2E-45 | not DE | -5.24 |
| TRINITY_DN1411_c0_g1 | piggyBac transposable element-derived protein 4-like | - | - | not DE | 1.22 |
| TRINITY_DN14898_c0_g1 | Reverse transcriptase (RNA-dependent DNA polymerase) | GAG_CoDi4.3 | 0.00000001 | not DE | 1.93 |
| TRINITY_DN16114_c0_g1 | transposase IS4 | - | - | not DE | -1.59 |
| TRINITY_DN16133_c0_g1 | Reverse transcriptase (RNA-dependent DNA polymerase) | RT_CoDi2.4 | 1E-64 | not DE | -2.58 |
| TRINITY_DN18354_c0_g2 | Reverse transcriptase (RNA-dependent DNA polymerase) | - | - | not DE | 3.04 |
| TRINITY_DN18740_c0_g1 | Reverse transcriptase (RNA-dependent DNA polymerase) | RT_CoDi4.5 | 9E-62 | not DE | -2.82 |
| TRINITY_DN19720_c0_g1 | gag-pol polyprotein | RT_CoDi6.3 | 8E-62 | not DE | -2.64 |
| TRINITY_DN20314_c0_g1 | Reverse transcriptase (RNA-dependent DNA polymerase) | RT_CoDi3.1 | 0.0006 | not DE | 1.23 |
| TRINITY_DN21162_c0_g2 | Reverse transcriptase (RNA-dependent DNA polymerase) | RNaseH_CopiaSL_23 | 1E-13 | not DE | -1.76 |
| TRINITY_DN21460_c0_g1 | reverse transcriptase domain-containing protein | RNaseH_17.6 | 1E-30 | not DE | -5.52 |

| | | | | | |
|---|---|---|---|---|---|
| TRINITY_DN21635_c0_g1 | transposase IS4 | - | - | not DE | 2.00 |
| TRINITY_DN2165_c6_g1 | Reverse transcriptase (RNA-dependent DNA polymerase) | RT_CoDi4.5 | 8E-47 | not DE | 1.75 |
| TRINITY_DN21933_c0_g1 | Reverse transcriptase (RNA-dependent DNA polymerase) | RT_CoDi6.3 | 3E-96 | not DE | -2.41 |
| TRINITY_DN22707_c1_g1 | Pogo transposable element | - | - | not DE | -3.41 |
| TRINITY_DN23550_c0_g1 | piggyBac transposable element-derived protein 3-like | - | - | not DE | -2.51 |
| TRINITY_DN2369_c0_g1 | tigger transposable element-derived protein 4-like | - | - | not DE | 1.41 |
| TRINITY_DN24163_c0_g1 | Reverse transcriptase (RNA-dependent DNA polymerase) | RT_CoDi4.3 | 1E-64 | not DE | -1.68 |
| TRINITY_DN24357_c0_g1 | reverse transcriptase domain-containing protein | - | - | not DE | -2.09 |
| TRINITY_DN24824_c0_g1 | Reverse transcriptase (RNA-dependent DNA polymerase) | RT_CoDi2.4 | 2E-87 | not DE | -3.18 |
| TRINITY_DN26423_c0_g1 | transposase IS4 | TR_LsGINGER2-1_Repbaseaccession_Ginger2-1_LS | 0.0003 | not DE | -2.58 |
| TRINITY_DN26905_c3_g1 | Reverse transcriptase (RNA-dependent DNA polymerase) | RT_CoDi4.4 | 4E-84 | not DE | -3.28 |
| TRINITY_DN2791_c1_g1 | Reverse transcriptase (RNA-dependent DNA polymerase) | TAV_TVCV | 0.057 | not DE | -1.09 |
| TRINITY_DN2829_c0_g1 | Reverse transcriptase (RNA-dependent DNA polymerase) | RT_CoDi6.6 | 0.00000001 | not DE | -3.07 |
| TRINITY_DN28670_c0_g1 | Reverse transcriptase (RNA-dependent DNA polymerase) | RNaseH_CoDi4.5 | 9E-72 | not DE | -5.17 |
| TRINITY_DN2996_c1_g2 | Reverse transcriptase (RNA-dependent DNA polymerase) | - | - | not DE | -1.32 |
| TRINITY_DN3028_c0_g1 | tigger transposable element-derived protein 4-like | - | - | not DE | 1.46 |
| TRINITY_DN31435_c1_g1 | Reverse transcriptase (RNA-dependent DNA polymerase) | RNaseH_CopiaSL_23 | 2E-19 | not DE | -3.18 |
| TRINITY_DN31914_c0_g1 | Reverse transcriptase (RNA-dependent DNA polymerase) | RNaseH_CoDi5.2 | 3E-62 | not DE | -3.26 |
| TRINITY_DN3204_c1_g1 | Reverse transcriptase (RNA-dependent DNA polymerase) | RT_CoDi5.5 | 4E-49 | not DE | 5.6 |
| TRINITY_DN32229_c0_g1 | Reverse transcriptase (RNA-dependent DNA polymerase) | - | - | not DE | -2.97 |
| TRINITY_DN32405_c0_g2 | Reverse transcriptase (RNA-dependent DNA polymerase) | CHR_CoDi4.3 | 5E-17 | not DE | -4.74 |
| TRINITY_DN32657_c0_g1 | Reverse transcriptase (RNA-dependent DNA polymerase) | INT_CoDi4.5 | 6E-69 | not DE | 1.51 |
| TRINITY_DN33107_c0_g1 | Reverse transcriptase (RNA-dependent DNA polymerase) | RT_CoDi6.3 | 2E-41 | not DE | -3.62 |
| TRINITY_DN33424_c0_g1 | Reverse transcriptase (RNA-dependent DNA polymerase) | RT_CoDi3.1 | 2E-48 | not DE | 3.85 |
| TRINITY_DN36162_c0_g1 | Reverse transcriptase (RNA-dependent DNA polymerase) | AP_CoDi4.3 | 3E-24 | not DE | -4.68 |

| | | | | | |
|---|---|---|---|---|---|
| TRINITY_DN3853_c1_g2 | piggyBac transposable element-derived protein 3-like | - | - | not DE | 3.00 |
| TRINITY_DN42522_c0_g1 | Reverse transcriptase (RNA-dependent DNA polymerase) | - | - | not DE | -6.29 |
| TRINITY_DN4356_c0_g1 | Transposase IS4 | - | - | not DE | 1.64 |
| TRINITY_DN4947_c0_g1 | Reverse transcriptase (RNA-dependent DNA polymerase) | RNaseH_CopiaSL_23 | 2E-23 | not DE | -1.08 |
| TRINITY_DN5897_c0_g1 | transposase IS4 | - | - | not DE | -2.55 |
| TRINITY_DN6360_c3_g1 | DDE superfamily endonuclease | - | - | not DE | -2.72 |
| TRINITY_DN6615_c0_g1 | Reverse transcriptase (RNA-dependent DNA polymerase) | RT_CoDi2.4 | 1E-55 | not DE | -5.93 |
| TRINITY_DN66948_c0_g1 | gag-pol polyprotein | GAG_CoDi6.3 | 7E-12 | not DE | -5.37 |
| TRINITY_DN7181_c0_g1 | Reverse transcriptase (RNA-dependent DNA polymerase) | RT_CoDi4.3 | 2E-57 | not DE | -1.46 |
| TRINITY_DN7449_c0_g1 | Reverse transcriptase (RNA-dependent DNA polymerase) | RT_CoDi4.3 | 3E-56 | not DE | -5.37 |
| TRINITY_DN7903_c0_g1 | transposase IS4 | TR_LsGINGER2-1_Repbaseaccession_Ginger2-1_LS | 0.005 | not DE | -3.03 |
| TRINITY_DN794_c0_g2 | Tigger transposable element-derived protein 6 | - | - | not DE | 1.88 |
| TRINITY_DN8255_c0_g1 | Copia protein | RNaseH_CoDi6.2 | 4E-28 | not DE | -3.13 |
| TRINITY_DN8268_c0_g1 | Reverse transcriptase (RNA-dependent DNA polymerase) | RT_1731 | 0.00000006 | not DE | -2.86 |
| TRINITY_DN9052_c0_g1 | Reverse transcriptase (RNA-dependent DNA polymerase) | RT_CoDi6.6 | 0.000003 | not DE | 2.12 |
| TRINITY_DN9584_c0_g1 | Reverse transcriptase (RNA-dependent DNA polymerase) | RT_CoDi4.3 | 2E-82 | not DE | -2.28 |
| TRINITY_DN5173_c0_g2 | piggyBac transposable element-derived protein 3-like | - | - | 4.28 | -2.80 |
| TRINITY_DN14869_c0_g1 | Transposase IS4 | - | - | 2.91 | -2.13 |
| TRINITY_DN25027_c0_g1 | Reverse transcriptase (RNA-dependent DNA polymerase) | RT_Ty1B | 0.027 | 2.82 | -5.5 |
| TRINITY_DN21635_c0_g3 | Transposase IS4 | - | - | 2.45 | not DE |
| TRINITY_DN30274_c0_g1 | Transposase IS4 | RNaseH_ComYMV | 0.0006 | 2.23 | -3.46 |
| TRINITY_DN4022_c0_g1 | Transposase IS4 | - | - | 2.1 | -1.60 |
| TRINITY_DN10002_c0_g1 | Transposase IS4 | - | - | 1.83 | -1.13 |
| TRINITY_DN7083_c3_g1 | Transposase IS4 | - | - | 1.77 | -1.25 |
| TRINITY_DN11900_c0_g1 | Reverse transcriptase (RNA-dependent DNA polymerase) | RT_CoDi4.3 | 2E-58 | 1.68 | 1.19 |
| TRINITY_DN3114_c0_g1 | rve integrase | - | - | 1.58 | not DE |
| TRINITY_DN15623_c0_g1 | Reverse transcriptase (RNA-dependent DNA polymerase) | AP_CatDceg | 0.07 | 1.50 | 0.14 |
| TRINITY_DN164_c1_g1 | Reverse transcriptase (RNA-dependent DNA polymerase) | RT_CoDi4.3 | 2E-60 | 1.44 | -2.09 |
| TRINITY_DN3114_c0_g4 | DDE superfamily endonuclease | - | - | 1.05 | not DE |
| TRINITY_DN5085_c2_g1 | Reverse transcriptase (RNA-dependent DNA polymerase) | - | - | -1.05 | 1.13 |

| | | | | | |
|---|---|---|---|---|---|
| TRINITY_DN9615_c1_g1 | Reverse transcriptase (RNA-dependent DNA polymerase) | - | - | -1.21 | not DE |
| TRINITY_DN7972_c0_g1 | Reverse transcriptase (RNA-dependent DNA polymerase) | RNaseH_Hydra1-2 | 0.0000004 | -1.28 | not DE |
| TRINITY_DN12637_c0_g1 | Reverse transcriptase (RNA-dependent DNA polymerase) | RT_CoDi4.3 | 3E-73 | -1.31 | not DE |
| TRINITY_DN4301_c0_g2 | Reverse transcriptase (RNA-dependent DNA polymerase) | RNaseH_CopiaSL_23 | 9E-23 | -1.44 | not DE |
| TRINITY_DN1726_c0_g2 | Reverse transcriptase (RNA-dependent DNA polymerase) | RNaseH_Xanthias | 1E-19 | -1.55 | not DE |
| TRINITY_DN2814_c0_g1 | Reverse transcriptase (RNA-dependent DNA polymerase) | RNaseH_CopiaSL_23 | 6E-25 | -1.56 | not DE |
| TRINITY_DN14681_c0_g1 | Reverse transcriptase (RNA-dependent DNA polymerase) | RT_CoDi6.3 | 0.0004 | -1.58 | 1.38 |
| TRINITY_DN28117_c0_g1 | Reverse transcriptase (RNA-dependent DNA polymerase) | RNaseH_pCretro6 | 2E-21 | -1.58 | not DE |
| TRINITY_DN21298_c0_g1 | Reverse transcriptase (RNA-dependent DNA polymerase) | RNaseH_CopiaSL_23 | 6E-22 | -1.63 | not DE |
| TRINITY_DN11427_c0_g1 | Reverse transcriptase (RNA-dependent DNA polymerase) | - | - | -1.71 | not DE |
| TRINITY_DN17284_c0_g1 | Reverse transcriptase (RNA-dependent DNA polymerase) | - | - | -1.72 | not DE |
| TRINITY_DN4976_c0_g1 | Retrovirus Polyprotein | RT_DRM | 7E-38 | -1.75 | not DE |
| TRINITY_DN23488_c0_g2 | DDE-type integrase /transposase/recombinase | RT_SPM | 2E-23 | -1.80 | not DE |
| TRINITY_DN9202_c0_g1 | Reverse transcriptase (RNA-dependent DNA polymerase) | RT_CoDi2.4 | 8E-76 | -1.84 | not DE |
| TRINITY_DN14242_c0_g1 | Reverse transcriptase (RNA-dependent DNA polymerase) | RNaseH_Galadriel | 2E-22 | -1.93 | not DE |
| TRINITY_DN17627_c0_g1 | hypothetical protein INT48_004898 | - | - | -2.04 | not DE |
| TRINITY_DN32266_c0_g1 | pol protein | RT_DRM | 1E-40 | -2.05 | not DE |
| TRINITY_DN7036_c0_g1 | Reverse transcriptase (RNA-dependent DNA polymerase) | RT_CoDi4.3 | 9E-60 | -2.12 | not DE |
| TRINITY_DN48152_c0_g1 | tigger transposable element-derived protein 4-like | - | - | -2.15 | not DE |
| TRINITY_DN6398_c0_g1 | Reverse transcriptase (RNA-dependent DNA polymerase) | RNaseH_CoDi6.3 | 6E-20 | -2.23 | not DE |
| TRINITY_DN20105_c0_g1 | Reverse transcriptase (RNA-dependent DNA polymerase) | RT_CoDi6.3 | 4E-58 | -2.29 | not DE |
| TRINITY_DN42297_c0_g2 | Reverse transcriptase (RNA-dependent DNA polymerase) | INT_CoDi4.4 | 5E-20 | -2.29 | not DE |
| TRINITY_DN11942_c0_g1 | endonuclease-reverse transcriptase domain-containing protein | INT_GypsySL_11 | 0.051 | -2.38 | not DE |
| TRINITY_DN21842_c1_g1 | Reverse transcriptase (RNA-dependent DNA polymerase) | RNaseH_pCretro6 | 1E-24 | -2.46 | not DE |
| TRINITY_DN16719_c0_g1 | Reverse transcriptase (RNA-dependent DNA polymerase) | - | - | -2.50 | not DE |
| TRINITY_DN30181_c0_g1 | Reverse transcriptase (RNA-dependent DNA polymerase) | RNaseH_HMS-Beagle | 3E-25 | -2.51 | not DE |
| TRINITY_DN16969_c0_g1 | gag-pol polyprotein | RT_CoDi2.4 | 2E-92 | -2.59 | not DE |

| | | | | | |
|---|---|---|---|---|---|
| TRINITY_DN13529_c1_g1 | Reverse transcriptase (RNA-dependent DNA polymerase) | RNaseH_pCretro6 | 3E-21 | -2.89 | not DE |
| TRINITY_DN13789_c2_g1 | Reverse transcriptase (RNA-dependent DNA polymerase) | RNaseH_pCretro6 | 3E-24 | -2.91 | not DE |
| TRINITY_DN47095_c1_g1 | Reverse transcriptase (RNA-dependent DNA polymerase) | - | - | -3.43 | not DE |
| TRINITY_DN62023_c0_g1 | Pogo transposable element with KRAB domain | - | - | -3.46 | not DE |
| TRINITY_DN16115_c1_g1 | Reverse transcriptase (RNA-dependent DNA polymerase) | RNaseH_Oryco1-1 | 4E-17 | -3.47 | 2.44 |
| TRINITY_DN78189_c0_g1 | Reverse transcriptase (RNA-dependent DNA polymerase) | RT_1731 | 0.0000001 | -3.65 | not DE |
| TRINITY_DN21841_c0_g2 | transposase | - | - | -3.66 | not DE |
| TRINITY_DN36654_c0_g1 | Reverse transcriptase (RNA-dependent DNA polymerase) | RT_SURL | 6E-29 | -3.66 | not DE |
| TRINITY_DN62844_c0_g1 | Reverse transcriptase (RNA-dependent DNA polymerase) | - | - | -3.91 | not DE |
| TRINITY_DN26406_c0_g1 | reverse transcriptase family protein | RT_SPM | 0.0000003 | -4.50 | not DE |
| TRINITY_DN24847_c0_g1 | Reverse transcriptase (RNA-dependent DNA polymerase) | - | - | -4.76 | not DE |
| TRINITY_DN36064_c1_g1 | reverse transcriptase domain-containing protein | RNaseH_HMS-Beagle | 2E-19 | -5.39 | not DE |

**Table S7.** Shared DEGs encoding enzymes involved in biosynthesis and degradation of fatty acid and chrysolaminarin (1,3-*β*-glucan) and their expression levels. The first column indicates the area on the Venn diagrams in Fig. 1.

| Venn diagram | Gene | Pathway | Enzyme | $Log_2FC$ | |
|---|---|---|---|---|---|
| | | | | HA-01 | HA-02 |
| (a) | TRINITY_DN7305_c0_g1 | Fatty acid biosynthesis | [acyl-carrier-protein] S-malonyltransferase [EC:2.3.1.39] | 3.14 | 1.35 |
| (b) | TRINITY_DN95_c1_g2 | Fatty acid biosynthesis & Fatty degradation | long-chain acyl-CoA synthetase [EC:6.2.1.3] | -2.15 | -1.09 |
| (a) | TRINITY_DN484_c2_g1 | Fatty acid degradation | acyl-CoA oxidase [EC:1.3.3.6] | 1.44 | 1.44 |
| (a) | TRINITY_DN3892_c1_g1 | | butyryl-CoA dehydrogenase [EC:1.3.8.1], acyl-CoA dehydrogenase [EC:1.3.8.7] | 1.11 | 1.86 |
| (a) | TRINITY_DN17472_c0_g2 | | short-chain 2-methylacyl-CoA dehydrogenase [EC:1.3.8.5] | 1.58 | 2.39 |
| (b) | TRINITY_DN88_c1_g2 | Chrysolaminarin biosynthesis (UDP-glucose → 1,3-β-Glucan) | 1,3-beta-glucan synthase [EC:2.4.1.34] | -3.23 | -3.48 |
| (a) | TRINITY_DN3822_c0_g1 | Chrysolaminarin degradation (1,3-beta-Glucan → Glucose) | glucan 1,3-beta-glucosidase [EC:3.2.1.58] | 2.25 | 2.46 |

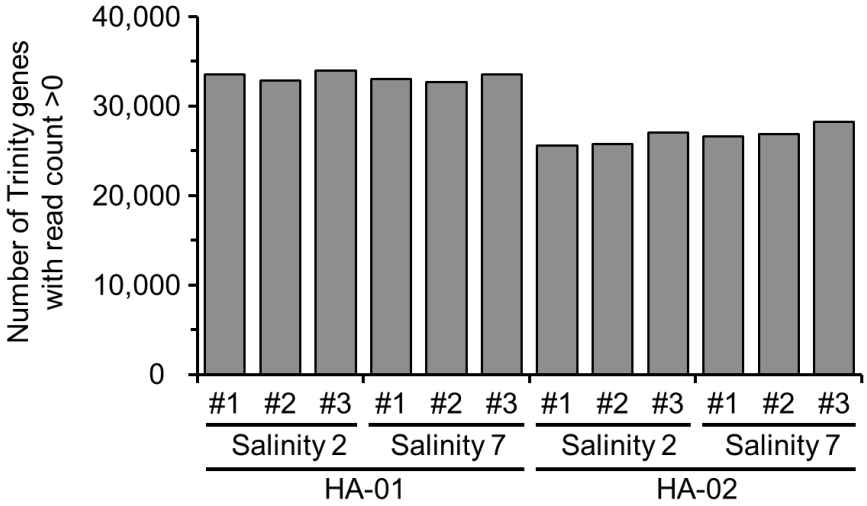


**Fig. S1.** Number of genes in the 12 samples with read count greater than 0. The numbers are based on the read counts after TMM normalization. Genes possibly derived from contamination were eliminated from this result.

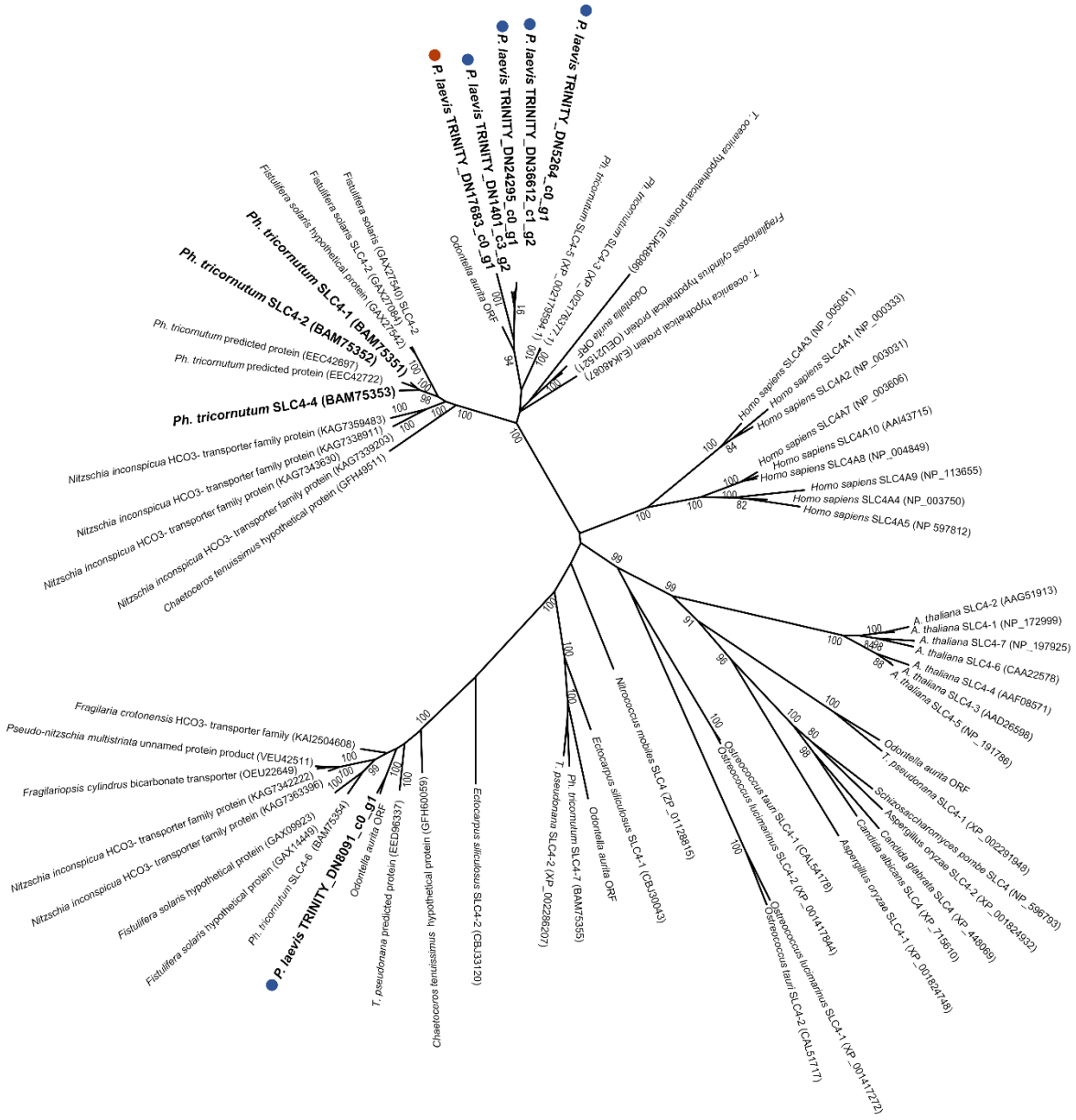


**Fig. S2.** Phylogenetic tree of bicarbonate transporters of mammal, plant, fungi, and eukaryotic algae, based on the amino acid sequences. Values are shown only for branches supported by bootstrap values >80. Brackets indicate GenBank accession. Bolded characters indicate the SLC 4-1, 2, 4 of *Ph. tricornutum*, whose activity has been demonstrated to be dependent on $Na^+$ or other cations (Nakajima et al. 2013, Nawaly et al. 2023), and the $HCO_3^-$ transporters of *P. laevis*. Brown circle indicates the gene up-regulated in salinity 2, and blue circles indicate the gene down-regulated in salinity 2.

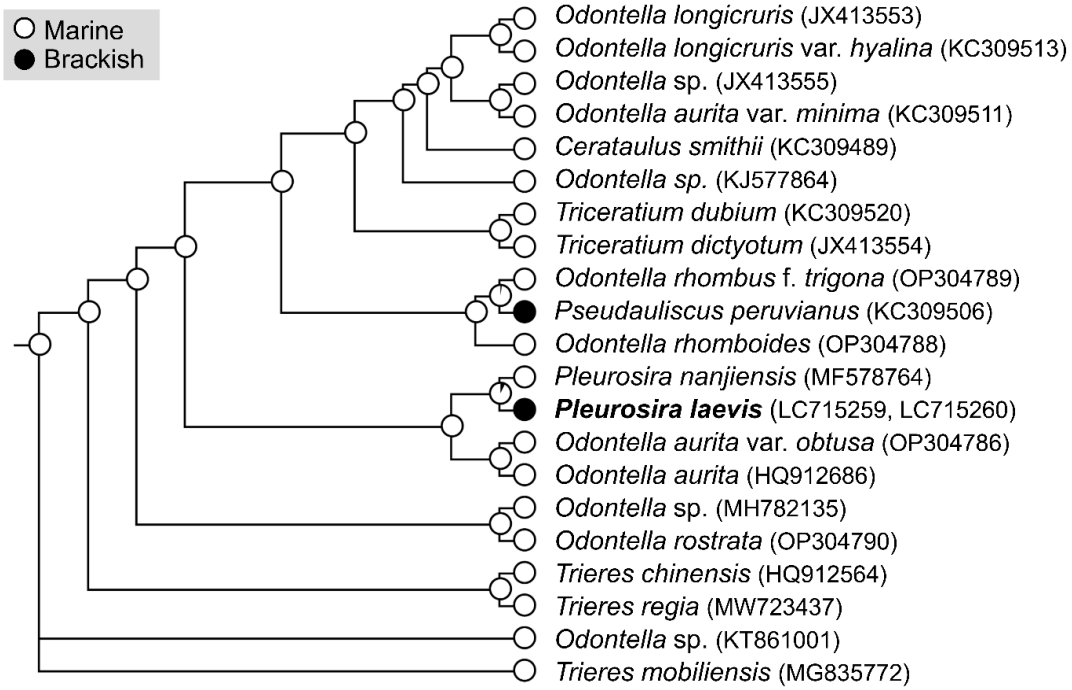


**Fig. S3.** Maximum likelihood ancestral state reconstructions based on SSU rDNA sequences. Pie graphs at internal nodes indicate the relative maximum likelihood support for the inferred ancestral habitat type. Brackets indicate GenBank accessions. *Pseudauliscus peruvianus* was described from the Hudson River by Schmidt (1875), while was found from marine environment in Ashworth et al. (2013), therefore it was assumed here to be a brackish species.

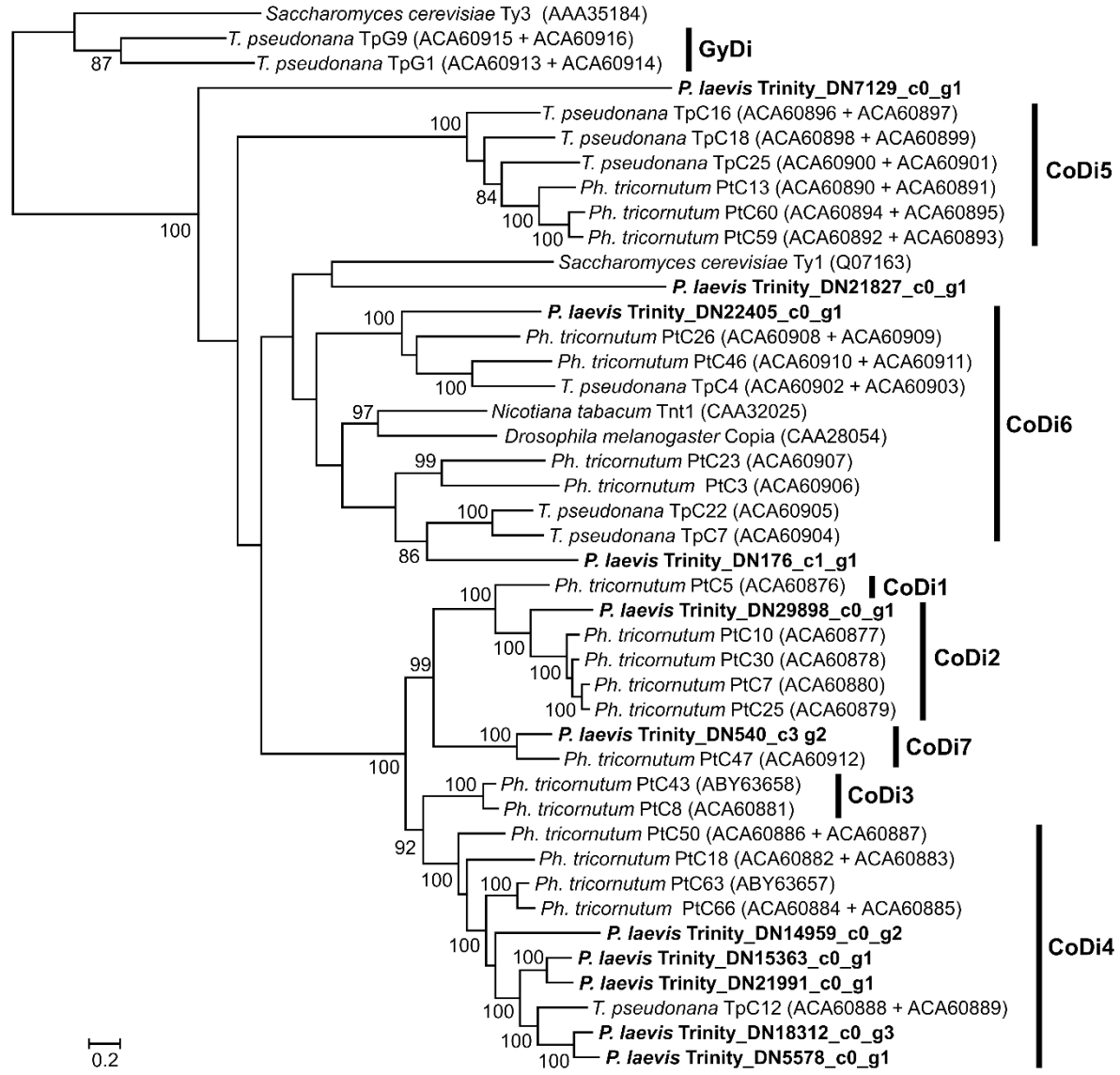


**Fig. S4**. Phylogenetic tree of retrotransposons based on amino acid sequences. Values are shown only for branches supported by bootstrap values >80. Brackets indicate GenBank accessions. The designation of each TE and CoDi1-7 adheres to the numbering by Maumus et al. (2009).

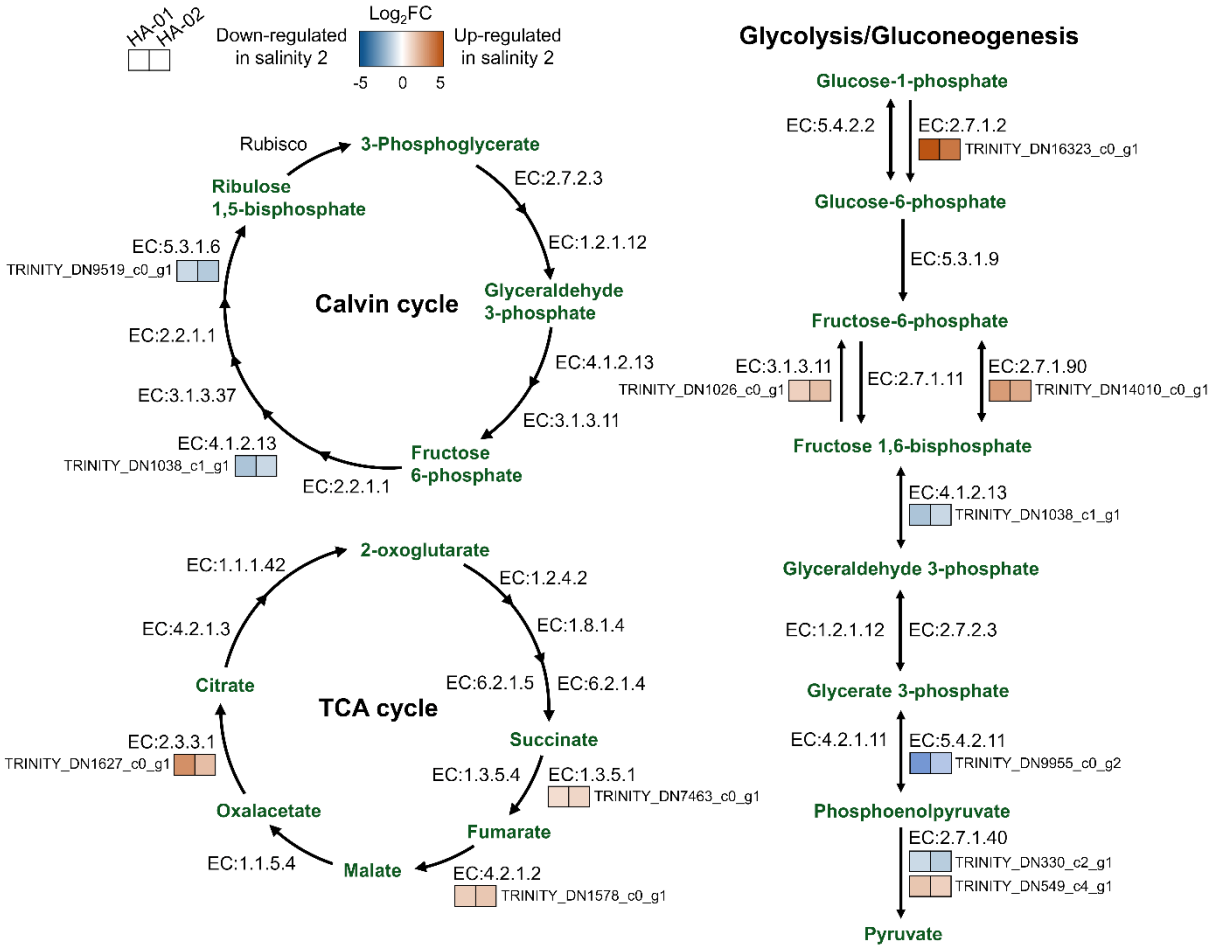


**Fig. S5.** Log2 fold changes of shared DEGs involved in the Calvin cycle, TCA cycle, and glycolysis/glycogenesis.

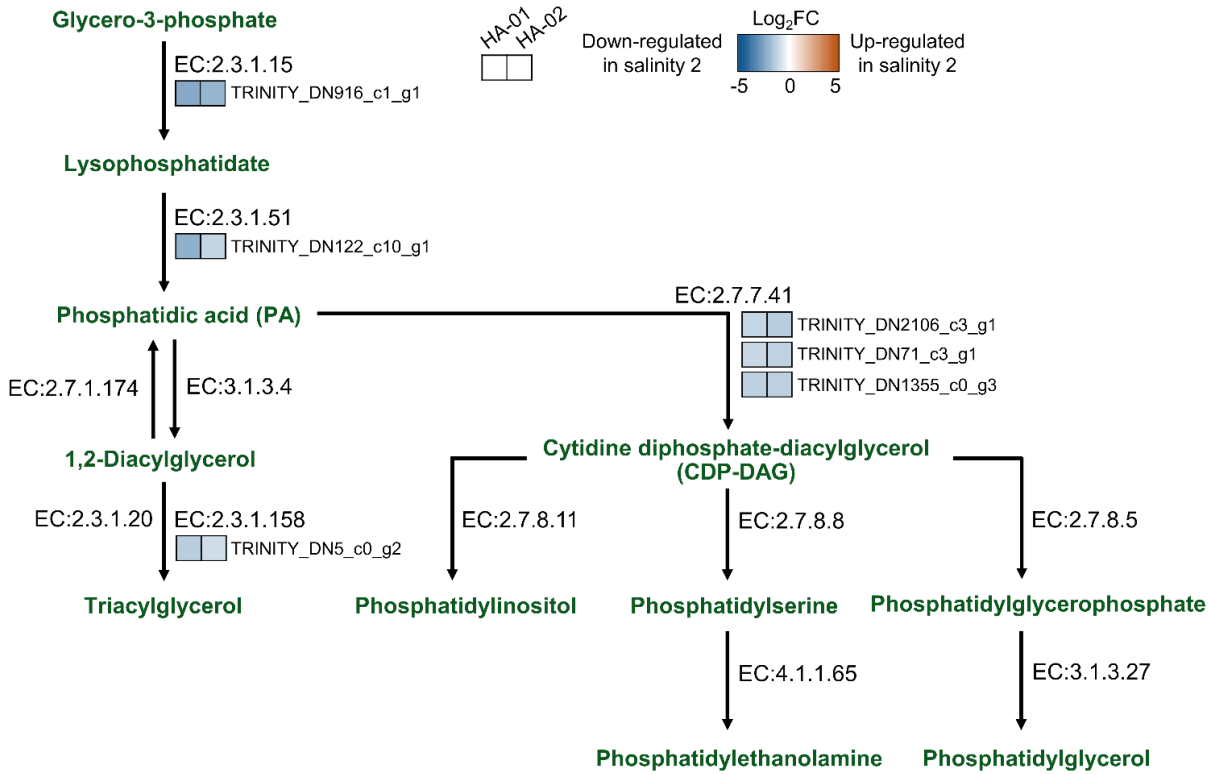


**Fig. S6.** Log2 fold changes of the shared DEGs involved in triacylglycerol and phospholipids biosynthesis.

# GENERAL DISCUSSION

## Review of the chapters

In **Chapter 1**, the inheritance mode of spheroid bodies in *Epithemia gibba* var. *ventricosa* was revealed to be randomly inherited from only one parent. This implies that the host diatom has already developed a system that ensures uniparental inheritance of this newly established organelle. It was also found that the parental origin of plastid and spheroid bodies can differ from each other, suggesting that the removal mechanisms of plastid and spheroid bodies are independent of each other. Further validation through genotyping with polymorphisms on the spheroid body genome, as conducted in this study, would be useful to determine if there is a bias between parental strains in the inheritance of spheroid bodies when multiple parental strains are used. It will be interesting to see if our result showing the random uniparental inheritance would be affected by the number of spheroid bodies per cell, which have been shown to vary with the nitrogen availability of the environment (DeYoe et al. 1992).

There are only a limited number of diatom species in which sexual reproduction can be induced in a culture condition. Nevertheless, since Klebahn (1896) observed sexual reproduction of *E. gibba* var. *gibba* in field samples, it was not surprising that *E. gibba* var. *ventricosa*, which is phylogenetically and morphologically closely related to *E. gibba* var. *gibba* (see Discussion in Chapter 2, Kamakura & Sato 2018), was also capable of sexual reproduction. I could induce sexual reproduction in *E. gibba* var. *ventricosa* by simply mixing the strains, making it a suitable material for this study. This diatom may allow us to understand uniparental inheritance mechanism of spheroid bodies in the process of organellogenesis thorough a cell biological approach, as has been done for the studies of organellar inheritance of the green alga *Chlamydomonas reinhardii* (as reviewed in Nishimura et al. 2010).

In **Chapter 2**, the differences in the life cycles of sympatric *Epithemia* taxa were shown. While *E. gibba* var. *ventricosa* inevitably decreased in cell size and required sexual reproduction for size restoration, *Epithemia* sp. showed very little or no reduction in cell size. The emergence of the sexual phase in diatoms is regulated solely by cell size, and the avoidance of size reduction is tied to the absence of sexual reproduction (Chepurnov et al. 2004). *Epithemia gibba* var. *ventricosa*, reached to the lower size limit for cell division (mentioned in Chapter 1) after long term clonal culture, directly supporting the importance of cell size recovery in this taxon. The different degrees of cell size reduction in the two taxa were possibly due to differences in cell wall mechanics as Geitler (1932) proposed. When girdle bands are more elastic, the cytoplasm beneath them can expand during cell division, and the size of newly formed hypovalve can be same as that of the epivalve, or be even larger (Geitler 1932). Görlich et al. (2019) revealed that the gene *Silicanin-1*, which encodes a protein localized to the SDV membrane, controls the stiffness of the cell wall. Such genes may regulate diatom life cycles by enabling or hindering the avoidance of cell size reduction through the control of mechanical properties of the silica cell wall. I consider that *Epithemia* sp. is an undescribed taxon, although it has been found sporadically in Japan (Kihara et al. 2009, Takano et al. 2009, Sato et al. 2020, Ohtsuka & Kitano 2020). Morphological comparison and phylogenetic

analysis among this diatom and other *Epitheima* taxon i.g., *E. gibberula* and *E. michelorum* is needed clarify its taxonomic position.

In **Chapter 3**, I tracked the formation of newly formed valves of *Pleurosira laevis* under several salinity conditions. The result clearly demonstrated the morphological plasticity of the valves was controlled by environmental salinity. The *laevis* form, characterized by flat valve faces, and the *polymorpha* form, characterized by domed valve faces, were both produced at salinities of 2 and 7, respectively. The striking feature seen in *P. laevis* is that the distinct morphological change readily recognizable under LM can be induced by only a subtle change in salinity. The morphological response to salinity in this diatom would be a potential indicator for water quality and for paleoenvironmental studies. Furthermore, the highly reproducible and easily manipulated morphological plasticity makes this diatom an ideal model for lab experiments focusing on the molecular and genetic factors involved with valve morphogenesis. A similar morphology to the *polymorpha* form was reproduced in a freshwater medium with the addition of sorbitol, suggesting that osmotic pressure plays a key role in this morphological plasticity. The plasticity of a domed valve face under higher osmotic conditions was also observed in *Skeletonema* species (Paasche et al. 1975, Hasle & Evensen 1976) and *Pleurosira socotrensis* (Li & Chiang 1979). *Melosira varians*, found in freshwater, is characterized by a flat valve face, whereas brackish or marine species such as *M. moniliformis* and *M. nummuloides* have a rounded valve face. Morphological differences in valve shape among *Melosira* species may be partly influenced by environmental salinity. The present study demonstrated that the mechanical force of osmotic pressure, which is one of the potential factors that have been estimated to provide the diatoms with morphological diversity (Mann 1984, Schmid 1984, 1987, Round et al. 1990), could drive a common flat/domed morphology in at least some genera.

In **Chapter 4**, I characterized gene expression of *P. laevis* cultivated at salinities of 2 and 7, which were found to produce flat (*laevis* form) and domed valve faces (*polymorpha* form), respectively. Using two strains, I found that the strain-dependent variation (i.e., intraspecific variation) in gene expression patterns in response to salinity was greater than the variation between salinity conditions. The intraspecific variations were reported by the recent transcriptomic studies using multiple strains of planktonic species *Leptocylindrus aporus* (Pargana et al. 2019), *Cyclotella cryptica* (Nakov et al. 2020) and *Skeletonema marinoi* (Pinseel et al. 2022). Our study and those of previous cases highlight the importance of using multiple strains if the goal is to reveal the core transcriptional response patterns conserved in the species. Since the morphological plasticity of *P. laevis* is not affected by differences of strains and conserved within the species (as described in Chapter 3), I focused on the genes that were differentially expressed by salinity in both strains. The results suggested that in salinity 2, which produces a flat valve face, the intracellular $Ca^{2+}$ levels are regulated to be enhanced by the up-regulation of genes encoding mechanosensitive ion channels and down-regulation of genes encoding $Ca^{2+}$ ATPases. In addition, genes encoding annexin, which mediates membrane-actin filament association in a $Ca^{2+}$-dependent manner, and Arp2/3, which serves as nucleation sites for new actin filaments, were up-regulated in salinity 2. I hypothesized the morphogenesis related to osmotic pressure may be achieved through 1) an upstream response involving osmotic pressure- and membrane tension-dependent regulation of intracellular $Ca^{2+}$ levels through the gating of transporters such as mechanosensitive ion channels, and 2) a downstream response involving $Ca^{2+}$-dependent regulation of actin

dynamics at membrane contact sites. It is noteworthy that I detected the sensing of membrane tension by cells, with the change in valve morphology that has been thought to be dependent on membrane tension (Schmid 1987). The function of the candidate genes involved in this sequence of reactions could be revealed by gene knockout or knockdown techniques as is used in studies of morphogenesis in the model diatom *Thalassiosira pseudonana* (Görlich et al. 2019, Heintze et al. 2022). In addition, it was found that even small differences between salinity 2 and 7 induced regulations of transporter activity, response to oxidative stress, physiological regulation, and transposable element activity in the euryhaline diatom *P. laevis*.

## Synthesis

In this dissertation, the life history of benthic diatom species was investigated in terms of sexual reproduction, organellar inheritance and endosymbiosis, life cycles, morphological and transcriptional response to environment. Through these studies, parts of the process of diversification and adaptation of benthic diatoms to new environments were revealed, leading to some new research questions such as:

- What are the cellular mechanisms underlying the uniparental inheritance of spheroid bodies of *Epithemia*?
- What are physical or genomic differences between sexual and asexual diatoms?
- Why do only a limited number of species exhibit morphological plasticity by environmental change?
- Does the morphological plasticity of *P. laevis* contribute to the fitness and adaptation?

Uniparental inheritance includes the elimination of uniparental organelles during sexual reproduction, such as organellar segregation through cell division following the receipt of organelles from parents, degradation of uniparental organelles through ubiquitin-mediated degradation and autophagy, and DNA degradation through nucleases that target only uniparental organellar DNA (as reviewed in Nishimura 2010, Sato & Sato 2013). Although the mechanisms of organellar elimination have been largely understood in some model organisms, nothing has been known in diatoms. Additionally, the genes responsible for regulating the emergence of vegetative and sexual phases in the life cycle of diatoms are yet to be fully understood. Studies on the model diatoms *Seminavis robsta* and *Pseudo-nitzschia multistriata* have been revealing how diatoms perceive chemical cue of extracellular sex-inducing pheromones, change cell motility and gene expression in gametes, thus achieving the pairing of sexually compatible cells and the formation of gametes (Moeys et al. 2016, Basu et al. 2017, Russo et al. 2018, Fiorini et al. 2020, Bilcke et al. 2021). However, there is still a lack of clarity regarding the distinctions between vegetative and sexual phases, as well as the differences between sexual and asexual species. Comparative transcriptomics will enable us to identify genes responsible for the such cellular processes and behaviors of diatoms. This dissertation, focusing on non-model benthic diatoms, provides ideal materials for researches of life cycles and morphogenesis, and insights that would have been overlooked through studies using only a few model species.

# ABSTRACT

Diatoms are unicellular algae distributed in a variety of aquatic environments throughout the world. It is believed that they contribute approximately 20% to global primary productivity and significantly impact the biogeochemical cycling of carbon and silica. A notable feature of diatoms is the presence of a cell wall made of silica, known as a frustule, enclosing their cells. The frustule consists of parts called valves and girdle bands, and the morphology of the valves is commonly used in diatom taxonomy. There are two life forms of diatoms: planktonic and benthic. In this dissertation, the life histories of the benthic pinnate *Epithemia* and the centric *Pleurosira laevis* were examined using microscopic and molecular biological techniques, focusing on life cycle, sexual reproduction, endosymbiosis, and morphological and transcriptional responses to the environment.

Diatoms belonging to the family Epithemiaceae have endosymbiont 'spheroid bodies', which have received attention as a model to provide new insights into the early stages of organelle evolution. Uniparental organelle inheritance, known in a wide range of sexually reproducing eukaryotes, is considered to be one of the key characteristics acquired during the evolution of an endosymbiont into an organelle. However, there has been no information about the inheritance of spheroid bodies. The aim of the present study was, therefore, to investigate the inheritance modes of the spheroid bodies and plastids in the isogamous diatom *Epithemia gibba* var. *ventricosa*, which the author established to be heterothallic. Sexual reproduction of *E. gibba* var. *ventricosa* was induced in culture using sexually compatible mating strains that differed in nucleotide polymorphisms in the spheroid body genomes. The F1 strains were genotyped to determine the parental origin of the spheroid bodies using parent-specific polymorphisms. The results suggested that inheritance of the spheroid bodies was uniparental (i.e. progeny have the spheroid body genome from either parent but not both) and random (i.e. with an unbiased ratio of parental origins), while that of the plastids was more complex, being predominantly uniparental but with a few biparental cases. This study is the first to report the inheritance pattern of the spheroid body and will contribute to better understand the evolutionary state of this organelle.

The life cycle of diatoms is associated with their cell size, and characterized by a gradual decrease in size in the vegetative stage and a recovery in size through sexual reproduction. Sexual reproduction is trigged when cells become smaller than a species-specific size threshold and receive species-specific environmental cues. Few studies involving both field observation and laboratory culture have documented the life cycles and frequency of sexual reproduction in diatoms. The author investigated cell size in two congeneric taxa, *E. gibba* var. ventricosa and *Epithemia* sp. collected monthly over almost 3 years from a pond in Nakaikemi Wetland. Cultures of both taxa were established to examine rates of cell size reduction, which affects the duration of the vegetative stage. It was suggested that congeneric taxa sharing a common habitat and substratum exhibit distinct sexual and asexual strategies.

*Pleurosira laevis* is a salt-tolerant diatom distributed around the world. The valve of *P. laevis* has distinct structures called ocelli, which are sharply defined areas with fine, densely packed pores. Two formae of this diatom, *P. laevis* f. *laevis* and *P. laevis* f. *polymorpha*, are distinguished from each other by their flat or dome-shaped valve faces and degree of elevation of the ocelli, respectively. In this study, the author established 4 strains of *P. laevis* isolated from freshwaters or coastal areas in Japan and the United States, and tracked the formation of newly formed valves with

the fluorescent SDV-specific dye PDMPO in culture under several salinity conditions. The result clearly demonstrated the morphological plasticity of the valves, controlled by environmental salinity. The *laevis* form and *polymorpha* form valves were produced at salinities of 2 and 7, respectively. The salinity thresholds dictating the morphological plasticity of the valve were consistent in all 4 strains. A similar morphology to the *polymorpha* form was reproduced in a freshwater medium with the addition of sorbitol, suggesting that osmotic pressure plays a key role in this morphological plasticity. The highly reproducible and easily manipulated change in morphology makes this diatom an ideal model for lab experiments focusing on the molecular and genetic factors involved with valve morphogenesis.

The mechanism of diatom morphogenesis has received attention both in the biological and nanomaterials engineering fields. However, little is known about the genetic mechanisms that regulate the morphology. The author therefore aimed to search for genes that may be involved in determining the morphology using *P. laevis* though comparative transcriptomes between salinities 2 and 7, in which this diatom changes its valve morphology. *Pleurosira laevis* exhibited regulation of transporter activity, transposable element activity, metabolic pathway, and response to oxidative stress. Under the condition in which *P. laevis* produces a flat valve face, the expression of genes encoding mechanosensitive (MS) ion channels, which sense changes in membrane tension and osmotic pressure and uptake $Ca^{2+}$ into cytosol, was up-regulated. In contrast, expression of genes encoding $Ca^{2+}$ ATPases, which pump $Ca^{2+}$ out of the cell, was decreased, suggesting that intracellular $Ca^{2+}$ levels are regulated to increased. Furthermore, genes encoding annexins, which mediate $Ca^{2+}$-dependent membrane-actin filament association, and Arp2/3, the nucleation site of new actin filaments, were up-regulated. The author hypothesized that the morphogenesis related to osmotic pressure observed in some genera of diatoms may be achieved thorough 1) an upstream response involving osmotic pressure- and membrane tension-dependent regulation of intracellular $Ca^{2+}$ levels through the gating of transporters such as mechanosensitive ion channels, and 2) a downstream response involving $Ca^{2+}$-dependent regulation of actin dynamics at membrane contact sites.

The insights into the life history of non-model benthic diatoms obtained through the aforementioned studies have unveiled a part of the process of diatom diversification. The transcriptomic approach will not only be effective for morphogenesis, but also for other cellular events. It may be possible to identify genes involved in uniparental organellar inheritance and genes controlling the transition between the vegetative and sexual phases, which is defined by cell size. This dissertation provides ideal materials for researches of life cycles and morphogenesis, and insights that would have been overlooked through studies using only a few model species.

# ACKNOWLEDGEMENTS

I extend my sincerest gratitude to Professors Shinya Sato, Hiroaki Suetake, and David G. Mann for their academic supervision and critical review of my dissertation. I am also deeply indebted to Prof. Shinya Yoshikawa and Dr. Kazumasa Yamada for their constructive suggestions. Furthermore, I am greatly appreciative of the contributions of my co-authors, Drs. Matt P. Ashworth, Masahiko Idei, Taisuke Ohtsuka, Tamotsu Nagumo, Atsushi Kobayashi, and Gust Bilcke, as well as Mr. Noriaki Nakamura and Mr. Daichi Mikami, for their invaluable support in conducting experiments and composing the manuscript. I would like to express my gratitude to the staff of the NPO Nakaikemi Net and the staff of the Fukui Coast Nature Center for their kind permission to collect samples. I had been greatly supported by Morishita-Jintan Scholarship Foundation for three years.

佐藤晋也先生と末武弘章先生には，研究を進めるうえで丁寧なご指導を賜りました。Prof. David G. Mann には，執筆にあたって多くの建設的なコメントをいただきました。また，学位審査は佐藤先生，末武先生, Prof. Mann によって行われました。心より感謝申し上げます。

海洋生物学研究室の吉川伸哉先生と山田和正先生には日々さまざまな助言をいただきました。投稿論文の共著者である Dr. Matt P. Ashworth，出井雅彦先生，大塚泰介先生，南雲保先生，小林敦先生, Dr. Gust Bilcke，中村憲章氏，三上大智氏には，実験と執筆で大変お世話になりました。皆様に心より感謝申し上げます。

本研究は, NPO 法人 中池見ねっとスタッフの皆様と，福井県海浜自然センタースタッフの皆様からサンプル採集を快諾いただいて遂行することができました。深く御礼申し上げます。

著者は 3 年間にわたり公益財団法人森下仁丹奨学会の奨学生として多大なご支援をいただきました。深く御礼申し上げます。

# REFERENCES

Basu, S., Patil. S., Mapleson, D., Russo, M.T., Vitale, L., Fevola, C., et al. (2017) Finding a partner in the ocean: molecular and evolutionary bases of the response to sexual cues in a planktonic diatom. New Phytologist 215: 140–156.

Bondoc, K.G.V., Lembke, C., Lang, S. N., Germerodt, S., Schuster, S., Vyverman, W. & Pohnert, G. (2019) Decision-making of the benthic diatom *Seminavis robusta* searching for inorganic nutrients and pheromones. The ISME journal 13: 537–546.

Bilcke, G., Osuna-Cruz, C. M., Santana Silva, M., Poulsen, N., D'hondt, S., Bulankova, P., Vyverman, W., De Veylder, L. & Vandepoele, K. (2021) Mating type specific transcriptomic response to sex inducing pheromone in the pennate diatom *Seminavis robusta*. The ISME Journal 15: 562–576.

Bussard, A., Corre, E., Hubas, C., Duvernois-Berthet, E., Le, Corguillé, G., Jourdren, L., Coulpier, F., Claquin, P. & Lopez, P.J. (2017) Physiological adjustments and transcriptome reprogramming are involved in the acclimation to salinity gradients in diatoms. Environmental Microbiology 19: 909–925.

Cox, E.J. (1995) Morphological variation in widely distributed diatom taxa: taxonomic and ecological implications. *In* Donate, M. & Montresor, M. [Eds] Proceedings of the 13th International Diatom Symposium, Maratea, 1994. Biopress, Bristol, pp. 335–345.

Cox, E.J. (2014) Diatom identification in the face of changing species concepts and evidence of phenotypic plasticity. Journal of Micropalaeontology 33: 111–120.

Cheng, R.L., Feng, J., Zhang, B.X., Huang, Y., Cheng, J. & Zhang, C.X. (2014) Transcriptome and gene expression analysis of an oleaginous diatom under different salinity conditions. BioEnergy Research 7: 192–205.

Chepurnov, V.A., Mann, D.G., Sabbe, K. & Vyverman, W. (2004) Experimental studies on sexual reproduction in diatoms. International Review of Cytology 237: 91–154.

Davidovich, N. & Davidovich, O. (2022) Diatoms with studied sexual reproduction. Fottea 22: 292–296.

Drum, R.W. & Pankratz, S. (1965) Fine structure of an unusual cytoplasmic inclusion in the diatom genus, *Rhopalodia*. Protoplasma 60: 141–149.

DeYoe, H.R., Lowe, R.L. & Marks, J.C. (1992) Effects of nitrogen and phosphorus on the endosymbiont load of *Rhopalodia gibba* and *Epithemia turgida* (Bacillariophyceae). Journal of Phycology 28: 773–777.

Dyall, S.D., Brown, M.T. & Johnson, P.J. (2004) Ancient invasions: from endosymbionts to organelles. Science 304: 253–257.

Edlund, M.B. & Stoermer, E.F. (1997) Ecological, evolutionary and systematic significance of diatom life histories. Journal of Phycology 33: 897–918.

Fattorini, N. & Maier, U.G. (2021) Targeting of proteins to the cell wall of the diatom *Thalassiosira pseudonana*. Discover Materials 1: 5.

Ferrante, M.I., Entrambasaguas, L., Johansson, M., Töpel, M., Kremp, A., Montresor, M. & Godhe, A. (2019) Exploring molecular signs of sex in the marine diatom *Skeletonema marinoi*. Genes 10: 494.

Finkel, Z.V. & Kotrc, B. (2010) Silica use through time: macroevolutionary change in the morphology of the diatom frustule. Geomicrobiology Journal 27: 596–608.

Fiorini F, Borgonuovo C, Ferrante MI, Brönstrup M. (2020) A metabolomics exploration of the sexual phase in the marine diatom *Pseudo-nitzschia multistriata*. Marine Drugs 18: 313.

Foster, R.A. & Zehr, J.P. (2019) Diversity, genomics, and distribution of phytoplankton-cyanobacterium single-cell symbiotic associations. Annual Review of Microbiology 73: 435–456.

Gallagher, J.C. (1983) Cell enlargement in *Skeletonema costatum* (Bacillariophyceae). Journal of Phycology 19: 539–542.

Geitler, L. (1932) Der Formwechsel der pennaten Diatomeen (Kieselalgen). Archiv für Protistenkunde 78: 1–226.

Geitler, L. (1977) Zur Entwicklungsgeschichte der Epithemiaceen *Epithemia, Rhopalodia* und *Denticula* (Diatomophyceae) und ihre vermutlich symbiotischen Sphäroidkörper. Plant Systematics and Evolution 128: 259–275.

Görlich, S., Pawolski, D., Zlotnikov, I. & Kröger, N. (2019) Control of biosilica morphology and mechanical performance by the conserved diatom gene *Silicanin-1*. Communication Biology 2: 245.

Hallegraeff, G.M. (1993) A review of harmful algal blooms and their apparent global increase. Phycologia 32: 79–99.

Hasle, G.R. & Evensen, D.L. (1976) Brackish water and freshwater species of the diatom genus *Skeletonema*. II. *Skeletonema potamos* comb. nov. Journal of Phycology 12: 73–82.

Heintze, C., Babenko, I., Zackova Suchanova, J., Skeffington, A., Friedrich, B.M. & Kröger, N. (2022) The molecular basis for pore pattern morphogenesis in diatom silica. Proceedings of the National Academy of Sciences 119: e2211549119.

Huang, R., Ding, J., Gao, K., Cruz de Carvalho, M.H., Tirichine, L., Bowler, C. & Lin, X. (2019) A potential role for epigenetic processes in the acclimation response to elevated $pCO_2$ in the model diatom *Phaeodactylum tricornutum*. Frontiers in Microbiology 9: 3342.

Kaczmarska, I., Poulíčková, A., Sato, S., Edlund, M.B., Idei, M., Watanabe, T. & Mann, D.G. (2013) Proposals for a terminology for diatom sexual reproduction, auxospores and resting stages. Diatom Research 28: 263–294.

Kamakura, S. & Sato, S. (2018) Morphology and phylogeny of 2 strains of *Epithemia* collected from Nakaikemi Wetland, Fukui, Japan. Diatom 34: 68–69.

Kihara, Y., Sahashi, Y., Arita, S. & Ohtsuka, T. (2009) Diatoms of Yamakado Moor in Shiga Prefecture, Japan. Diatom 25: 91–105.

Klebahn H. (1896) Beiträge zur Kenntniss der Auxosporenbildung I. *Rhopalodia gibba* (Ehrenb.) O. Müller. Jahrbücher für Wissenschaftliche Botanik 29: 595–654.

Kneip, C., Lockhart, P., Voß, C. & Maier, U.G. (2007) Nitrogen fixation in eukaryotes–new models for symbiosis. BMC Evolutionary Biology 7: Article 55.

Kociolek, J.P. & Stoermer, E.F. (2010) Variation and polymorphism in diatoms: the triple helix of development, genetics and environment. A review of the literature. Vie Milieu 60:75–87.

Kröger, N. & Poulsen, N. (2008) Diatoms—from cell wall biogenesis to nanotechnology. Annual Review of Genetics 42: 83–107.

Kuroiwa T. (2010) Review of cytological studies on cellular and molecular mechanisms of uniparental (maternal or paternal) inheritance of plastid and mitochondrial genomes

induced by active digestion of organelle nuclei (nucleoids). Journal of Plant Research 123: 207–230.

Levitan, O., Dinamarca, J., Zelzion, E., Lun, D.S., Guerra, L.T., Kim, M.K., Kim, J., Van Mooy. B.A.S., Bhattacharya, D. & Falkowski, P.G. (2015) Remodeling of intermediate metabolism in the diatom *Phaeodactylum tricornutum* under nitrogen stress. Proceedings of the National Academy of Sciences 112: 412–417.

Li, C. W. & Chiang, Y. (1979) A euryhaline and polymorphic new diatom, *Proteucylindrus taiwanensis* gen. et sp. nov. British Journal Phycology 14: 377–384.

Mann, D.G. (1984) An ontogenetic approach to diatom systematics. In Mann, D.G. [Ed.] Proceedings of the 7th International Diatom Symposium, Philadelphia, 1982. Koeltz, Koenigstein, pp. 113–144.

Mann, D.G. (1988) Why didn't Lund see sex in *Asterionella*? A discussion of the diatom life cycle in nature. In: Algae and the Aquatic Environment (ed Round, F.E.). Biopress, Bristol, pp. 383–412.

Mann, D.G. (1999) The species concept in diatoms. Phycologia 38: 437–495.

Mann, D.G. & Chepurnov, V.A. (2004) What have the Romans ever done for us? The past and future contribution of culture studies to diatom systematics. Nova Hedwigia 79: 237–291.

Mann, D.G. & Vanormelingen, P. (2013) An inordinate fondness? The number, distributions, and origins of diatom species. Journal of eukaryotic microbiology 60: 414–420.

Moeys, S., Frenkel, J., Lembke, C., Gillard, J.T.F., Devos, V., Van den Berge, K., Bouillon, B., Huysman, M.J.J., De Decker, S., Scharf, J., Bones, A., Brembu, T., Winge, P., Sabbe, K., Vuylsteke, M., Clement, L., De Veylder, L., Pohnert, G. & Vyverman, W. (2016) A sex-inducing pheromone triggers cell cycle arrest and mate attraction in the diatom *Seminavis robusta*. Scientific Reports 6: 19252.

Morozova, O., Hirst, M. & Marra, M.A. (2009) Applications of new sequencing technologies for transcriptome analysis. Annual review of genomics and human genetics 10: 135-151.

Nakayama, T., Ikegami, Y., Nakayama, T., Ishida, K., Inagaki, Y. & Inouye, I. (2011) Spheroid bodies in rhopalodiacean diatoms were derived from a single endosymbiotic cyanobacterium. Journal of Plant Research 124: 93–97.

Nakov, T., Judy, K.J., Downey, K.M., Ruck, E.C. & Alverson, A.J. (2020) Transcriptional response of osmolyte synthetic pathways and membrane transporters in a euryhaline diatom during long-term acclimation to a salinity gradient. Journal of Phycology 56: 1712–1728.

Nelson, D.M., Tréguer, P., Brzezinski, M.A., Leynaert, A. & Quéguiner B. (1995) Production and dissolution of biogenic silica in the ocean: revised global estimates, comparison with regional data and relationship to biogenic sedimentation. Global Biogeochemical Cycles 9: 359–372.

Nishimura, Y. (2010) Uniparental inheritance of cpDNA and the genetic control of sexual differentiation in *Chlamydomonas reinhardtii*. Journal of Plant Research 123: 149–162.

Ogura, A., Akizuki, Y., Imoda, H., Mineta, K., Gojobori, T. & Nagai, S. (2018) Comparative genome and transcriptome analysis of diatom, *Skeletonema costatum*, reveals evolution of genes for harmful algal bloom. BMC Genomics 19: 765.

Ohtsuka, T. & Kitano, D. (2020) Diatom flora of a wet grassland on mineral soil conserved in the Ritsumeikan University Biwako-Kusatsu Campus in Shiga Prefecture, central Japan. Diatom 36: 1–12.

Ovide, C., Kiefer-Meyer, MC., Bérard, C., Vergne, N., Lecroq, T., Plasson, C., Burel, C., Bernard, S., Driouich, A., Lerouge, P., Tournier, I., Dauchel, H. & Bardor, M. (2018) Comparative in depth RNA sequencing of *P. tricornutum*'s morphotypes reveals specific features of the oval morphotype. Scientific Reports 8: 14340.

Paasche, E., Johansson, S. & Evensen, D.L. (1975) An effect of osmotic pressure on the valve morphology of the diatom *Skeletonema subsalsum* (A. Cleve) Bethge. Phycologia 14: 205–211.

Pargana, A., Musacchia, F., Sanges, R., Russo, M.T., Ferrante, M.I., Bowler, C. & Zingone, A. (2019) Intraspecific diversity in the cold stress response of transposable elements in the diatom *Leptocylindrus aporus*. Genes 11: 9.

Pickett-Heaps, J., Schmid, A.M.M. & Edgar, L.A. (1990) The cell biology of diatom valve formation. *In* Round, F.E. & Chapman, D.J. [Eds] Progress in phycological research 7. Biopress, Bristol, pp. 1–168.

Pinseel, E., Nakov, T., Van den Berge, K., Downey, K. M., Judy, K. J., Kourtchenko, O., Kremp, A., Ruck, E.C., Sjöqvist, C., Töpel, M., Godhe, A. & Alverson, A.J. (2022) Strain-specific transcriptional responses overshadow salinity effects in a marine diatom sampled along the Baltic Sea salinity cline. The ISME Journal 16: 1776–1787.

Prechtl, J., Kneip, C., Lockhart, P., Wenderoth, K. & Maier, U.G. (2004) Intracellular spheroid bodies of *Rhopalodia gibba* have nitrogen-fixing apparatus of cyanobacterial origin. Molecular Biology and Evolution 21: 1477–1481.

Rose, D.T. & Cox, E.J. (2013) Some diatom species do not show a gradual decrease in cell size as they reproduce. Fundamental and Applied Limnology 182: 117–122.

Round, F.E. (1972) The problem of reduction of cell size during diatom cell division. Nova Hedwigia 23: 291–303.

Round, F.E., Crawford, R.M. & Mann, D.G. (1990) The Diatoms: biology and morphology of the genera. Cambridge University Press, Cambridge, 747 pp.

Russo, M.T., Vitale, L., Entrambasaguas, L., Anestis, K., Fattorini, N., Romano, F., et al. (2018) MRP3 is a sex determining gene in the diatom *Pseudo-nitzschia multistriata*. Nature Communications 9: 5050.

Sato, M. & Sato, K. (2013) Maternal inheritance of mitochondrial DNA by diverse mechanisms to eliminate paternal mitochondrial DNA. Biochimica et Biophysica Acta (BBA) Molecular Cell Research 1833: 1979–1984.

Sato, S., Mann, D.G., Nagumo, T., Tanaka, J., Tadano, T. & Medlin, L.K. (2008) Auxospore fine structure and variation in modes of cell size changes in *Grammatophora marina* (Bacillariophyta). Phycologia 47: 12–27.

Sato, Y., Takashimizu, Y. & Urabe, A. (2020) Diatom assemblages in the 2011 Tohoku-oki tsunami deposits and underlying soil in the Sendai Plain. Diatom 36: 85–91.

Shimizu, K., Del Amo, Y., Brzezinski, M.A., Stucky, G.D. & Morse, D.E. (2001) A novel fluorescent silica tracer for biological silicification studies. Chemistry & Biology 8: 1051–1060.

Shirokawa, Y. & Shimada, M. (2013) Sex allocation pattern of the diatom *Cyclotella meneghiniana*. Proceedings of the Royal Society B: Biological Sciences 280: 20130503.

Schmid, A.M.M. (1984) Tricornate spines in *Thalassiosira eccentrica* as a result of valve modelling. In Mann, D.G. [Ed.] Proceedings of 7th International Diatom Symposium, Philadelphia, 1982. Koeltz, Koenigstein, pp. 71–95.

Schmid, A.M.M. (1987) Morphogenetic forces in diatom cell wall formation. Cytomechanics. Springer, Berlin, Heidelberg. pp. 183–199.

Su, Y., Lundholm, N. & Ellegaard, M. (2018) Effects of abiotic factors on the nanostructure of diatom frustules—ranges and variability. Applied Microbiology and Biotechnology 102: 5889–5899.

Suzuki, S., Ota, S., Yamagishi, T., Tuji, A., Yamaguchi, H., & Kawachi, M. (2022) Rapid transcriptomic and physiological changes in the freshwater pennate diatom *Mayamaea pseudoterrestris* in response to copper exposure. DNA Research 29: dsac037.

Takano, S., Akaneya, K., Watanabe, T. & Katano, N. (2009) Diatoms from Akita Prefecture, northern part of Japan, part II－Diatoms from Toyokawa River. Diatom 25: 120–133.

Tesson, B. & Hildebrand, M. (2010a) Extensive and intimate association of the cytoskeleton with forming silica in diatoms: control over patterning on the meso- and micro-scale. PloS one 5: e14300.

Tesson, B. & Hildebrand, M. (2010b) Dynamics of silica cell wall morphogenesis in the diatom *Cyclotella cryptica*: substructure formation and the role of microfilaments. Journal of Structural Biology 169: 62–74.

Theissen, U. & Martin, W. (2006) The difference between organelles and endosymbionts. Current Biology 16: R1016–R1017.

Thompson, S.D., Prahalad, S. & Colbert, R.A. (2016) Integrative genomics. In Textbook of pediatric rheumatology. Seventh ed. WB Saunders, Elsevier Inc. pp. 43–53.

Trapp, E.M., Adler, S., Zau-ner, S. & Maier, U.G. (2012) *Rhopalodia gibba* and its endosymbionts as a model for early steps in a cyanobacterial primary endosymbiosis. Endocytobiosis and Cell Research 23: 21–24.

von Stosch, H.A. (1965) Manipulierung der Zellgrösse von Diatomeen im experiment. Phycologia 5: 21–44.

Wilhelm, B., Marguerat, S. & Watt, S. (2008) Dynamic repertoire of a eukaryotic transcriptome surveyed at single-nucleotide resolution. Nature 453: 1239–1243.

Zachar, I. & Boza, G. (2020) Endosymbiosis before eukaryotes: mitochondrial establishment in protoeukaryotes. Cellular and Molecular Life Sciences 77: 3503–3523.